

University of Montana

ScholarWorks at University of Montana

Graduate Student Theses, Dissertations, &
Professional Papers

Graduate School

2009

Biosignature storage in sulfate minerals- synthetic and natural investigations of the jarosite group minerals

Julia Michelle Kotler
The University of Montana

Follow this and additional works at: <https://scholarworks.umt.edu/etd>

Let us know how access to this document benefits you.

Recommended Citation

Kotler, Julia Michelle, "Biosignature storage in sulfate minerals- synthetic and natural investigations of the jarosite group minerals" (2009). *Graduate Student Theses, Dissertations, & Professional Papers*. 1275.
<https://scholarworks.umt.edu/etd/1275>

This Dissertation is brought to you for free and open access by the Graduate School at ScholarWorks at University of Montana. It has been accepted for inclusion in Graduate Student Theses, Dissertations, & Professional Papers by an authorized administrator of ScholarWorks at University of Montana. For more information, please contact scholarworks@mso.umt.edu.

BIOSIGNATURE STORAGE IN SULFATE MINERALS- SYNTHETIC AND
NATURAL INVESTIGATIONS OF THE JAROSITE GROUP MINERALS

By

JULIA MICHELLE KOTLER

Bachelor of Science Chemistry, University of Montana, Missoula, Montana, 2004

Dissertation

presented in partial fulfillment of the requirements
for the degree of

Doctor of Philosophy
in Geosciences

The University of Montana
Missoula, MT

Official Graduation Date - July 2009

Approved by:

Perry Brown, Associate Provost for Graduate Education
Graduate School

Nancy Hinman, Chair
Geosciences

Julia Baldwin
Geosciences

Steven Sheriff
Geosciences

James Sears
Geosciences

Edward Rosenberg
Chemistry

Jill Scott
Chemical Sciences, Idaho National Laboratory

Biosignature storage in sulfate minerals- synthetic and natural investigations of the jarosite group minerals

Chairperson: Nancy Hinman

ABSTRACT

The discovery of jarosite on Mars in 2004 generated increased interest in the properties of the mineral related to the search for life on other planets. Several studies indicate that the formation of jarosite can be linked to biological activity on Earth and biomolecules such as amino acids have been found associated with terrestrial jarosite samples. A series of natural and synthetic investigations using different jarosite end-members has been conducted and is presented in this dissertation to investigate the possibility that jarosite can store biosignatures. Natural samples were analyzed by X-ray diffraction, elemental carbon analysis and laser-desorption Fourier transform mass spectrometry (LD-FTMS) and were found to contain the amino acid glycine. Synthetic experiments were conducted in which the different end-members were synthesized in the presence of glycine as well as the amino acid alanine and the amino acid breakdown product methylamine. These samples were analyzed by X-ray diffraction, neutron diffraction, LD-FTMS and thermogravimetric analysis (TGA) techniques. Results of these experiments show that the detection of the biosignature and the effect that biomolecule has on the jarosite minerals is dependent on the end-member and indicate that the jarosite minerals are an excellent target for detecting potential signs of past life on other planets.

ACKNOWLEDGEMENTS

So many people have contributed both personally and scientifically to this project over the years. Every time I thought I couldn't continue, someone was there to help me find a way to push forward. To everyone who had to listen to endless hours of discussion about jarosite or the latest theories about Mars, I thank you. I thank you for the support, encouragement and even the blank stares. Sometimes all I needed was someone to listen.

I would like to thank my family, my friends, my dissertation committee, and all of the colleagues I have worked with over the years who have helped me make this possible. I would like to thank the three most influential scientists in my life, Dr. Kent Sugden, Dr. Nancy Hinman, and Dr. Jill Scott for giving me the foundation in which to build this project and achieve success. Kent's influence still holds today, many years later, as I remember the things he taught me in my early days of research. Nancy's support has been unyielding, and I couldn't imagine a better person to have spent time with both in the field and in the laboratory. She has given me so many opportunities to succeed and grow as a scientist. Lastly, to Jill, you have always found a way to help me stand up again no matter how many times I would fall down. Your patience has never gone unnoticed or unappreciated.

I would like to dedicate this dissertation to my grandmother, Patricia Brigati. Had she not been willing to take a chance on me so many years ago when she co-signed my first student loan, none of this would have possible. Thanks G! Thanks for believing in me and enduring the harassment from Wells Fargo.

PREFACE

This dissertation represents the final research work for my Ph.D conducted from 2004 – 2009 at the University of Montana Geosciences Department. What follows are five chapters and two appendices. Chapter 1 provides a general introduction to the subjects covered within the research chapters including; background information on the formation of the jarosite minerals on Earth and Mars, extraterrestrial amino acids, jarosite chemistry and crystallography, and an overview of techniques used that are less common in the geosciences. Chapter 2 is a research chapter that was published in the journal *Astrobiology* in April 2008. Chapter 2 covers X-ray diffraction, carbon elemental analysis, and Laser Desorption- Fourier Transform Mass Spectrometry (LD-FTMS) analysis conducted on natural samples of jarosite from various locations around the world in which the amino acid glycine was found associated with the mineral samples. Chapter 3 is a research chapter that was accepted for publication in the journal *Planetary and Space Science* in June of 2009. This chapter represents of a series of synthetic experiments with several jarosite end-members that were synthesized in the presence of glycine and then analyzed by thermal gravimetric analysis (TGA) techniques. Chapter 4 is a research chapter that was submitted to the *Journal of Thermal Analysis and Calorimetry* that was accepted July 2009. The chapter presents the results of jarosite end-members synthesized in the presence of the amino acid alanine and the amino acid degradation product methylamine studied by TGA. Chapter 5 is the last research chapter and represents X-ray and neutron diffraction studies of jarosite end-members synthesized in the presence of glycine.

Appendix 1 is a review chapter titled “The Stellar Stew: Distribution of Extraterrestrial Organics in the Universe”. It was accepted for publication in August of 2008 in the book “Astrobiology: from simple molecules to primitive life” published by American Scientific Publishers. This chapter reviews current literature related to the formation and detection of organic molecules in the universe including the interstellar medium, interplanetary dust particles, asteroids/chondritic meteorites and comets, planetary bodies and meteorites. Appendix 2 is a research chapter that covers some of the initial X-ray and LD-FTMS studies of the synthetic jarosite samples that provided the groundwork for the later research chapters.

Since many of the chapters were submitted as manuscripts, the formatting for those chapters remained similar to the journal format with the exception of header, figure and table numbering. As a consequence of this, each of the chapters has its own reference section and an amount of redundancy within the introductions of those chapters was unavoidable.

ABSTRACT.....	ii
ACKNOWLEDGEMENT.....	iii
PREFACE.....	iv
TABLE OF FIGURES.....	ix
TABLE OF TABLES.....	xi
CHAPTER 1: INTRODUCTION.....	1
1.1 GENERAL INTRODUCTION.....	1
1.2 FORMATION OF JAROSITE MINERALS ON EARTH AND MARS	3
1.3 ROLE OF SULFUR IN SHAPING THE MARTIAN SURFACE	6
1.4 EXTRATERRESTRIAL AMINO ACIDS	14
1.5 JAROSITE CHEMISTRY AND CRYSTALLOGRAPHY	23
1.6 OVERVIEW OF TECHNIQUES	29
1.6.2 DETECTION OF BIOSIGNATURES BY GEOMATRIX-ASSISTED LASER DESORPTION/IONIZATION (GALDI) MASS SPECTROMETRY	30
1.6.3 POWDER DIFFRACTION STRUCTURE SOLUTION METHODS	32
1.7 REFERENCES	39
CHAPTER 2: GLYCINE IDENTIFICATION IN NATURAL JAROSITES USING LASER DESORPTION FOURIER TRANSFORM MASS SPECTROMETRY: IMPLICATIONS FOR THE SEARCH FOR LIFE ON MARS	51
2.1 ABSTRACT	51
2.2 INTRODUCTION	52
2.3 MATERIALS AND METHODS	55
2.3.1 NATURAL SAMPLES-	55
2.3.2 SYNTHETIC SAMPLES-	56
2.3.3 X-RAY POWDER DIFFRACTION.....	56
2.3.4 TOTAL CARBON ANALYSIS	57
2.3.5 LASER DESORPTION FOURIER TRANSFORM MASS SPECTROMETRY.....	57
2.4 RESULTS.....	58

2.5 DISCUSSION.....	69
2.6 CONCLUSIONS.....	72
2.7 ACKNOWLEDGEMENTS	74
2.8 REFERENCES	74
2.8 ADDENDUM.....	75

CHAPTER 3: LABORATORY SIMULATIONS OF PREBIOTIC MOLECULE STABILITY IN THE JAROSITE MINERAL GROUP; END MEMBER EVALUATION OF DETECTION AND DECOMPOSITION BEHAVIOR RELATED TO MARS SAMPLE RETURN 80

3.1 ABSTRACT	80
3.2 INTRODUCTION	81
3.3 METHODS.....	85
3.3.1 SYNTHESSES.....	85
3.3.2 THERMAL ANALYSIS	86
3.4 RESULTS.....	86
3.4.1 THERMOGRAVIMETRIC ANALYSIS	86
3.5 DISCUSSION.....	98
3.6 ACKNOWLEDGEMENTS	104
3.7 REFERENCES	105

CHAPTER 4: THERMAL DECOMPOSITION BEHAVIOR OF POTASSIUM AND SODIUM JAROSITE SYNTHESIZED IN THE PRESENCE OF METHYLAMINE AND ALANINE..... 116

4.1 ABSTRACT	116
4.2 INTRODUCTION	118
4.3 EXPERIMENTAL	120
4.4 RESULTS AND DISCUSSION.....	122
4.5 CONCLUSIONS.....	133
4.6 ACKNOWLEDGEMENTS	134
4.7 REFERENCES	134

CHAPTER 5: NEUTRON AND X-RAY DIFFRACTION ANALYSIS OF POTASSIUM JAROSITE, SODIUM JAROSITE, AND AMMONIUM JAROSITE SYNTHESIZED IN THE PRESENCE OF THE AMINO ACID GLYCINE..... 137

5.1 ABSTRACT	137
5.2 INTRODUCTION	138
5.3 METHODS.....	141
5.3.1 SYNTHESSES.....	141
5.3.2 X-RAY DIFFRACTION	141
5.3.3 NEUTRON DIFFRACTION	142
5.4 RESULTS.....	143
5.4.2 NEUTRON DIFFRACTION.....	146
5.5 DISCUSSION.....	152
5.6 CONCLUSIONS.....	154
5.7 REFERENCES	154

APPENDIX 1: THE STELLAR STEW: DISTRIBUTION OF EXTRATERRESTRIAL ORGANIC COMPOUNDS IN THE UNIVERSE..... 159

A1 1.1 INTRODUCTION	160
A1 2.1 INTERSTELLAR MEDIUM ORGANIC COMPOUNDS	162
A1 2.2 DIFFUSE MOLECULAR CLOUDS.....	170
A1 2.3 DENSE DARK MOLECULAR CLOUDS.....	173
A1 2.4 HOT MOLECULAR CORES.....	176
A1 3.1 INTERPLANETARY DUST PARTICLES, ASTEROIDS/CHONDRITIC METEORITES, AND COMETS	180
A1 3.2 INTERPLANETARY DUST PARTICLES	182
A1 3.3 ASTEROIDS/CHONDRITIC METEORITES	184
A1 3.4 COMETS	197
A1 4.1 PLANETARY BODIES	199
A1 4.2 THE KUIPER BELT AND CENTAURS	200
A1 4.3 GIANT PLANETS	202
A1 4.4 SATURN'S ICY MOONS.....	203
A1 4.4.1 PHOEBE.....	203
A1 4.4.2 IAPETUS	204
A1 4.4.3 ENCELADUS.....	204
A1 4.5 TITAN	205
A1 4.6 TRITON	206
A1 4.7 GALILEAN SATELLITES	207
A1 4.7.1 EUROPA	207

A1 4.7.2 GANYMEDE AND CALLISTO	208
A1 4.8 THE TERRESTRIAL PLANETS	208
A1 4.8.1 MERCURY	208
A1 4.8.2 VENUS	209
A1 4.8.3 MARS	209
A1 4.10 SNC METEORITES	210
A1 5.1 CONCLUSION	214
A1 6.1 ACKNOWLEDGEMENTS	215
A1 7.1 REFERENCES	215
APPENDIX 2: INVESTIGATION OF SYNTHETIC JAROSITE END MEMBERS (K, Na, NH₄, Rb, AND Pb) USING LASER DESORPTION FOURIER TRANSFORM MASS SPECTROMETRY AND X-RAY DIFFRACTION	246
A2.1 ABSTRACT	246
A2.2 INTRODUCTION	246
A2.3 METHODS	249
A2.3.1 SYNTHESSES	249
A2.3.2 X-RAY DIFFRACTION	249
A2.3.3 LASER DESORPTION-FOURIER TRANSFORM MASS SPECTROMETRY (LD-FTMS) ..	250
A2.4 RESULTS/DISCUSSION	251
A2.4.1 X-RAY DIFFRACTION	251
A2.4.2 LD-FTMS	255
A2.5 CONCLUSIONS	257
A2.6 REFERENCES	259

TABLE OF FIGURES

Figure 1.1 The abundances of N ₂ , CO ₂ , and various noble gas isotopes trapped in impact-melted glass from the EETA79001 shergotite meteorite	8
Figure 1.2 Oxygen isotopic composition of four differentiated planetary bodies: Earth, Moon, Mars (SNC), and the howardite-eucrite-diogenite parent body (HED) ..	8
Figure 1.3 The sulfur cycle presented in Farquhar et al. (2000)	13
Figure 1.4 Chemical reaction for the formation of amino acids in the Strecker synthesis.	22
Figure 1.5 Step 1 in the mechanism of the Strecker synthesis	22
Figure 1.6 Step 2 of the Strecker synthesis	23
Figure 1.7 Modeled jarosite structure showing sites of probable substitution.	24

Figure 1.8 Modeled jarosite structure showing triangular arrangement of iron atoms that form the kagome lattice..	26
Figure 1.9 Modeled jarosite structure with trigonal symmetry and space group R-3m..	28
Figure 1.10 Modeled jarosite structure with trigonal symmetry and space group R3m..	28
Figure 1.11 Zwitterion form of l-glutamic acid..	37
Figure 1.12 Evolutionary progress plots.	38
Figure 1.13 Comparison between the position of the structural fragment in the best structure solution obtained by the GA calculations..	39
Figure 2.2 LD-FTMS positive mode spectrum of synthetic jarosite..	61
Figure 2.3. LD-FTMS positive mode spectra of jarosites from Arizona (AZ), Australia (AUS), New Mexico, and New Zealand (NZ)..	63
Figure 2.4. Expanded region (A) LD-FTMS positive mode spectrum from m/z 270 to m/z 280 of jarosite-New Zealand sample.	65
Figure 3.1 Thermal decomposition and derivative mass curves for glycine.	87
Figure 3.2 The results of the thermal decomposition and derivative mass curves of K-jarosite, K-jarosite-SWG, and K-jarosite-PMG.	91
Figure 3.3 Thermal decomposition and derivative mass curves for K-jarosite, K-jarosite-SWG, and K-jarosite-PMG	93
Figure 3.4. Thermal decomposition and derivative mass curves for NH ₄ -jarosite, NH ₄ -jarosite-SWG, and NH ₄ -jarosite-PMG	96
Figure 3.5. Relative decomposition rates of the jarosite end member syntheses (K ⁺ , Na ⁺ , and NH ₄ ⁺) and jarosite-SWG.	98
Figure 4.1 Thermal degradation (TG) and derivative mass (DG) curves for methylamine and alanine.	125
Figure 4.2 Thermal degradation (TG) and derivative mass (DG) curves for K-jarosite, K-jarosite-SWMA, K-jarosite-PMMA, K-jarosite-SWAla, and K-jarosite- PMAla.	127
Figure 4.3 Thermal degradation (TG) and derivative mass (DG) curves for Na-jarosite, Na-jarosite-SWMA, Na-jarosite-PMMA, Na-jarosite-SWAla, Na-jarosite-PMAla.	131
Figure 5.1- X-ray diffraction patterns for K-jarosite, Na-jarosite, and NH ₄ -jarosite.	145
Figure 5.2- X-ray diffraction patterns for K-jarosite-SWG, Na-jarosite-SWG, and NH ₄ -jarosite-SWG.	146
Figure 5.3- Neutron diffraction patterns for dK-jarosite and dK-jarosite-SWG	148
Figure 5.4- Subtracted neutron pattern (dK-jarosite – dK-jarosite-SWG).	149
Figure 5.5- Neutron diffraction patterns for dNa-jarosite and dNa-jarosite-SWG.	150
Figure 5.6 - Subtracted neutron pattern (dNa-jarosite – dNa-jarosite-SWG).	150
Figure 5.7- Neutron diffraction patterns for dNH ₄ -jarosite and dNH ₄ -jarosite-SWG	151
Figure 5.8- Subtracted neutron pattern (dNH ₄ -jarosite – dNa-jarosite-SWG).	152
Figure A1.1 Illustration of the various extraterrestrial environments relevant to organic species.	161
Figure A1.2 Comparison of laboratory acquired spectrum of a 1:10 mixture of dimethyl ether (CH ₃ OCH ₃) and H ₂ O at 105 K with the observed spectrum from the protostar W33A.	165
Figure A1. 3 Spectral bands indicative of PAHs acquired from several sources	166

Figure A1.4 Purported glycine spectra for A–C) line 21 at 206,468 MHz and D–F) line 26 240,899 MHz from the three sources Sgr B2(N-LMH), Orion KL, and W51 el /e2, respectively.....	177
Figure A1.5 Potential gas-phase reaction for synthesis of glycolaldehyde involving four steps.....	180
Figure A1.6. Comparison of RAMAN spectra from a laboratory sample with that of an IDP..	183
Figure A1.7. Solid-state ¹³ C Nuclear Magnetic Resonance (NMR) spectra of macromolecular material from the Orgueil and Tagish Lake meteorites	186
Figure A1.8. Tagish Lake and Murchison meteorite laser desorption mass spectra illustrating the detection of fullerene molecules.....	187
Figure A1.9. Chemical reaction for the formation of amino acids in the Strecker synthesis.....	195
Figure A1.10 Step 1 in the mechanism of the Strecker synthesis illustrating the formation of the α - aminonitrile intermediate.	196
Figure A.11 Step 2 of the Strecker synthesis showing the mechanism of formation from the α -aminonitrile to the formation of the amino acid and the ammonia by product.	197
Figure A1.12 Chemical analyses of organic matter from the carbonaceous chondrites EET92042, CR2, and Tieschitz, L3.6 compared to Stardust Comet 81P/Wild 2 samples.....	199
Figure A1.13 Near-infrared spectra of Pluto, Pluto’s moon Charon, and the large Kuiper belt object Quasar.....	199

TABLE OF TABLES

Table 1.1 The terrestrial protein amino acids listed with formulas and side chain polarity.	16
Table 2.1 Natural jarosite sample names, locations, and sources.....	55
Table 2.3 Major LD-FTMS positive peaks (m/z) observed in the natural jarosite samples.	62
Table 3.1. Thermal analysis of the jarosite standard synthetic samples, jarosite glycine syntheses (jarosite-SWG), and jarosite glycine mixtures (jarosite-PMG) including transition temperatures, total mass loss, total decomposition rates, rates per step, and total temperature change (ΔT_{total}) from onset to final.....	88
Table 4.1. Thermal analysis of methylamine and alanine, K-jarosite and Na-jarosite standard synthetic samples, synthesis and mixture experiments including transition temperatures, total mass loss, and total temperature change (ΔT_{total}) from onset to final.	122
Table 5.1- X-ray diffraction unit cell dimensions for jarosite end-members and jarosite-SWG.....	144
Table 5.2- Neutron diffraction unit cell dimensions for the dueterated jarosite end-members and jarosite-SWG.	149
Table A1.1 Organic molecules and ions detected in interstellar medium and circumstellar envelopes.....	159
Table A1.2 Soluble organic compounds in the Tagish Lake and Murchison meteorites	

Table A1.3 Compilation of selected organic compounds found in carbonaceous chondrites including generic structural examples and references.....	162
Table A1.4 The terrestrial protein amino acids listed with formulas and side chain polarity	
Table A1.5 Chemical composition of atmospheres of the Jovian planets.....	172
Table A1.6 Organic Inventory on Titan.....	194

CHAPTER 1: INTRODUCTION

1.1 GENERAL INTRODUCTION

In the search for life on other planets, detection of organic molecules and their assignment as biological evidence are key goals. During the *Viking* mission, pyrolysis gas chromatography/mass spectrometry was used on the surface of Mars to detect organic molecules (BIEMANN, 1977). Although the *Viking* mission was unsuccessful in providing evidence for significant quantities of organic molecules on Mars (BENNER et al., 2000), the search continues for new ways to identify organic molecules in geologic materials.

Jarosite is a prime mineral candidate for harboring organic compounds. Recently, Skelley *et al.*, (2004) reported the detection of amino acids associated with terrestrial jarosite samples through the use of a portable capillary electrophoresis instrument called the Mars Organic Analyzer with a sensitivity of 0.5 parts per trillion. Aubrey et al., (2006) also reported the association of amino acids with a single jarosite sample using a vapor-phase acid hydrolysis/desalting/micro-diffusion method followed by reverse-phase high performance liquid chromatography analysis (RP-HPLC). Thermodynamic evaluation of the two most common jarosite group minerals (jarosite- $\text{KFe}_3(\text{SO}_4)_2(\text{OH})_6$, and natrojarosite- $\text{NaFe}_3(\text{SO}_4)_2(\text{OH})_6$) has shown that these two members should be stable on the Martian surface (NAVROTSKY et al., 2005). The mineral group is also stable on Earth, and samples dating to several million years old have been reported (HOFSTRA et al., 1999; STOFFREGEN et al., 2000). The jarosite group minerals were first predicted to occur on Mars by Burns in the late 1980's (BURNS, 1987a; BURNS, 1987b; BURNS, 1989). In 2004, the Mars Exploration Rover *Opportunity* confirmed the presence

of jarosite group minerals on the Martian surface (CHRISTENSEN et al., 2004; KLINGELHOFER et al., 2004; SQUYRES et al., 2004b).

The jarosite group minerals can accommodate a wide variety of substitutions in several crystallographic sites of the unit cell. These substitutions often cause a distortion in the crystal lattice that creates vacancies in certain crystallographic sites (DUTRIZAC and JAMBOR, 2000). The general chemical formula for jarosite is $XFe_3(SO_4)_2(OH)_6$ where the X represents both monovalent and divalent cations that can occupy the axial positions in the crystal structure. Commonly found ions include K^+ , Na^+ , H_3O^+ , NH_4^+ , and Pb^{2+} with reports of foreign ions also occupying this position (DUTRIZAC and CHEN, 2004; DUTRIZAC et al., 1996; GIERE et al., 2003). A foreign ion is used to describe any atomic or molecular ion that is found associated in an unidentified manner, either trapped, included, or possibly substituted, in the mineral structure that is not considered common to the mineral chemistry. Becker and Gasharova (BECKER and GASHAROVA, 2001) investigated the ability of jarosite to incorporate foreign ions and determined that jarosite could act as a storage mineral for heavy metals. The acidic conditions ($pH < 2.5$) at which jarosite forms suggest that certain amino acids such as glycine ($C_2H_5O_2$) present in solution would be charged ($pK_a \alpha-COOH = 2.3$; $pK_a \alpha-NH_3^+ = 9.6$) (MATHEWS et al., 2000). This could provide a charge balancing substitution especially in rapidly precipitating systems where the inclusion of foreign ions would likely occur. Unless the system were supersaturated with respect to these foreign ions, the amount of substitution would be below the detection limits of standard powder diffraction methods (generally, 3-5%) including particle size considerations and could go undetected without the use of sensitive microprobe techniques.

Discussed individually in the following sections is the information related to topics covered in the various research chapters. Although each research chapter contains its own introduction and methods sections, this introductory chapter is intended to provide additional background information that links all of the research chapters together.

1.2 FORMATION OF JAROSITE MINERALS ON EARTH AND MARS

On Earth, the major environments that host jarosite mineralization are varied. They include: oxidized regions of sulfide ore deposits including oxidation of surface pyrite deposits, acid soils (DILL and POLLMAN, 2002; DUTRIZAC and JAMBOR, 2000), acid saline lakes (ALPERS and RYE, 1992), acid fumaroles (FULIGNATI and SBRANA, 2002), hot springs (JONES and RENAUT, 2003; KAWANO and TOMITA, 2001), and magmatic hydrothermal environments (ARMSTRONG, 1995; HUTTON and BOWEN, 1950; JOHNSTON, 1977; MARTINEZ-FRIAS and LUNAR, 2004). The rate of sulfide oxidation in these systems can be greatly enhanced by bacterial activity, and numerous sources have shown that jarosite precipitation can be influenced or mediated by sulfur and iron metabolizing microorganisms (AKAI et al., 1999; BRIDGE and JOHNSON, 2000; CLARK et al., 1993; ENEROTH and KOCH, 2004; GRISHIN et al., 1988; GRISHIN and TUOVINEN, 1988; KARAMANEV, 1991; SASAKI and KONNO, 2000).

Microorganisms are ubiquitous on Earth and have not yet been identified on Mars. This represents a possible major difference in the chemical weathering of bedrock between the planets. The processes of chemical weathering on Earth are rarely unaffected by the influence of microorganisms since they can modulate red-ox conditions (AKAI et al., 1999), pH (ARMSTRONG, 1995), and the surface reactivity of minerals (BRIDGE and JOHNSON, 2000). Microorganisms inhabit nearly every surface and many subsurface

environments on Earth including high and low temperature environments, extremes of ionic strength in acid-saline lakes and evaporative environments, and all ranges of aqueous environments including water of extreme alkalinity and acidity.

The sedimentary-layered formations that contain jarosite and other secondary iron minerals observed at Meridiani Planum by MER-*Opportunity* (CHRISTENSEN et al., 2004; KLINGELHOFER et al., 2004; SQUYRES et al., 2004a; SQUYRES et al., 2004b) could be explained by the weathering of fayalitic olivine, iron-rich pyroxenes, and pyrrhotite-pentlandite mineral assemblages present in the komatiitic basalts near the surface. These assemblages are highly vulnerable to chemical weathering, particularly in the presence of oxygenated acidic aqueous solutions (SIEVER and WOODFORD, 1979). Burns and Fisher (1990a) summarized the oxidative weathering process as follows: deep weathering of primary igneous iron sulfides (pyrrhotite or troilite) is initiated by dissolved Fe^{3+} ions in percolating groundwater which can proceed in the absence of oxygen. The dissolved oxygen in the near-surface environment then initiates the formation of the hydrated alteration minerals (jarosite, goethite) from the secondary FeS_2 minerals (pyrite or marcasite).

The details of the chemical reactions show how the formation of hydronium jarosite $((\text{H}_3\text{O})\text{Fe}_3(\text{SO}_4)_2(\text{OH})_6)$ (eqn. 4b) precedes the formation of the more insoluble and thermodynamically stable forms of jarosite $((\text{K},\text{Na})\text{Fe}_3(\text{SO}_4)_2(\text{OH})_6)$ (STOFFREGEN et al., 2000) from the interaction with near surface weathering of feldspars that provide the alkali cations. The formation of the other hydrated mineral phase goethite can proceed by the oxidation of Fe^{2+} (eqn. 6), the hydrolysis of Fe^{3+} (eqn. 7), and the decomposition of hydronium jarosite (eqn. 8). Jarosite formation occurs through the decomposition of

secondary iron-sulfides (eqn.2, 3), the production of sulfate anions, and the release of protons to lower the pH of the aqueous environment.

- (1) $\text{Fe}_7\text{S}_8 + 6 \text{Fe}^{3+} \rightarrow 4 \text{FeS}_2 + 9 \text{Fe}^{2+}$
- (2) $\text{FeS}_2 + 14 \text{Fe}^{3+} + 8 \text{H}_2\text{O} \rightarrow 15 \text{Fe}^{2+} + 2 \text{SO}_4^{2-} + 16 \text{H}^+$
- (3) $2 \text{FeS}_2 + 2 \text{H}_2\text{O} + 7 \text{O}_2 (\text{aq}) \rightarrow 2 \text{Fe}^{2+} + 4 \text{SO}_4^{2-} + 4 \text{H}^+$
- (4) (a) $3 \text{Fe}^{3+} + 2 \text{SO}_4^{2-} + 7 \text{H}_2\text{O} \rightarrow (\text{H}_3\text{O})\text{Fe}_3(\text{SO}_4)_2(\text{OH})_6 + 6 \text{H}^+$
 (b) $2 \text{FeSO}_4^- + \text{FeOH}^{2+} + 6 \text{H}_2\text{O} \rightarrow (\text{H}_3\text{O})\text{Fe}_3(\text{SO}_4)_2(\text{OH})_6 + 4 \text{H}^+$
- (5) $6 \text{Fe}^{2+} + 4 \text{SO}_4^{2-} + 9 \text{H}_2\text{O} + \frac{3}{2} \text{O}_2 (\text{aq}) + 2 (\text{K}^+, \text{Na}^+, \text{H}_3\text{O}) \rightarrow$
 $2 (\text{K,Na}, (\text{H}_3\text{O}))\text{Fe}_3(\text{SO}_4)_2(\text{OH})_6 + 6 \text{H}^+$
- (6) $4 \text{Fe}^{2+} + 6 \text{H}_2\text{O} + \text{O}_2 (\text{aq}) \rightarrow 4 \text{FeOOH} + 8 \text{H}^+$
- (7) $\text{Fe}^{3+} + 2 \text{H}_2\text{O} \rightarrow \text{FeOOH} + 3 \text{H}^+$
- (8) $(\text{H}_3\text{O})\text{Fe}_3(\text{SO}_4)_2(\text{OH})_6 \rightarrow 3 \text{FeOOH} + 2 \text{SO}_4^{2-} + 4 \text{H}^+ + \text{H}_2\text{O}$

Mars and Earth differ in chemical weathering potentials inherent in the amount of liquid surface water that is available to initiate potential chemical reactions. The surface area of the Earth is more than 70 % water. Since alteration of basalts is occurring at water-rock interfaces on the ocean floor (ALT et al., 1986), this represents a major weathering environment that Mars lacks.

It is not yet possible to determine what chemical, physical, and possibly biological influences affected the formation of jarosite on Mars. It is clear however, that the most likely path of jarosite formation was initiated by and originated in the chemical weathering of basalts (SQUYRES and KNOLL, 2005). It is also clear that sulfur played a critical role in shaping the Martian surface and influenced jarosite formation.

1.3 ROLE OF SULFUR IN SHAPING THE MARTIAN SURFACE

The evolution of magmatic sulfides, volcanic outgassing of H_2S and SO_2 , photochemical atmospheric reactions, and eolian and/or aqueous deposition of sulfur species has shaped the surface of Mars. Sulfur cycling on Mars likely began with partial melting of the Martian mantle, which is estimated to contain 4.5 wt. % sulfur (CARROLL and RUTHERFORD, 1985). The production of iron and sulfur-rich komatiitic magmas (BAIRD and CLARK, 1984; MCGETCHIN and SMYTH, 1978) then transported high concentrations of dissolved S^{2-} and HS^- to the Martian surface (CARROLL and RUTHERFORD, 1988). Chemical analyses of near-surface basalts in shergottite Martian meteorites indicate that only 0.16-0.22 wt % sulfur remained in the magmas after they reached the surface (LAUTH et al., 1986; MCSWEEN and JAROSEWICH, 1983). Chlorine and sulfur are thought to be more abundant in Martian soils and dust than in underlying rocks (RIEDER et al., 2004), implying deposition by volcanism, chemical transformation in the atmosphere, and eolian or aqueous deposition (BOGARD et al., 2001).

Clark and Baird (CLARK and BAIRD, 1979) suggested a pathway for sulfur cycling that involves thermal decomposition or reduction of FeS leading to the production of H_2S that escapes into the atmosphere during volcanism where oxidation by O , O_2 , and O_3 produce SO_2 , leading to SO_3 by third body reactions (SETTLE and GREELEY, 1979) and eventual precipitation of H_2SO_4 in acid rain. Complex chemical reactions in the Martian atmosphere may be reflected in data collected for sulfur isotope distributions in SNC meteorites that indicate interactions between the Martian atmosphere and regolith (GREENWOOD et al., 2000; SHEARER et al., 1996).

The SNC (shergotite-nakhlite-chassignite) meteorite classification is based primarily on oxygen isotope fractionation values in meteoritic materials that indicate an extraterrestrial origin (CLAYTON and MAYEDA, 1996) and also correlate with compositional measurements of the Martian atmosphere taken by the Viking spacecraft (PEPIN and CARR, 1992). The Martian atmosphere is considered to be unique, and therefore the geochemical remnants of atmospheric gases trapped in meteorites can serve as the geochemical fingerprint linking a material to its parent planet, in this case Mars (MARTI et al., 1995; TURNER et al., 1997). Figure 1.1 shows the relationship between the isotopic compositions and abundances found in the impact-melted glass of the shergotite meteorite EETA79001 and the Martian atmosphere (taken from Treiman and McSween, 2000). The oxygen isotope compositions of different planetary bodies are shown in figure 1.2. The measurements are relative to SMOW (standard mean ocean water) and terrestrial values were determined using the common fractionation line TF (TF = terrestrial fractionation line) in which Moon and Earth materials define. The Martian meteorites (SNC class) have a mean $\Delta^{17}\text{O}$ value of 0.28, which is the departure from the TF defined as $\delta^{17}\text{O} = 0.52 \delta^{18}\text{O}$ (Clayton and Mayeda, 1996). All of the SNC meteorites are above the TF and indicate a common parent body that has been linked to Mars by the atmospheric relationships shown in 1.1.

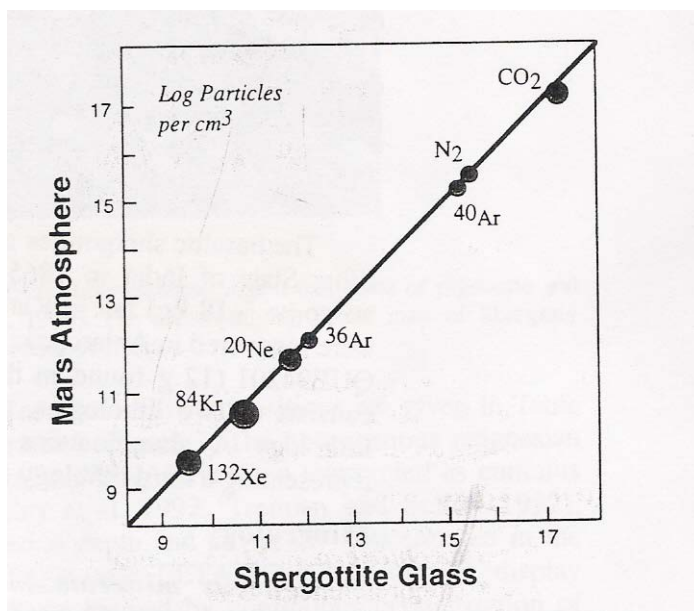


Figure 1.1. The abundances of N_2 , CO_2 , and various noble gas isotopes trapped in impact-melted glass from the EETA79001 shergotite that correlate to measurements of the Martian atmosphere by Viking spacecraft (modified from Pepin and Carr 1992). Uncertainties in the analyses are encompassed within the circles. (Taken from McSween and Treiman, 2000).

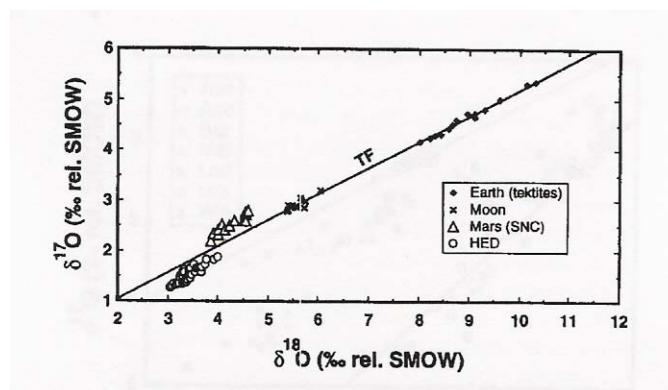


Figure 1.2. Oxygen isotopic composition of four differentiated planetary bodies: Earth, Moon, Mars (SNC), and the howardite-eucrite-diogenite parent body (HED) that illustrate the differences in oxygen isotopic compositions that group materials to their parent bodies. The Earth and Moon fall on a common fractionation line (TF), indicating their origin from a single reservoir. The Mars (SNC) meteorites have a mean $\Delta^{17}O$ value of 0.28 and plot above the TF. (Taken from Clayton and Mayeda, 1996).

The shergotites are named after Shergotty, a 5 kg meteorite that fell in the Bihar State of India in 1865 (TSCHERMAK, 1872). There are 6 identified shergotites that have

been recovered from India, Nigeria and various localities in Antarctica (CLAYTON and MAYEDA, 1996). The term “shergotites” includes meteorites with basaltic and lherzolitic composition, although the lherzolitic shergotites have only been found in Antarctica (TREIMAN et al., 2000). The Nakhrites are also igneous rocks and the type meteorite, Nakhla, fell in 1911 at El-Nakhla el-Bahariya in northern Egypt (MCSWEEN and TREIMAN, 1998). Two other nakhrites, Lafayette and Governador Valadares, have uncertain histories. It has been postulated that they are all pieces of the Nakhla fall (TREIMAN, 1993). Since 2000, four additional nakhrites have been discovered, two in northwest Africa and two from separate localities in Antarctica (TREIMAN, 2005). There is only one chassignite (Chassigny) meteorite and it is the only known Martian dunite sample. It's fall was observed in Haute-Marne, France in 1815 (MEYER, 1996).

Meteorite ALH84001 does not fall specifically into the SNC classification but is still considered to have a Martian origin (MCSWEEN and TREIMAN, 1998). The oxygen isotopic composition and atmospheric relationships links ALH84001 to the other SNC meteorites (CLAYTON and MAYEDA, 1996). Geochronological investigations estimated the age of the meteorite to be 4.5 ± 0.13 Ga which is 3 to 4 billion years older than the other SNC class meteorites and has raised questions about its origin as the oldest discovered Martian meteorite (NYQUIST et al., 1995). Despite controversies associated with ALH84001 that include the presence of possible nanofossils (MCKAY et al., 1996), it is classified as a Martian meteorite based on oxygen isotope fractionation and mineralogical properties and has been generally accepted to have originated from Mars (MCSWEEN and TREIMAN, 1998).

Anomalous values for $\delta^{33}\text{S}$ have been reported for some Martian meteorites (nakhlikes and shergottites). These values have been explained by non-mass-dependent chemical reactions involving UV photolysis of volcanogenic SO_2 and H_2S in the Martian atmosphere (FARQUAR et al., 2000). Few mechanisms are known in nature that can fractionate isotopes independently of mass. Only atmospheric or nuclear processes (as recorded in meteorites) are likely agents for producing the isotopic heterogeneity seen in the SNC meteorites (GREENWOOD et al., 2000). Therefore, cycling between atmospheric sulfur and the Martian surface has been shown to occur where these isotopic signatures have been imparted into secondary pyrite grains analyzed from Martian meteorites (FARQUAR et al., 2000; GREENWOOD et al., 2000).

Clayton et al. (CLAYTON et al., 1973) reported the first observations of mass-independent isotope fractionation of oxygen isotopes in calcium-aluminum rich inclusions (CAIs) from chondritic meteorites. Since then, numerous studies have been conducted to understand the phenomenon, and progress has been made toward developing the possible chemical and physical mechanisms that underlie the process with the majority of work being focused on oxygen isotopes (MARCUS, 2004). These mechanisms are still being developed, and contradictory theories have led to the claim that “the development of a quantitative model still presents a formidable challenge to the chemical physics community” (THEIMANS, 1999).

It has been suggested that isotopic anomalies observed in atmospheric ozone reactions that lead to enrichment of ^{17}O may be due to symmetry constraints where an isotopically asymmetric ozone molecule has a longer lifetime for dissociation due to a smaller effective density of quantum states of the vibrationally excited molecule (GAO

and MARCUS, 2001). In addition to symmetry considerations, mass-independent isotope fractionation of oxygen isotopes has been linked to the nuclear spin associated with ^{17}O that has a hyperfine interaction that reduces the “spin-forbidedness” of electron spin-nuclear spin coupling (BHATTACHARYA et al., 2000) that would cause ^{17}O incorporation to be favored (MARCUS, 2004).

Because the mechanisms developed for oxygen isotopes are based more on physical than chemical processes, the mass independent isotope fractionations are being used to distinguish early solar system and atmospheric processes from more evolved systems where chemically driven mass-dependent isotope fractionations will dominate (THEIMANS, 1999). Therefore, sulfur isotope mass-independent fractionations are being investigated with the same assumptions (FARQUAR et al., 2000). Despite a clear mechanism for how the process of mass-independent isotope fractionation occurs, the phenomenon is clearly observed in both oxygen and sulfur systems (THEIMANS, 1999).

The formation of secondary pyrite from primary komatiitic basalts on Mars has been proposed to occur by the oxidation of pyrrhotite in acidic groundwater percolating from the surface (BURNS, 1990). The formation of ferric sulfates such as jarosite ($\text{K,Na,(H}_3\text{O)Fe}_3(\text{SO}_4)_2(\text{OH})_6$) are thought to occur when highly acidic, sulfate-rich solutions such as those formed by acidic rain (BAIRD and CLARK, 1979), enter the groundwater adjacent to weathering of sulfide minerals (BURNS, 1990). This would explain the modification of the original sulfur signatures by interaction with these fluids and would produce heterogeneous sulfur isotope distributions (GREENWOOD et al., 2000). Until more oxidized samples of the Martian surface such as the jarosite found at Meridiani Planum (CHRISTENSEN et al., 2004; KLINGELHOFER et al., 2004; SQUYRES et

al., 2004a; SQUYRES et al., 2004b) can be analyzed for sulfur isotope anomalies, the constraints of atmospheric sulfur interactions with the Martian regolith based on isotopic distributions will remain poorly understood.

A complete cycling of sulfur on Mars by atmospheric photochemical reactions has been developed by Farquhar et al., 2000 and is consistent with the observed sulfur isotopic distributions from the SNC meteorites. The details of the cycle are as follows and are shown in figure 1.3 with the major reservoir for sulfur found in the regolith as magmatic sulfur:

- 1) volcanic injections of SO_2 and H_2S introduce sulfur into the atmosphere
- 2) photochemical reactions in the atmosphere are split into 3 types
 - a) H_2S photodissociation
 - b) SO_2 photooxidation
 - c) photochemical decomposition of airborne sulfate
- 3) deposition of oxidized sulfate onto surface as dust
- 4) dust storms loft and homogenize surface sulfate reintroducing it into the atmosphere to continue the cycle.

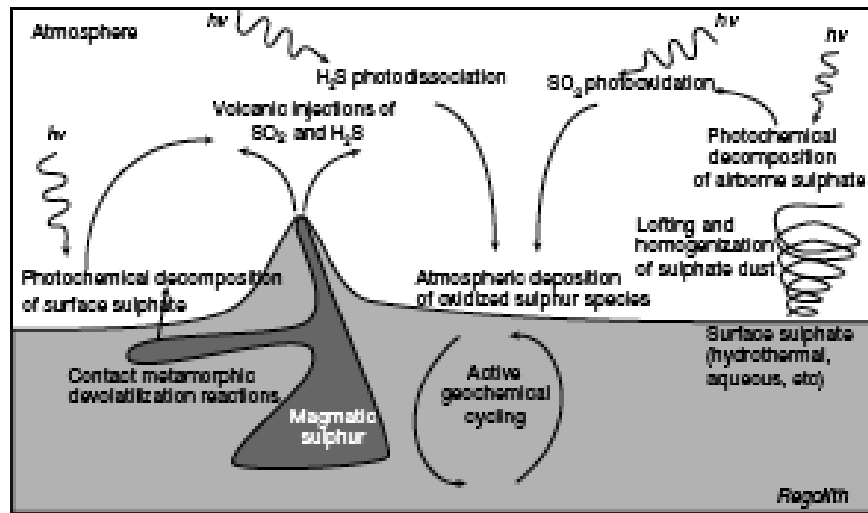


Figure 1.3 The sulfur cycle presented in Farquhar et al. (2000). Major reservoir for sulfur is found in the regolith as magmatic sulfur. Transfer of sulfur between the atmosphere and regolith takes place by ejection of SO_2 and H_2S . The SO_2 and H_2S are altered by photochemical reactions and deposited onto the surface as dust that is either incorporated into surface materials or is re-entered into the cycle by dust storms or photochemical reactions at the surface.

This model of sulfur cycling does not explicitly take into account the influence of groundwater that has been incorporated into other models that have been proposed (GREENWOOD et al., 2000; NEWSOM et al., 1999). These models suggest that a late meteoric veneer on Mars should be considered to explain the isotopic anomalies in the Martian meteorites and the geochemical requirements of secondary hydrous mineral formation.

Greenwood et al. (2000) suggest that the ALH84001 sulfur isotope analysis results are consistent with a short-lived impact-driven hydrothermal system and that Nakhla experienced a magmatic hydrothermal system (KARLSSON et al., 1992; ROMANEK et al., 1998) and that these results are consistent with a Martian regolith that remained isotopically distinct from the Martian mantle. Since widespread and long-lived plate

tectonic activity did not occur on Mars (CARR and WANKE, 1992), effective crustal recycling did not occur to homogenized sulfur isotope distributions.

Therefore, a modification to the sulfur cycle proposed by Farquhar et al. (2000) should be considered that implicitly considers the possibility of evaporation of meteoric fluids to the atmosphere to cycle sulfur by the following steps:

- 1) volcanic ejection of H₂S and SO₂ into the atmosphere
- 2) photochemical reactions (photodissociation and or photooxidation)
- 3) groundwater reaction with surface minerals to produce hydrous secondary ferric sulfates either from precipitation, impact-driven hydrothermal systems or magmatic hydrothermal systems
- 4) evaporation of residual groundwater to undergo further photochemical reactions
- 5) deposition of oxidized sulfate onto surface as dust
- 6) dust storms loft and homogenize surface sulfate reintroducing it into the atmosphere to continue the photochemical cycle.

This cycle would allow for the formation of evaporite minerals that have been observed on Mars (CLARK et al., 2005; MCLENNAN et al., 2005; TOSCA et al., 2005), fulfill the geochemical requirements for hydrous ferric sulfates proposed by Burns (BURNS, 1987a), and fits with observations of sulfur isotope distributions in Martian meteorites (FARQUAR et al., 2000; GREENWOOD et al., 2000) that require the cycling between the atmosphere and regolith to produce heterogeneous sulfur isotope distributions.

1.4 EXTRATERRESTRIAL AMINO ACIDS

The most complex extraterrestrial bio/organic molecules, such as prebiotic amino acids, were discovered by directly analyzing extraterrestrial objects that were delivered to Earth, such as chondritic meteorites (the most abundant source), the SNC class martian meteorites, and grains returned from comet 81/P from the Stardust Mission. This section will focus primarily on the amino acids that are related to biotic and prebiotic chemical processes that may be of interest to the astrobiology community including some of the accepted abiotic mechanisms for their formation. For a more comprehensive review, please see Sephton (2002), Pizzarello et al. (2006) and Kotler et al. (2009).

The presence of amino acids in the carbonaceous chondrites has generated a great deal of excitement as a possible indicator of prebiotic chemistry in the proto-solar nebula (PIZZARELLO, 2006). Glycine, methylamine, and ethylamine were detected in several grains returned from the Stardust Mission, generating excitement about the possibility of prebiotic molecules in comets (SANDFORD, 2007; SANDFORD et al., 2006). Our understanding of martian organic matter is limited to what is known from the SNC meteorites because of the lack of detection of organic matter by Viking landers. In 1996, (MCKAY et al., 1996) issued an astonishing report that ALH84001 contained signs of extraterrestrial life, supported by the appearance of nanofossils, biogenic magnetite, and PAHs. The amino acids (glycine, serine, alanine) were also detected using LD-MS and HPLC, but some were considered to be products of terrestrial contamination (BECKER et al., 1999a; BECKER et al., 1999b), especially the amino acids that are thought to be contaminants from Antarctic meltwater (BADA et al., 1998).

Amino acids in meteorites have produced a wealth of information and speculation regarding early synthetic pathways for prebiotic chemistry on Earth. Approximately 20

common amino acids comprise proteins in living systems on Earth (see Table x). Amino acids are organic compounds that contain both an α -NH₂ (α - amino group) and an α -COOH (α - carboxylic acid) attached to a common carbon atom. The carbonyl carbon can then accommodate several molecular constituents on the side chain of the amino acid. In terrestrial protein amino acids, a hydrogen (called the α -H) occupies the fourth bonding site on the common carbon. When four different atoms or molecules are bound to the common carbon, that carbon is chiral. Chirality is used to represent molecules of identical composition that differ structurally by how they rotate light. This property can be explained easily by using the term ‘handedness.’ This term becomes useful when describing chirality because human hands are mirror images of one another, but they are not super-imposable. Handedness is pervasive in biomolecules; terrestrial organisms usually prefer one orientation to another, resulting in the concept of homochirality. Chirality is indicated by terms such as R,S enantiomers (organic chemistry nomenclature) and L,D enantiomers (biochemistry nomenclature). Enantiomers are molecules with opposite chirality. Abiotic syntheses of amino acids tend to produce equal quantities of enantiomers (i.e., a 50/50 racemic mixture). Enantiomeric excesses imply preferential synthesis, which could be biologically directed, or preferentially use of one form over another in biological processes; either process would result in an excess of one enantiomer over the other.

Table 1.1 The terrestrial protein amino acids listed with formulas and side chain polarity.

Terrestrial protein amino Acid	Side Chain formula	Side chain polarity
Alanine	CH₃-CH(NH₂)-COOH	nonpolar

Arginine	$\text{HN}=\text{C}(\text{NH}_2)\text{-NH}(\text{CH}_2)_3\text{-CH}(\text{NH}_2)\text{-COOH}$	polar
Asparagine	$\text{H}_2\text{N-CO-CH}_2\text{-CH}(\text{NH}_2)\text{-COOH}$	polar
Aspartic Acid	$\text{HOOC-CH}_2\text{-CH}(\text{NH}_2)\text{-COOH}$	polar
Cysteine	$\text{HS-CH}_2\text{-CH}(\text{NH}_2)\text{-COOH}$	polar
Glutamic Acid	$\text{HOOC}(\text{CH}_2)_2\text{-CH}(\text{NH}_2)\text{-COOH}$	polar
Glutamine	$\text{H}_2\text{N-CO}(\text{CH}_2)_2\text{-CH}(\text{NH}_2)\text{-COOH}$	polar
Glycine	$\text{NH}_2\text{-CH}_2\text{-COOH}$	nonpolar
Histidine	$\text{NH-CH}=\text{N-CH}=\text{C-CH}_2\text{-CH}(\text{NH}_2)\text{-COOH}$	polar
Isoleucine	$\text{CH}_3\text{-CH}_2\text{-CH}(\text{CH}_3)\text{-CH}(\text{NH}_2)\text{-COOH}$	nonpolar
Leucine	$(\text{CH}_3)_2\text{-CH-CH}_2\text{-CH}(\text{NH}_2)\text{-COOH}$	nonpolar
Lysine	$\text{H}_2\text{N}(\text{CH}_2)_4\text{-CH}(\text{NH}_2)\text{-COOH}$	polar
Methionine	$\text{CH}_3\text{-S}(\text{CH}_2)_2\text{-CH}(\text{NH}_2)\text{-COOH}$	nonpolar
Phenylalanine	$\text{Ph-CH}_2\text{-CH}(\text{NH}_2)\text{-COOH}$	nonpolar
Proline	$\text{NH}(\text{CH}_2)_3\text{-CH-COOH}$	nonpolar
Serine	$\text{HO-CH}_2\text{-CH}(\text{NH}_2)\text{-COOH}$	polar
Threonine	$\text{CH}_3\text{-CH}(\text{OH})\text{-CH}(\text{NH}_2)\text{-COOH}$	polar

Tryptophan	Ph-NH-CH=C-CH₂-CH(NH₂)-COOH	nonpolar
Tyrosine	HO-Ph-CH₂-CH(NH₂)-COOH	polar
Valine	(CH₃)₂-CH-CH(NH₂)-COOH CH(NH₂)-COOH	nonpolar

Over 100 amino acids were found in the Murchison meteorite, while only approximately 20 amino acids are common in terrestrial systems. Hence, terrestrial biological systems have already trimmed the number of amino acids from the original extraterrestrial inputs; determining the role that exogeneous organic compounds might have played in the origins of life on this planet will be challenging (PIZZARELLO, 2006). Organics were likely introduced to Earth by carbonaceous chondrites, which may have seeded the planet with prebiotic molecules (CHYBA and SAGAN, 1992; DELSEMME, 1992). Life might have been based on achiral molecules, but through evolutionary processes enzymatic processes selected generally only one enantiomer. Biochemical processes use one enantiomer (i.e., L-amino acids and D-sugars) to build proteins (polypeptides), RNA, and DNA; the enantiomers dictate the tertiary structures of biopolymers and ultimately control biopolymer function. Therefore, homochirality is considered essential to terrestrial life (CRONIN and REISSE, 2005). Meteoritic enantiomeric excesses might have provided a chiral basis capable of directing biosynthesis towards this homochirality (PIZZARELLO and CRONIN, 2000).

Enantiomeric excesses found during analyses of amino acids in carbonaceous chondrites should be initially regarded as products of terrestrial contamination, and their

extraterrestrial origin suspect until proven otherwise because non-racemic mixtures of non-terrestrial amino acids play an important role in demonstrating the extraterrestrial origin of amino acids in carbonaceous chondrites (PIZZARELLO and CRONIN, 2000). Several amino acids indigenous to the Murchison meteorite have been carefully selected to investigate this phenomenon. The amino acid, 2-amino-2,3-dimethylpentanoic acid (2-a-2,3-dmpa), has two chiral centers and, consequently, four stereoisomers and has not been found in terrestrial samples. Thus, aqueous processing on the original meteoritic body probably did not alter the configuration of the enantiomeric ratios (i.e., the meteorite has not been affected by terrestrial contamination) (CRONIN and PIZZARELLO, 1997). Sarcosine (N-methyl glycine), N-methyl alanine, α -methylnorvaline, isovaline, α -amino-n-butyric acid, and norvaline have also been found in Murchison extracts and are negligible in the terrestrial biosphere (BADA, 1991). Enantiomeric excesses favoring the L-enantiomer observed in these amino acids; most excesses are considered to be statistically significant (CRONIN and PIZZARELLO, 1997). Extraterrestrial amino acids differ from the terrestrial amino acids shown in Table 3. Terrestrial biological amino acids are all α -H amino acids, while extraterrestrial amino acids include α -methyl ($-\text{CH}_3$) amino acids. The α -H amino acids and sugars easily racemize in water, making the task of determining and interpreting enantiomeric enrichments in meteorites difficult (BADA and MILLER, 1987). However, the amino acid, isovaline, which is not found in terrestrial organisms, is stereochemically stable because it lacks the α -H, thus preventing interconversion between chiral configurations. Meteoritic bombardment early in Earth's history could have provided an extended supply of isovaline, which has an enantiomeric

enrichment in meteorites of up to 15% that could have influenced chirality in prebiotic sugar synthesis (PIZZARELLO and WEBER, 2004).

The amino acid enantiomeric enrichment data from the Murchison, Murray, and Tagish Lake meteorites suggest that the α -methyl ($-\text{CH}_3$) amino acids may be associated with a distinct meteoritic phase because their concentrations vary systematically relative to the α -H amino acids (BADA and MILLER, 1987). Deuterium (D) enrichments in the amino acids suggest that they might be related to interstellar molecules (EPSTEIN et al., 1987). These α -methyl amino acids coexist with and structurally correspond to a suite of α -hydroxy acids, which could be explained if both were formed by a Strecker-type synthesis (PELTZER and BADA, 1978). Since the carbonaceous chondrites have experienced some degree of aqueous processing, Cronin et al. (CRONIN and PIZZARELLO, 1997) suggested a two-step formation process. The first step is incorporation of precursors to the amino acids, such as the aldehydes, ketones, HCN, and ammonia formed in the molecular cloud, into the meteoritic body; these compounds are often enriched in deuterium, which then provides an isotopic signature for the α -methyl amino acid. Subsequently, a Strecker-type synthesis involving the incorporated components might occur in the meteoritic body, forming amino acids. In 1974, asymmetric organic compounds appeared to have been produced in recurrent photolytic processes by ultraviolet circularly polarized light (UV CPL) (BALAVOIN et al., 1974); these experiments mimicked recurrent exposure during interstellar cloud collapse (CRONIN and REISSE, 2005), which might lead to give large enantiomeric excesses. In UV CPL theory, losses of low-anisotropy organic compounds, such as the amino acids, and higher-anisotropy organic compounds are predicted, which could then act as catalysts for the

secondary propagation of optical activity (PIZZARELLO et al., 2003). However, the range of variability for isovaline (upper limit of L-ee = 15.2%) extends well beyond the theoretical boundaries set for amino acid decomposition by UV CPL and would seem to refute the suggestion that UV CPL was the sole causation of the asymmetry observed in certain meteoritic amino acids (PIZZARELLO et al., 2003).

Many authors invoke the Strecker-type synthesis as the primary formation mechanism for amino acids in carbonaceous chondrites (PIZZARELLO, 2006). The Strecker-type synthesis of amino acids from aldehydes and ketones was proposed in the 1850's by Adolph Strecker (RIANT and HANNEDOUCHE, 2007); an aldehyde condenses with ammonium in the presence of cyanide to form the intermediate compound, α -aminonitrile. The nitrile group is hydrolyzed and replaced by the carboxylic acid to form an amino acid. However, the Strecker-type synthesis does not explain enantiomeric excesses observed in carbonaceous chondrites. Bonner and Rubenstein (MEIERHENRICH et al., 1999) propose that amino acids formed entirely in the interstellar medium. If true, then the two-stage interstellar-parent body hypothesis (aldehyde and ketone formation followed by the amino acids by Strecker-type synthesis) is not applicable to the non-racemic amino acids. If all of the meteorite amino acids were formed in the interstellar medium, then enantiomeric excesses might be expected in a broader range of organic compounds in comets than in carbonaceous chondrites; comets, discussed below, probably have not experienced aqueous processing, with the attendant possibility of racemization, to the same extent as may have occurred in carbonaceous chondrites (CRONIN and PIZZARELLO, 1997).

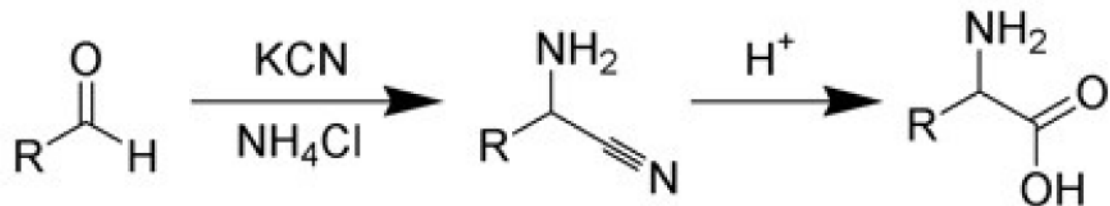


Figure 1.4 Chemical reaction for the formation of amino acids in the Strecker synthesis.

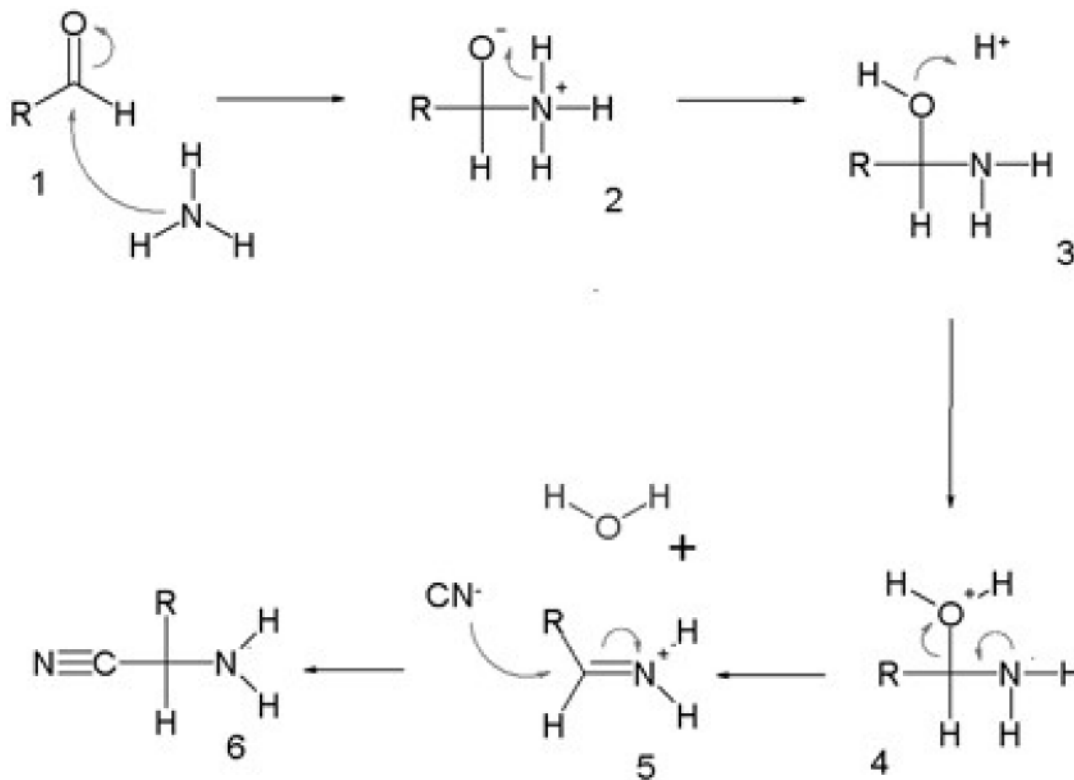


Figure 1.5 Step 1 in the mechanism of the Strecker synthesis illustrating the formation of the α -aminonitrile intermediate.

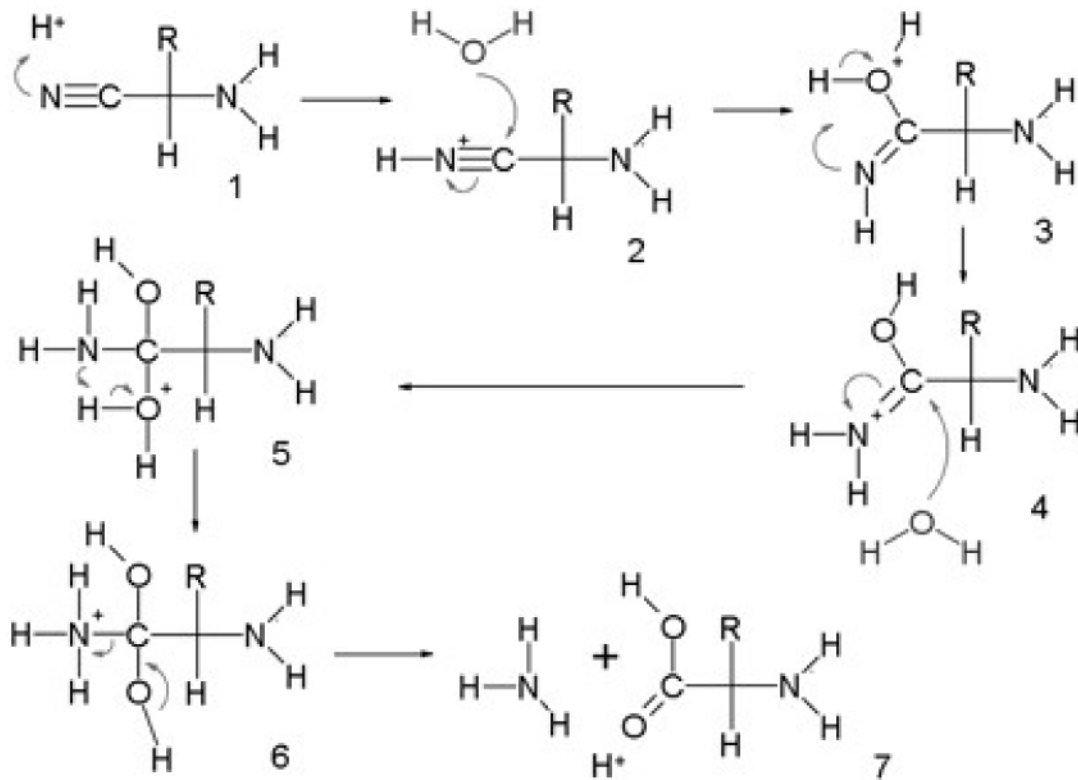


Figure 1.6 Step 2 of the Strecker synthesis showing the mechanism of formation from the α -aminonitrile to the formation of the amino acid and the ammonia by product.

1.5 JAROSITE CHEMISTRY AND CRYSTALLOGRAPHY

As stated briefly in the general introduction, the jarosite group minerals belong to the alunite supergroup, which contains over 40 minerals. The supergroup is subdivided based on the trivalent metal cation present in tetrahedral coordination that forms the backbone of the mineral (JAMBOR, 1999). In the jarosite group, the dominant transition metal cation that occupies this site is Fe^{3+} . The jarosite group minerals have the general formula $XFe_3(SO_4)_2(OH)_6$, where X is a monovalent cation, the identity of which depends on chemistry of the depositional environment. The most common cations to fill this position are the monovalent K^+ , Na^+ , Ag^+ , NH_4^+ , and H_3O^+ ions. Other ions to fill this position include both divalent and trivalent ions such as Ca^{2+} , Sr^{2+} , Ba^{2+} , Pb^{2+} , REE

(typically trivalent), and Bi^{3+} . (STOFFREGEN et al., 2000). Figure 1.7 shows the general jarosite structure with the X sites highlighted indicating the sites where the most variability occurs in the structure.

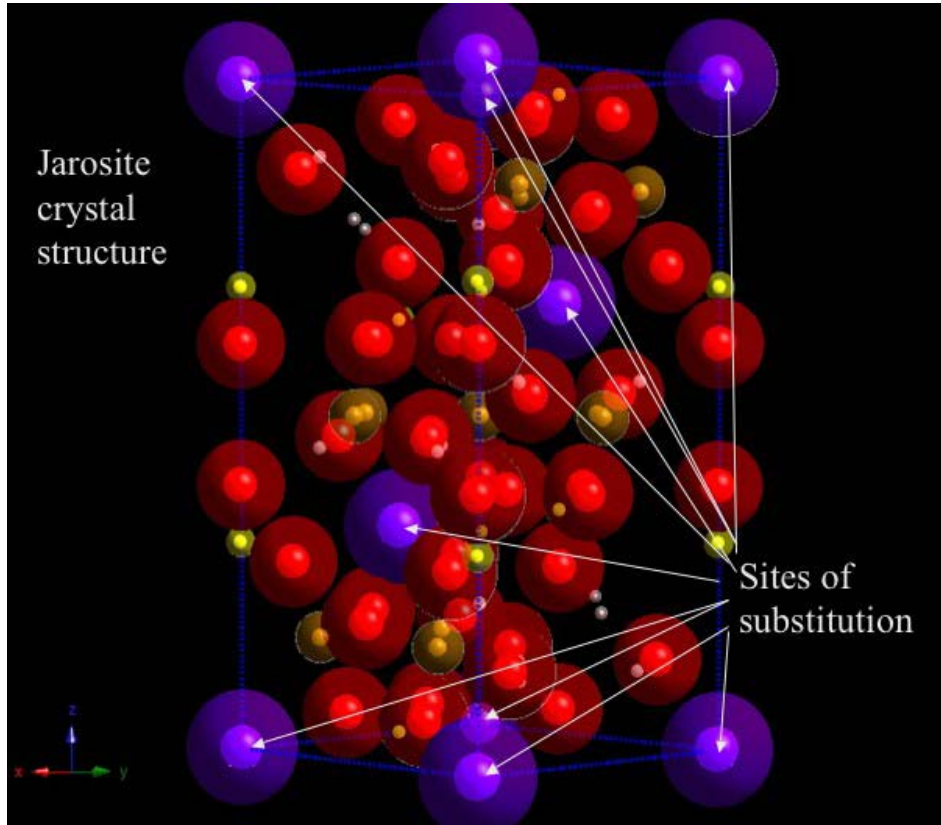


Figure 1.7 Modeled jarosite structure showing sites of probable substitution. Atom colors represent: Purple = potassium, red = oxygen, yellow = sulfur, brown = iron, and white = hydrogen.

Rarely, true end members within the group are found in nature. Most researchers attribute this to the presence of hydronium ions within the primary cation site (X site) that leads to non-stoichiometry (STOFFREGEN et al., 2000). Deficiencies are also observed for Fe^{3+} leading to incomplete occupation of this site in the crystal lattice. Extensive work has been done with synthetic varieties of jarosite and recent report show that full occupancy of the iron site can be obtained in the laboratory (BASCIANO and PETERSON,

2008). Although infrequently mentioned in the geologic literature, the arrangement of the iron atoms within the crystal lattice has generated numerous reports within the mineral physics and chemical physics community because the atoms are arranged in what is called a kagome lattice (BARTLETT and NOCERA, 2005; BISSON and WILLS, 2007; BISSON and WILLS, 2008; BONVILLE et al., 2006; COOMER et al., 2006; FAK et al., 2008; INAMI et al., 2001; MAEGAWA et al., 2007; NISHIYAMA et al., 2003; NOCERA et al., 2004; TOWNSEND et al., 1986; YILDIRIM and HARRIS, 2006). This generates what is termed “a classic kagome lattice antiferromagnet” (TOWNSEND et al., 1986).

The triangular arrangement of the iron atoms that forms the kagome lattice is shown in figure 1.8. What separates a typical triangular antiferromagnet from a kagome lattice, is that in the kagome lattice the triangles only share vertices, not sides. Interesting properties result from this arrangement, including suppression to total lack of magnetic ordering, successive phase transitions, unconventional spin structures and large fluctuations in behavior at low temperatures (NISHIYAMA et al., 2003). The kagome lattice antiferromagnet has classical Heisenberg spins, with a large number of degenerate ground states causing long-range-order not to occur at any temperatures, instead, novel ground states are predicted as temperatures go to 0 K (INAMI et al., 2001). One of the interesting properties of geometrically frustrated antiferromagnets is the ability to undergo a spin glass transition. In particular for jarosite, it is the ability of the ground states to be frozen into a random pattern, similar by analogy to the random arrangement of silica in glass (GREEDAN, 2001). A specific temperature at which this transition occurs characterizes the spin transition, and the jarosite group minerals show a fairly wide distribution of these temperatures depending on the primary cation identity (X site) and

the amount of iron deficiency in the lattice (HARRISON et al., 2000; WILLIS and HARRISON, 1996; WILLIS et al., 2000). A practical up side to the antiferromagnet behavior of the jarosite minerals, is that this property has allowed authors to conduct nuclear magnetic resonance (NMR) studies on the mineral group, which would not normally be possible with iron containing materials (MAEGAWA et al., 2007; NIELSEN et al., 2008).

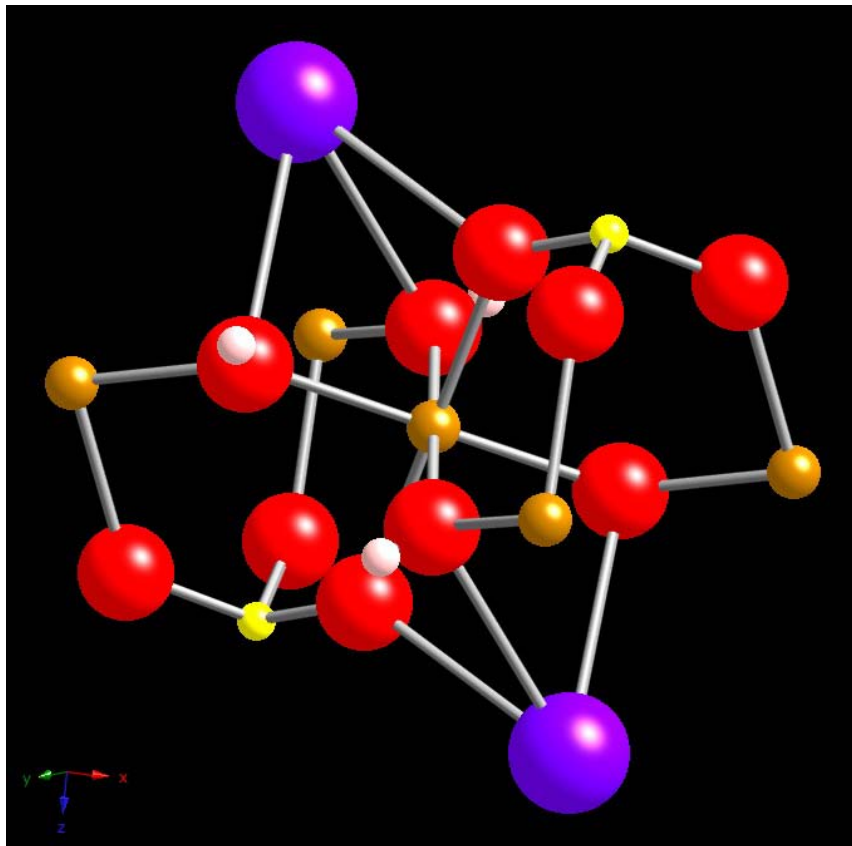


Figure 1.8 Modeled jarosite structure showing triangular arrangement of iron atoms (brown) that form the kagome lattice. Atom colors represent: Purple = potassium, red = oxygen, yellow = sulfur, brown = iron, and white = hydrogen.

Intimately related to the iron deficiencies in the lattice and other crystal site vacancies, is variability in space group designations for the jarosite mineral group. The idealized symmetry for jarosite is trigonal, with space group R-3m and $Z = 3$. It has been

suggested that these values should be assumed for jarosite unless structural can confirm otherwise (STOFFREGEN et al., 2000). The R-3m space group has a $Z = 3$ meaning that the formula unit ($XFe_3(SO_4)_2(OH)_6$) is repeated three times within the unit cell with no stoichiometric deficiencies. Some authors assert that since nonstoichiometry is more the rule than the exception, the space group R3m might be a more appropriate approximation for the space group (SZYMANSKI, 1988; TOWNSEND et al., 1986). 1. 9 shows the modeled jarosite structure with trigonal symmetry and space group R-3m. The unit cell contains 81 atoms and 36 symmetry operations. 1. 10 show the modeled jarosite structure with trigonal symmetry and space group R3m. This unit cell contains 45 ions and 18 symmetry operations. The crystallographic rationalization for the reduction in symmetry between the two structures is that ordering is reduced due to distortion effects in the X site (STOFFREGEN et al., 2000).

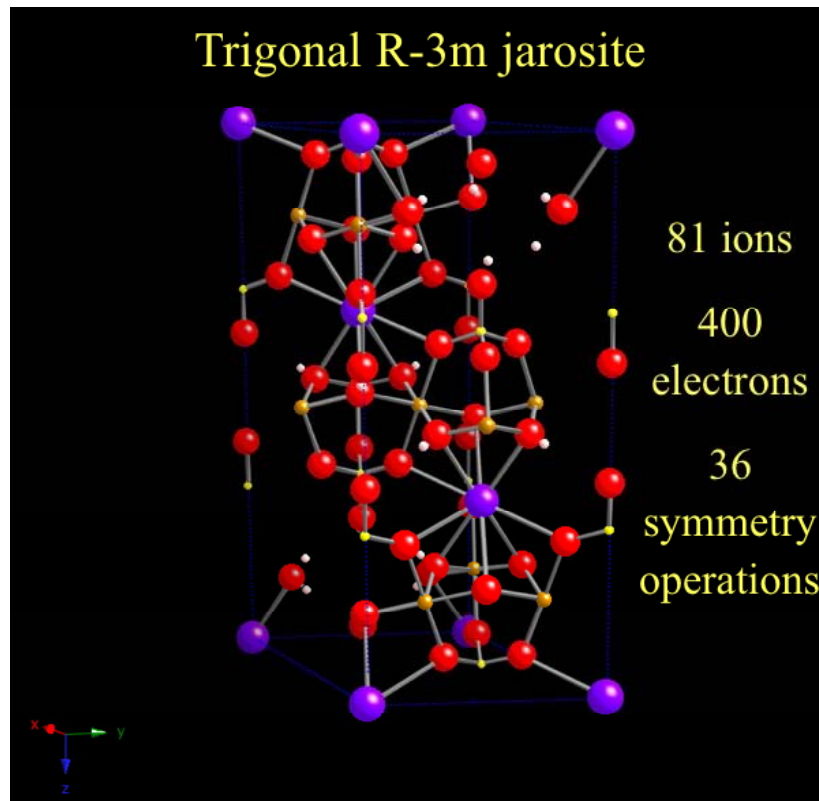


Figure 1.9 Modeled jarosite structure with trigonal symmetry and space group R-3m. This structure contains 81 atoms, 400 electrons and has 36 symmetry operations. Atom colors represent: Purple = potassium, red = oxygen, yellow = sulfur, brown = iron, and white = hydrogen.

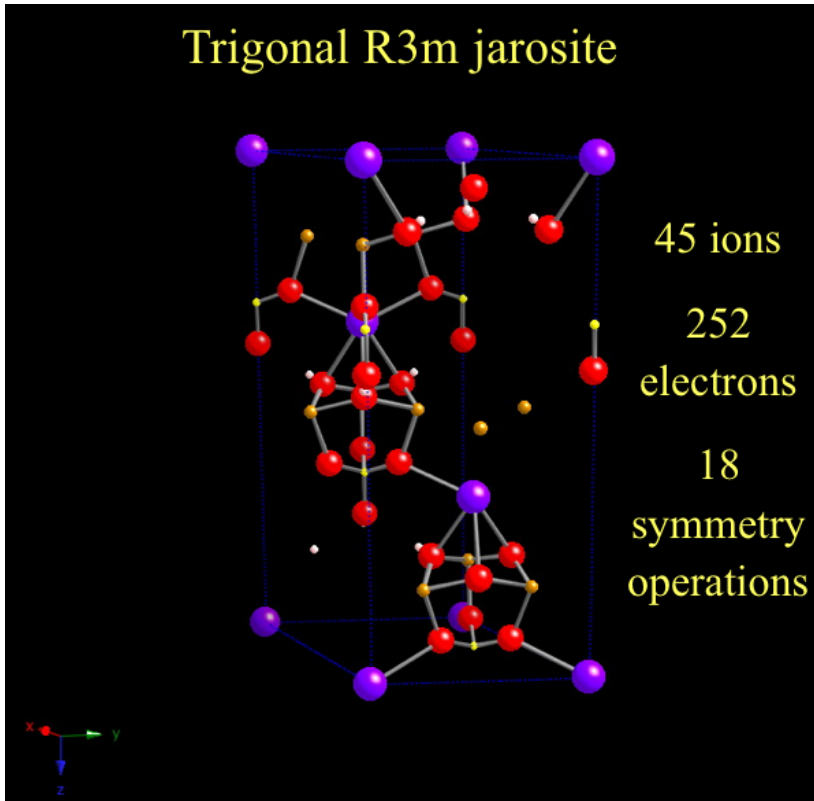


Figure 1.10 Modeled jarosite structure with trigonal symmetry and space group R3m. This structure contains 45 atoms, 252 electrons and has 18 symmetry operations. Atom colors represent: Purple = potassium, red = oxygen, yellow = sulfur, brown = iron, and white = hydrogen.

The X site distortions and symmetry issues introduces the problem of where the hydronium ion is within the unit cell. The first reported crystal structure for jarosite (HENDRICKS, 1937) indicated that the hydronium ion did not occupy the axial position that is referred to as the X site as all subsequent reports have indicated. The coordinates for the X site are generally as $x = 0$, $y = 0$, and $z = 0$. Hendricks (1937) reported the coordinates as $x = 0.150$, $y = -0.150$, and $z = 0.126$ indicating that the hydronium ion is

shifted inwards from the axial positions. It should be noted that workers do not evaluate the positions of the individual atoms in the hydronium ion. For example, coordinates are not given for each of the 3 hydrogen atoms, just the overall ion (H_3O). This is surprising given the numerous number of structures published on the jarosite group minerals (BARTLETT and NOCERA, 2005; BOND and JONES, 2002; HARRIS and TREMAYNE, 1996; HENDRICKS, 1937; JOHNSTON et al., 2002; SOLOVYOV et al., 2005; SZYMANSKI, 1988) including deuterated synthetic samples analyzed by neutron diffraction that would in theory be capable of discerning the positions. Overall, the jarosite minerals exhibit complex magnetic and structural behaviors making them a continuing target for mineralogical investigations by both the geologic community and the chemical physics community.

1.6 OVERVIEW OF TECHNIQUES

Within this section is a discussion of techniques that may be less commonly used in the geosciences, but were used at length in the dissertation. The first section is an overview of the technique termed Geomatrix-Assisted Laser Desorption/Ionization that was developed as way to identify organic materials in geologic samples (YAN et al., 2007a; YAN et al., 2007b). The second section discusses powder diffraction structure solution methods. Although the techniques of Rietveld refinement (RIETVELD, 1969) have been used by geoscientists for decades, the advent of sophisticated computer algorithms and new software designs have contributed greatly to the technique. Included in this discussion is also the use of the techniques applied to organic materials.

1.6.2 DETECTION OF BIOSIGNATURES BY GEOMATRIX-ASSISTED LASER DESORPTION/IONIZATION (GALDI) MASS SPECTROMETRY

Direct identification of biomolecules in association with minerals is vital for exploring the spatial relationships between biomolecules and minerals in natural environments (LOWER et al., 2001a; LOWER et al., 2001b); retrieving biomolecular information from fossils on Earth (SCHWEITZER et al., 2005); detecting trace amounts of organic compounds in meteorites (GLAVIN et al., 1999; MCKAY et al., 1996); and identifying biosignatures on Mars and other planets (BADA and McDONALD, 1996). By applying imaging laser-desorption Fourier transform mass spectrometry (LD-FTMS) to detect biosignatures in sedimentary materials, examine the interaction of microorganisms with minerals, and chemically image the mineral and organic phases within meteorite samples, a new technique has been developed. Critical to these efforts is the ability to detect and identify molecules that range in size from low molecular weight compounds, such as amino acids to high molecular weight biomolecules (e.g., proteins, lipopolysaccharides, and peptidoglycans) that are derived from microbial biomass.

Direct detection of biomolecules by mass spectrometry (MS) from solids has become an active field of research since its combination with a variety of soft ionization techniques that allow direct analysis of polar biomolecules. Currently used soft ionization techniques for solids include particle bombardment, laser desorption/ionization (LDI), and matrix-assisted laser desorption/ionization (MALDI). Among those techniques, LDI has not been widely used because of the fragmentation and difficulty of vaporizing polar compounds under UV laser radiation (STUMP et al., 2002). Since its introduction in 1988 (KARAS and HILLENKAMP, 1988; TANAKA et al., 1988), MALDI has become the dominant laser desorption technique because it overcame the limitations of LDI by

utilizing photoreactive matrix molecules to transfer large and/or nonvolatile biomolecules (e.g., protein, DNA, and RNA) into the gas-phase as intact ions (Stults, 1995; Stump *et al.*, 2002). In MALDI sample preparation, the analyte and an excessive amount of matrix is dissolved in an organic solvent and then deposited and dried onto a sample holder (Yao *et al.*, 1998). The excess amount of matrix molecules is thought to isolate analyte molecules from each other, protect the analyte molecules from the damaging laser radiation, and assist in the ionization of the analyte, usually by acting as a protonation or deprotonation agent (STULTS, 1995).

MALDI, however, is not suitable for in-situ analysis of biomolecular constituents in some natural samples where biomolecules are strongly associated with minerals. For example, Bada *et al.* (1998) found that the amino acids in a Martian meteorite (ALH 84001) were strongly associated with the carbonate mineral globules as bound acids. The MALDI solvents cannot effectively extract Biomolecules strongly associated with insoluble minerals, thereby leading to inefficiencies in co-crystallization and subsequent desorption/ionization of the analytes. In addition, the use of liquid solvents in outer space would be impractical. Consequently, laser desorption and ionization of mineral-associated biomolecules may have to rely on the minerals themselves. Successful usage of some inorganic matrices that are compositionally similar to natural minerals encourages our application of minerals as geomatrices. Zhang *et al.* (2001) used porous silicon powder and silica gel as matrices for the analysis of small biomolecules (< 2,000 Da). Other researchers have reported the use of other types of solid inorganic materials such as metal oxide powders or graphite as matrices to detect proteins, peptides, or low molecular weight biomolecules (KINUMI *et al.*, 2000; LAI *et al.*, 1998; YALCIN *et al.*,

2002; ZHANG et al., 2001). Accordingly, we initiated this study to explore whether or not minerals can play the role of matrix to assist desorption and ionization of associated biomolecules; hence, the naissance of the phase geomatrix-assisted laser desorption/ionization (GALDI).

1.6.3 POWDER DIFFRACTION STRUCTURE SOLUTION METHODS

Methods to solve crystal structures from powder diffraction patterns have evolved significantly with the advance of powerful computer algorithms. Presented herein are several examples of these algorithms with specific examples. Included also is a brief history of the development of these methods.

Single crystal diffraction data have been used successfully since the 1950's (ROBERTSON, 1953) to determine structure solutions of molecules in the solid state. It is inherently difficult to grow single crystals, and therefore the ability to determine crystal structures from powder X-ray diffraction (PXRD) data of microcrystalline materials has been greatly desired in the structural sciences. Single crystal diffraction data and PXRD data contain the same intrinsic information. However, in single crystal diffraction data the information is distributed in 3-dimensional space, and PXRD data is compressed into 1-dimensional space (REYNOLDS, 1989). This 1-d compression in PXRD data leads to peak overlap in the diffraction pattern. Overlap can obscure information on the intensities of individual peak maxima, information that is necessary to solve structure solutions in molecular solids. This problem is especially evident in solids with large unit cells and low symmetry where peak overlap is particularly severe (HARRIS, 2003).

The stages for crystal structure determination from diffraction data are similar for both single crystal and PXRD data and are as follows: (i) unit cell determination and space group designation, (ii) structure solution, and (iii) structure refinement (ZHIGANG et al, 2005). The structure solution stage (ii) has been most problematic when solving molecular structures from PXRD data. Since the early 1990's, advances have been made using the "direct-space strategy" to obtain structure solutions from PXRD data (CHEETHAM and WILKINSON, 1992; HARRIS and TREMAYNE, 1996; HARRIS et al., 2001; LANGFORD and LOUER, 1996).

Direct-space strategies involve the use of sophisticated software programs that generate "trial" structures that are then compared to the experimental diffraction patterns and assigned a quantitative weighted powder R-factor (R_{wp}) value (HARRIS, 2003). This is the same R-factor that is employed in Rietveld refinement (RIETVELD, 1969) and takes into account the entire digitized intensity profile instead of the integrated intensities of individual diffraction maxima, which allows the problem of peak overlap to be considered (HARRIS and TREMAYNE, 1996). The direct-space strategy aims to find the trial structure with the lowest R_{wp} resulting in the closest match to experimental data. This technique uses a set of variables to define the coordinates (x, y, z) of the individual atoms, the orientation of rotational angles (θ , ϕ , ψ) around a set of orthogonal axes, and the set of variable torsion angles (τ_1 , τ_2 ... τ_n) for each molecule in the asymmetric unit cell (HARRIS, 2003). These variables and the generation of trial structures have been successfully employed using the Monte Carlo/simulated annealing technique, the genetic algorithm technique (GA), and variations between the two techniques (HARRIS et al., 2001).

1.6.3.1 MONTE CARLO/SIMULATED ANNEALING ALGORITHM TECHNIQUE-

Monte Carlo techniques are in general, stochastic nondeterministic random sampling methods that are used extensively in mathematics, chemistry, and physics (ROBERT and CASELLA, 2004). In the Monte Carlo/simulated annealing technique each trial structure is generated from the previous structure by making small random displacements to the structure variables such as the atomic coordinates, rotation and torsion angles (Harris et al, 1994). Trial structures are accepted or rejected by invoking the Metropolis importance sampling algorithm (METROPOLIS et al., 1953), that uses the following rules:

$$\begin{aligned} Z &= R_{wp}(\text{trial structure 1}) - R_{wp}(\text{trial structure 2}) \\ Z \leq 0, & \text{ the trial structure is accepted} \\ Z > 0, & \text{ structure is either accepted with probability} = \exp(-Z/S) \\ & \text{Or rejected with probability} = (1 - \exp(-Z/S)) \end{aligned}$$

The parameter S is an appropriate scaling factor and may be fixed or varied during the calculations. The higher the S value, the higher the probability the structure will be accepted. The treatment of the S parameter is what differentiates the Monte Carlo technique from the Simulated Annealing technique. In the Monte Carlo technique, the S parameter can be varied or fixed. In the simulated anneal technique, S is decreased systematically according to the individual experimental design and varies dramatically in this field (HARRIS, 2003; VAN LAARHOVEN and AARTS, 1987).

The Monte Carlo technique has been successfully used to solve the structure of a melaminium polyphosphate from PXRD data with additional structural conformational support from solid-state NMR data (BRODSKI et al., 2005). Several other structures including capsaicin (Johnston et al, 2002), 3-bromophenylboronic acid and tris(4-bromophenyl)boroxine (BHUVANESH et al., 2005), and the anti-ulcer drug famotidine

(SHANKLAND et al., 2002) have been solved using a hybrid Monte Carlo/simulated annealing techniques.

1.6.2.3 GENETIC ALGORITHM (GA) TECHNIQUE-

The genetic algorithm technique is based on the principles of natural selection analogous to evolutionary processes in biology. Each of the trial structures has a “genetic code” based on its atomic coordinates, orientation angles, and torsion angles within the unit cell (ZHIGANG et al, 2005). In the GA technique, a population of trial structures is allowed to evolve according to rules and operations such as mating, mutation, and natural selection (HARRIS et al., 1998). Trial structures mate by distributing parts of their genetic codes to offspring structures. Mutant structures are created by random mutation operations that alter the genetic codes of the offspring. The offspring structures are subjected to natural selection where only the structures with the highest “fitness” (lowest R_{wp}) are permitted to pass to the next generation. Once a sufficient population of structures has been produced, the one with the lowest R_{wp} is selected for structure refinement (HARRIS, 2003).

Impressive examples of the GA method’s successful application to structure solution include: the previously solved structures of the α and β phases of L-Glutamic Acid, the previously unsolved structures of several oligopeptides (Harris, 2003), and the monohydrate structure of 3,5-bis((3,4,5-trimethoxybenzyl)oxy)benzyl alcohol (ZHIGANG, 2005).

1.6.2.4 DISCUSSION-

Although the direct-space strategies Monte Carlo/Simulated Annealing and GA were developed around the same time, more structures have been solved using the Monte Carlo/Simulated Annealing techniques, and the majority of the published literature reviewed showed a bias toward using the Monte Carlo/Simulated annealing techniques. This may be due in part to the ubiquity of Monte Carlo algorithms in various modeling programs that can be altered to run variations of the technique.

Other algorithms mentioned in the literature involved variations on the direct-space strategy that used quantum-chemical density-functional theory algorithms such as CASTEP and DMol to perform geometry optimizations on limited numbers of trial structures (SOLOVYOV et al., 2005). These algorithms are not specifically designed to provide structure solutions for powder X-ray diffraction data, but they can be used when potential structures can be inferred. This fundamentally differs from the direct-space strategy that assumes no previously determined atomic coordinates and begins the search for trial structures *ab initio* (HARRIS, 2003).

The primary points to consider when solving crystal structures from PXRD data are to assess whether the final structure gives an acceptable fit to the experimental PXRD pattern, and to assess whether the final refined structure is structurally and chemically sensible. It is therefore of great importance to obtain difference spectra between the proposed structure generated powder X-ray diffraction pattern and the experimental pattern (ZHIGANG et al., 2005). This final procedure insures the quality of the obtained structure solution.

The major limitations of the procedures discussed are the costs of obtaining the algorithm codes and the costs associated with obtaining multi-processor workstations

with technical support staff to maintain them. Other limitations associated with using these algorithms are that many structure solutions need to be verified or corroborated by other more validated methods such as solid-state NMR (Brodski et al., 2005; Harper et al, 2006).

1.6.2.5 STEP-BY-STEP EXAMPLE

Harris et al. (2003) demonstrated the GA structure solution method in the polymorphic system of the α and β phases of L-glutamic acid. Both phases exist in the zwitterions form shown in Figure 1.11. Powder diffraction patterns were recorded on a Siemens D5000 diffractometer using Ge-monochromated $\text{CuK}_{\alpha 1}$ radiation and a linear position-sensitive detector covering 8° in 2θ . The space group and unit cell dimensions for the two polymorphs were determined from the data and indicated that both molecules were $P2_12_12_1$. The unit cell dimensions were determined to be $a=10.28$ angstroms, $b=8.78$ angstroms, and $c=7.07$ angstroms for the α phase. The unit cell dimensions for the β phase were $a=5.16$ angstroms, $b=17.30$ angstroms, and $c=6.95$ angstroms.

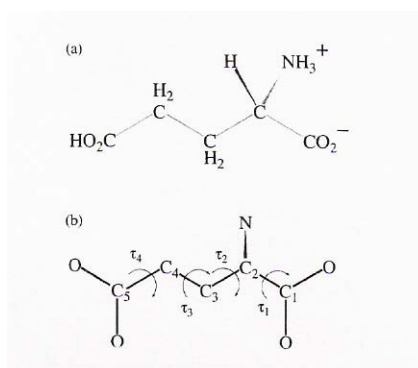


Figure 1.11 Zwitterion form of l-glutamic acid (a) and the structural fragment used in the GA structure solution calculations showing the variable torsion angles (b). Taken from Harris et al. (2003).

For the GA structure solution calculations the structural fragment consisted of all non-hydrogen atoms. Standard molecular geometry (bond lengths and angles) was assumed with all C-O bonds taken to be equal. The torsion angles were defined using the molecular conformation seen in 1.11b. The space group, unit cell parameters, diffraction patterns, standard molecular geometry assumptions and torsion angles were inputted to the program EAGER for the GA analysis. The progress of the GA calculation is assessed from the evolutionary progress plot seen in figure 1.12. The best (R_{\min}) and average (R_{ave}) of the R_{wp} for the population as a function of generation number.

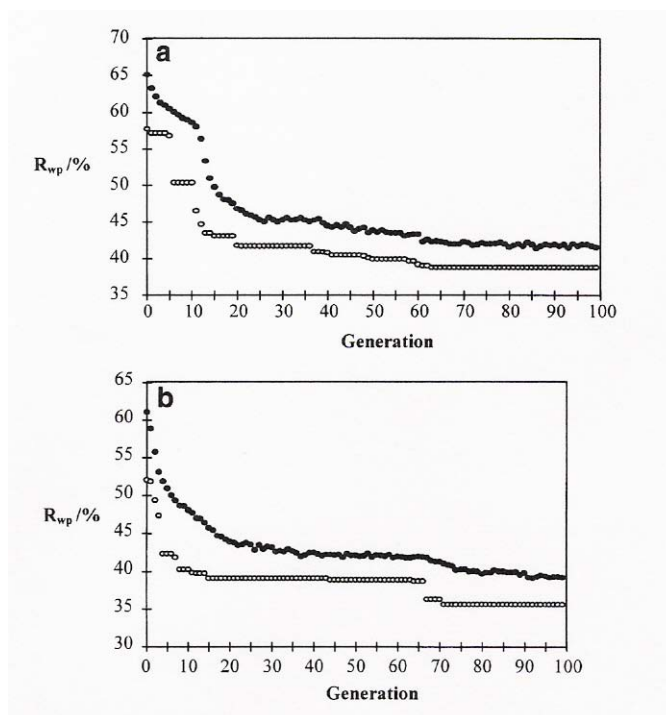


Figure 1.12 Evolutionary progress plots showing the R_{ave} (filled circles) and R_{\min} (open circles) as a function of generation number for the α l-glutamic acid phases (a) and β l-glutamic acid phase (b). Taken from Harris et al. (2003).

The best structure solutions for both phases are shown in figure 1.13. They are overlapped with the previously single crystal structure solutions to show how well the

GA calculation technique agrees with single crystal diffraction solutions for both the α and β phases of l-glutamic acid. The maximum divergence between the single crystal structure and the GA solved structure was 0.5 angstroms. After Rietveld refinement the structures are in exact agreement.

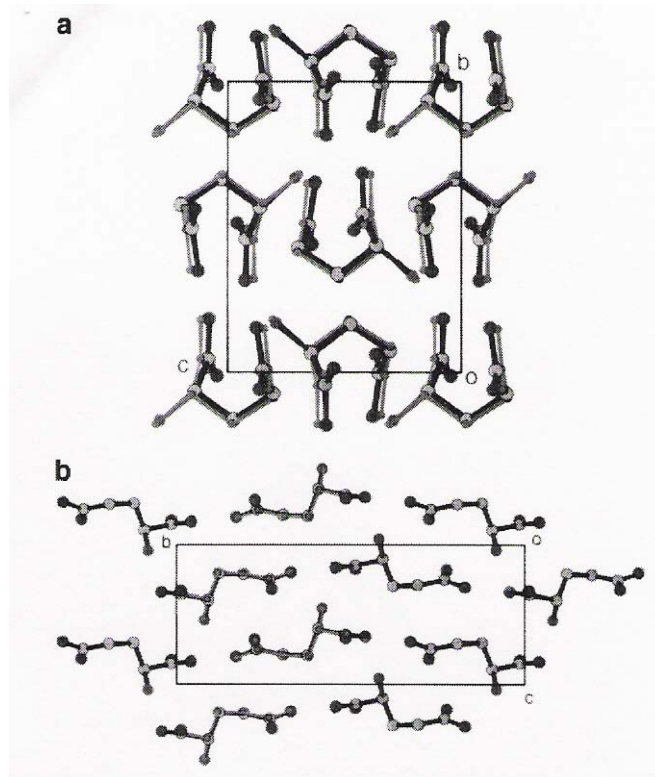


Figure 1.13 Comparison between the position of the structural fragment in the best structure solution obtained by the GA calculations for both the α (a) and β (b) phases of l-glutamic acid before Rietveld refinement. Light shading indicates the GA calculated structure and dark shading is the previously defined positions from single crystal diffraction solution.

1.7 REFERENCES

Akai, J., Akai, K., Ito, M., Nakano, S., Maki, Y., and Sasagawa, I., 1999. Biologically induced iron ore at Gunma iron mine, Japan. *American Mineralogist* **84**, 171-182.

- Alpers, C. N. and Rye, R. O., 1992. Chemical, Crystallographic and Stable Isotope Properties of Alunite and Jarosite from Acid Hypersaline Australian Lakes. *Chemical Geology* **96**, 203-226.
- Alt, J. C., Honnorez, J., Laverne, C., and Emmerman, R., 1986. Hydrothermal alteration of a 1 km section through the upper oceanic crust, deep sea drilling project hole 504B: mineralogy, chemistry, and evolution of seawater-basalt interactions. *Journal of Geophysical Research* **91**, 10309-10336.
- Armstrong, D. C., 1995. Acid Sulfate Alteration in a Magmatic Hydrothermal Environment, Barton Peninsula, King George Island, Antarctica. *Mineralogical Magazine* **59**, 429-441.
- Bada, J. L., 1991. Amino-Acid Cosmogeochimistry. *Philosophical Transactions Of The Royal Society Of London Series B-Biological Sciences* **333**, 349-358.
- Bada, J. L., Glavin, D. P., McDonald, G. D., and Becker, L., 1998. A search for endogenous amino acids in Martian meteorite ALH84001. *Science* **279**, 362-365.
- Bada, J. L. and McDonald, G. D., 1996. Detecting amino acids on Mars. *Analytical Chemistry* **68**, A668-A673.
- Bada, J. L. and Miller, S. L., 1987. Racemization And The Origin Of Optically-Active Organic-Compounds In Living Organisms. *Biosystems* **20**, 21-26.
- Baird, A. K. and Clark, B. C., 1979. Volatiles in the Martian Regolith. *Geophysical Research Letters* **6**, 811-814.
- Baird, A. K. and Clark, B. C., 1984. Did Komatiitic lavas erode channels on Mars? *Nature* **311**.
- Balavoin, G., Moradpou, A., and Kagan, H. B., 1974. Preparation Of Chiral Compounds With High Optical Purity By Irradiation With Circularly Polarized-Light, A Model Reaction For Prebiotic Generation Of Optical-Activity. *Journal Of The American Chemical Society* **96**, 5152-5158.
- Bartlett, B. M. and Nocera, D. G., 2005. Long-range magnetic ordering in iron jarosites prepared by redox-based hydrothermal methods. *Journal Of The American Chemical Society* **127**, 8985-8993.
- Basciano, L. C. and Peterson, R. C., 2008. Crystal chemistry of the natrojarosite-jarosite and natrojarosite-hydronium jarosite solid-solution series: A synthetic study with full Fe site occupancy. *American Mineralogist* **93**, 853-862.
- Becker, L., Popp, B., Rust, T., and Bada, J. L., 1999a. The origin of organic matter in the Martian meteorite ALH84001. *Earth and Planetary Science Letters* **167**, 71-79.
- Becker, L., Popp, B., Rust, T., and Bada, J. L., 1999b. The origin of organic matter in the Martian meteorite ALH84001, *Life Sciences: New Insights Into Complex Organics In Space*. Pergamon Press Ltd, Oxford.
- Becker, U. and Gasharova, B., 2001. AFM observations and simulations of jarosite growth at the molecular scale: probing the basis for the incorporation of foreign ions into jarosite as a storage mineral. *Physics and Chemistry of Minerals* **28**, 545-556.
- Benner, S. A., Devine, K. G., Matveeva, L. N., and Powell, D. H., 2000. The missing organic molecules on Mars. *Proceedings of the National Academy of Sciences of the United States of America* **97**, 2425-2430.
- Bhattacharya, S. K., Savarino, J., and Theimans, M. H., 2000. A new class of oxygen isotopic fractionation in photodissociation of carbon dioxide: potential

- implications atmospheres of Earth and Mars. *Geophysical Research Letters* **27**, 1459-1462.
- Bhuvanesh, N. S. P., Reibenspies, J. H., Zhang, Y., and Lee, P. L., 2005. A novel strategy for ab initio structure determination using micro-powder X-ray diffraction: structure solution and refinement of 3-bromophenylboronic acid and tris(4-bromophenyl) boroxine *Journal of Applied Crystallography* **38**, 632-638.
- Biemann, K., 1977. Composition of Lower Atmosphere and Search for Organic-Compounds in Surface of Mars. *Abstracts of Papers of the American Chemical Society* **173**, 57-57.
- Bisson, W. and Wills, A. S., 2007. Intermediate phase in the oxidative hydrothermal synthesis of potassium jarosite, a model kagome antiferromagnet. *Zeitschrift Fur Kristallographie*, 511-516.
- Bisson, W. G. and Wills, A. S., 2008. Anisotropy-driven spin glass transition in the kagome antiferromagnet hydronium jarosite, $(\text{H}_3\text{O})\text{Fe}_3(\text{SO}_4)_2(\text{OH})_6$.
- Bogard, D. D., Clayton, R. N., Marti, K., Owen, T., and Turner, G., 2001. Martian Volatiles: Isotopic Composition, Origin, and Evolution. *Chronology and Evolution of Mars* **96**, 425-458.
- Bond, A. D. and Jones, W., 2002. Structure prediction as a tool for solution of the crystal structures of metallo-organic complexes using powder X-ray diffraction data. *Acta Crystallography* **B58**, 233-243.
- Bonville, P., Dupuis, V., Vincent, E., Lippens, P. E., and Wills, A. S., 2006. Fe-57 Mossbauer spectra and magnetic data from the kagome antiferromagnet H_3O -jarosite. *Hyperfine Interactions* **168**, 1085-1089.
- Bridge, T. A. M. and Johnson, D. B., 2000. Reductive dissolution of ferric iron minerals by *Acidiphilium* SJH. *Geomicrobiology Journal* **17**, 193-206.
- Brodski, V., Peshar, R., Schenk, H., Brinkmann, A., Bloemberg, T. G., Van Eck, E. R. H., Kentgens, A. P. M., and Arno, P. M., 2005. Structural analysis of a melaminium polyphosphate from X-ray powder diffraction and solid-state NMR data *Journal of Physical Chemistry B* **109**, 13529-13537.
- Burns, R. G., 1987a. Ferric Sulfates on Mars. *Journal of Geophysical Research-Solid Earth and Planets* **92**, E570-E574.
- Burns, R. G., 1987b. Gossans on Mars: spectral features attributed to jarosite *Lunar and Planetary Science XVIII*.
- Burns, R. G., 1989. Terrestrial analogues of the surface rocks of Mars? *Nature* **320**.
- Burns, R. G., 1990. Iron-sulfur mineralogy of Mars: magmatic evolution and chemical weathering products. *Journal of Geophysical Research* **95**, 14415-14421.
- Carr, M. H. and Wanke, H., 1992. Earth and Mars: water inventories as clues to accretional histories. *Icarus* **98**, 775-784.
- Carroll, M. R. and Rutherford, M. J., 1985. Sulfide and sulfate saturation in hydrous silicate melts. *Journal of Geophysical Research* **90**, C601-C612.
- Carroll, M. R. and Rutherford, M. J., 1988. Sulfur speciation in hydrous experimental glasses of varying oxidation states: Results from measured wavelength shifts of sulfur X-rays. *American Mineralogist* **73**, 845-849.
- Cheetham, A. K. and Wilkinson, A. P., 1992. SYNCHROTRON X-RAY AND NEUTRON-DIFFRACTION STUDIES IN SOLID-STATE CHEMISTRY *Angew. Int. Chem. Int. Ed. Engl.* **31**, 1557.

- Christensen, P. R., Wyatt, M. B., Glotch, T. D., Rogers, A. D., Anwar, S., Arvidson, R. E., Bandfield, J. L., Blaney, D. L., Budney, C., Calvin, W. M., Faracaro, A., Ferguson, R. L., Gorelick, N., Graff, T. G., Hamilton, V. E., Hayes, A. G., Johnson, J. R., Knudson, A. T., McSween, H. Y., Mehall, G. L., Mehall, L. K., Moersch, J. E., Morris, R. V., Smith, M. D., Squyres, S. W., Ruff, S. W., and Wolff, M. J., 2004. Mineralogy at Meridiani Planum from the Mini-TES experiment on the Opportunity Rover. *Science* **306**, 1733-1739.
- Chyba, C. and Sagan, C., 1992. Endogenous Production, Exogenous Delivery And Impact-Shock Synthesis Of Organic-Molecules - An Inventory For The Origins Of Life. *Nature* **355**, 125-132.
- Clark, B. C. and Baird, A. K., 1979. Is the Martian lithosphere sulfur rich? *Journal of Geophysical Research* **84**, 8395-8403.
- Clark, B. C., Morris, R. V., McLennan, S. M., Gellert, R., Jolliff, B., Knoll, A. H., Squyres, S. W., Lowenstein, T. K., Ming, D. W., Tosca, N. J., Yen, A., Christensen, P. R., Gorevan, S., Bruckner, J., Calvin, W., Dreibus, G., Farrand, W., Klingelhofer, G., Waenke, H., Zipfel, J., Bell, J. F., Grotzinger, J., McSween, H. Y., and Rieder, R., 2005. Chemistry and mineralogy of outcrops at Meridiani Planum. *Earth and Planetary Science Letters* **240**, 73-94.
- Clark, T. R., Baldi, F., and Olson, G. J., 1993. Coal Depyritization by the Thermophilic Archaeon *Metallosphaera-Sedula*. *Applied and Environmental Microbiology* **59**, 2375-2379.
- Clayton, R. N., Grossman, L., and Mayeda, T. K., 1973. A component of primitive nuclear composition in carbonaceous chondrites. *Science* **182**, 485.
- Clayton, R. N. and Mayeda, T. K., 1996. Oxygen isotope studies of achondrites. *Geochimica Et Cosmochimica Acta* **60**, 1999-2017.
- Coomer, F. C., Harrison, A., Oakley, G. S., Kulda, J., Stewart, J. R., Stride, J. A., Fak, B., Taylor, J. W., and Visser, D., 2006. Inelastic neutron scattering study of magnetic excitations in the kagome antiferromagnet potassium jarosite. *Journal of Physics-Condensed Matter* **18**, 8847-8858.
- Cronin, J. and Risse, J., 2005. Chirality and the origin of homochirality. *Lectures In Astrobiology, Vol 1*, 473-515.
- Cronin, J. R. and Pizzarello, S., 1997. Enantiomeric excesses in meteoritic amino acids. *Science* **275**, 951-955.
- Delsemme, A. H., 1992. Cometary Origin Of Carbon And Water On The Terrestrial Planets. *Iau Symposia*, 421-422.
- Dill, H. G. and Pollman, H., 2002. Supergene mineralization in mining residues of the Matchless cupreous pyrite deposit (Namibia)- a clue to the origin of modern and fossil duricrusts in semiarid climates. *Journal of Geochemical Exploration* **75**, 43-70.
- Dutrizac, J. E. and Chen, T. T., 2004. Factors affecting the incorporation of cobalt and nickel in jarosite-type compounds. *Canadian Metallurgical Quarterly* **43**, 305-319.
- Dutrizac, J. E., Hardy, D. J., and Chen, T. T., 1996. The behaviour of cadmium during jarosite precipitation. *Hydrometallurgy* **41**, 269-285.

- Dutrizac, J. E. and Jambor, J. L., 2000. Jarosites and their application in hydrometallurgy. *Sulfate Minerals - Crystallography, Geochemistry and Environmental Significance* **40**, 405-452.
- Eneroth, E. and Koch, C. B., 2004. Fe-hydroxysulphates from bacterial Fe²⁺ oxidation. *Hyperfine Interactions* **156**, 423-429.
- Epstein, S., Krishnamurthy, R. V., Cronin, J. R., Pizzarello, S., and Yuen, G. U., 1987. Unusual Stable Isotope Ratios In Amino-Acid And Carboxylic-Acid Extracts From The Murchison Meteorite. *Nature* **326**, 477-479.
- Fak, B., Coomer, F. C., Harrison, A., Visser, D., and Zhitomirsky, M. E., 2008. Spin-liquid behavior in a kagome antiferromagnet: Deuterium jarosite. *Epl* **81**.
- Farquar, J., Savarino, J., Jackson, T. L., and Theimans, M. H., 2000. Evidence of atmospheric sulfur in the martian regolith from sulfur isotopes in meteorites. *Nature* **404**, 50-52.
- Fulignati, P. and Sbrana, A., 2002. Formation of rock coating induced by the acid fumarole of plume of the actively degassing volcano of La Fossa (Vulcano Island, Italy). *Journal of Volcanology and Geothermal Research* **115**, 397-410.
- Gao, Y. Q. and Marcus, R. A., 2001. Strange and unconventional isotope effects in ozone formation. *Science* **293**, 259.
- Giere, R., Sidenko, N. V., and Lazareva, E. V., 2003. The role of secondary minerals in controlling the migration of arsenic and metals from high-sulfide wastes (Berikul gold mine, Siberia). *Applied Geochemistry* **18**, 1347-1359.
- Glavin, D. P., Bada, J. L., Brinton, K. L. F., and McDonald, G. D., 1999. Amino acids in the Martian meteorite Nakhla. *Proceedings Of The National Academy Of Sciences Of The United States Of America* **96**, 8835-8838.
- Greedan, J. E., 2001. Geometrically frustrated magnetic materials. *Journal of Materials Chemistry* **11**, 37-53.
- Greenwood, J. P., Mojzsis, S. J., and Coath, C. D., 2000. Sulfur isotopic compositions of individual sulfides in Martian meteorites ALH84001 and Nakhla: implications for crust-regolith exchange on Mars. *Earth and Planetary Science Letters* **184**, 23-25.
- Grishin, S. I., Bigham, J. M., and Tuovinen, O. H., 1988. Characterization of Jarosite Formed Upon Bacterial Oxidation of Ferrous Sulfate in a Packed-Bed Reactor. *Applied and Environmental Microbiology* **54**, 3101-3106.
- Grishin, S. I. and Tuovinen, O. H., 1988. Fast Kinetics of Fe-2+ Oxidation in Packed-Bed Reactors. *Applied and Environmental Microbiology* **54**, 3092-3100.
- Harris, K. D. M., 2003. New opportunities for structure determination of molecular materials directly from powder diffraction data *Crystal Growth and Design* **3**, 887-895.
- Harris, K. D. M., Johnston, R. L., and Kariuki, B. M., 1998. The genetic algorithm: Foundations and applications in structure solution from powder diffraction data. *Acta Crystallography A* **54**, 632.
- Harris, K. D. M. and Tremayne, M., 1996. Crystal structure determination from powder diffraction data. *Chemistry of Materials* **8**, 2554.
- Harris, K. D. M., Tremayne, M., and Kariuki, B. M., 2001. Contemporary advances in the use of powder X-ray diffraction for structure determination *Agnew. Int. Chem. Int. Ed.* **40**, 1626.

- Harrison, A., Willis, A. S., and Ritter, C., 2000. μ SR studies of the kagome antiferromagnet $(\text{H}_3\text{O})\text{Fe}_3(\text{OH})_6(\text{SO}_4)_2$. *Physica B* **289**, 217-220.
- Hendricks, S. B., 1937. The crystal structure of alunite and the jarosites. *American Mineralogist* **22**, 773-784.
- Hofstra, A. H., Snee, L. W., Rye, R. O., Folger, H. W., Phinisey, J. D., Loranger, R. J., Dahl, A. R., Naeser, C. W., Stein, H. J., and Lewchuk, M., 1999. Age constraints on Jerritt Canyon and other Carlin-type gold deposits in the western United States-relationship to mid-tertiary extension and magmatism. *Economic Geology and the Bulletin of the Society of Economic Geologists* **94**, 769-802.
- Hutton, C. O. and Bowen, O. E., 1950. An Occurrence of Jarosite in Altered Volcanic Rocks of Stoddard Mountain, San-Bernadino County, California. *American Mineralogist* **35**, 556-561.
- Inami, T., Nishiyama, M., Maegawa, S., and Oka, Y., 2001. Magnetic structure of the kagome lattice antiferromagnet postassium jarosite. *Physical Review B* **61**, 1281-1286.
- Jambor, J. L., 1999. Nomenclature of the alunite supergroup. *Canadian Mineralogist* **37**, 1323-1341.
- Johnston, J. C., David, W., Markvardsen, A. J., and Shankland, K., 2002. A hybrid Monte Carlo method for crystal structure determination from powder diffraction data. *Acta Crystallography A* **58**, 441-447.
- Johnston, J. H., 1977. Jarosite and Akaganeite from White Island Volcano, New Zealand-an X-ray and Mossbauer study. *Geochimica Et Cosmochimica Acta* **41**, 539-544.
- Jones, B. and Renaut, R. W., 2003. Hot spring and geyser sinters: the integrated product of precipitation, replacement, and deposition. *Canadian Journal of Earth Sciences* **40**, 1549-1569.
- Karamanev, D. G., 1991. Model of the Biofilm Structure of Thiobacillus-Ferrooxidans. *Journal of Biotechnology* **20**, 51-64.
- Karas, M. and Hillenkamp, F., 1988. Laser Desorption Ionization Of Proteins With Molecular Masses Exceeding 10000 Daltons. *Analytical Chemistry* **60**, 2299-2301.
- Karlsson, H. R., Clayton, R. N., Gibson, E. K., and Mayeda, T. K., 1992. Water in SNC meteorites: evidence for a Martian hydrosphere. *Science* **255**, 1409-1411.
- Kawano, M. and Tomita, K., 2001. Geochemical modeling of bacterially induced mineralization of schwertmannite and jarosite in sulfuric acid spring water. *American Mineralogist* **86**, 1156-1165.
- Kinumi, T., Saisu, T., Takayama, M., and Niwa, H., 2000. Matrix-assisted laser desorption/ionization time-of-flight mass spectrometry using an inorganic particle matrix for small molecule analysis. *Journal Of Mass Spectrometry* **35**, 417-422.
- Klingelhofer, G., Morris, R. V., Bernhardt, B., Schroder, C., Rodionov, D. S., de Souza, P. A., Yen, A., Gellert, R., Evlanov, E. N., Zubkov, B., Foh, J., Bonnes, U., Kankleit, E., Gutlich, P., Ming, D. W., Renz, F., Wdowiak, T., Squyres, S. W., and Arvidson, R. E., 2004. Jarosite and hematite at Meridiani Planum from Opportunity's Mossbauer spectrometer. *Science* **306**, 1740-1745.
- Lai, E. P. C., Owega, S., and Kulczycki, R., 1998. Time-of-flight mass spectrometry of bioorganic molecules by laser ablation of silver thin film substrates and particles. *Journal Of Mass Spectrometry* **33**, 554-564.

- Langford, J. I. and Louer, D., 1996. Powder diffraction *Reports on the Progress of Physics* **59**, 131.
- Lauth, J. C., Smith, M. R., Wanke, H., Jagoutz, G., Dreibus, H., Palme, B., and Spettel, B., 1986. Chemical systematics of the Shergotty meteorite and the composition of its parent body (Mars). *Geochimica Et Cosmochimica Acta* **50**, 909-926.
- Lower, S. K., Hochella, M. F., and Beveridge, T. J., 2001a. Bacterial recognition of mineral surfaces: Nanoscale interactions between *Shewanella* and alpha-FeOOH. *Science* **292**, 1360-1363.
- Lower, S. K., Hochella, M. F., and Beveridge, T. J., 2001b. Bacterial recognition of mineral surfaces: Nanoscale interactions between *Shewanella* and alpha-FeOOH. *Science* **292**, 1360-1363.
- Maegawa, S., Kaji, R., Kanou, S., Oyamada, A., and Nishiyama, M., 2007. Spin dynamics in classical and quantum Kagome lattice magnets studied by NMR.
- Marcus, R. A., 2004. Mass independent isotope effect in the earliest processed solids in the solar system: A possible chemical mechanism. *Journal of Chemical Physics* **21**, 8201-8211.
- Marti, K., Kim, J. S., Thakur, A. N., McCoy, T. J., and Keil, K., 1995. Signatures of the martian atmosphere in glass of the Zagami meteorite. *Science* **267**.
- Martinez-Frias, J. and Lunar, R., 2004. The volcanism-related multistage hydrothermal system El Jaroso (SE Spain): Implications for the exploration of Mars. *Earth Planets and Space* **56**, 5-8.
- Mathews, C., van Holde, K., and Ahern, K., 2000. *Biochemistry*. Addison Wesley Longman, San Francisco.
- McGetchin, T. R. and Smyth, J. R., 1978. The mantle of Mars: some possible implications of its high density. *Icarus* **34**, 512-536.
- McKay, D. S., Gibson, E. K., Thomas-Keprta, K. L., Vali, H., Romanek, C. S., Clemett, S. J., Chillier, X. D. F., Maechling, C. R., and Zare, R. N., 1996. Search for past life on Mars: Possible relic biogenic activity in Martian meteorite ALH84001. *Science* **273**, 924-930.
- McLennan, S. M., Bell, J. F., Calvin, W. M., Christensen, P. R., Clark, B. C., de Souza, P. A., Farmer, J., Farrand, W. H., Fike, D. A., Gellert, R., Ghosh, A., Glotch, T. D., Grotzinger, J. P., Hahn, B., Herkenhoff, K. E., Hurowitz, J. A., Johnson, J. R., Johnson, S. S., Jolliff, B., Klingelhofer, G., Knoll, A. H., Learner, Z., Malin, M. C., McSween, H. Y., Pockock, J., Ruff, S. W., Soderblom, L. A., Squyres, S. W., Tosca, N. J., Watters, W. A., Wyatt, M. B., and Yen, A., 2005. Provenance and diagenesis of the evaporite-bearing Burns formation, Meridiani Planum, Mars. *Earth and Planetary Science Letters* **240**, 95-121.
- McSween, H. Y. J. and Jarosewich, E., 1983. Petrogenesis of the Elephant Martian A79001 meteorite: Multiple magma pulses on the shergottite parent body. *Geochimica Et Cosmochimica Acta* **47**, 1501-1513.
- McSween, H. Y. J. and Treiman, A. H., 1998. Martian meteorites. In: Papike, J. J. (Ed.), *Planetary materials. Reviews in Mineralogy. Vol. 36*.
- Meierhenrich, U., Thiemann, W. H. P., and Rosenbauer, H., 1999. Molecular parity violation via comets? *Chirality* **11**, 575-582.

- Metropolis, N., Rosenbluth, A. W., Rosenbluth, M. N., Teller, A. H., and Teller, E., 1953. Equation of State Calculations by Fast Computing Machines. *Journal of Chemical Physics* **21**, 1087.
- Meyer, C., 1996. Mars Meteorite Compendium-1996. NASA/Johnson Space Center, Houston, TX.
- Navrotsky, A., Forray, F. L., and Drouet, C., 2005. Jarosite stability on Mars. *Icarus* **176**, 250-253.
- Newsom, H. E., Haggerty, J. J., and Goff, F., 1999. Mixed hydrothermal fluids and the origin of martian soil. *Journal of Geophysical Research* **104**, 8717-8728.
- Nielsen, U. G., Majzlan, J., and Grey, C. P., 2008. Determination and quantification of the local environments in stoichiometric and defect jarosite by solid-state H-2 NMR spectroscopy. *Chemistry of Materials* **20**, 2234-2241.
- Nishiyama, M., Maegawa, S., Inami, T., and Oka, Y., 2003. Magnetic ordering and spin dynamics in potassium jarosite: A Hiesenberg kagome lattice antiferromagnet. *Physical Review B* **67**, 224435.
- Nocera, D. G., Bartlett, B. M., Grohol, D., Papoutsakis, D., and Shores, M. P., 2004. Spin frustration in 2D kagome lattices: A problem for inorganic synthetic chemistry. *Chemistry-a European Journal* **10**, 3851-3859.
- Nyquist, L. E., Bansal, B., Weissmann, N., and Shih, C. Y., 1995. Martians- young and old: Zagami and ALH84001. *Lunar and Planetary Science XXVI*, 106-1066.
- Peltzer, E. T. and Bada, J. L., 1978. Alpha-Hydroxycarboxylic Acids In Murchison Meteorite. *Nature* **272**, 443-444.
- Pepin, R. O. and Carr, M. H., 1992. *Major issues and outstanding problems*. University of Arizona Press, Tuscon, AZ.
- Pizzarello, S., 2006. The chemistry of life's origin: A carbonaceous meteorite perspective. *Accounts Of Chemical Research* **39**, 231-237.
- Pizzarello, S. and Cronin, J. R., 2000. Non-racemic amino acids in the Murray and Murchison meteorites. *Geochimica Et Cosmochimica Acta* **64**, 329-338.
- Pizzarello, S. and Weber, A. L., 2004. Prebiotic amino acids as asymmetric catalysts. *Science* **303**, 1151-1151.
- Pizzarello, S., Zolensky, M., and Turk, K. A., 2003. Nonracemic isovaline in the Murchison meteorite: Chiral distribution and mineral association. *Geochimica Et Cosmochimica Acta* **67**, 1589-1595.
- Reynolds, R. C., 1989. *Principles of Powder Diffraction*. Mineralogical Society of America, Chelsea, MI.
- Riant, O. and Hannedouche, J., 2007. Asymmetric catalysis for the construction of quaternary carbon centres: nucleophilic addition on ketones and ketimines. *Organic & Biomolecular Chemistry* **5**, 873-888.
- Rieder, R., Gellert, R., Anderson, R. C., Bruckner, J., Clark, B. C., Dreibus, G., Economou, T., Klingelhoffer, G., Lugmair, G. W., Ming, D. W., Squyres, S. W., d'Uston, C., Wanke, H., Yen, A., and Zipfel, J., 2004. Chemistry of rocks and soils at Meridiani Planum from the alpha particle X-ray spectrometer. *Science* **306**, 1746-1749.
- Rietveld, H. M., 1969. A profile refinement method for nuclear and magnetic structures. *Journal of Applied Crystallography* **2**, 65.

- Robert, C. P. and Casella, G., 2004. *Monte Carlo Statistical Methods*. Springer Verlag, New York.
- Robertson, J. M., 1953. *Organic Crystals and Molecules*. Cornell University Press, Ithaca, NY.
- Romanek, C. S., Perry, E. C., Treiman, R. A., Socki, J. H., and Gibson, E. K., 1998. Oxygen isotope record of silicate alteration in the Shergotty-Nakhla-Chassigny meteorite Layfayette. *Meteoritics & Planetary Science* **33**, 775-784.
- Sandford, S. A., 2007. Organics in the samples returned by the Stardust spacecraft from Comet 81P/Wild 2. *Astrobiology* **7**, 493-494.
- Sandford, S. A., Aleon, J., Alexander, C. M. O., Araki, T., Bajt, S., Baratta, G. A., Borg, J., Bradley, J. P., Brownlee, D. E., Brucato, J. R., Burchell, M. J., Busemann, H., Butterworth, A., Clemett, S. J., Cody, G., Colangeli, L., Cooper, G., D'Hendecourt, L., Djouadi, Z., Dworkin, J. P., Ferrini, G., Fleckenstein, H., Flynn, G. J., Franchi, I. A., Fries, M., Gilles, M. K., Glavin, D. P., Gounelle, M., Grossemy, F., Jacobsen, C., Keller, L. P., Kilcoyne, A. L. D., Leitner, J., Matrajt, G., Meibom, A., Mennella, V., Mostefaoui, S., Nittler, L. R., Palumbo, M. E., Papanastassiou, D. A., Robert, F., Rotundi, A., Snead, C. J., Spencer, M. K., Stadermann, F. J., Steele, A., Stephan, T., Tsou, P., Tyliszczak, T., Westphal, A. J., Wirick, S., Wopenka, B., Yabuta, H., Zare, R. N., and Zolensky, M. E., 2006. Organics captured from comet 81P/Wild 2 by the Stardust spacecraft. *Science* **314**, 1720-1724.
- Sasaki, K. and Konno, H., 2000. Morphology of jarosite-group compounds precipitated from biologically and chemically oxidized Fe ions. *Canadian Mineralogist* **38**, 45-56.
- Schweitzer, M. H., Chiappe, L., Garrido, A. C., Lowenstein, J. M., and Pincus, S. H., 2005. Molecular preservation in Late Cretaceous sauropod dinosaur eggshells. *Proceedings Of The Royal Society B-Biological Sciences* **272**, 775-784.
- Settle, M. and Greeley, R., 1979. Formation and deposition of volcanic sulfate aerosols on Mars. *Journal of Geophysical Research* **84**, 8343-8354.
- Shankland, K., McBride, L., David, W., Shankland, N., and Steele, G., 2002. Molecular, crystallographic and algorithmic factors in structure determination from powder diffraction data by simulated annealing *Journal of Applied Crystallography* **35**, 443-454.
- Shearer, C. K., Layne, G. D., Papike, J. J., and Spilde, M. N., 1996. Sulfur isotopic systematics in alteration assemblages of Martian meteorite ALH84001. *Geochimica Et Cosmochimica Acta* **60**, 2921-2926.
- Siever, R. and Woodford, N., 1979. Dissolution kinetics and the weathering of mafic minerals. *Geochimica Et Cosmochimica Acta* **43**, 717-724.
- Solovyov, L. A., Astachov, A. M., Molokeyev, M. S., and Vasiliev, A. D., 2005. Powder diffraction crystal structure analysis using derivative difference minimization: example of the potassium salt of 1-(tetrazol-5-yl)-2-nitroguanidine *Acta Crystallographica B: Structural Science* **B61**, 435-442.
- Squyres, S. W., Arvidson, R. E., Bell, J. F., Bruckner, J., Cabrol, N. A., Calvin, W., Carr, M. H., Christensen, P. R., Clark, B. C., Crumpler, L., Des Marais, D. J., d'Uston, C., Economou, T., Farmer, J., Farrand, W., Folkner, W., Golombek, M., Gorevan, S., Grant, J. A., Greeley, R., Grotzinger, J., Haskin, L., Herkenhoff, K. E., Hviid,

- S., Johnson, J., Klingelhofer, G., Knoll, A. H., Landis, G., Lemmon, M., Li, R., Madsen, M. B., Malin, M. C., McLennan, S. M., McSween, H. Y., Ming, D. W., Moersch, J., Morris, R. V., Parker, T., Rice, J. W., Richter, L., Rieder, R., Sims, M., Smith, M., Smith, P., Soderblom, L. A., Sutlivan, R., Wanke, H., Wdowiak, T., Wolff, M., and Yen, A., 2004a. The Opportunity Rover's Athena science investigation at Meridiani Planum, Mars. *Science* **306**, 1698-1703.
- Squyres, S. W., Grotzinger, J. P., Arvidson, R. E., Bell, J. F., Calvin, W., Christensen, P. R., Clark, B. C., Crisp, J. A., Farrand, W. H., Herkenhoff, K. E., Johnson, J. R., Klingelhofer, G., Knoll, A. H., McLennan, S. M., McSween, H. Y., Morris, R. V., Rice, J. W., Rieder, R., and Soderblom, L. A., 2004b. In situ evidence for an ancient aqueous environment at Meridiani Planum, Mars. *Science* **306**, 1709-1714.
- Squyres, S. W. and Knoll, A. H., 2005. Sedimentary rocks at Meridiani Planum: Origin, diagenesis, and implications for life on Mars. *Earth and Planetary Science Letters* **240**, 1-10.
- Stoffregen, R. E., Alpers, C. N., and Jambor, J. L., 2000. Alunite-jarosite crystallography, thermodynamics, and geochronology. *Sulfate Minerals - Crystallography, Geochemistry and Environmental Significance* **40**, 453-479.
- Stults, J. T., 1995. Matrix-assisted laser-desorption ionization mass-spectrometry (MALDI-MS). *Current Opinion In Structural Biology* **5**, 691-698.
- Stump, M. J., Fleming, R. C., Gong, W. H., Jaber, A. J., Jones, J. J., Surber, C. W., and Wilkins, C. L., 2002. Matrix-assisted laser desorption mass spectrometry. *Applied Spectroscopy Reviews* **37**, 275-303.
- Szymanski, J. T., 1988. The crystal structure of beudantite, $Pb(Fe, Al)_3[(As, S)_4]_2(OH)_6$. *The Canadian Mineralogist* **26**, 923-932.
- Tanaka, K., H. W., Ido, Y., Akita, A., Yoshida, Y., and Yoshida, T., 1988. Protein and polymer analyses up to m/z 100,000 by laser ionization time-of-flight mass spectrometry. *Rapid Communications in Mass Spectrometry* **2**, 151-153.
- Theimans, M. H., 1999. Mass-Independent Isotope Effects in Planetary Atmosphere and the Early Solar System. *Science* **283**, 341-345.
- Tosca, N. J., McLennan, S. M., Clark, B. C., Grotzinger, J. P., Hurowitz, J. A., Knoll, A. H., Schroder, C., and Squyres, S. W., 2005. Geochemical modeling of evaporation processes on Mars: Insight from the sedimentary record at Meridiani Planum. *Earth and Planetary Science Letters* **240**, 122-148.
- Townsend, M. G., Longworth, G., and Roudaut, E., 1986. Triangular-spin, kagome plane in jarosites. *Physical Review B* **33**, 4919-4926.
- Treiman, A. H., 1993. The parent magmas of the Nakhla (SNC) meteorite, inferred from magmatic inclusions. *Geochimica Et Cosmochimica Acta* **57**, 4753-4767.
- Treiman, A. H., 2005. The nakhlite meteorites: Augite-rich igneous rocks from Mars. *Chemie der Erde* **65**, 203-270.
- Treiman, A. H., Gleason, J. D., and Bogard, D. D., 2000. The SNC meteorites are from Mars. *Planetary and Space Science* **48**, 1213-1230.
- Tschermak, G., 1872. Die Meteoriten von Shergotty and Gopalpur. *Sitzungsber. Akad. Wiss. Wien Math Naturwiss. Kl.* **65**, 122-146.

- Turner, G., Knott, S. F., Ash, R. D., and Gilmour, J. D., 1997. Ar-Ar chronology of the Martian meteorite ALH84001, evidence for the early bombardment of Mars. *Geochimica Et Cosmochimica Acta* **61**, 3835-3850.
- Van Laarhoven, P. J. M. and Aarts, E. H. L., 1987. *Simulated Annealing: Theory and Applications*. Reidel Publishing, Holland.
- Willis, A. S. and Harrison, A., 1996. Structure and magnetism of hydronium jarosite, a model Kagome antiferromagnet *Journal of The American Chemical Society-Faraday Transactions* **92**, 2161.
- Willis, A. S., Harrison, A., Ritter, C., and Smith, R. I., 2000. Magnetic properties of pure and diamagnetically doped jarosites: Model kagome antiferromagnets with variable coverage of the magnetic lattice *Physical Review B* **61**, 6156.
- Yalcin, T., Wallace, W. E., Guttman, C. M., and Li, L., 2002. Metal powder substrate-assisted laser desorption/ionization mass spectrometry for polyethylene analysis. *Analytical Chemistry* **74**, 4750-4756.
- Yan, B. Z., Stoner, D. L., Kotler, J. M., Hinman, N. W., and Scott, J. R., 2007a. Detection of biosignatures by geomatrix-assisted laser desorption/ionization (GALDI) mass spectrometry. *Geomicrobiology Journal* **24**, 379-385.
- Yan, B. Z., Stoner, D. L., and Scott, J. R., 2007b. Direct LD-FTMS detection of mineral-associated PAHs and their influence on the detection of co-existing amino acids. *Talanta* **72**, 634-641.
- Yao, J., Scott, J. R., Young, M. K., and Wilkins, C. L., 1998. Importance of matrix : analyte ratio for buffer tolerance using 2,5-dihydroxybenzoic acid as a matrix in matrix-assisted laser desorption/ionization Fourier transform mass spectrometry and matrix-assisted laser desorption/ionization time of flight. *Journal Of The American Society For Mass Spectrometry* **9**, 805-813.
- Yildirim, T. and Harris, A. B., 2006. Magnetic structure and spin waves in the Kagome jarosite compound $\text{KFe}_3(\text{SO}_4)_2(\text{OH})_6$. *Physical Review B* **73**.
- Zhang, Q. C., Zou, H. F., Guo, Z., Zhang, Q., Chen, X. M., and Ni, J. Y., 2001. Matrix-assisted laser desorption/ionization mass spectrometry using porous silicon and silica gel as matrix. *Rapid Communications In Mass Spectrometry* **15**, 217-223.

CHAPTER 2: GLYCINE IDENTIFICATION IN NATURAL JAROSITES USING LASER DESORPTION FOURIER TRANSFORM MASS SPECTROMETRY: IMPLICATIONS FOR THE SEARCH FOR LIFE ON MARS

J. Michelle Kotler¹, Nancy W. Hinman^{1*}, Beizhan Yan², Daphne L. Stoner², and Jill R. Scott³

¹Geosciences Department, University of Montana, Missoula, MT 59812

²Department of Chemistry, University of Idaho, Idaho Falls, ID 83402

³Chemistry Department, Idaho National Laboratory, Idaho Falls, ID 83415

* Corresponding author. Tel.: 406-243-5277; fax: 406-243-4028.

E-mail address: nancy.hinman@umontana.edu

Running title- Glycine found in jarosites using LD-FTMS

2.1 ABSTRACT

The jarosite group minerals have received increasing attention since the discovery of jarosite on the martian surface by the Mars Exploration Rover Opportunity. Given that jarosite can incorporate foreign ions within its structure, we have investigated the use of jarosite as an indicator of aqueous and biological processes on Earth and Mars. The use of laser desorption Fourier transform mass spectrometry has revealed the presence of organic matter in several jarosite samples from various locations worldwide. One of the ions from the natural jarosites has been attributed to glycine because it was systematically observed in combinations of glycine with synthetic ammonium and potassium jarosites, Na₂SO₄, and K₂SO₄. The ability to observe these organic signatures in jarosite samples with an “*in situ*” instrumental technique, such as employed in this study, furthers the goals of planetary geologists to determine whether signs of life (e.g., the presence of biomolecules or biomolecule precursors) can be detected in the rock record of terrestrial and extraterrestrial samples.

Key words: jarosite, Mars, mass spectrometry, organic matter, biosignatures

2.2 INTRODUCTION

In the search for life on other planets, the detection of organic molecules and their assignment as biological evidence are key goals. During the *Viking* mission, pyrolysis gas chromatography/mass spectrometry was used on the surface of Mars to detect organic molecules (BIEMANN, 1977). Although the *Viking* mission was unsuccessful in providing evidence for significant quantities of organic molecules on Mars (Benner *et al.*, 2000), the search continues for new ways to identify organic molecules in geologic materials (NAVARRO-GONZALEZ *et al.*, 2006). Jarosite is a prime mineral candidate for harboring organic compounds. Recently, Skelley *et al.* (SKELLEY *et al.*, 2005) reported the detection of amino acids associated with terrestrial jarosite samples through the use of a portable capillary electrophoresis instrument called the Mars Organic Analyzer. Quantities of amino acids were also detected by Aubrey *et al.* (AUBREY *et al.*, 2006) in gypsum and jarosite samples with a complex extraction procedure. Thermodynamic evaluation of the two most common jarosite group minerals (i.e., jarosite– $\text{KFe}_3(\text{SO}_4)_2(\text{OH})_6$ and natrojarosite– $\text{NaFe}_3(\text{SO}_4)_2(\text{OH})_6$) has shown that these two members should be stable on the martian surface (NAVROTSKY *et al.*, 2005). The mineral group is stable on Earth; reported occurrences of samples date to several million years old (HOFSTRA *et al.*, 1999; STROFFREGEN *et al.*, 2000). The jarosite group minerals were first postulated to occur on Mars by Burns (1987a, 1987b, 1989). In 2004, the Mars Exploration Rover Opportunity confirmed the presence of jarosite group minerals on the martian surface (CHRISTENSEN *et al.*, 2004; KLINGELHOFER *et al.*, 2004; SQUYRES *et al.*, 2004).

Since the discovery of jarosite group minerals on Mars, interest has focused on linking the origin and characteristics of the mineral group to the existence of extant or extinct life on Mars (SQUYRES AND KNOLL, 2005). On Earth, jarosite group mineral formation can be influenced or mediated by sulfur- and iron-metabolizing microorganisms (ENEROTH AND KOCH, 2004; BRIDGE et al., 2000; SASAKI AND KONNO, 2000; AKAI et al., 1999; KARAMANEV, 1991; CLARK et al., 1993; GRISHIN et al. 1988). It is therefore possible that biological “fingerprints” left over from jarosite formation can be used to identify extant or extinct signs of life in the geologic record on Earth and, potentially, Mars.

The jarosite group minerals can accommodate a wide variety of substitutions in several crystallographic sites of the unit cell. These substitutions often cause a distortion in the crystal lattice that creates vacancies in certain crystallographic sites (DUTRIZAC AND JAMBOR, 2000). The general chemical formula for jarosite is $XFe_3(SO_4)_2(OH)_6$, where the X represents both monovalent and divalent cations that can occupy the axial positions in the crystal structure. Commonly found ions include K^+ , Na^+ , H_3O^+ , NH_4^+ , and Pb^{2+} with reports of “foreign ions” also occupying this position (DUTRIZAC et al., 1996; GIERÉ et al., 2003; DUTRIZAC, 2004). The term foreign ion is used to describe any atomic or molecular ion that is found associated in an unidentified manner - either trapped, included, or possibly substituted - in the mineral structure and is not considered common to the mineral chemistry. Becker and Gasharova (2001) investigated the ability of jarosite to incorporate foreign ions and determined that jarosite could act as a storage mineral for heavy metals. Under the acidic conditions ($pH < 2.5$) at which jarosite forms, certain amino acids such as glycine ($C_2H_5NO_2$) present in solution would be charged

($pK_a \alpha\text{-COOH} = 2.3$; $pK_a \alpha\text{-NH}_3^+ = 9.6$) (MATHEW et al., 1999). This could provide a charge balancing substitution, especially in rapidly precipitating systems where the inclusion of foreign ions would likely occur. Unless the system was supersaturated with respect to these foreign ions, the amount of substitution would be below the detection limits of standard powder diffraction methods (generally 3–5%) and could go undetected without the use of sensitive microprobe techniques. Also, if the foreign ions exist as a separate phase within the mineral matrix or are adsorbed to the mineral surface, they would not be detected by conventional methods at low concentrations. For this study, natural jarosite samples were analyzed with a laser desorption microprobe Fourier transform mass spectrometer (LD-FTMS) to determine whether this technique could provide the high resolution chemical data needed to detect organic matter incorporated or associated with jarosite.

The LD-FTMS used in this study is housed at the Idaho National Laboratory and was created for highly reproducible laser beam scanning and collection of sensitive high resolution chemical data (SCOTT AND TREMBLAY, 2002). With the new technique of geomatrix-assisted laser desorption/ionization (GALDI) (YAN et al., 2007a), which is based on principles established from matrix-assisted laser desorption/ionization (MALDI), it is possible to use jarosite as the geomatrix to aid in organic matter detection. Direct laser desorption of biomolecules often does not result in production of ions; hence, the addition of a matrix that aids desorption and ionization processes is necessary. In MALDI, the matrices are usually aromatic acids that result in protonation or cationization of biomolecules (KARAS et al., 1987). Yan et al. (2007a) demonstrated that minerals or geomatrices can also assist in the detection of biomolecules.

Herein, we report our use of the GALDI technique to identify mass spectral signatures of organic matter associated with natural jarosite samples collected from seven different locations around the world. Additional characterization by X-ray powder diffraction (XRPD) studies and total carbon analysis were performed. Synthesized jarosite standards were also analyzed to assist in identification of organic matter present in the natural samples.

2.3 MATERIALS AND METHODS

2.3.1 NATURAL SAMPLES-

Natural jarosite samples were acquired from the University of Montana Dana Collection, commercial sources, or the authors (Table 1). Samples were isolated from the parent rock matrices and ground to a fine powder with a corundum mortar and pestle. Synthetic samples were also ground to ensure homogeneity. Samples were mounted on glass slides for random X-ray powder diffraction (XRPD) analysis.

Table 2.1 Natural jarosite sample names, locations, and sources.

Sample Name	Location	Source
Jarosite-MT	West of Agency Fort Belknap Reservation, Montana	UM Dana Collection
Jarosite-AZ	Toughnut Mine-Tombstone, Cochise Co., Arizona	UM Dana Collection
Jarosite-NM	Copiapo Jarosite Mine, Dona Ana County, New Mexico	UM Dana Collection
Jarosite-AUS	Bolcummata, S. Australia	UM Dana Collection
Jarosite-NZ	Te Karo Bay- Coromandal Peninsula, New Zealand	Collected April 4, 2005

Jarosite- RUS	Perm, Russia	Purchased from Rubelev Colours, Natural Pigments- USA (707-539-8215)
Jarosite- SPA	El Jaroso, Spain (type locality)	Purchased from De Steenen Kamer- Mineralen, Edelstenen Sieraden- Netherlands (www.desteenenkamer.nl)
Jarosite (synthetic)	-	synthesized

2.3.2 SYNTHETIC SAMPLES-

Potassium jarosite ($\text{KFe}_3(\text{SO}_4)_2(\text{OH})_6$) was prepared according to Dutrizac's (2003) method. Potassium sulfate (0.4 M K_2SO_4) was added to a 0.4M FeCl_3 solution in a 100-mL round bottom flask with a stoichiometric ratio of 2:3 sulfate salt to ferric iron. The solution was stirred under reflux conditions at 100° C for 24 hours. To collect the precipitate, the solutions were vacuum filtered while hot with a Buchner funnel and Whatman #4 filter paper. The precipitates were washed under vacuum three times with 1L of deionized water and air-dried. The synthesis of ammonium jarosite ($\text{NH}_4\text{Fe}_3(\text{SO}_4)_2(\text{OH})_6$) was accomplished with an identical procedure, except that $(\text{NH}_4)_2\text{SO}_4$ was used in place of K_2SO_4 . Experimental mixtures of glycine or alanine with sodium or potassium sulfate (Sigma-Aldrich, MA) or a synthetic jarosite were prepared by mixing ~3–5% analyte with the sulfate or jarosite matrix before LD-FTMS preparations.

2.3.3 X-RAY POWDER DIFFRACTION

Powdered samples were mounted on glass slides for random X-ray powder diffraction (XRPD) analysis. X-ray diffraction analyses were performed with a Philips APD 3720

X-ray diffractometer with a step size of $0.02^\circ 2\theta$ and a rate of $0.750^\circ 2\theta/\text{min}$. Patterns were compared to jarosite synthetic Joint Committee on Powder Diffraction Standards (JCPDS) file 22-0827, and unit cell dimensions were calculated from the hkl {003} and {110} crystallographic reflections.

2.3.4 TOTAL CARBON ANALYSIS

Powdered jarosite samples underwent total carbon and sulfur analysis by SGS Mineral Services of Canada for total carbon and sulfur analysis by the furnace/IR method (Leco SC632-Series, ASTM method E-1915-97).

2.3.5 LASER DESORPTION FOURIER TRANSFORM MASS SPECTROMETRY

Samples were formed into pellets with a half-inch Beckman dye with a Carver Laboratory Press at a pressure of 3.4×10^7 Pa before mounting onto a 316 SS probe tip with epoxy (Devcon 5 minute epoxy, Danvers, MA). Epoxy was allowed to cure to ~70 % dryness before pellet was applied to prevent the sample from absorbing the epoxy. Mass spectra were obtained with a Fourier transform mass spectrometer equipped with a 7-Tesla Oxford (Oxford, England) superconducting magnet, a 2-inch cubic cell, and an Odyssey control and data acquisition system (Thermo-Finnigan FT/MS, Bremen, Germany) (SCOTT AND TREMBLAY, 2002; YAN et al., 2007a). An Nd:YAG laser (Continuum, Santa Clara, CA) operating at 355 nm with a 6 ns pulse width was used for desorption/ionization at a laser fluence of 8600 J/m^2 focused to a $\sim 6 \mu\text{m}$ diameter spot, measured as described previously (SCOTT AND TREMBLAY, 2002). All spectra were

collected from single laser shots. The sample was positioned ~0.5 cm from the front electrostatic trap plate of the ionization cell. During the ionization event, the potential on the front and rear trap plates was maintained at 0 V. After ionization, a trapping potential of 2 V was applied to both trap plates and maintained until the quench event at the end of the sequence. A delay of 0.5 s was imposed prior to application of a radio frequency chirp excitation applied to opposing plates of the cubic cell over the range of 50 Hz to 4 MHz with a sweep rate of 3600 Hz/ μ s. The ions were detected in direct mode with 64 to 128 K data points with resolution ranging from 5000 to 50,000 and mass errors of less than ± 0.002 u for known masses. Raw data were baseline corrected, Hamming apodized, zero filled, and Fourier transformed to produce the mass spectra. Pressure during analysis was $\leq 2 \times 10^{-7}$ Pa (2×10^{-9} Torr). External calibration of the FTMS was performed with Na-attached polyethylene glycol 1000.

2.4 RESULTS

XRPD patterns indicated that the natural samples were dominated by a jarosite mineral phase with few contaminants present. A range of jarosite compositions were indicated in the samples by the unit cell variations. The unit cell dimensions of all the natural and synthetic jarosite samples in this study are plotted in Fig. 1 and listed in Table 2. The reference values for jarosite, natrojarosite, and hydronium jarosite are also plotted for comparison with standard compositions assigned to various jarosite group end-members. Unit cell dimensions may vary in jarosite group minerals. The unit cell dimensions are dependent on cation substitution characteristics and indicate deviations from strict formula constraints between jarosite ($\text{KFe}_3(\text{SO}_4)_2(\text{OH})_6$) and natrojarosite ($\text{NaFe}_3(\text{SO}_4)_2(\text{OH})_6$). Hydronium ion substitution may also affect unit cell dimensions

in the jarosite group minerals by altering the length values along both a- and c-axes. Solid solutions exist among jarosite, natrojarosite, and hydronium jarosite, and end-member compositions are rarely found in natural or synthetic samples (DUTRIZAC AND JAMBOR, 2000). The unit cell lengths for the samples along the a-axis ranged between 7.25 —7.50 angstroms. Values for the c-axis ranged between 16.64 —17.70 angstroms. The synthetic jarosite sample has unit cell dimensions of $a = 7.32$ and $c = 17.13$ angstroms. The JCPDS reference values for jarosite were the dimensions $a = 7.29$ and $c = 17.16$ angstroms.

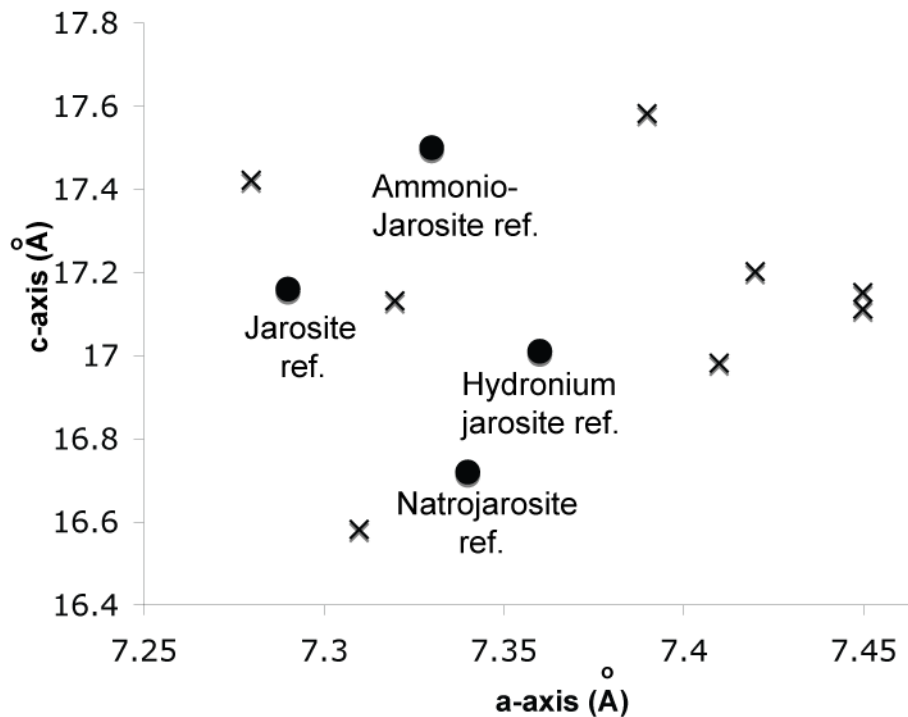


Figure 2.1 Plot of synthetic jarosite and natural jarosite unit cell dimension (x) compared to standard reference values for end member compositions of jarosite, natrojarosite, hydronium jarosite, and ammoniojarosite.

Table 2.2 Unit cell dimension of the natural and synthetic jarosite samples.

Sample	Unit Cell Dimensions	
	a (Å)	c (Å)
Jarosite (synthetic)	7.32	17.13
Jarosite- Arizona	7.45	17.11
Jarosite- Australia	7.41	16.98
Jarosite- Montana	7.42	17.20
Jarosite- New Mexico	7.45	17.15
Jarosite- New Zealand	7.28	17.42
Jarosite- Russia	7.31	16.58
Jarosite- Spain	7.39	17.58

Fig. 2 shows the LD-FTMS positive mode spectra of synthetic potassium jarosite. The primary mass-to-charge (m/z) peaks in the potassium jarosite sample corresponded to potassium (K^+ , m/z 38.96) and iron (Fe^+ , m/z 55.93) ions. Small isotope peaks of potassium and iron were also visible in the spectrum. Relative abundances for potassium corresponded to standard isotopic distributions for the two stable potassium isotopes ($^{39}K = 93.25\%$ with mass = 38.96 u and $^{41}K = 6.73\%$ with mass = 40.96 u). For iron, the visible isotope peaks corresponded to standard distributions for the two most abundant stable isotopes ($^{54}Fe = 5.84\%$ with mass = 53.93 u and $^{56}Fe = 91.75\%$ with mass = 55.93 u). No high mass cluster ions were produced in the positive mode spectra of synthetic jarosite, which indicates that the only positive ions formed were those expected from the formula unit with a laser wavelength of 355 nm.

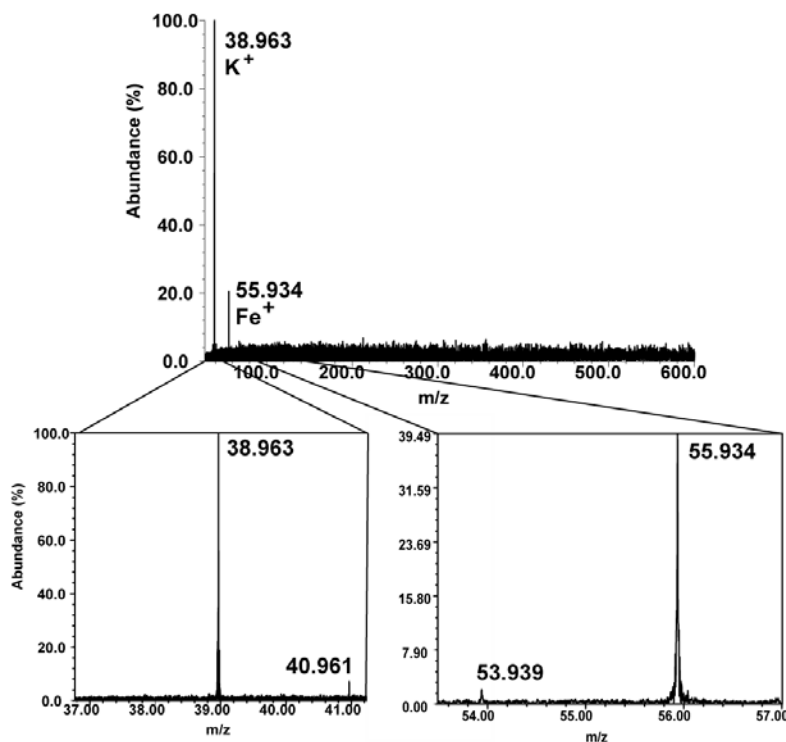


Figure 2.2 LD-FTMS positive mode spectrum of synthetic jarosite. Potassium and iron atoms are observed at m/z 38.963 and m/z 55.934, respectively.

No attempt was made to quantify relationships between the various types of cations present in the jarosite samples in this study because the signal intensities, expressed as relative peak abundances, are dependent on both the ionization efficiencies and the concentrations of the elements or compounds in the sample (YAN et al., 2006). The variation in ionization efficiencies can be significant not only for molecules but also for elements. For example, the unit formula indicates that iron occurs at higher concentrations than potassium in potassium jarosite (3:1, $\text{KFe}_3(\text{SO}_4)_2(\text{OH})_6$), but this was not observed in the synthetic potassium jarosite spectra (Fig. 2.1) because potassium ionizes more efficiently at a wavelength of 355 nm than does iron. Therefore, no attention was focused on the quantitative relationships between one ion type relative to another. However, the isotopic abundances for a particular element or compound are

more quantitative than abundances between different species because the ionization energies for the isotopes are very close to each other. Therefore, relative isotopic abundances can be very useful for assisting in the identification of elemental compositions; however, the accuracy of isotope ratios does vary with mass analyzer and ionization method. For FTMS, electron ionization provides isotope ratio accuracy of ~1%, while the accuracy can be as poor as ~6% even for abundant element isotopes with laser desorption ionization (SPELL et al., 1993). Laser desorption or ablation produces less accurate isotope ratios because the slightly different ionization energies of the isotopes and the wider range of kinetic energies cause fractionation that obscures the results.

Similar to synthetic jarosite, the natural mineral showed potassium and iron peaks at m/z ratios of 38.96 and 55.93 respectively. In addition, all natural samples contained peaks at higher masses, which indicated the presence of other ions or molecules in the samples (Table 3). One particular peak at m/z 275 was common to the jarosite samples from Arizona, Australia, New Mexico, and New Zealand (Fig. 3.). Expanding the spectral region from m/z 270 to 280 revealed that this peak had a set of associated isotope peaks that were less abundant than the primary peak (Fig. 4 and Table 4).

Table 2.3 Major LD-FTMS positive peaks (m/z) observed in the natural jarosite samples.

<i>Samples</i>	<i>Major m/z positive mode peaks</i>									
Jarosite-AZ	38.963	55.934				212.844		275.091		317.138
Jarosite-AUS	38.963	55.934	84.911		196.872			275.093		317.126
Jarosite-MT	38.963	55.934					259.116			
Jarosite-NM	38.963	55.934		128.409	195.579			275.092		373.218
Jarosite-NZ	38.963	55.934		128.418			259.112	275.084		317.136

Jarosite-RUS	38.963	55.934							301.857	317.109	
Jarosite-SPA	38.963	55.934		128.418	195.372						

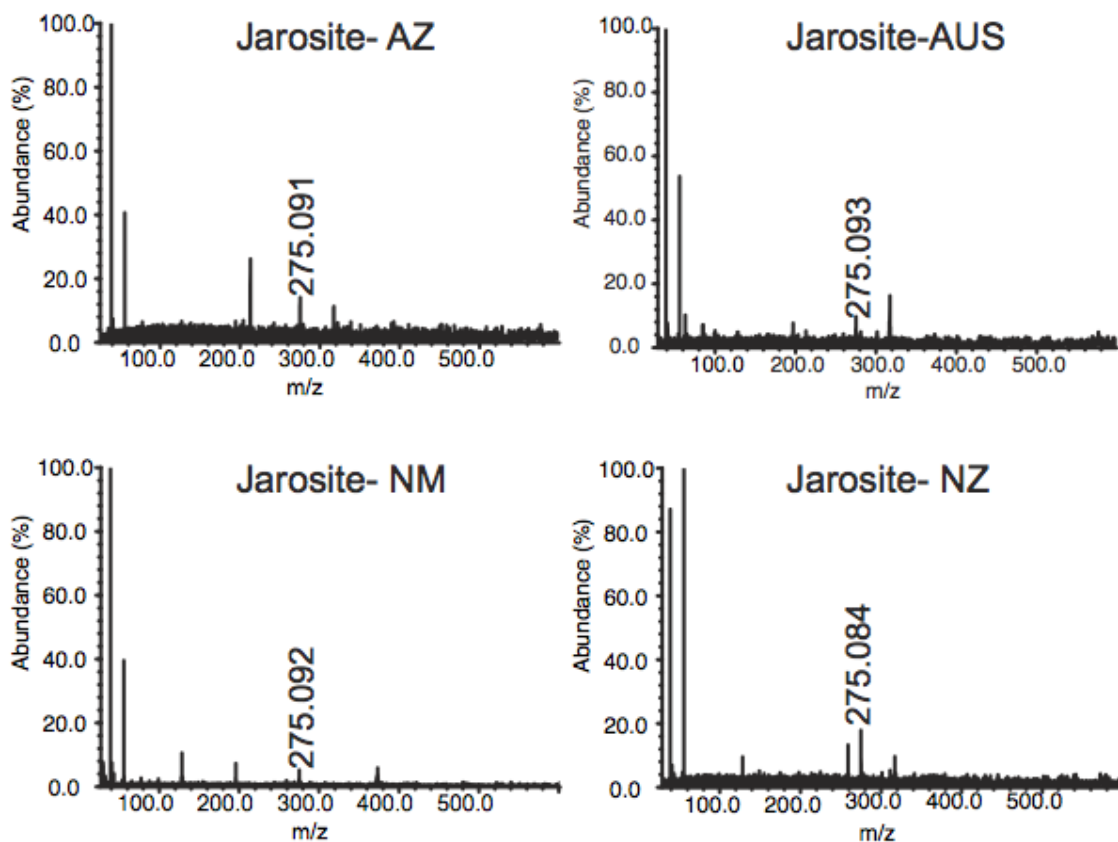


Figure 2.3 LD-FTMS positive mode spectra of jarosites from (A) Arizona (AZ), (B) Australia (AUS), (C) New Mexico, and (D) New Zealand (NZ), showing a common peak at m/z 275. All other major peaks are listed in Table 3.

To determine the elemental composition of the main peak at m/z 275, elemental and isotopic composition searches were performed with the Odyssey Interpretation software (Thermo-Finnigan FT/MS, Bremen, Germany). Potential elemental compositions with all possible combinations of inorganic and organic elements that were likely to be present in the samples were identified (i.e., C, N, O, S, H, Si, Na, K, Fe, Pb, P, Cu, and Zn). Carbon was included because analyses indicated that all natural samples

had levels of carbon that were above the detection limits of the Leco carbon analyzer (Table 5). Higher quality spectra revealed that the mass of the peak was 275.087 u, where the non-integer portion represents the total mass defect from the combined mass defects of the elements present (the mass defects of elemental isotopes are a result of using ^{12}C (12.00000000 u) as the standard). To ensure that a sufficiently wide range of likely candidates was identified, the computer was queried for any combinations of element isotopes within ± 0.005 u of 275.087. Several compositions that contained carbon, nitrogen, sulfur, oxygen, and hydrogen met this requirement. Some of these combinations were easily dismissed by following standard mass spectral interpretation procedures (MCLAFFERTY AND TUREČEK, 1993; SACK et al., 1984; KIM et al., 2006). The remaining possibilities were further subjected to the requirements that the mass of the compound had to be very close to the target value (within ± 0.005 u or less) and the calculated isotopic abundance patterns had to be similar to those observed.

Based on these criteria, the most likely identity of the peak at m/z 275 was determined to be a cluster ion with the composition $\text{C}_{11}\text{H}_{19}\text{N}_2\text{O}_2\text{S}_2$ (Fig. 4. and Table 4). The mass for this cluster ion is 275.088 u, which would give a mass accuracy of ~ 3 ppm. To illustrate that a small change in composition can dramatically affect the mass defect and, therefore, the mass accuracy, the substitution of a combination of NH_2 for one O would create a cluster ($\text{C}_{11}\text{H}_{21}\text{N}_3\text{OS}_2$) that would have a mass of 275.112 u, while a substitution of two Os for one S would create a cluster ($\text{C}_{11}\text{H}_{19}\text{N}_2\text{O}_4\text{S}$) with a mass of 275.106 u. Both alternative clusters have masses that are too high for the reported accuracy of the instrument.

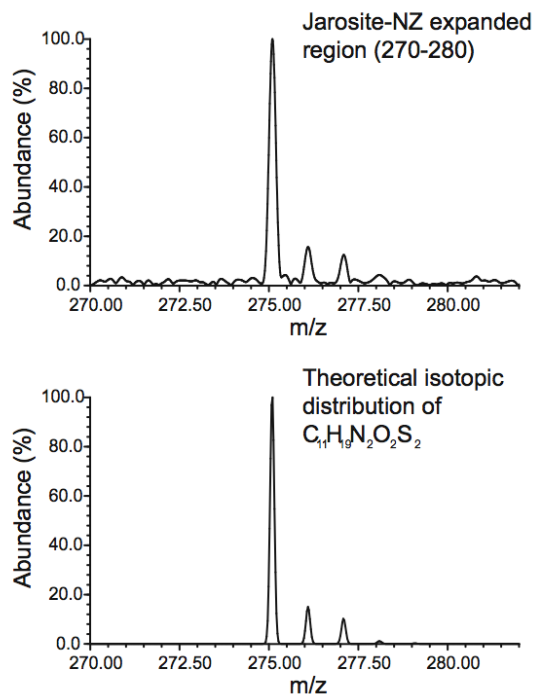


Figure 2.4. Expanded region (A) LD-FTMS positive mode spectrum from m/z 270 to m/z 280 of jarosite-New Zealand sample that shows the isotopic distribution of the major peak at m/z 275 and (B) the theoretical isotopic distribution of compound $C_{11}H_{19}N_2O_2S_2$ predicted to form during gas-phase ionization of the jarosite samples.

The possibility was considered that potassium could play a role in the cluster composition, resulting in a cluster with an elemental composition of $C_{14}H_{20}OSK$ with a mass of 275.087 u along with associated isotopes given in Table 4. Another key for assigning a composition for m/z 275 was to account for the peak intensity for the isotope peak at m/z 277 ($[M + 2]^{+1}$), which is higher than would be expected for an organic compound composed of only C, H, O, and N. Two S atoms or an SK combination would account for the increased abundance of the $[M + 2]^{+1}$ peak. However, the difference between isotopic abundances for $C_{11}H_{19}N_2O_2S_2$ and $C_{14}H_{20}OSK$ is that the abundance of the $[M + 1]^{+1}$ peak for the $C_{14}H_{20}OSK$ cluster is 20% higher than that for $C_{11}H_{19}N_2O_2S_2$. One caveat to using isotopic distribution patterns is that they can be

corrupted by the presence of other ions, especially those that differ in the number of hydrogen atoms present (HAM et al., 2003; YAN et al., 2007b). The possibility of such interferences can be ruled out in this case because of the mass difference between the $[M]^{+1}$ and $[M + 2]^{+1}$ isotope peaks (Table 4), which is 1.997 u. If the $[M + 2]^{+1}$ peak was due to addition of two hydrogens (i.e., $[M + 2H]^{+1}$), then the mass difference would be 2.016 u based on the theoretical masses given in Table 4. The “contraction” in the mass difference between the $[M]^{+1}$ and $[M + 2]^{+1}$ peaks is due to the presence of a heteroatom, such as S or K. The experimental mass difference between the $[M]^{+1}$ and $[M + 2]^{+1}$ peaks of 1.997 u is between the theoretical mass differences of the isotopes for the two clusters, which are 1.996 u and 1.998 u for $C_{11}H_{19}N_2O_2S_2$ and $C_{14}H_{20}OSK$, respectively. While this mass difference does not help to distinguish between these two composition choices, it does rule out interference from $[M + 2H]^{+1}$. Participation of cations (e.g., K or Na) in the cluster formation was ruled out based on experiments with glycine combined with synthetic ammonium jarosite, synthetic potassium jarosite, Na_2SO_4 , or K_2SO_4 as discussed below. Therefore, $C_{11}H_{19}N_2O_2S_2$ was believed to be the best fit for the elemental composition for m/z 275, and comparison of the experimental spectrum with the theoretical spectrum of $C_{11}H_{19}N_2O_2S_2$ revealed that the two spectra were virtually identical (Fig. 4.).

Interestingly, there appeared to be a peak at m/z 259 that occurred occasionally and may be related to the m/z 275 peak. The nominal mass difference between these two peaks was 16 u. Such a difference is common for peaks that differ only in the presence of Na (22.989 u) and K (38.963 u), which have a Δm of 15.974 u. Another alternative to account for this difference is the substitution of O for S, which gives a Δm of 15.977 u

that is close to the difference between the two peaks observed at m/z 259 and 275 (Δm of 15.976 u). Therefore, the peak at m/z 259 is most likely to be the cluster ion $C_{11}H_{19}N_2O_3S$, which also matched the observed isotopic distribution. While unequivocal characterization of these cluster ions requires extensive tandem (MS/MS) and isotope exchange studies, the cluster ions observed at m/z 275 and m/z 259 were clearly organic in nature.

Glycine, the smallest amino acid, was physically mixed with synthetic ammonium or potassium jarosite to investigate how jarosite interacted with biomolecules in the laser desorption plume. Interestingly, the physical mixtures produced the same cluster ion at m/z 275 as observed in the natural samples (Fig. 2.5). In a traditional MALDI experiment, one would have expected to see a peak at m/z 76 that corresponded to the protonated version of glycine ($C_2H_5O_2NH^+$) or a peak that corresponded to a cationized glycine molecule (e.g., $C_2H_5O_2NX^+$, where $X = Na$ or K) neither of which was observed. In addition to the set of peaks around m/z 275 that had the same isotopic distribution pattern seen in the natural samples and the theoretical isotopic distribution of $C_{11}H_{19}N_2O_2S_2$ (Figs. 2.3 and 2.4), the spectrum (Fig. 2.5) also showed the same distribution of potassium and iron present in the standard synthetic jarosite spectrum. To test whether the peak at m/z 275 was distinct for glycine or general to the presence of any amino acid, the experiments were run with alanine in place of glycine. Alanine was chosen because it is the second smallest amino acid compared to glycine; in alanine one additional methyl group replaces the hydrogen side chain of glycine in the chemical structure. When synthetic jarosite was mixed homogeneously with the amino acid alanine (Fig. 6), a complex mass spectrum was observed with the most abundant peak in the

spectrum at m/z 266 and no peak observed at m/z 275. The additional methyl group affects the molecular mass of alanine, which suggests that the detection of alanine in the mass spectrometer would be different than glycine by a net change of 14 u ($-\text{CH}_2$).

Since a net change of 14 u (or multiples thereof) was not observed in the alanine-jarosite spectrum, the formation of the cluster ions is a complex gas-phase phenomenon whose mechanism is not yet understood. Comparison of the glycine and alanine results does suggest that the identity of the peak at m/z 275 is not likely to be related to any amino acid other than glycine; however, not all amino acids have been tested.

Because the LD-FTMS spectrum of glycine alone did not show any peaks (data not shown) and because there is sulfur in the cluster ion ($\text{C}_{11}\text{H}_{19}\text{N}_2\text{O}_2\text{S}_2$) of samples with jarosite, it is possible that the sulfur comes from the sulfate in the jarosite crystal lattice and is responsible for formation of the cluster ion in the laser-induced plume created during LD-FTMS analysis. When glycine was mixed homogeneously with potassium sulfate (K_2SO_4), a series of high mass fragmentation patterns were observed (Fig. 7.). The expanded region of this spectrum from m/z 270–280 showed the same peaks that were present in the natural jarosite samples, synthetic glycine-jarosite mixture, and theoretical isotopic distribution of $\text{C}_{11}\text{H}_{19}\text{N}_2\text{O}_2\text{S}_2$ (m/z 275). The potassium sulfate glycine mixture sample also produced a strong peak at m/z 259. Similar peak patterns were observed when glycine was mixed with Na_2SO_4 , which suggests that neither Na or K participate in formation of the ions. However, the most convincing evidence that Na or K cations in jarosite were not participating in the formation of the cluster ion at m/z 275 was that the combination of glycine with synthetic ammonium jarosite, which should be free from Na or K, also produced this peak.

2.5 DISCUSSION

The XRPD results shown in Fig. 2.1 indicated that the unit cell dimensions of natural jarosite samples varied. These variations indicated that an end-member composition in the natural samples was unlikely. A definitive classification of the natural samples as jarosite, natrojarosite, hydronium jarosite or ammoniojarosite based on the XRPD unit cell calculations is problematic without the addition of complete elemental analysis to determine the ratios of substituting cations relative to each other. This additional analysis would not have assisted in the determination of hydronium or ammonium ratios due to the inability of ICP-MS techniques to determine these elemental compositions. These analyses were not performed due to sample quantity limitations. Therefore, the samples were tentatively classified only by the XRPD data. Based on XRPD results, the samples from Arizona, Montana, and New Mexico are most likely jarosite. The samples from Australia and Russia are natrojarosite, while the samples from Spain and New Zealand could potentially be ammoniojarosite. The classification of the New Zealand and Spain samples as ammoniojarosite is speculative, given the rarity of this mineral subclass within the jarosite group minerals. The large unit cell dimensions could possibly be attributed to the presence of foreign ions in the structure, whose identities were not determined in this study. Potassium ions were observed in all of the LD-FTMS spectra (see Table 3.), which indicated that all of the samples contained at least some quantity of potassium in their structures.

The LD-FTMS results demonstrated that glycine was present in jarosite samples from Arizona, Australia, New Mexico, and New Zealand as evidenced by the presence of the peak at m/z 275 and its associated isotopes. The determination that the peak at m/z

275 resulted from the presence of glycine was based on a variety of mixture experiments that suggest this peak is a systematic signature when glycine was present in an ionization matrix that contains sulfate. There is no evidence from this study that conclusively determined how the glycine is associated with the mineral structure. However, because glycine could not be ionized alone by LD-FTMS, the presence of the geomatrix (i.e., jarosite) was necessary to ionize the biomolecule, as observed by Yan *et al.* (2007a). This study further validates the GALDI technique's ability to detect biomolecule impurities in geologic samples and, if applied to relevant minerals of interest to planetary geology, to aid in the search for signs of life on other planets. The ability to detect biomolecules *in situ* without extensive sample preparation is a key advantage of this technique because the mineral itself acts as the ionizing matrix. This is clearly demonstrated when glycine was analyzed alone by LD-FTMS and no peaks were observed in the spectrum until a matrix (jarosite) was present (Figs. 5 and 7).

Of equal importance is the identification of minerals or mineral groups that are capable of storing biomolecules in the geologic record and an understanding of the signatures they produce. This study has shown that jarosite samples from various worldwide locations produced ion signatures representative of organic matter, and that one of these signatures can be produced by glycine. Sulfur that is present as sulfate seems to be responsible for the ionization and detection of glycine related peaks in the samples, as evidenced by its presence in the cluster ion observed at m/z 275 in the LD-FTMS spectra of all glycine- and sulfate-containing samples (Figs. 3, 5, and 7). While the formation pathway is currently not understood, it is possible that the rather high laser fluence used means that the laser-matter interaction represents an ablation, as opposed to

a desorption, regime where recombination processes are more likely to take place (AUBRIET et al., 2005). While the other high mass peaks seen in the jarosite LD-FTMS spectra have yet to be identified, it is likely that they are organic, because their masses and isotopic distributions are consistent with combinations of carbon and hydrogen. Searches for purely inorganic combinations of ions did not result in any matches for the masses or isotopic distributions. The corresponding isotope peaks that surround these additional high mass peaks have similar distributions as those observed for glycine and likely represent combinations of the less abundant isotopes in the organic compounds, such as ^{13}C , ^{15}N , and ^{18}O , which combine to form the smaller isotope peaks (such as those in observed in the m/z 275 cluster ion). The parent molecules responsible for the charged clusters can be difficult to determine without undertaking a variety of mixture experiments like those performed in this study, which aided in the determination that the m/z 275 peak is a product of glycine ionization (see Chapter 2 Addendum). Cluster ions can be unique to specific molecules and geomatrix combinations as demonstrated by the spectrum of the synthetic jarosite-alanine mixture (Fig. 2.6), which did not produce the same m/z ions as the synthetic jarosite-glycine mixture (Fig. 2.5).

The fragmentation and cluster ion patterns also seem to be unique to the matrix-molecule combination. Synthetic jarosite, mixed with glycine, produced a simple mass spectrum where only the peak at m/z 275 and its associate isotopes were detected (Fig. 2.5) along with the jarosite signature pattern observed without glycine (Fig. 2.2).

However, when synthetic jarosite was mixed with alanine, a complex fragmentation and cluster ion pattern was observed that produced a large number of mass spectral peaks.

The mass spectrum was strikingly dissimilar to the glycine-jarosite pattern, which

supports the conclusion that the signatures observed in the natural samples could be attributed to glycine and not a simple combination of carbon, nitrogen, oxygen, and sulfur atoms that randomly produced a peak at m/z 275. A complex mass spectrum was also observed when potassium sulfate was mixed with glycine, which indicates that a wide variety of gas-phase or laser plume interactions occur that lead to many combinations of ions that can be detected by LD-FTMS. It is likely that each geomatrix-molecule combination yields a distinctive signature that can be detected by LD-FTMS and identifies both the matrix and the additional molecules present in the samples.

Jarosite has become a target mineral because it was found on the surface of Mars in 2004 (SQUYRES et al., 2004), and jarosite was chosen for this study based on its mineralogical characteristics and the possible biological influences on its formation that would lead to biosignature detection. The results in this study not only validate the GALDI technique and use of LD-FTMS, but also show that jarosite is an attractive target for identifying biosignatures in the geologic record. It is unclear from this study how glycine or the other, yet to be identified, organic molecules interact with the jarosite mineral structure. These molecules may be intercalated between crystal layers during deposition, adsorbed as surface-related contaminants, or incorporated into the crystal lattices. If the organic molecules are somehow incorporated into the jarosite crystal lattices, it is possible that they could persist throughout geologic time.

2.6 CONCLUSIONS

Our studies indicated that glycine was present in intact natural jarosite samples from 4 out of 7 worldwide locations. Additional high mass, complex ions were also observed in all 7 samples. These results are complimentary to extraction analyses that

have also shown that glycine is present in natural jarosite samples (Aubrey *et al.*, 2006). The source of the glycine or other organic molecules detected in the jarosite samples (i.e., whether they were biologically produced) and how the organic molecules are associated with the mineral matrix are unknown. While a biological origin for the organic matter is possible, because jarosite formation can be microbially mediated (ENEROTH AND KOCH 2004; BRIDGE *et al.* 2000; SASAKI AND KONNO, 2000; AKAI *et al.* 1999; KARAMANEV, 1991; CLARK *et al.*, 1993; GRISHIN *et al.* 1988), it is impossible to ascertain biogenicity without further information. Glycine may be produced abiotically (MITA *et al.*, 2002 and references therein). We cannot be certain of the origin of the glycine in the natural samples used in this study without further information. It is difficult to dismiss the possibility of a biological origin for these molecules, when the ubiquity of microorganisms in the surface environments where jarosite is typically found on Earth is considered, regardless of whether the molecules were present during deposition or were emplaced after formation. In any case the current experiments have demonstrated the direct detection of organic molecules associated with natural jarosite by LD-FTMS and suggest that the use of laser desorption mass spectrometry is an appropriate approach for the analysis of minerals returned to Earth from other planets or for *in situ* exploration on Earth.

The overall advantage of our method and instrumental approach is the ability to detect the presence of organic molecules from fragment or cluster ions observed in the LD-FTMS spectra in a relatively short time and without extensive sample preparation. This study has shown that cluster ion patterns are unique to the geomatrix-molecule combination and that organic molecules can be identified within terrestrial jarosite

samples. In addition, jarosite has been shown to be an attractive mineral for investigating biosignatures in the geologic record.

2.7 ACKNOWLEDGEMENTS

Funding for this research at the University of Montana, University of Idaho, and the Idaho National Laboratory (INL) comes from the NASA exobiology program (EXB03-0000-0054). We would like to thank the University of Montana Geology Department for the donation of several of the jarosite samples used in this study. J.M.K. and N.W.H. would like to thank John Mocko and Murray Baker for field assistance during the collection of jarosite samples from the Coromandel Peninsula, New Zealand. We would also like to thank Rohn Wood and Eric Nugent at the University of Montana as well as Tim McJunkin at the Idaho National Laboratory for technical support on this project. J.M.K would also like to thank John Maclean for many useful discussions and advise about this manuscript. LD-FTMS analysis was performed at the INL under DOE/NE Idaho Operations Office Contract DE-AC07-05ID14517.

2.8 REFERENCES

Akai, J., Akai, K., Ito, M., Nakano, S., Maki, Y., and Sasagawa, I. (1999) Biologically induced iron ore at Gunma iron mine, Japan. *American Mineralogist*, 84, 171-182.

Aubrey, A., Cleaves, H.J., Chalmer, J.H., Skelley, A.M., Mathies, R.A., Grunthaler, F.J., Ehrenfreund, P., and Bada, J.L. (2006) Sulfate minerals and organic matter on Mars. *Geology*, 34, 357-360.

Aubriet, F., Carré, V., and Muller, J.-F. (2005) Laser desorption and laser ablation Fourier transform mass spectrometry for the analysis of pollutants in complex matrices. *Spectroscopy Europe*, 17, 14-22.

Becker, U., and Gasharova B. (2001) AFM observations and simulations of jarosite

growth at the molecular scale: probing the basis for the incorporation of foreign ions into jarosite as a storage mineral. *Physics and Chemistry of Minerals*, 28, 545-556.

Beimann, K., Oro, J., Toulmin, P., Orgel, L. E., Nier, A. O., Anderson, D. M., Simmonds, P. G., Flory, D., Diaz, A. V., Rushneck, D. R., et al. (1977) The search for organic substances and inorganic volatile compounds in the surface of Mars. *Journal of Geophysical Research*, 82, 4641-4658.

Benner, S. A., Devine, K. G., Matveeva, L. N., and Powell, D. H. (2000) The missing organic molecules on Mars. *Proceedings of the National Academy of Science*, 97, 2425-2430.

Bridge, T. A. M. and Johnson, D. B. (2000) Reductive dissolution of ferric iron minerals by *Acidiphilium* SJH. *Geomicrobiology Journal* 17, 193-206.

Burns, R. G. (1987a) Ferric sulfates on Mars. *Journal of Geophysical Research*., 92, E570- E574.

Burns, R. G. (1987b) Gossans on Mars: spectral features attributed to Jarosite. *Lunar Planet. Sci. XVIII*. Abstract 141.

Burns, R. G. (1989) Terrestrial analogues to the surface rocks of Mars? *Nature*, 320, 55-56.

Christensen, P. R., Wyatt, M. B., Glotch, T.D., Rogers, A.D., Anwar, S., Arvidson, R.E., Bandfield, J.L., Blaney, D.L., Budney, C., Calvin, W.M., Fallacaro, A., Ferguson, R. L., Gorelick, N., Graff, T.G., Hamilton, V.E., Hayes, A.G., Johnson, J.R., Knudson, A.T. McSween, H.Y. Jr., Mehall, G.L., Mehall, L.K., Moersch, J.E., Morris, R.V., Smith, M.D., Squyres, S.W., Ruff, S.W., and Wolff, M.J. (2004) Mineralogy at Meridiani Planum from the Mini-TES experiment on the Opportunity Rover. *Science*, 306, 1733-1739.

Clark, T. R., Baldi, F., and Olson, G.J. (1993) Coal depyritization by the thermophilic Archaeon *Metallosphaera-Sedula*. *Applied and Environmental Microbiology*, 59, 2375-2379.

Dutrizac, J. E. (2004) The behaviour of the rare earths during precipitation of sodium, potassium and lead jarosites. *Hydrometallurgy*, 73, 11-30.

Dutrizac, J.E. and Chen, T.T. (2003) Synthesis and properties of V^{3+} analogues of Jarosite-group minerals. *The Canadian Mineralogist*, 41, 479-488.

Dutrizac, J. E. and Jambor, J. L. (2000) Jarosites and their application in hydrometallurgy. In: Alpers, C. N., Jambor, J. L., and Nordstrom, D. K. (Eds.) *Sulfate Minerals: Crystallography, Geochemistry, and Environmental Significance*. Mineralogical Society of America. Washington, DC, pp. 405-452.

Dutrizac, J. E., Hardy, D. J., and Chen, T. T. (1996) The behaviour of cadmium during jarosite precipitation. *Hydrometallurgy*, 41, 269-285.

Eneroth, E. and Koch, C. B. (2004) Fe-hydroxysulphates from bacterial Fe²⁺ oxidation. *Hyperfine Interactions*, 156, 423-429.

Gieré, R., Sidenko, N. V., and Lazareva, E. V. (2003) The role of secondary minerals in controlling the migration of arsenic and metals from high sulfide waters (Berikul Gold mine, Siberia). *Applied Geochemistry*, 18, 1347-1359.

Grishin, S. I., Bigham, J. M., and Tuovinen, O.H. (1988) Characterization of Jarosite Formed Upon Bacterial Oxidation of Ferrous Sulfate in a Packed-Bed Reactor. *Applied and Environmental Microbiology*, 54, 3101-3106.

Ham, J.E., Durham, B., and Scott, J.R. (2003) Comparison of Laser Desorption and Matrix-assisted Laser Desorption/Ionization for Ruthenium and Osmium Trisbipyridine Complexes using Fourier Transform Mass. *Journal of American Society for Mass Spectrometry* 17, 393-400.

Hofstra, A. H., Snee, L. W., Rye, R. O., Folger, H. W., Phinisey, J. D., Loranger, R. J., Dahl, A. R., Naeser, C. W., Stein, H. J., and Lewchuck, M. T. (1999) Age constraints on Jerritt Canyon and other Carlin-type gold deposits in the western United States: Relationship to mid-tertiary extension and magmatism. *Economic Geology*, 94, 769-802.

Karamanev, D. G. (1991) Model of the Biofilm Structure of Thiobacillus-Ferrooxidans. *Journal of Biotechnology*, 20, 51-64.

Karas, M., Bachman, D., Bahr, U., and Hillenkamp, F. (1987) Matrix-Assisted Ultraviolet Laser Desorption of Non-Volatile Compounds. *Int. J Mass Spectrom Ion Proc*, 78, 53-68.

Kim, S., Rogers, R.P., and Marshall, A.G. (2006) Truly "exact" mass: Elemental Compositions can be determined uniquely from molecular mass measurement at ~0.1 mDa accuracy for molecules up to ~500 Da. *International Journal of Mass Spectrometry*, 251, 260-265.

Klingelhofer, G., Morris, R. V., Bernhardt, B., Schröder, C., Rodionov, D.S., de Souza, P.A. Jr., Yen, A. Gellert, R., Evlanov, E.N., Zubkov, B., Foh, J., Bonnes, U. Kankeleit, E., Gütlich, P., Ming, D.W., Renz, F., Wdowiak, T., Squyres, S.W., and Arvidson, R.E. (2004) Jarosite and hematite at Meridiani Planum from Opportunity's Mossbauer spectrometer. *Science*, 306, 1740-1745.

Mathews, C. K., van Holde, K. E., and Ahern, K. G. (1999) Biochemistry: 3rd Edition. An imprint of Addison Wesley Longman, Inc. San Francisco, CA, USA.

- McLafferty, F. W. and Tureček, F. (1993) Interpretation of Mass Spectra: 4th Edition. University Science Books, Sausalito, CA, USA.
- Mita, H., Shirakura, N., Yokoyama, H., Nomoto, S., and Shimoyama, A. (2002) Kinetic Studies of abiotic amino acid formation by UV-irradiation. *Advances in Space Research*, 33, 1282-1288.
- Navarro-González, R., Navarro, K.F., de la Rosa, J., Iñiguez, E., Molina, P., Miranda, L.D., Morales, P., Cienfuegos, E., Coll, P., Raulin, F., Amilis, R., and McKay, C.P. (2006) The limitations on organic detection in Mars-like soils by thermal volatilization-gas chromatography-MS and their implications for the Viking results. *Proceedings of the National Academy of Sciences*, 103, 16089-16094.
- Navrotsky, A., Forray, F. L., and Drouet, C. (2005) Jarosite stability on Mars. *Icarus*, 176, 250-252.
- Sack, T. M., Lapp, R. L., Gross, M. L., and Kimble, B. J. (1984) A method for the statistical evaluation of accurate mass measurement quality. *International Journal of Mass Spectrometry and Ion Processes*, 61, 191-213.
- Sasaki, K. and Konno, H. (2000) Morphology of jarosite-group compounds precipitated from biologically and chemically oxidized Fe ions. *Canadian Mineralogist*, 38, 45-56.
- Scott, J. R. and Tremblay, P.L. (2002) Highly reproducible laser beam scanning device for an internal source laser desorption microprobe Fourier transform mass spectrometer. *Review of Scientific Instruments*, 73, 1108-1116.
- Skelley, A. M., Scherer, J. R., Aubrey, A. D., Grover, W. H., Ivester, R. H. C., Ehrenfreund, P., Grunthaner, F. J., Bada, J. L., and Mathies, R. A. (2004) Development and evaluation of a microdevice for amino acid detection and analysis on Mars. *Proceedings of the National Academy of Science*, 102, 1041-1046.
- Spell, T. L, DeLong, S. E., and Creasy, W. R., (1993) Characterization of Fourier transform ion cyclotron resonance mass spectrometry for quantitative isotope ratio measurements. *Int. J. Mass Spectrom. Ion Processes* 124, 223-239.
- Squyres, S. W., Grotzinger, J. P., Arvidson, R.E., Bell, J.F., III, Calvin, W., Christensen, P.R., Clark, B.C., Crisp, J.A., Farrand, W.H., Herkenhoff, K.E., Johnson, J.R., Klingelhöfer, G., Knoll, A.H., McLennan, S.M., McSween, H.Y. Jr., Morris, R.V., Rice, J.W. Jr., Rieder, R., and Soderblom, L.A. (2004) In situ evidence for an ancient aqueous environment at Meridiani Planum, Mars. *Science*, 306, 1709-1714.
- Squyres, S. W. and Knoll, A. H. (2005) Sedimentary rocks at Meridiani Planum: Origin, diagenesis and implications for life on Mars. *Earth and Planetary Letters*, 240, 1-10.

Stroffegen, R. E., Alpers, C. N., and Jambor, J. L. (2000) "Alunite-jarosite crystallography, thermodynamics, and geochronology." In: Alpers, C. N., Jambor, J. L., and Nordstrom, D. K. (Eds.) Sulfate minerals: Crystallography, Geochemistry, and Environmental Significance. Mineralogical Society of America. Washington, DC, pp. 453-479.

Yan, B., McJunkin, T.J., Stoner, D.L., and Scott, J.R. (2006) Validation of Fuzzy Logic Method for Automated Mass Spectral Classification for Mineral Imaging. *Applied Surface Science*, 253, 2011–2017.

Yan, B., Stoner, D.L., Kotler, J.M., Hinman, N.W., and Scott, J.R. (2007a) Detection of Biosignatures by Geomatrix-Assisted Laser Desorption/Ionization (GALDI) Mass Spectrometry. *Geomicrobiology Journal*, in press.

Yan, B., Stoner, D.L., and Scott, J.R. (2007b) Direct LDI-FTMS Detection of Mineral-Associated PAHs and Their Influence on the Detection of Other Organics," *Talanta*. [in press]

CHAPTER 2 :ADDENDUM

The exact structure of the cluster ion ($C_{11}H_{19}N_2O_2S_2^+$) attributed to glycine at m/z 275 is unknown. The ion does not appear to be a simple gas-phase version of a traditional organic molecule or a dimer or trimer of a traditional organic molecule as is often observed in mass spectrometry (SCOTT et al., 2000; TOMLINSON et al., 1999).

Instead, it is likely to be similar to a matrix adduct, a phenomenon observed in MALDI (HAM et al., 2003). Odd rearrangements, including loss of hydrogen atoms with and without addition of other fragments as well as sulfur for oxygen exchanges have been reported (GREENWOOD et al., 2000; GROENEWOLD et al., 2001a; GROENEWOLD et al., 2001b; GROENEWOLD et al., 2001c). These scenarios are likely because the laser fluence on the LD-FTMS (see methods sections Chapter 2) may put us in the ablation regime, where rearrangements are more likely (BOUILLY et al., 2007; FAN et al., 2008; VLADOIU

et al., 2008). Additionally, there is evidence for an oxygen for sulfur exchange converting m/z 275 to m/z 259 as discussed in Chapter 2 (page 67). Such O for S exchanges have been reported (GROENEWOLD et al., 2001a) and tend to be dependent on the vacuum chamber pressure.

REFERENCES

- Bouilly, D., Perez, D., and Lewis, L. J., 2007. Damage in materials following ablation by ultrashort laser pulses: A molecular-dynamics study. *Physical Review B* **76**, 453-461.
- Fan, X., Little, M. W., and Murray, K. K., 2008. Infrared laser wavelength dependence of particles ablated from glycerol. *Applied Surface Science* **255**, 1699-1704.
- Groenewold, G. S., Hodges, B. D. M., Scott, J. R., Gianotto, A. K., Appelhans, A. D., Kessinger, G. F., and Wright, J. B., 2001a. Oxygen-for-sulfur exchange in the gas phase: Reactions of Al and Si oxyanions with H₂S. *Journal of Physical Chemistry A* **105**, 4059-4064.
- Groenewold, G. S., Kessinger, G. F., Scott, J. R., Gianotto, A. K., Appelhans, A. D., Delmore, J. E., and Avci, R., 2001b. Secondary ion mass spectrometry of zeolite materials: Observation of abundant aluminosilicate oligomers using an ion trap. *Analytical Chemistry* **73**, 226-232.
- Groenewold, G. S., Scott, J. R., Gianotto, A. K., Hodges, B. D. M., Kessinger, G. F., Benson, M. T., and Wright, J. B., 2001c. Gas-phase condensation reactions of Si_xO_yH_z⁻ oxyanions with H₂O. *Journal of Physical Chemistry A* **105**, 9681-9688.
- Ham, J. E., Durham, B., and Scott, J. R., 2003. Comparison of laser desorption and matrix-assisted laser desorption/ionization for ruthenium and osmium trisbipyridine complexes using Fourier transform mass spectrometry. *Journal of the American Society for Mass Spectrometry* **14**, 393-400.
- Scott, J. R., Groenewold, G. S., Gianotto, A. K., Benson, M. T., and Wright, J. B., 2000. Experimental and computational study of hydration reactions of aluminum oxide anion clusters. *Journal of Physical Chemistry A* **104**, 7079-7090.
- Tomlinson, M. J., Scott, J. R., Wilkins, C. L., Wright, J. B., and White, W. E., 1999. Fragmentation of an alkali metal-attached peptide probed by collision-induced dissociation Fourier transform mass spectrometry and computational methodology. *Journal of Mass Spectrometry* **34**, 958-968.

CHAPTER 3: LABORATORY SIMULATIONS OF PREBIOTIC MOLECULE STABILITY IN THE JAROSITE MINERAL GROUP; END MEMBER EVALUATION OF DETECTION AND DECOMPOSITION BEHAVIOR RELATED TO MARS SAMPLE RETURN

J. Michelle Kotler^a, Nancy W. Hinman^{a*}, C. Doc Richardson^a, Andrew G. Conly^b and Jill R. Scott^c

^aGeosciences Department, 32 Campus Drive University of Montana, Missoula, MT USA 59812; ^bDepartment of Geology, Lakehead University, 955 Oliver Road, Thunder Bay, ON Canada P7B 5E1; ^cChemical Sciences, Idaho National Laboratory 1765 N. Yellowstone Hwy, Idaho Falls USA, ID 83415

*Corresponding author- Nancy W. Hinman, Geosciences Department, 32 Campus Drive University of Montana, Missoula, MT USA 59812, email- nancy.hinman@umontana.edu, Phone- (406) 243- 4277, Fax – (406) 243-4026

3.1 ABSTRACT

Recently, the prebiotic amino acid glycine has been found associated with natural jarosite samples from locations around the world. Since the discovery of jarosite on Mars, extensive research focuses on linking this mineral group with possible detection of biosignatures in the geologic record on Earth and Mars. Multiple analytical methods, including extraction and mass spectrometry techniques, have identified glycine and other biomolecules in jarosite samples. The jarosite end members jarosite (*sensu stricto*-potassium jarosite), natrojarosite (sodium jarosite), and ammoniojarosite (ammonium jarosite) have different thermodynamic stabilities, decompose at different rates, and have potentially different susceptibilities to substitution. The relationship between the thermodynamic stability of the jarosite end members and the effect that glycine has on

the thermal decomposition behavior of each end member was investigated using thermal gravimetric analysis. Introducing glycine into the synthesis procedure (75 ppm) of the potassium, sodium and ammonium jarosite end-member has elucidated the effects that glycine has on the thermal stability of the mineral group. Potassium jarosite appears to be the least susceptible to the effects of glycine, with the sodium and ammonium end members showing marked changes in thermal decomposition behavior and decomposition rates. These results suggest that the sodium and ammonium jarosites are more suitable targets for identifying signs of prebiotic or biotic activity on Mars and Earth than the potassium jarosites. These results have implications for current *in situ* investigations of the martian surface and future sample return missions.

Keywords- jarosite, glycine, thermodynamic stability, prebiotic, Mars, Sample return

3.2 INTRODUCTION

Sample return missions from Mars present an exciting possibility to enhance our knowledge about the planet using analytical instrumentation and techniques that are not viable for space flight (DesMarais et al., 2008). The scientific community has compiled various recommendations on how to appropriately plan a sample return mission from Mars (NRC, 1978; NRC, 1990a; NRC, 1990b; NRC, 1994; NRC, 1996; NRC, 2001; NRC, 2002; NRC, 2007). In a recently published report by the Mars Exploration Program Analysis Group (MEPAG) Next Decade Science Analysis Group (ND-SAG), high priority geologic and astrobiological targets were identified for Mars sample return (DesMarais et al., 2008). Mineral targets included aqueous phyllosilicate clay minerals,

such as nontronite and montmorillonite, that were identified by the Mars Express Orbiter (Bibring et al., 2006; Bibring et al., 2005; Poulet et al., 2005), and sulfate minerals, such as jarosite, that were identified by the Mars Exploration Rover Mission (Klingelhofer et al., 2004; Knoll et al., 2005; Squyres et al., 2004a; Squyres et al., 2004b; Squyres and Knoll, 2005).

The hydrous sulfate mineral jarosite is found in many environments on Earth, in meteorites and asteroids, and on the martian surface (Christensen et al., 2004; Cochran and Vilas, 1997; Klingelhofer et al., 2004; Madden et al., 2004; Osawa et al., 2003; Squyres et al., 2004a; Squyres et al., 2004b). Squyres and Knoll (2005) suggested that the origin and characteristics of the mineral group make it an ideal candidate to store evidence for the existence of extant or extinct life on Mars. Jarosite is an attractive mineral in the search for biosignatures in the geologic record and an excellent target for Mars sample return because researchers have identified several amino acids associated with jarosite on Earth (Aubrey et al., 2006; Kotler et al., 2008; Skelley et al., 2005).

Sample sterilization and/or heat treatment to maintain planetary protection is discussed in the MEPAG ND-SAG (DesMarais et al., 2008) report. The group concluded that heat sterilization would have a detrimental effect on the samples, especially those samples targeted for biological and/or aqueous studies (DesMarais et al., 2008). Thermal analysis techniques (Wendlandt, 1986), although destructive, can provide valuable information while heating the samples to temperatures within the sterilization range (up to 500 °C). Thermal analysis has been shown to differentiate biotic and abiotic minerals by changes in on-set temperatures (Stalport et al., 2005; Stalport et al., 2007), and thermal analysis techniques were recently used on the Phoenix Mission that landed in the

martian arctic (Banks, 2008; Guinn et al., 2008). Combining sterilization with thermal analysis techniques could therefore provide a reasonable compromise between planetary protection and scientific payoff.

In addition to astrobiological interest, the jarosite minerals have characteristics that make them attractive in reconstructing geologic history. Jarosite minerals belong to the alunite supergroup, which contains over 40 minerals. The supergroup is subdivided based on the trivalent metal cation present in tetrahedral coordination that forms the backbone of the mineral (Jambor, 1999). In the jarosite group, the dominant transition metal cation that occupies this site is Fe^{3+} . The jarosite group minerals have the general formula $\text{XFe}_3(\text{SO}_4)_2(\text{OH})_6$, where X is a monovalent cation, the identity of which depends on the chemistry of the depositional environment. The most common cations to fill this position are K^+ (jarosite, sensu stricto), Na^+ (natrojarosite), Ag^+ (argentojarosite), NH_4^+ (ammoniojarosite), and H_3O^+ (hydronium jarosite) (Stoffregen et al., 2000). Rare earth elements (REEs) have been shown to incorporate into jarosite minerals in proportions as high as 3.7 % (Dutrillac, 2004), and atomic force microscopy studies of jarosite indicate that the mineral is capable of incorporating many different ions into its crystal structure (Becker and Gasharova, 2001). Thermodynamic values vary for jarosite end members with jarosite (potassium jarosite, sensu-stricto) being the most stable (Baron, 1996). Understanding which jarosite minerals to target for astrobiological investigations based on stability and susceptibility to substitution, could help refine sample selection criteria for sample return missions. Additionally, valuable composition information could aid in reconstructing the geologic history of Mars.

Our recent studies of natural jarosite samples with a technique called geomatrix-assisted laser desorption/ionization Fourier transform mass spectrometry (GALDI-FTMS) (Yan et al., 2007) indicate that the amino acid, glycine, was present in several samples (Kotler et al., 2008). Herein we report the results of experiments to determine the effect that glycine has on stability and thermal properties of the jarosite group minerals. By adding glycine to the jarosite synthetic procedure, we sought to determine whether a structural relationship exists that would indicate possible incorporation of glycine into the jarosite structure and if there is a correlated thermodynamic relationship between jarosites that would affect the degradation rates. Thermal Gravimetric Analysis (TGA) has been used extensively in the study of the jarosite minerals and has been shown to be a technique that is highly sensitive to jarosite composition (Frost et al., 2005; Frost et al., 2006a; Frost et al., 2006b). Thermal analyses of the jarosite end members (K-jarosite, Na-jarosite, and NH₄-jarosite), end member glycine syntheses (jarosite-SWG), and physical mixtures of the jarosite end member with glycine (jarosite-PMG) are presented to determine the relative rates of degradation within the samples. Additionally, a method to determine composition and site occupancy from TGA for *in situ* analysis on Mars and for sample return missions is presented should heat treatment of the samples render them useless for crystallographic studies.

3.3 METHODS

3.3.1 SYNTHESSES

K-jarosite ($\text{KFe}_3(\text{SO}_4)_2(\text{OH})_6$), Na-jarosite ($\text{NaFe}_3(\text{SO}_4)_2(\text{OH})_6$), and NH_4 -jarosite ($\text{NH}_4\text{Fe}_3(\text{SO}_4)_2(\text{OH})_6$) were prepared according to the method described in Dutrizac and Chen, 2003, and also presented in Kotler et al. (2008). Potassium sulfate, sodium sulfate or ammonium sulfate (0.4 M K_2SO_4 , Na_2SO_4 , and $(\text{NH}_4)_2\text{SO}_4$) were added to a 0.4 M FeCl_3 solution in a 100-mL round bottom flask maintaining a stoichiometric ratio of 2:3 sulfate salt to ferric iron during reaction. The solution was stirred under reflux conditions at 100 °C for 24 hours. In order to collect the precipitate, the solutions were vacuum filtered while hot using a Buchner funnel and Whatman #4 filter paper. The precipitates were washed under vacuum three times with 1L of deionized water and air-dried. Substitution (jarosite-SWG) experiments were performed by adding 1 mM (75 ppm) concentrations of glycine (Sigma-Aldrich, MA) to the synthetic procedure using the same temperature, time, and washing procedures as the standard jarosite syntheses. Powdered samples were mounted on glass slides for random X-ray powder diffraction (XRD) analysis to ensure purity and for phase identification. X-ray diffraction analyses were performed on randomly oriented powders using a Philips APD 3720 X-ray diffractometer (Natick, MA) using a step size of 0.02 °2 θ and a rate of 0.750 °2 θ / min. Patterns were compared to jarosite synthetic Joint Committee on Powder Diffraction Standards (JCPDS) file 22-0827.

3.3.2 THERMAL ANALYSIS

Thermal analyses were obtained using a TA Instruments model 2950 thermogravimetric analyzer (TGA) (New Castle, DE). Mixture experiments using glycine with synthetic jarosite (jarosite-PMG) were prepared by mixing ~3-5 % analyte with jarosite matrix before TGA preparations. Sample masses varied between 15 – 20 mg and were heated in a platinum sample holder at a constant ramping of temperature between ambient and 950°C at a rate of 5°C/ min. Replicate analyses of the K-jarosite standard were performed to assess the reproducibility of the measurements. The standard deviation was calculated to be 0.176 °C/ min with a relative standard deviation (RSD) of 0.45 %. All rate calculations and analysis of TGA data was performed using TA Thermal Advantage Universal Analysis software. Instrument measurements are reported in weight % (elevation in Idaho Falls, ID \approx 1430 m), however, convention has shifted to report the units as Mass %.

3.4 RESULTS

3.4.1 THERMOGRAVIMETRIC ANALYSIS

Figure 3.1 shows the decomposition (A) and derivative mass (B) curves for glycine alone. The decomposition proceeds through two major steps starting at 37.99 °C and ends at 686.23 °C with a total mass loss of 100 %. The total decomposition rate is - 0.172 % °C⁻¹. The derivative mass curve shows one major peak at 240 °C. This 240 °C

peak was used an indicator peak for glycine in the jarosite thermal analyses for the synthesis experiments (jarosite-SWG) and physical mixture experiments (jarosite-PMG).

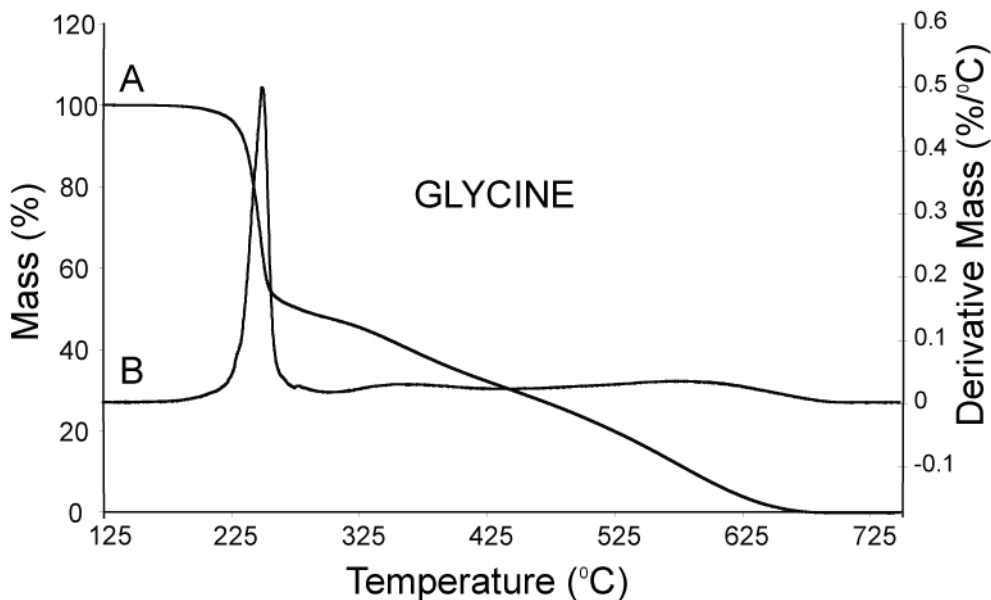


Figure 3.1 Thermal decomposition (A) and derivative mass (B) curves for glycine. Two major mass loss steps are shown from 37.99 – 260.14 (47.38 % loss), and 260.14 – 686.23 °C (100 % loss) with a decomposition rate of -0.172 % °C⁻¹ with a derivative mass peak observed at 240 °C.

Samples were not dried prior to analysis so minor mass losses did occur for some samples below 100 °C, these losses were attributed to ambient hydration and are not presented or discussed. Decomposition behavior between K-jarosite-SWG and K-jarosite varies slightly; the onset temperature was lower for K-jarosite-SWG (127.32 °C vs. 158.69 °C; see table 1) than for K-jarosite. After the onset of decomposition, both samples followed similar decomposition steps with little variation in temperature until the final decomposition step. The K-jarosite-SWG sample completes decomposition at 825.44°C with a total mass loss of 39.58 % compared to 762.61 °C and 39.22 % for K-

jarosite. Both decompositions occurred in a total of 6 steps. The total decomposition rates were slightly different; $-0.0579\% \text{ } ^\circ\text{C}^{-1}$ for K-jarosite and $-0.0555\% \text{ } ^\circ\text{C}^{-1}$ for K-jarosite-SWG. The total decomposition temperatures (ΔT_{total}) showed an increase between the K-jarosite and the K-jarosite-SWG. K-jarosite-SWG had a broader decomposition temperature range ($750.72\text{ } ^\circ\text{C}$) than the K-jarosite ($603.92\text{ } ^\circ\text{C}$). When the potassium jarosite standard was mixed with glycine instead of synthesized in the presence of, the decomposition behavior is markedly different. The onset temperature for the K-jarosite-PMG was $186.04\text{ } ^\circ\text{C}$ with a steady mass loss slope of $0.117\% \text{ } ^\circ\text{C}^{-1}$ and then leveled out again after $518.76\text{ } ^\circ\text{C}$. Final decomposition occurs at $757.68\text{ } ^\circ\text{C}$ where the total mass loss was 56.32% . Decomposition occurred in four steps with a total decomposition rate of $-0.0870\% \text{ } ^\circ\text{C}^{-1}$. The ΔT_{total} was $718.72\text{ } ^\circ\text{C}$.

Table 4Table 3.1. Thermal analysis of the jarosite standard synthetic samples, jarosite glycine syntheses (jarosite-SWG), and jarosite glycine mixtures (jarosite-PMG) including transition temperatures, total mass loss, total decomposition rates, rates per step, and total temperature change (ΔT_{total}) from onset to final.

<i>Sample</i>	<i>Step</i>	<i>Transition Temperatures ($^\circ\text{C}$)</i>	<i>% original weight</i>	<i>Rate per step ($\% \text{ } ^\circ\text{C}^{-1}$)</i>
K-jarosite Total weight loss: 39.22 % Decomposition rate = $-0.0579\% \text{ } ^\circ\text{C}^{-1}$ $\Delta T_{\text{total}} = 603.92\text{ } ^\circ\text{C}$	1	158.69 — 317.91	99.71	-0.025
	2	317.91 — 418.25	86.94	-0.104
	3	418.25 — 537.64	85.13	-0.007
	4	537.64 — 630.64	80.05	-0.059
	5	630.64 — 707.40	64.95	-0.219
	6	707.40 — 762.61	60.78	-0.087
K-jarosite-SWG Total weight loss: 39.58 % Decomposition rate =	1	127.32 — 320.80	96.04	-0.019
	2	320.80 — 429.63	86.15	-0.091

$-0.0555 \text{ \% } ^\circ\text{C}^{-1}$ $\Delta T_{\text{total}} = 750.72 \text{ } ^\circ\text{C}$	3	429.63 — 562.55	85.21	-0.007
	4	562.55 — 663.39	80.00	-0.058
	5	663.39 — 746.98	64.90	-0.189
	6	746.96 — 825.44	60.42	-0.033
K-jarosite-PMG Total weight loss: 56.32 % Decomposition rate = $-0.0870 \text{ \% } ^\circ\text{C}^{-1}$ $\Delta T_{\text{total}} = 718.72 \text{ } ^\circ\text{C}$	1	186.04 — 518.76	59.54	-0.117
	2	518.76 — 610.03	56.81	-0.023
	3	610.03 — 757.68	43.68	-0.109
Na-jarosite Total weight loss: 39.91 % Decomposition rate = $-0.0840 \text{ \% } ^\circ\text{C}^{-1}$ $\Delta T_{\text{total}} = 510.41 \text{ } ^\circ\text{C}$	1	251.61 — 370.97	97.61	-0.017
	2	370.97 — 452.51	87.44	-0.145
	3	452.51 — 589.69	84.49	-0.018
	4	589.69 — 762.02	60.09	-0.175
Na-jarosite-SWG Total weight loss: 40.39 % Decomposition rate = $-0.0788 \text{ \% } ^\circ\text{C}^{-1}$ $\Delta T_{\text{total}} = 606.24 \text{ } ^\circ\text{C}$	1	230.56 — 365.93	97.50	-0.016
	2	365.93 — 455.29	87.51	-0.124
	3	455.29 — 602.65	84.50	-0.018
	4	602.65 — 836.80	59.61	-0.119
Na-jarosite-PMG Total weight loss: 43.32 % Decomposition rate = $-0.0810 \text{ \% } ^\circ\text{C}^{-1}$ $\Delta T_{\text{total}} = 632.38 \text{ } ^\circ\text{C}$	1	182.51 — 382.68	86.83	-0.069
	2	382.68 — 448.73	77.12	-0.166
	3	448.73 — 582.72	73.22	-0.026
	4	582.72 — 814.89	52.37	-0.107
NH₄-jarosite Total weight loss: 50.68 % Decomposition rate = $-0.1007 \text{ \% } ^\circ\text{C}^{-1}$ $\Delta T_{\text{total}} = 520.51 \text{ } ^\circ\text{C}$	1	235.57 — 312.76	97.98	-0.021
	2	312.76 — 439.88	82.72	-0.132
	3	439.88 — 562.38	80.83	-0.014
	4	562.38 — 756.08	49.32	-0.216
NH₄-jarosite-SWG	1	154.66 — 216.98	99.54	-0.005

Total weight loss: 54.21 % Decomposition rate = $-0.0852 \text{ \% } ^\circ\text{C}^{-1}$ $\Delta T_{\text{total}} = 696.80 \text{ } ^\circ\text{C}$	2	216.98 — 242.95	95.85	-0.149
	3	242.95 — 303.57	93.71	-0.029
	4	303.57 — 442.22	78.53	-0.120
	5	442.22 — 610.76	75.66	-0.014
	6	610.76 — 851.46	45.79	-0.360
	NH₄-jarosite-PMG Total weight loss: 56.70 % Decomposition rate = $-0.0900 \text{ \% } ^\circ\text{C}^{-1}$ $\Delta T_{\text{total}} = 743.58 \text{ } ^\circ\text{C}$	1	180.62 — 238.01	96.74
2		238.01 — 241.21	94.88	-0.556
3		241.21 — 325.62	90.28	-0.048
4		325.62 — 445.47	75.40	-0.130
5		445.47 — 568.47	72.56	-0.019
6		568.47 — 924.20	43.13	-0.082

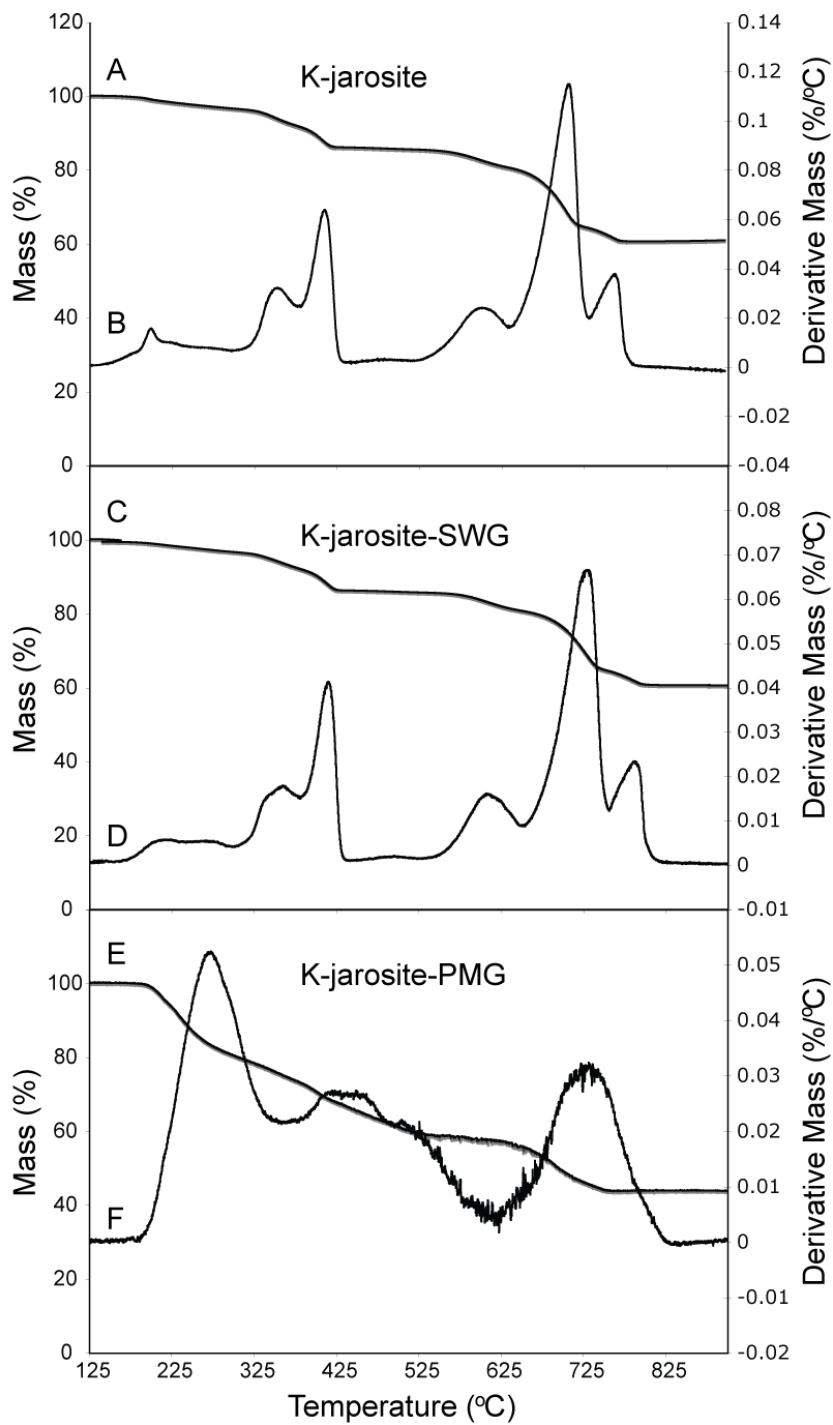


Figure 3.2 shows the results of the thermal decomposition and derivative mass curves of K-jarosite (A, B), K-jarosite-SWG (C, D), and K-jarosite-PMG (E, F).

The derivative mass curves for the K-jarosite (3.2 B) shows one minor peak at 210 °C, two prominent peaks from 325 – 425 °C and three major peaks from 550 – 825

°C. The derivative mass curve for K-jarosite-SWG (figure 3.2 D) has a similar peak pattern, but the minor peak at 210 °C is more diffuse. The derivative mass pattern for K-jarosite-PMG (figure 3.2 F) does not resemble either the K-jarosite or K-jarosite-SWG derivative mass curves. There is a major peak at 275 °C and three diffuse peaks from 400 – 825 °C. The indicator peak for glycine at 240 °C is not observed as a sharp peak as it is in the derivative mass curve of glycine alone (figure 3.1 B) for the K-jarosite-SWG or K-jarosite-PMG derivative mass curves, however, there is an increase in the derivative mass in the regions where glycine should be observed in both the K-jarosite-SWG and K-jarosite-PMG derivative mass curves.

Figure 3.3 displays the decomposition and derivative mass curves of Na-jarosite (A, B), Na-jarosite-SWG (C, D), and the Na-jarosite-PMG (E, F). The Na-jarosite-SWG sample began to degrade at a slightly lower temperature than the Na-jarosite (230.56 °C vs. 251.61 °C). The patterns were similar until the final decomposition step (step 4, see table 1) when the Na-jarosite-SWG was completely degraded at a higher temperature than that of the Na-jarosite (836.80 °C vs. 762.02 °C). The total mass loss for the Na-jarosite-SWG was 40.39 % and the Na-jarosite total mass loss was 39.91 %. The total decomposition rate was slower for the Na-jarosite-SWG than for the Na-jarosite (-0.0840 % °C⁻¹ vs. -0.0788 % °C⁻¹). The total decomposition temperatures also varied with the Na-jarosite-SWG degrading over a greater temperature range ($\Delta T_{\text{total}} = 632.38$ °C) than the Na-jarosite ($\Delta T_{\text{total}} = 606.24$ °C). The Na-jarosite-PMG begins to degrade at 182.51 °C at a mass loss rate of -0.069 % °C⁻¹ until 382.68 °C. The mixture sample continued to degrade until 708.92 °C with a total mass loss of 43.32 %. The Na-jarosite, Na-jarosite-SWG, and the Na-jarosite-PMG all degraded in a total of 4 steps.

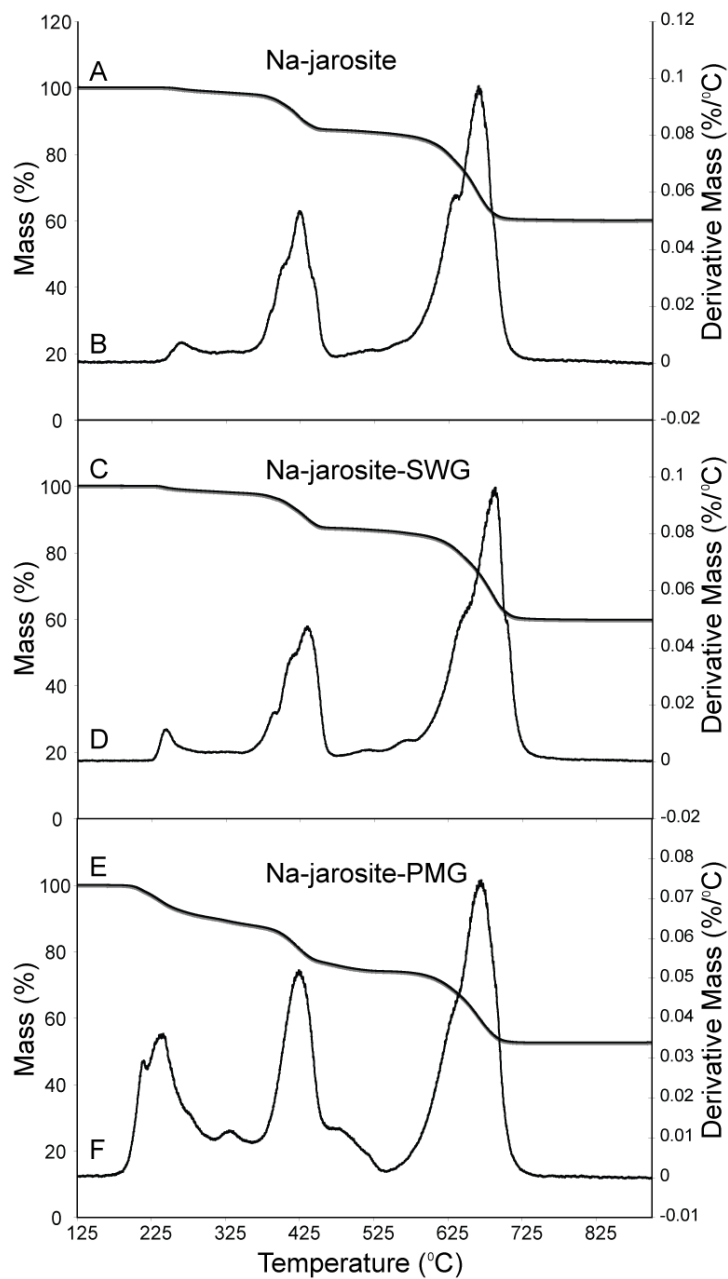


Figure 3.3. Thermal decomposition and derivative mass curves for Na-jarosite (A, B), Na-jarosite-SWG (C, D), and Na-jarosite-PMG (E, F).

The derivative mass curve for Na-jarosite (figure 3.3 B) shows a minor peak at 275 °C, another major peak from 375 – 450 °C that contains a minor shoulder peak at 400 °C, and another major peak from 600 – 725 °C with a shoulder peak at 650 °C. The derivate mass pattern for Na-jarosite-SWG (figure 3.3 D) has a similar peak pattern to

Na-jarosite (figure 3.3 B), however, the minor peak is shifted to a lower temperature (240 °C) than the minor peak in the Na-jarosite that occurs at 275 °C. Additionally, the other major peaks in the derivative mass pattern are shifted 10 °C towards higher temperature consistent with the temperature shifts seen in the decomposition curves for Na-jarosite (figure 3.3 A) and Na-jarosite-SWG (figure 3.3 C). The derivative mass curve for Na-jarosite-PMG (figure 3.2 F) resembles both the Na-jarosite derivative mass curve (figure 3.2 B) and Na-jarosite-SWG derivative mass curve (figure 3.3 D) however, there are two additional peaks. The first additional peak is observed at 200 °C. It is adjacent to the peak that is present at 240 °C in the same position as the first peak in the Na-jarosite-SWG derivative curve. The second additional peak is observed at 325 °C. The 240 °C glycine indicator peak is observed in the Na-jarosite-PMG derivative mass curve and also in the Na-jarosite-SWG derivative mass curve. It is unclear whether the peak observed at 240 °C in the Na-jarosite-SWG is a result of glycine or is related to the shift of the 275 °C peak in the Na-jarosite derivative mass curve.

Figure 3.3 shows the decomposition and derivative mass curves for NH₄-jarosite (A, B), NH₄-jarosite-SWG (C, D), and NH₄-jarosite-PMG (E, F). The decomposition behavior of the NH₄-jarosite differed from that of the NH₄-jarosite-SWG sample starting at the onset temperature. The NH₄-jarosite-SWG sample began to degrade at 154.66 °C and then proceeded through 6 decomposition steps ending at 851.46 °C with a total mass loss of 54.21 % (see table 1). There is very little similarity between the NH₄-jarosite-SWG and the NH₄-jarosite decomposition curve, which begins to degrade at 235.57 °C and proceeded through only 4 decomposition steps with a final decomposition temperature of 756.08 °C for a total mass loss of 50.68 %. The decomposition rates were

also different with the NH_4 -jarosite-SWG degrading at a slower rate ($-0.0852\% \text{ } ^\circ\text{C}^{-1}$) than NH_4 -jarosite ammonium ($-0.1007\% \text{ } ^\circ\text{C}^{-1}$). The NH_4 -jarosite-PMG decomposition is different from both the NH_4 -jarosite and the NH_4 -jarosite-SWG. The onset temperature for the NH_4 -jarosite-PMG was $180.62\text{ } ^\circ\text{C}$ and the sample proceeded through 6 decomposition steps ending at $924.20\text{ } ^\circ\text{C}$ with a total mass loss of 56.70% and a decomposition rate of $-0.0900\% \text{ } ^\circ\text{C}^{-1}$.

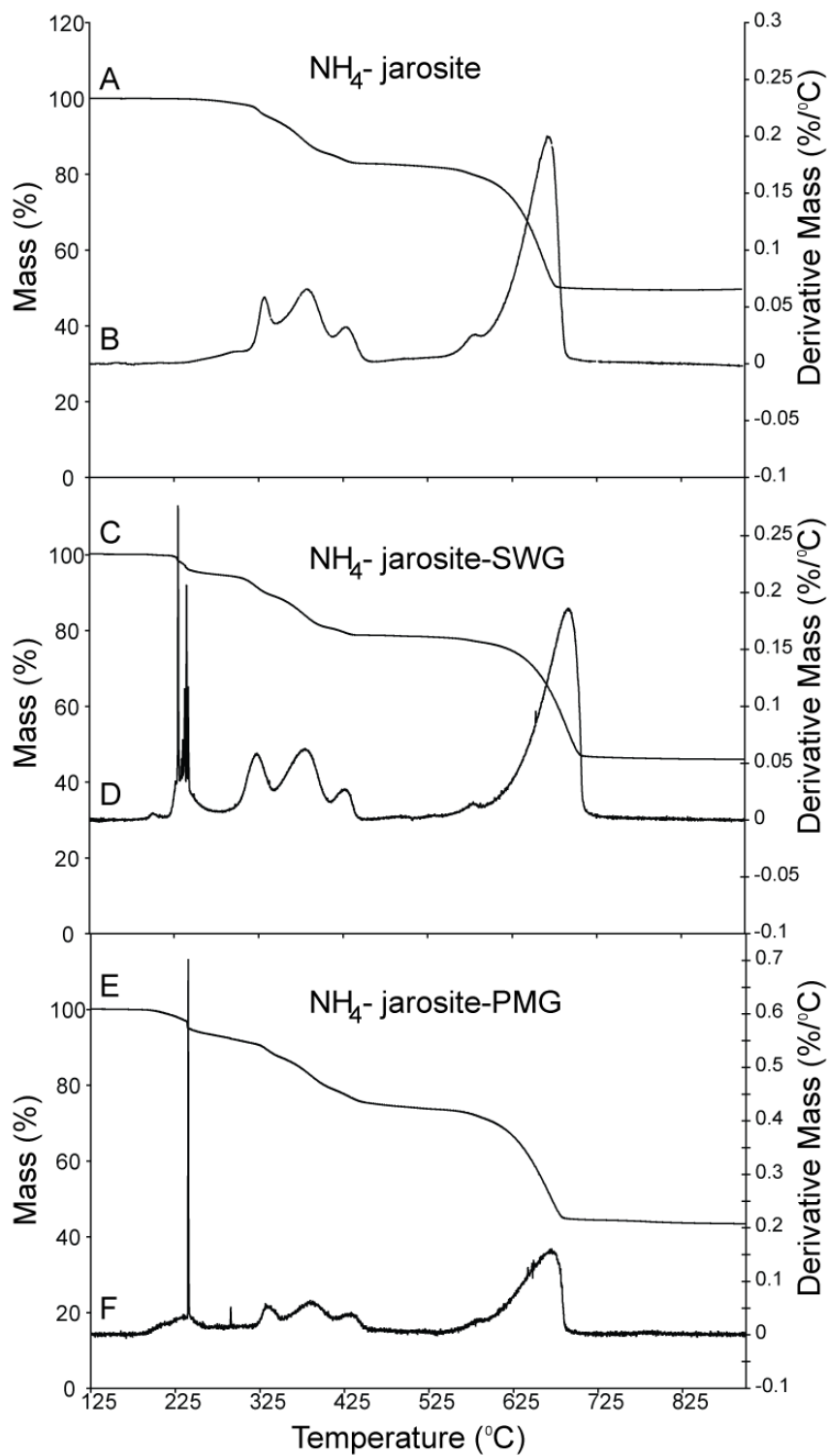


Figure 3.4. Thermal decomposition and derivative mass curves for NH_4 -jarosite (A, B), NH_4 -jarosite-SWG (C, D), and NH_4 -jarosite-PMG (E, F).

The derivative mass curve for NH_4 -jarosite (figure 3.3 B) shows 3 major peaks from 310 – 475 °C, a minor peak at 600 °C, and another major peak at 675 °C. The derivative mass curve for NH_4 -jarosite-SWG (figure 3.3 D) is similar to the derivative mass for NH_4 -jarosite, however, there are three additional peaks and several of the other peaks are shifted in comparison. The three additional peaks are present at 200, 210, and 240 °C. The peaks in the 310 – 475 °C region for NH_4 -jarosite-SWG derivative curve are shifted towards lower temperatures relative to the NH_4 -jarosite derivative curve (figure 3.3 B). In addition, the peaks in the higher temperature range (600 – 675 °C) are shifted towards higher temperatures, which is consistent with the shifts seen in the decomposition curves. The derivative mass curve for NH_4 -jarosite-PMG (figure 3.3 F) is similar to NH_4 -jarosite-SWG derivative curves except the first two peaks (200 and 210 °C) peaks are absent and the peak at 240 °C is the most prominent. There is a small peak at 280 °C that is present in the NH_4 -jarosite-PMG derivative mass curve that is absent in both the NH_4 -jarosite and NH_4 -jarosite-SWG derivative mass curves. The 240 °C glycine indicator peak is observed in both the NH_4 -jarosite-SWG and NH_4 -jarosite-PMG derivative mass curves.

The 240 °C peak found in the glycine derivative mass curve also occurs in the Na-jarosite-SWG, Na-jarosite-PMG, NH_4 -jarosite-SWG, and NH_4 -jarosite-PMG derivative mass curves. Although there is a variable response in the magnitude of decomposition rates and total decomposition temperatures between the potassium, sodium, and ammonium jarosites synthesized in the presence and absence of glycine, there is a trend that shows a slower decomposition rate and a greater temperature range for degradation that are indicative of the presence of glycine in the samples. Figure 3.5 illustrates the

effect that glycine has on the decomposition rate of jarosite relative to end member cation (K^+ , Na^+ , and NH_4^+), with relative decomposition rates being $K^+ < Na^+ < NH_4^+$.

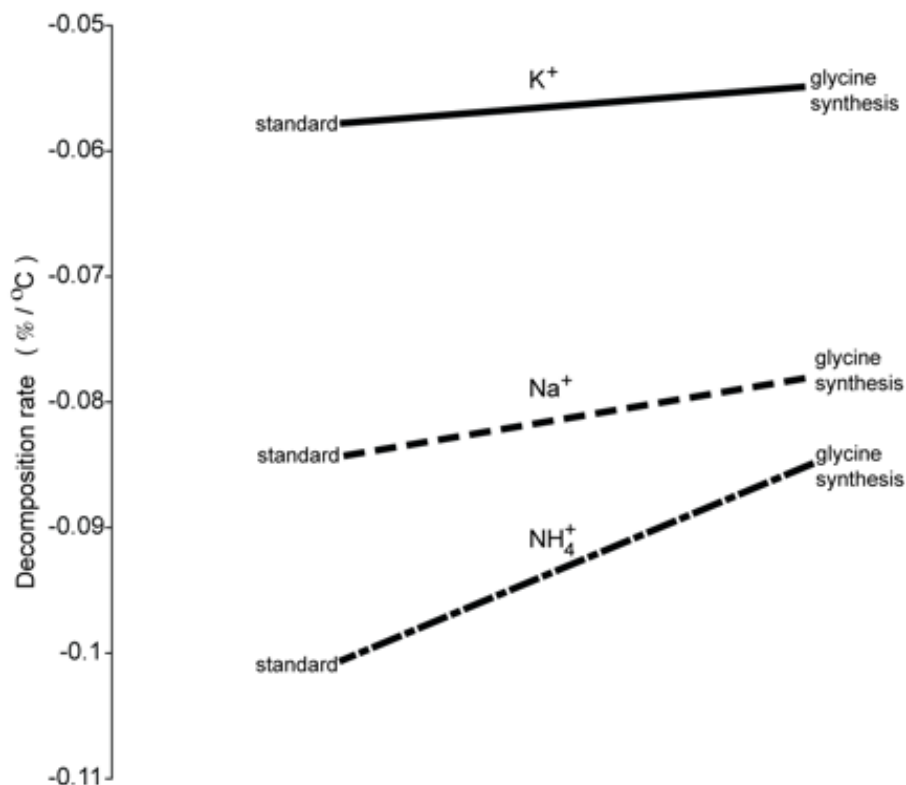


Figure 3.5 Relative decomposition rates of the jarosite end member syntheses (K^+ , Na^+ , and NH_4^+) and jarosite-SWG illustrating the relationship between cation type and the effect of glycine on thermal decomposition.

3.5 DISCUSSION

Peaks in the derivative mass curves, changes in the thermal decomposition curves, and thermal degradation rates indicate glycine is present in the jarosite-SWG and jarosite-PMG thermal analysis experiments. Additionally, GALDI-FTICR-MS analysis of the jarosite samples synthesized in the presence of glycine produced spectra (data not shown) similar to that observed in Kotler et al. 2008 for physically mixed jarosite and glycine samples. The peak at 240 °C observed in the glycine derivative mass curve (figure 3.1 B)

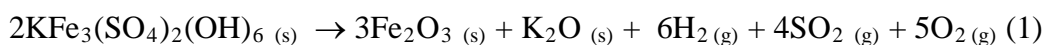
was most clearly seen in the NH₄-jarosite-SWG (figure 3.3 D) and NH₄-jarosite-PMG (figure 3.3 F) derivative mass curves. This could be due to the fact that the decomposition of NH₄-jarosite does not have derivative mass peaks within 75 °C of the glycine indicator region making identification more straightforward. K-jarosite and Na-jarosite both have derivative mass peak within the glycine indicator region, which may overlap or obscure a clear signature. The combustion of glycine during the thermal analysis experiments is likely the cause of shifts within the decomposition curves.

Thermal treatment of samples in response to planetary protection measures will remove the opportunity to acquire precise mineralogical and mineral chemical information from Mars samples by routine measures (e.g., XRD, electron microbeam, laser ablation-induced coupled plasma-mass spectrometry (LA-ICP-MS), and secondary ion mass spectrometry). Many of these techniques and variations were used to analyze samples returned during the Stardust Mission (Brownlee et al., 2006; Brownlee et al., 2003; Flynn et al., 2006; Horz et al., 2006; Lee et al., 2004; Liffman, 2006; Sandford, 2007; Sandford et al., 2006; Sandford and Brownlee, 2007; Spencer and Zare, 2007; Zolensky et al., 2008). Unless, the planetary community determines that samples returned from Mars carry no risk to Earth, the choice of analytical techniques could be limited by heat treatment. However, our work has shown that TGA can provide information regarding the cation composition, occurrence of organic components, and the structure of jarosite mineral species should it be implemented as part of a planetary protection protocol.

Since thermal analysis is a destructive method (Wendlandt, 1986), vital crystallographic information can be lost during analysis. By analyzing the total

decomposition reactions for each of the end members and making assumptions about hydronium ion substitution and full iron occupancy, it may be possible to estimate the site occupancies of the primary cations (K, Na, and NH₄) to determine more precise compositions. Site occupancy calculations normally require crystallographic information such as that obtained during Rietveld analysis of diffraction data (Rietveld, 1969). If samples from Mars are heat treated before they are returned to Earth, it is unlikely that crystallographic studies of the heat-treated material would provide the type of information needed to calculate the site occupancies of the original material. What follows is a potential method for estimating site occupancies based on the TGA data. Several assumptions need to be made about the material in order for these estimations to be made. They are discussed for each of the end members below.

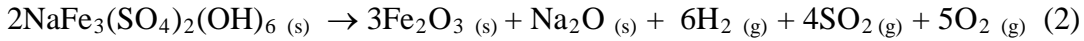
Hydronium ion substitution is common for each of the end member jarosites and true end member compositions are rarely found in natural and synthetic samples (Dutrizac and Jambor, 2000). The theoretical reaction for the complete degradation (ignoring intermediate steps that have been described previously by Frost et al. (Frost et al., 2005; Frost et al., 2006a; Frost et al., 2006b) of K-jarosite is as follows:



The theoretical molecular mass of a K-jarosite end-member is 1001.396 amu. The theoretical mass of solids left after decomposition ($3\text{Fe}_2\text{O}_3 \text{ (s)} + \text{K}_2\text{O} \text{ (s)}$) is 573.300 amu. The theoretical mass loss should therefore be 42.70 %. The experimental mass loss for K-jarosite was 39.22 %. This indicates a discrepancy of 3.48 % between the theoretical and actual mass losses. By assuming that this discrepancy is due to hydronium ion substitution, the estimated composition of the potassium jarosite standard synthesis is

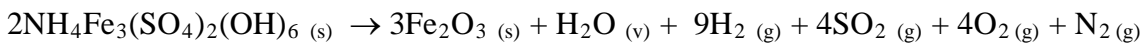
(K_{0.652}, H₃O_{0.348})Fe₃(SO₄)₂(OH)₆. Error calculations were described in the methods section and indicate a relative standard deviation (RSD) of 0.45 % for the analysis.

The theoretical reaction for the complete degradation of Na-jarosite is as follows:

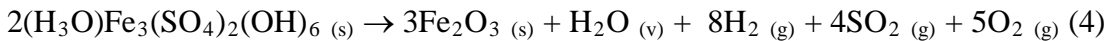


The theoretical molecular mass of the Na-jarosite end-member is 969.416, and the theoretical mass of solids left after decomposition (3Fe₂O₃, Na₂O) is 541.08 amu. The theoretical mass loss for the reaction is 44.10 %. The actual mass loss was 39.91%. The discrepancy is 5.0 %. This would give an estimated composition with nearly equal amounts of sodium and hydronium ions occupying the same crystallographic position. This estimate seems within the high end of synthetic compositions, but such equal occupancy is not outside reported values (Dutrizac and Jambor 2000). The estimated compositional formula would be (Na_{0.5}, H₃O_{0.5})Fe₃(SO₄)₂(OH)₆.

The theoretical decomposition reactions for NH₄-jarosite and hydronium jarosite (excluding intermediate steps) are as shown together below because of their similar theoretical mass losses:



(3)



The theoretical molecular mass for the NH₄-jarosite end-member is 959.68 amu. The total theoretical mass of solids (3Fe₂O₃) left after degradation is 479.10 amu. The theoretical mass loss is 50.07 %. The actual mass loss was 50.68 %. The discrepancy is

0.61 %. This small discrepancy makes it difficult to make a compositional estimate even though it is within the error measurement of the analysis. The true difficulty results from analyzing the degradation of a hydronium jarosite end-member (4). The theoretical molecular mass for hydronium jarosite is 961.484 amu and the resulting loss of solids is the same as the ammonium jarosite degradation (3). The theoretical mass loss for the hydronium jarosite degradation is 50.13 %. These values make estimates impossible since the mass loss values are too close to make any reasonable estimation.

Changes in decomposition curves between the standard jarosite syntheses and the jarosite-SWG can also be explained by considering that the presence of glycine in the synthetic procedure somehow effects competition for the main cation site and causes a disruption to crystal growth. Competition between K^+ , Na^+ , NH_4^+ , and, in this study, glycine for the X site is based on which ion is 'preferred' by the structure. This relates to the ability of the ion in question to fit in the available site based on its ionic radii and overall thermodynamic stability of the resulting structure. Since the K-jarosite is the most stable end member, it is possible that this competition scenario doesn't lead to a major difference in decomposition or structure. Regardless, there is an observed difference in behavior between potassium, sodium, ammonium jarosite synthesized in the presence of glycine. These differences include changes in total decomposition temperatures and rates. The jarosite-SWG degraded over a larger temperature range and at a slower rate compared to the standards (figure 3.3, and table 1). It is also clear that a simple physical mixture of the jarosite end-members and glycine (jarosite-PMG) do not mimic the decomposition behavior of the jarosite-SWG or the standards. Without further structural

data such as neutron diffraction analysis a firm conclusion about incorporation/substitution and occupancy cannot be made.

The results of the jarosite-PMG curves indicate that, if the glycine that has been observed in natural samples is not more intimately associated such as substituted or included rather than adsorbed or as an impurity within a mass of jarosite crystals, the signature will degrade more rapidly than if the glycine is incorporated into the structure. This has applications to the search for biosignatures on Mars because the harsh environment that surface materials encounter on the planet could easily destroy biomolecules such as glycine if they are not somehow protected. Terrestrial investigations of jarosite formation indicate that the process can be mediated by sulfur and iron metabolizing microorganisms (Akai et al., 1999; Bridge and Johnson, 2000; Clark et al., 1993; Eneroth and Koch, 2004; Grishin and Tuovinen, 1988; Karamanev, 1991; Sasaki and Konno, 2000) therefore making it likely that jarosite can hold clues to the presence of microbial activity in extraterrestrial environments. Sasaki and Konno (2000) determined that jarosites formed by biological processes could be differentiated from jarosites formed abiotically by slight changes in the crystal morphology and that impurities could be detected. This, along with the wide variety of atomic and molecular ions that substitute or can be incorporated into the jarosite lattice, indicate that capture of biomolecules is indeed possible. Therefore, the results of this study add to the growing body of knowledge suggesting that jarosite may be a useful mineral target for astrobiological investigations.

For Mars sample return, these studies show that thermal analysis of samples prior to their return to Earth could provide valuable information and also satisfy planetary

protection concerns. Information such as compositional estimates, detection of impurities such as biomolecules, and potentially the relationship between the biomolecules and the geologic material can in theory be determined. Coupling mass spectral techniques such as those used in the Thermal and Evolved Gas Analyzer (TEGA) (Boynton et al., 2001) that is being used on the surface of Mars as part of the Phoenix mission (Guinn et al., 2008) would allow researchers to identify the gases evolved during heat treatment to positively identify combustion gases that are due to organic matter (i.e., CO₂, CH₄, and NH₄). Investigations such as these and others conducted on other mineral groups of interest (Stalport et al., 2005) could provide the framework necessary to interpret the thermal analysis results should sterilization continue to be a criteria for planetary protection. In addition to sample return, these results could provide useful information should planned *in situ* investigations of the martian surface involve sites where jarosite minerals occur.

3.6 ACKNOWLEDGEMENTS

Funding for this research at the University of Montana and the Idaho National Laboratory (INL) comes from the NASA exobiology program (EXB03-0000-0054). We would like to thank Christopher Orme of the INL for assistance with thermal analysis and Timothy R. McJunkin of the INL for technical support on this project. JMK would also like to thank the Inland Northwest Research Alliance (INRA) for graduate support during this project. Research performed at the INL under DOE/NE Idaho Operations Office Contract DE-AC07-05ID14517.

3.7 REFERENCES

- Akai, J., Akai, K., Ito, M., Nakano, S., Maki, Y., and Sasagawa, I., 1999. Biologically induced iron ore at Gunma iron mine, Japan. *American Mineralogist* 84 (1-2), 171-182.
- Arabian, D. D., 1970. What made APOLLO a success - Action on mission evaluation and flight anomalies. *Astronautics & Aeronautics* 8 (3), 72-86.
- Aubrey, A., Cleaves, H. J., Chalmers, J. H., Skelley, A. M., Mathies, R. A., Grunthaner, F. J., Ehrenfreund, P., and Bada, J. L., 2006. Sulfate minerals and organic compounds on Mars. *Geology* 34 (5), 357-360.
- Banks, M., 2008. The life of NASA's Phoenix: highlights of its mission to Mars. *Physics World* 21 (12), 8-8.
- Baron, D., Palmer C.D., 1996. Solubility of jarosite at 4-35 degrees C. *Geochimica et Cosmochimica Acta* 60 (2), 285-195.
- Becker, U. and Gasharova, B., 2001. AFM observations and simulations of jarosite growth at the molecular scale: probing the basis for the incorporation of foreign ions into jarosite as a storage mineral. *Physics and Chemistry of Minerals* 28 (8), 545-556.
- Bibring, J., Langevin, Y., Mustard, J., Poulet, F., Arvidson, R., Gendrin, A., Gondet, B., Mangold, N., Pinet, P., and Forget, F., 2006. Global Mineralogical and Aqueous Mars History Derived from OMEGA/Mars Express Data. *Science* 312 (5772), 400.
- Bibring, J. P., Langevin, Y., Gendrin, A., Gondet, B., Poulet, F., Berthe, M., Soufflot, A., Arvidson, R., Mangold, N., Mustard, J., and Drossart, P., 2005. Mars surface diversity as revealed by the OMEGA/Mars Express observations. *Science* 307 (5715), 1576-1581.
- Boynton, W. V., Bailey, S. H., Hamara, D. K., Williams, M. S., Bode, R. C., Fitzgibbon, M. R., Ko, W. J., Ward, M. G., Sridhar, K. R., Blanchard, J. A., Lorenz, R. D., May, R.

D., Paige, D. A., Pathare, A. V., Kring, D. A., Leshin, L. A., Ming, D. W., Zent, A. P., Golden, D. C., Kerry, K. E., Lauer, H. V., and Quinn, R. C., 2001. Thermal and Evolved Gas Analyzer: Part of the Mars Volatile and Climate Surveyor integrated payload. *Journal of Geophysical Research-Planets* 106 (E8), 17683-17698.

Bridge, T. A. M. and Johnson, D. B., 2000. Reductive dissolution of ferric iron minerals by *Acidiphilium* SJH. *Geomicrobiology Journal* 17 (3), 193-206.

Brownlee, D., Tsou, P., Aleon, J., Alexander, C. M. O., Araki, T., Bajt, S., Baratta, G. A., Bastien, R., Bland, P., Bleuet, P., Borg, J., Bradley, J. P., Brearley, A., Brenker, F., Brennan, S., Bridges, J. C., Browning, N. D., Brucato, J. R., Bullock, E., Burchell, M. J., Busemann, H., Butterworth, A., Chaussidon, M., Chevront, A., Chi, M. F., Cintala, M. J., Clark, B. C., Clemett, S. J., Cody, G., Colangeli, L., Cooper, G., Cordier, P., Daghlian, C., Dai, Z. R., D'Hendecourt, L., Djouadi, Z., Dominguez, G., Duxbury, T., Dworkin, J. P., Ebel, D. S., Economou, T. E., Fakra, S., Fairey, S. A. J., Fallon, S., Ferrini, G., Ferroir, T., Fleckenstein, H., Floss, C., Flynn, G., Franchi, I. A., Fries, M., Gainsforth, Z., Gallien, J. P., Genge, M., Gilles, M. K., Gillet, P., Gilmour, J., Glavin, D. P., Gounelle, M., Grady, M. M., Graham, G. A., Grant, P. G., Green, S. F., Grossemy, F., Grossman, L., Grossman, J. N., Guan, Y., Hagiya, K., Harvey, R., Heck, P., Herzog, G. F., Hoppe, P., Horz, F., Huth, J., Hutcheon, I. D., Ignatyev, K., Ishii, H., Ito, M., Jacob, D., Jacobsen, C., Jacobsen, S., Jones, S., Joswiak, D., Jurewicz, A., Kearsley, A. T., Keller, L. P., Khodja, H., Kilcoyne, A. L. D., Kissel, J., Krot, A., Langenhorst, F., Lanzirotti, A., Le, L., Leshin, L. A., Leitner, J., Lemelle, L., Leroux, H., Liu, M. C., Luening, K., Lyon, I., et al., 2006. Research article - Comet 81P/Wild 2 under a microscope. *Science* 314 (5806), 1711-1716.

Brownlee, D. E., Tsou, P., Anderson, J. D., Hanner, M. S., Newburn, R. L., Sekanina, Z., Clark, B. C., Horz, F., Zolensky, M. E., Kissel, J., McDonnell, J. A. M., Sandford, S. A., and Tuzzolino, A. J., 2003. Stardust: Comet and interstellar dust sample return mission. *Journal of Geophysical Research-Planets* 108 (E-10), 8111.

Burnett, D. S., Barraclough, B. L., Bennett, R., Neugebauer, M., Oldham, L. P., Sasaki, C. N., Sevilla, D., Smith, N., Stansbery, E., Sweetnam, D., and Wiens, R. C., 2003. The Genesis Discovery mission: Return of solar matter to Earth. *Space Science Reviews* 105 (3-4), 509-534.

CETEX, 1958. Development of international efforts to avoid contamination of extraterrestrial bodies. *Science* 128, 887-889.

CETEX, 1959. Contamination by extra-terrestrial exploration. *Nature* 183, 925-928.

Christensen, P. R., Wyatt, M. B., Glotch, T. D., Rogers, A. D., Anwar, S., Arvidson, R. E., Bandfield, J. L., Blaney, D. L., Budney, C., Calvin, W. M., Faracaro, A., Fergason, R. L., Gorelick, N., Graff, T. G., Hamilton, V. E., Hayes, A. G., Johnson, J. R., Knudson, A. T., McSween, H. Y., Mehall, G. L., Mehall, L. K., Moersch, J. E., Morris, R. V., Smith, M. D., Squyres, S. W., Ruff, S. W., and Wolff, M. J., 2004. Mineralogy at Meridiani Planum from the Mini-TES experiment on the Opportunity Rover. *Science* 306 (5702), 1733-1739.

Clark, T. R., Baldi, F., and Olson, G. J., 1993. Coal depyritization by the thermophilic archaeon *Metallosphaera-sedula*. *Applied and Environmental Microbiology* 59 (8), 2375-2379.

Cochran, A. L. and Vilas, F., 1997. The McDonald observatory serendipitous UV/blue spectral survey of asteroids. *Icarus* 127 (1), 121-129.

DesMarais, D. J., Borg, L. E., and Beaty, D. W., 2008. Science priorities for Mars Sample Return. *Astrobiology* 8 (3), 489-535.

Dutrizac, J. E., 2004. The behaviour of the rare earths during precipitation of sodium, potassium and lead jarosites. *Hydrometallurgy* 73 (1-2), 11-30.

Dutrizac, J. E. and Chen, T. T., 2003. Synthesis and properties of V³⁺ analogues of jarosite-group minerals. *Canadian Mineralogist* 41, 479-488.

Dutrizac, J. E. and Jambor, J. L., 2000. Jarosites and their application in hydrometallurgy. *Sulfate Minerals - Crystallography, Geochemistry and Environmental Significance* 40, 405-452.

Eneroth, E. and Koch, C. B., 2004. Fe-hydroxysulphates from bacterial Fe²⁺ oxidation. *Hyperfine Interactions* 156 (1), 423-429.

Flynn, G. J., Bleuet, P., Borg, J., Bradley, J. P., Brenker, F. E., Brennan, S., Bridges, J., Brownlee, D. E., Bullock, E. S., Burghammer, M., Clark, B. C., Dai, Z. R., Daghljan, C. P., Djouadi, Z., Fakra, S., Ferroir, T., Floss, C., Franchi, I. A., Gainsforth, Z., Gallien, J. P., Gillet, P., Grant, P. G., Graham, G. A., Green, S. F., Grossemey, F., Heck, P. R., Herzog, G. F., Hoppe, P., Horz, F., Huth, J., Ignatyev, K., Ishii, H. A., Janssens, K., Joswiak, D., Kearsley, A. T., Khodja, H., Lanzirrotti, A., Leitner, J., Lemelle, L., Leroux, H., Luening, K., MacPherson, G. J., Marhas, K. K., Marcus, M. A., Matrajt, G., Nakamura, T., Nakamura-Messenger, K., Nakano, T., Newville, M., Papanastassiou, D. A., Pianetta, P., Rao, W., Riekkel, C., Rietmeijer, F. J. M., Rost, D., Schwandt, C. S., See, T. H., Sheffield-Parker, J., Simionovici, A., Sitnitsky, I., Snead, C. J., Stadermann, F. J., Stephan, T., Stroud, R. M., Susini, J., Suzuki, Y., Sutton, S. R., Taylor, S., Teslich, N., Troadec, D., Tsou, P., Tsuchiyama, A., Uesugi, K., Vekemans, B., Vicenzi, E. P., Vincze, L., Westphal, A. J., Wozniakiewicz, P., Zinner, E., and Zolensky, M. E., 2006. Elemental compositions of comet 81P/Wild 2 samples collected by Stardust. *Science* 314 (5806), 1731-1735.

Frost, R. L., Weier, M. L., and Martens, W., 2005. Thermal decomposition of jarosites of potassium, sodium, and lead. *Journal of Thermal Analysis and Calorimetry* 82 (1), 115-118.

Frost, R. L., Willis, R. A., Klopregge, J. T., and Martens, W., 2006a. Thermal decomposition of ammonium jarosite. *Journal of Thermal Analysis and Calorimetry* 84 (2), 489-496.

Frost, R. L., Willis, R. A., Klopregge, J. T., and Martens, W. N., 2006b. Thermal Analysis of hydronium jarosite. *Journal of Thermal Analysis and Calorimetry* 83 (1), 212-218.

Grishin, S. I. and Tuovinen, O. H., 1988. Fast kinetics of Fe-2+ oxidation in packed-bed reactors. *Applied and Environmental Microbiology* 54 (12), 3092-3100.

Guinn, J. R., Garcia, M. D., and Talley, K., 2008. Mission design of the Phoenix Mars Scout mission. *Journal of Geophysical Research-Planets* 113, EE00A26.

Horz, F., Bastien, R., Borg, J., Bradley, J. P., Bridges, J. C., Brownlee, D. E., Burchell, M. J., Chi, M. F., Cintala, M. J., Dai, Z. R., Djouadi, Z., Dominguez, G., Economou, T. E., Fairey, S. A. J., Floss, C., Franchi, I. A., Graham, G. A., Green, S. F., Heck, P., Hoppe, P., Huth, J., Ishii, H., Kearsley, A. T., Kissel, J., Leitner, J., Leroux, H., Marhas, K., Messenger, K., Schwandt, C. S., See, T. H., Snead, C., Stadermann, F. J., Stephan, T., Stroud, R., Teslich, N., Trigo-Rodriguez, J. M., Tuzzolino, A. J., Troadec, D., Tsou, P., Warren, J., Westphal, A., Wozniakiewicz, P., Wright, I., and Zinner, E., 2006. Impact features on Stardust: Implications for comet 81P/Wild 2 dust. *Science* 314 (5806), 1716-1719.

Jambor, J. L., 1999. Nomenclature of the alunite supergroup. *Canadian Mineralogist* 37, 1323-1341.

Karamanev, D. G., 1991. Model of the biofilm structure of *Thiobacillus-ferrooxidans*. *Journal of Biotechnology* 20 (1), 51-64.

Klingelhofer, G., Morris, R. V., Bernhardt, B., Schroder, C., Rodionov, D. S., de Souza, P. A., Yen, A., Gellert, R., Evlanov, E. N., Zubkov, B., Foh, J., Bonnes, U., Kankeleit, E., Gutlich, P., Ming, D. W., Renz, F., Wdowiak, T., Squyres, S. W., and Arvidson, R. E., 2004. Jarosite and hematite at Meridiani Planum from Opportunity's Mossbauer spectrometer. *Science* 306 (5702), 1740-1745.

Knoll, A. H., Carr, M., Clark, B., Marais, D. J. D., Farmer, J. D., Fischer, W. W., Grotzinger, J. P., McLennan, S. M., Malin, M., Schroder, C., Squyres, S., Tosca, N. J., and Wdowiak, T., 2005. An astrobiological perspective on Meridiani Planum. *Earth and Planetary Science Letters* 240 (1), 179-189.

Kotler, J. M., Hinman, N., and Tenesch, A., 2005. Laser and optical chemical imaging of diagenesis in iron-oxide deposits. *Geochimica et Cosmochimica Acta* 69 (10), A622-A622.

Kotler, J. M., Hinman, N. W., Yan, B., Stoner, D. L., and Scott, J. R., 2008. Glycine identification in natural jarosites using laser desorption Fourier transform mass spectrometry: Implications for the search for life on Mars. *Astrobiology* 8 (2), 253-266.

Kraft, C. C., Mayer, J. P., Huss, C. R., and Parten, R. P., 1970. What made APOLLO a success - flexible yet disciplined mission planning. *Astronautics & Aeronautics* 8 (3), 84-98.

Lee, T., Calaway, W. F., Chen, C. Y., Moore, J. F., Pellin, M. J., and Veryovkin, I. V., 2004. Dust-buster isotope TOF-MS for stardust. *Meteoritics & Planetary Science* 39 (8), A59-A59.

Liffman, K., 2006. Stardust mission results: Hot in cold. *Science* 312 (5780), 1599-1599.

Madden, M. E. E., Bodnar, R. J., and Rimstidt, J. D., 2004. Jarosite as an indicator of water-limited chemical weathering on Mars. *Nature* 431 (7010), 821-823.

NRC, 1978. Strategy for the Exploration of the Inner Planets: 1977- 1987. National Academy of Sciences, Washington, DC, 1-97.

NRC, 1990a. International Cooperation for Mars Exploration and Sample Return. National Academy of Sciences, Washington, D.C, 1-44.

NRC, 1990b. Update to Strategy for the Exploration of the Inner Planets. National Academy of Sciences, Washington, D.C, 1-47.

NRC, 1994. An Integrated Strategy for the Planetary Sciences: 1995-2010. National Academy of Sciences, Washington, D.C, 1-199.

NRC, 1996. Review of NASA's Planned Mars Program. National Academy of Sciences, Washington D.C, 1-43.

NRC, 2001. Assessment of Mars' Science and Mission Priorities. National Academy of Sciences, Washington D.C, 1-132.

NRC, 2002. Safe on Mars: Precursor Measurements. National Academy of Sciences, Washington D.C, 1-64.

NRC, 2007. An Astrobiology Study for the Exploration of Mars. National Academy of Sciences, Washington D.C, 1-130.

Osawa, T., Nakamura, T., and Nagao, K., 2003. Noble gas isotopes and mineral assemblages of Antarctic micrometeorites collected at the meteorite ice field around the Yamato Mountains. *Meteoritics & Planetary Science* 38 (11), 1627-1640.

Poulet, F., Bibring, J.-P., Mustard, J. F., Gendrin, A., Mangold, N., Langevin, Y., Arvidson, R. E., Gondet, B., and Gomez, C., 2005. Phyllosilicates on Mars and implications for early Martian climate. *Nature* 438 (7068), 623-627.

Richardson, C. D., Hinman, N. W., McJunkin, T. R., Kotler, J. M., and Scott, J. R., 2008. Exploring biosignatures associated with thenardite by geomatrix-assisted laser desorption/ionization Fourier transform ion cyclotron resonance mass spectrometry (GALDI-FTICR-MS). *Geomicrobiology Journal* 25 (7-8), 432-440.

Rietveld, H. M., 1969. A profile refinement method for nuclear and magnetic structures. *Journal of Applied Crystallography* 2, 65.

Rummel, J. D., 2001. Planetary exploration in the time of astrobiology: Protecting against biological contamination. *Proceedings of the National Academy of Sciences of the United States of America* 98 (5), 2128-2131.

Sandford, S. A., 2007. Organics in the samples returned by the Stardust spacecraft from Comet 81P/Wild 2. *Astrobiology* 7 (3), 493-494.

Sandford, S. A., Aleon, J., Alexander, C. M. O., Araki, T., Bajt, S., Baratta, G. A., Borg, J., Bradley, J. P., Brownlee, D. E., Brucato, J. R., Burchell, M. J., Busemann, H., Butterworth, A., Clemett, S. J., Cody, G., Colangeli, L., Cooper, G., D'Hendecourt, L., Djouadi, Z., Dworkin, J. P., Ferrini, G., Fleckenstein, H., Flynn, G. J., Franchi, I. A., Fries, M., Gilles, M. K., Glavin, D. P., Gounelle, M., Grossemy, F., Jacobsen, C., Keller, L. P., Kilcoyne, A. L. D., Leitner, J., Matrajt, G., Meibom, A., Mennella, V., Mostefaoui, S., Nittler, L. R., Palumbo, M. E., Papanastassiou, D. A., Robert, F., Rotundi, A., Snead, C. J., Spencer, M. K., Stadermann, F. J., Steele, A., Stephan, T., Tsou, P., Tylliszczak, T., Westphal, A. J., Wirick, S., Wopenka, B., Yabuta, H., Zare, R. N., and Zolensky, M. E., 2006. Organics captured from comet 81P/Wild 2 by the Stardust spacecraft. *Science* 314 (5806), 1720-1724.

Sandford, S. A. and Brownlee, D. E., 2007. Response to comment on "Organics captured from Comet 81P/Wild 2 by the Stardust spacecraft". *Science* 317 (5845), 493-494.

Sasaki, K. and Konno, H., 2000. Morphology of jarosite-group compounds precipitated from biologically and chemically oxidized Fe ions. *Canadian Mineralogist* 38, 45-56.

Scott, J. R. and Tremblay, P. L., 2002. Highly reproducible laser beam scanning device for an internal source laser desorption microprobe Fourier transform mass spectrometer. *Review of Scientific Instruments* 73 (3), 1108-1116.

Simpkins, S., 1970. What made APOLLO a success - testing to insure mission success. *Astronautics & Aeronautics* 8 (3), 50-89.

Skelley, A. M., Scherer, J. R., Aubrey, A. D., Grover, W. H., Ivester, R. H. C., Ehrenfreund, P., Grunthaner, F. J., Bada, J. L., and Mathies, R. A., 2005. Development and evaluation of a microdevice for amino acid biomarker detection and analysis on Mars. *Proceedings of the National Academy of Sciences of the United States of America* 102 (4), 1041-1046.

Spencer, M. K. and Zare, R. N., 2007. Comment on "Organics captured from Comet 81P/Wild 2 by the Stardust spacecraft". *Science* 317 (5845).

Squyres, S. W., Arvidson, R. E., Bell, J. F., Bruckner, J., Cabrol, N. A., Calvin, W., Carr, M. H., Christensen, P. R., Clark, B. C., Crumpler, L., Des Marais, D. J., d'Uston, C., Economou, T., Farmer, J., Farrand, W., Folkner, W., Golombek, M., Gorevan, S., Grant, J. A., Greeley, R., Grotzinger, J., Haskin, L., Herkenhoff, K. E., Hviid, S., Johnson, J., Klingelhofer, G., Knoll, A. H., Landis, G., Lemmon, M., Li, R., Madsen, M. B., Malin, M. C., McLennan, S. M., McSween, H. Y., Ming, D. W., Moersch, J., Morris, R. V., Parker, T., Rice, J. W., Richter, L., Rieder, R., Sims, M., Smith, M., Smith, P., Soderblom, L. A., Sutlivan, R., Wanke, H., Wdowiak, T., Wolff, M., and Yen, A., 2004a.

The Opportunity Rover's Athena science investigation at Meridiani Planum, Mars. *Science* 306 (5702), 1698-1703.

Squyres, S. W., Grotzinger, J. P., Arvidson, R. E., Bell, J. F., Calvin, W., Christensen, P. R., Clark, B. C., Crisp, J. A., Farrand, W. H., Herkenhoff, K. E., Johnson, J. R., Klingelhofer, G., Knoll, A. H., McLennan, S. M., McSween, H. Y., Morris, R. V., Rice, J. W., Rieder, R., and Soderblom, L. A., 2004b. In situ evidence for an ancient aqueous environment at Meridiani Planum, Mars. *Science* 306 (5702), 1709-1714.

Squyres, S. W. and Knoll, A. H., 2005. Sedimentary rocks at Meridiani Planum: Origin, diagenesis, and implications for life on Mars. *Earth and Planetary Science Letters* 240 (1), 1-10.

Stalport, F., Coll, P., Cabane, M., Person, A., Gonzalez, R. N., Raulin, F., Vaulay, M. J., Ausset, P., McKay, C. P., Szopa, C., and Zarnecki, J., 2005. Search for past life on Mars: Physical and chemical characterization of minerals of biotic and abiotic origin: part 1 - Calcite. *Geophysical Research Letters* 32 (23), L24102.

Stalport, F., Coll, P., Szopa, C., Person, A., Navarro-Gonzalez, R., Cabane, M., Ausset, P., and Vaulay, M. J., 2007. Search for past life on Mars: Physical and chemical characterization of minerals of biotic and abiotic origin. *Geophysical Research Letters* 34 (24), L2320.

Stoffregen, R. E., Alpers, C. N., and Jambor, J. L., 2000. Alunite-jarosite crystallography, thermodynamics, and geochronology. *Sulfate Minerals - Crystallography, Geochemistry and Environmental Significance* 40, 453-479.

UN, 1967. Treaty on Principles Governing the Activities of States in the Exploration and Use of Outer Space Including the Moon and Other Celestial Bodies. United Nations.

Wendlandt, W. W., 1986. *Thermal Analysis*. John Wiley and Sons, New York.

Yan, B. Z., Stoner, D. L., Kotler, J. M., Hinman, N. W., and Scott, J. R., 2007. Detection of biosignatures by geomatrix-assisted laser desorption/ionization (GALDI) mass spectrometry. *Geomicrobiology Journal* 24 (3-4), 379-385.

Zolensky, M., Nakamura-Messenger, K., Fletcher, L., and See, T., 2008. Curation, spacecraft recovery, and preliminary examination for the Stardust mission: A perspective from the curatorial facility. *Meteoritics & Planetary Science* 43 (1-2), 5-21.

CHAPTER 4: THERMAL DECOMPOSITION BEHAVIOR OF POTASSIUM AND SODIUM JAROSITE SYNTHESIZED IN THE PRESENCE OF METHYLAMINE AND ALANINE

J. Michelle Kotler¹, Nancy W. Hinman^{1*}, C. Doc Richardson¹, Jill R. Scott²

(1) Geosciences Department, University of Montana, Missoula, MT 59812

(2) Chemical Sciences, Idaho National Laboratory, Idaho Falls, ID 83415

4.1 ABSTRACT

Biomolecules, methylamine and alanine, found associated with natural jarosite samples peaked the interest of astrobiologists and planetary geologists. How the biomolecules are associated with jarosite remains unclear although the mechanism could be important for detecting biosignatures in the rock record on Earth and other planets. A series of thermal gravimetric experiments using synthetic K-jarosite and Na-jarosite were conducted to determine if thermal analysis could differentiate physical mixtures of alanine and methylamine with jarosite from samples where the methylamine or alanine was incorporated into the synthesis procedure. Physical mixtures and synthetic experiments with methylamine and alanine could be differentiated from one another and from the standards by thermal analysis for both the K-jarosite and Na-jarosite end-member suites. Changes included shifts in on-set temperatures, total temperature changes from on-set to final, and the presence of indicator peaks for methylamine and alanine in the physical mixture experiments.

Key Words: jarosite, Mars, methylamine, alanine, biosignatures

***Corresponding author- Nancy Hinman, nancy.hinman@umontana.edu, 406-243-5277**

4.2 INTRODUCTION

Jarosite ($\text{KFe}_3(\text{SO}_4)_2(\text{OH})_6$) was found on Mars in 2004 by the Mars Exploration Rover (MER) mission [1] after first being proposed for the martian surface in the late 1980's by Roger Burns [2, 3]. The mineral group is associated with biologic activity on Earth; microbes oxidize both iron and sulfur in primary minerals for energy, forming jarosite as a by-product [4, 5]. The same primary iron and sulfur minerals (pyrrhotite, marcasite, and pyrite) associated with jarosite on Earth are inferred to occur on Mars [2, 3, 6-13]. The chemical and physical properties of the mineral could allow biomolecules left over from biogenic formation to be incorporated into the crystal structure and serve as potential biosignatures [14]. Several analytical techniques have identified biomolecules, such as amino acids and amino acid degradation products, in natural jarosite samples from various locations around the world [14-16].

These previous studies did not show how the biomolecules are associated with the jarosite structure. Determination of how the biomolecules are associated with jarosite may provide clues to the stability of the potential signature in the rock record. If the biomolecule is not chemically or physically bound to the mineral structure, it has a greater chance of loss during exposure to harsh weathering environments, thereby, hindering the ability to detect signs of pre-biotic or biotic activity in the geologic record on Earth and other planets. By adding the amino acid breakdown product methylamine (CH_3NH_2) and the amino acid alanine ($\text{C}_3\text{H}_7\text{NO}_2$) to the jarosite

synthetic procedure, we sought to determine if a chemical or physical relationship between the amino acids and the mineral structure could be determined.

The degradation or combustion of methylamine and alanine relate to either biosynthesis or biodegradation by organisms in energy processing pathways [17]. Alanine is important as an intermediate in the formation of more complex amino acids and is integral to biochemical pathways due to its reaction to form pyruvate, an essential molecule in energy pathways such as glycolysis, gluconeogenesis, and the citric acid cycle [18]. Methylamine is linked with the decay of organic matter and is a substrate for methanogenesis [19]. The detection of methane in the martian atmosphere has been suggested as a possible link to biological activity [20-22]. Additionally, alanine is a chiral amino acid; the ratio of one isomer to another could potentially assist in determining a biological origin of the molecule [23]. The detection of either or both of these biomolecules in martian samples could help determine if biological activity ever occurred on Mars.

Very few discussions focus on the abiotic degradation mechanisms of alanine and methylamine except those related to the origins of life on Earth [24, 25]. The mechanisms involve the synthesis of amino acid precursors, such as aldehydes, by a process mimicked in the famous Stanley-Miller volcanic spark experiments [26]. The next step involves the Strecker synthesis of the amino acids by condensation of the aldehyde with ammonium chloride in the presence of potassium cyanide [27]. The reverse reactions (i.e., degradation or combustion) involves the release of methane (CH_4) and ammonia (NH_3) gases and, depending on the environmental conditions, molecular oxygen, hydrogen, and or nitrogen [27, 28].

Thermal analysis techniques are highly sensitive to jarosite composition [29-37], and several studies show that thermogravimetric analysis can differentiate biotic and abiotic samples of calcite and aragonite for astrobiological applications [38, 39]. Herein, we present a thermogravimetric study of the two most stable jarosite group minerals (potassium jarosite and sodium jarosite) [40, 41] synthesized in the presence of methylamine and alanine, simple physical mixtures of methylamine and alanine with the jarosites, and the synthetic mineral standards to determine if the physical mixtures, synthesis experiments and mineral standards can be differentiated from one another based on thermal decomposition processes.

4.3 EXPERIMENTAL

Syntheses

K-jarosite ($\text{KFe}_3(\text{SO}_4)_2(\text{OH})_6$) and Na-jarosite ($\text{NaFe}_3(\text{SO}_4)_2(\text{OH})_6$) were prepared according to the method described in Dutrizac and Chen [42], and also presented in Kotler et al. (2008) [14]. Potassium sulfate or sodium sulfate (0.4 M K_2SO_4 , Na_2SO_4) were added to a 0.4 M FeCl_3 solution in a 100-mL round bottom flask maintaining a stoichiometric ratio of 2:3 sulfate salt to ferric iron during reaction. The solution was stirred under reflux conditions at 100 °C for 24 hours. In order to collect the precipitate, the solutions were vacuum filtered while hot using a Buchner funnel and Whatman #4 filter paper. The precipitates were washed under vacuum three times with 1 L of deionized water and air-dried. Synthesis experiments were performed by adding 1 mM concentrations of methylamine (labeled SWMA,

synthesized with methylamine) or alanine (labeled SWAla, synthesized with alanine) (Sigma-Aldrich, MA) to the synthesis procedure using the same temperature, time, and washing procedures as the standard jarosite syntheses. Powdered samples were mounted on glass slides for random X-ray powder diffraction (XRD) analysis to ensure purity and for phase identification. X-ray diffraction analyses were performed on randomly oriented powders using a Philips APD 3720 X-ray diffractometer using a step size of $0.02^\circ 2\theta$ and a rate of $0.750^\circ 2\theta/\text{min}$. Patterns were compared to jarosite synthetic Joint Committee on Powder Diffraction Standards (JCPDS) file 22-0827.

Thermal Analysis

Thermal analyses were obtained using a TA Instruments model 2950 thermogravimetric analyzer (TGA). Mixture experiments using methylamine and alanine with synthetic jarosite (jarosite-PMMA and jarosite-PMAAla) were prepared by mixing ~3 – 5% analyte with jarosite matrix before TGA preparations. Sample masses varied between 15 – 20 mg and were heated in a platinum sample holder at a constant ramping of temperature between ambient and 950°C at a rate of $5^\circ\text{C}/\text{min}$. Replicate analyses of the K-jarosite standard were performed to assess the reproducibility of the measurements. The standard deviation was calculated to be $0.176^\circ\text{C}/\text{min}$ with a relative standard deviation (RSD) of 0.45 %. All rate calculations and analyses of TGA data were performed using TA Thermal Advantage Universal Analysis (TA instruments, New Castle, DE, USA) software. Instrument measurements are reported in weight % (elevation in Idaho Falls, ID ≈ 1430 m), however, convention has shifted to report the units as Mass %.

4.4 RESULTS AND DISCUSSION

The thermal degradation and derivative mass curves for methylamine and alanine are shown in Fig. 1 (a, b, c, d). Methylamine (CH_3NH_2) (Fig. 1 a) begins to degrade at 140 °C, and proceeded through three decomposition steps until the mass loss ceased at 521 °C (see Table 1, Fig. 1 a). The derivative mass curve for methylamine (Fig. 1 b) shows the presence of two peaks at 270 °C and 350 °C. Alanine ($\text{C}_3\text{H}_7\text{NO}_2$) begins to degrade at 206 °C, continues through one continuous step until 448 °C, when nearly 100 % of the total mass is lost (Fig. 1 c, Table 1). The derivative mass curve for alanine (Fig. 1 d) shows the presence of a single peak at 320 °C. For the purposes of this discussion, it is the shape of the degradation curves, the onset temperatures, and the presence of indicator peaks within the derivative mass curves that will be compared to the jarosite syntheses and mixture experiment analyses.

Table 1. Thermal analysis of methylamine and alanine, K-jarosite and Na-jarosite standard synthetic samples, synthesis and mixture experiments including transition temperatures, total mass loss, and total temperature change (ΔT_{total}) from onset to final.

<i>Sample</i>	<i>Step</i>	<i>Transition Temperatures</i> (°C)	<i>% original mass</i>
Methylamine (MA) Total mass loss: 92.81 % $\Delta T_{\text{total}} = 301.11$ °C	1	140.02 – 306.78	44.06
	2	306.78 – 372.93	13.75
	3	372.93 – 521.13	7.18

Alanine (Ala) Total mass loss: 99.62 % $\Delta T_{\text{total}} = 241.63 \text{ }^{\circ}\text{C}$	1	206.36 – 331.44	1.23
	2	331.44 – 447.99	0.38
K-jarosite Total mass loss: 39.22 % $\Delta T_{\text{total}} = 646.81 \text{ }^{\circ}\text{C}$	1	158.69 — 317.91	99.71
	2	317.91 — 418.25	86.94
	3	418.25 — 630.64	80.05
	4	630.64 — 707.40	64.95
	5	707.40 — 805.02	60.78
K-jarosite-SWMA Total mass loss: 39.38 % $\Delta T_{\text{total}} = 603.27 \text{ }^{\circ}\text{C}$	1	185.50 – 319.30	95.73
	2	319.30 – 425.26	86.00
	3	425.26 – 657.92	79.32
	4	657.92 – 736.63	64.57
	5	736.63 – 788.77	60.32
K-jarosite-PMMA Total mass loss: 63.81 % $\Delta T_{\text{total}} = 587.81 \text{ }^{\circ}\text{C}$	1	180.31 – 412.73	48.15
	2	412.73 – 768.12	60.32
K-jarosite-SWAla Total mass loss: 39.70 % $DT_{\text{total}} = 591.45 \text{ }^{\circ}\text{C}$	1	176.25 – 317.45	95.33
	2	317.45 – 422.27	85.54
	3	422.27 – 557.97	84.31
	4	557.97 – 644.57	78.99
	5	644.57 – 724.32	64.46
	6	724.32 – 767.60	60.28
K-jarosite-PMAla Total mass loss: 50.55 % $\Delta T_{\text{total}} = 607.88 \text{ }^{\circ}\text{C}$	1	190.27 – 224.64	97.33
	2	224.64 – 241.30	86.38
	3	241.30 – 420.19	71.03
	4	420.19 – 653.37	65.56

	5	653.37 – 745.28	53.10
	6	745.28 – 798.25	49.45
Na-jarosite	1	251.61 — 370.97	97.61
Total mass loss: 39.91 %	2	370.97 — 452.51	87.44
$\Delta T_{\text{total}} = 510.41 \text{ }^{\circ}\text{C}$	3	452.51 — 589.69	84.49
	4	589.69 — 762.02	60.09
Na-jarosite-SWMA	1	240.12 – 376.87	97.25
Total mass loss: 39.60 %	2	376.87 – 457.56	87.28
$\Delta T_{\text{total}} = 485.21 \text{ }^{\circ}\text{C}$	3	457.56 – 590.59	84.72
	4	590.59 – 725.33	60.48
Na-jarosite-PMMA	1	183.59 – 376.16	54.23
Total mass loss: 62.64 %	2	376.16 – 607.56	50.43
$\Delta T_{\text{total}} = 558.47 \text{ }^{\circ}\text{C}$	3	607.56 – 742.06	27.36
Na-jarosite-SWAla	1	244.71 – 374.03	97.63
Total mass loss: 39.74 %	2	374.03 – 456.96	87.47
$\Delta T_{\text{total}} = 489.89 \text{ }^{\circ}\text{C}$	3	456.96 – 606.87	84.09
	4	606.87 – 709.91	60.78
	5	709.91 – 734.70	60.26
Na-jarosite-PMAla	1	165.12 – 246.58	93.75
Total mass loss: 43.12 %	2	246.58 – 390.07	90.21
$\Delta T_{\text{total}} = 584.07 \text{ }^{\circ}\text{C}$	3	390.07 – 450.59	80.83
	4	450.59 – 642.75	77.50
	5	642.75 – 749.19	56.88

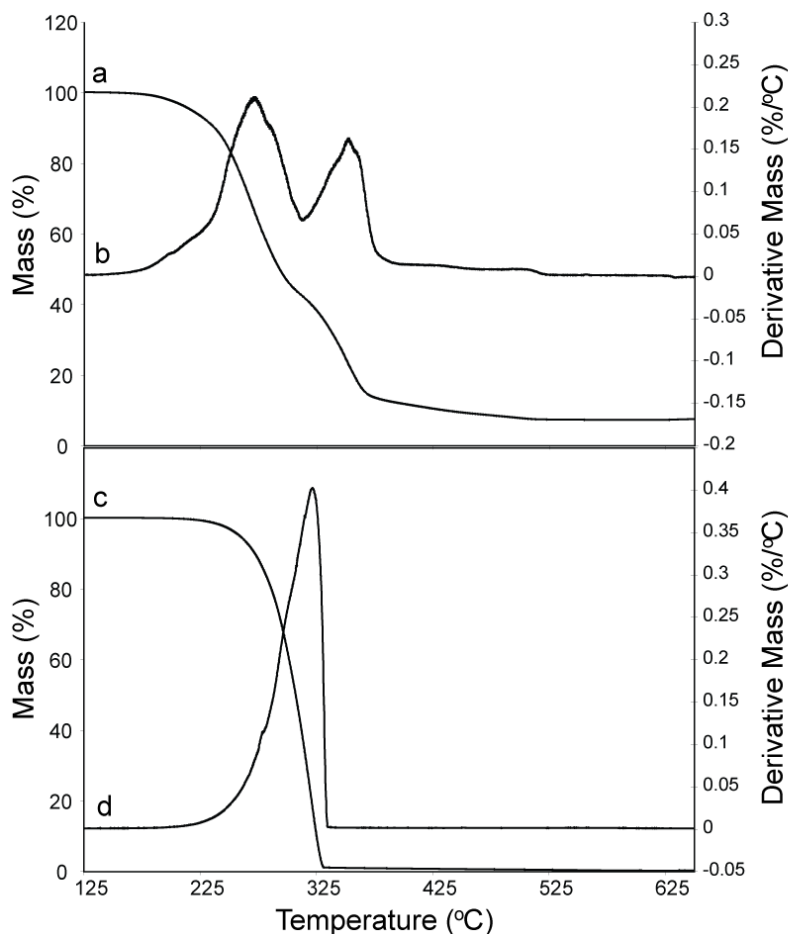


Fig. 4.1 Thermal degradation (TG) and derivative mass (DG) curves for methylamine (a, b) and alanine (c, d).

Interestingly, when methylamine and alanine are present in physical mixtures with K-jarosite and Na-jarosite (K-jarosite-PMMA, K-jarosite-PMAla, Na-jarosite-PMMA, and Na-jarosite-PMAla), the experiments are conducted to temperatures of 950 °C (Fig. 2 and 3). Yet, in all of the methylamine mixture experiments (K-jarosite-PMMA, and Na-jarosite-PMAla), the samples regain mass after 750 °C, indicating that the degradation pathway for methylamine likely involves the formation of carbon ash that cannot escape as a gas unlike the alanine degradation in which nearly all the

mass is lost as gaseous material. Without the attachment of a gas analyzer to the TGA experimental apparatus, degradation mechanisms and products are speculative.

The thermal degradation and derivative mass curves for the K-jarosite standard (Fig. 2 a, b) and Na-jarosite standard (Fig. 3 a, b) display distinct decomposition behavior including differences in onset temperature, degradation steps, number of derivative mass peaks and total temperature changes [43]. These experiments show that the K-jarosite and Na-jarosite onset temperatures differ by almost 100 °C (158.69 and 251.61 °C, respectively, Table 1). When the temperatures finally level out (final degradation step), the temperatures for the K-jarosite and Na-jarosite are within 50.0 °C of one another (805.02 and 762.61 °C). In addition to onset temperatures, and final degradation temperatures, the jarosite end members can be distinguished by the number of degradation steps, the number derivative mass peaks and overall shape of the degradation curves (see Fig. 2, 3 and Table 1). K-jarosite degrades in 5 steps with 6 distinct derivative mass peaks and the Na-jarosite in 4 steps with only 3 distinct derivative mass peaks, indicating that composition can be inferred from the thermal degradation and derivative mass curves. It is likely that these differences are directly related to the thermodynamic stability of the two end members. Direct comparison of the $\Delta G_{f, 298 \text{ K}, 1 \text{ bar}}$ values for K-jarosite (-3309.8 kJ/mol) and Na-jarosite (-3256.7 kJ/mol) show that free energy of formation values differ by approximately 50 kJ/mol [40, 44].

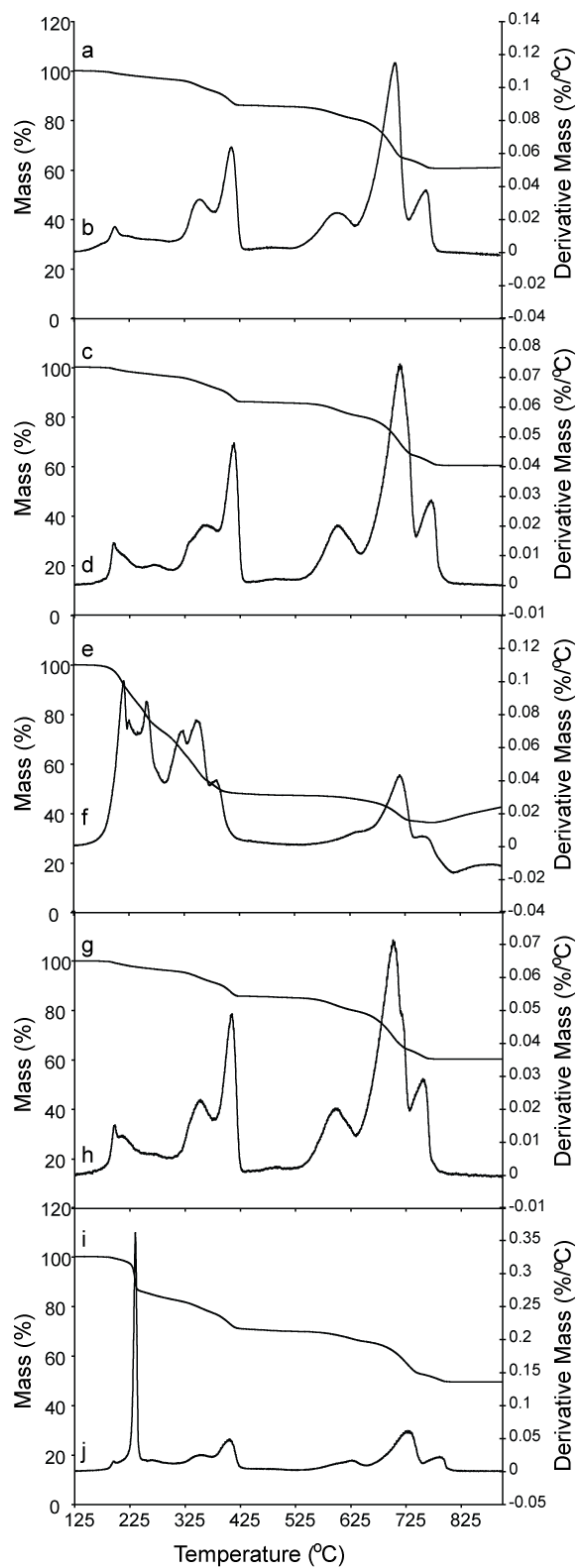


Fig. 4.2 Thermal degradation (TG) and derivative mass (DG) curves for K-jarosite (a, b), K-jarosite-SWMA (c, d), K-jarosite-PMMA (e, f), K-jarosite-SWAla (g, h), and K-jarosite- PMAla (i, j).

The K-jarosite-SWMA thermal decomposition and derivative mass curves are shown in Fig. 2 c, d. The onset temperature was 185.50 °C, preceded through 5 steps and mass loss levels out at 788.77 °C (Fig. 2 c, table 1). The number of degradation steps between the K-jarosite and the K-jarosite-SWMA are the same, and qualitatively, the curves appear similar until the K-jarosite-SWMA began to deviate near 600 °C. The derivative mass curve for K-jarosite-SWMA (Fig. 2 d) shows a slight shift in the higher temperature peaks, the presence of a diffuse small peak at 270 °C and a small shoulder peak at 350 °C. Both of these additional peaks occur in the indicator region for methylamine (Fig. 1 b). The small shoulder peak at 350 °C for K-jarosite-SWMA is likely obscured by the peak for the K-jarosite standard (Fig. 2 b) that occurs in the same region.

The K-jarosite-PMMA thermal decomposition curve (Fig. 2 e) deviates significantly from both the K-jarosite and K-jarosite-SWMA by degrading in only two steps. The onset temperature is intermediate between K-jarosite and K-jarosite-SWMA at 180.31 °C (Table 1). The derivative mass curve for K-jarosite-PMMA (Fig. 2 f) shows several additional peaks in the region where the methylamine indicator peaks should occur. The slight differences between the K-jarosite and K-jarosite-SWMA derivative mass curves indicate that a small quantity of methylamine remained associated with the K-jarosite during the synthesis experiment that can be detected by comparison of the derivative mass curves. It is unknown how much of the methylamine was retained during the synthesis, however a difference is observed

between the physical mixture and the synthesis indicating potentially a much lower concentration of methylamine or a different type of association.

The K-jarosite-SWAla thermal degradation and derivative mass curves are shown in Fig. 2 g, h. The K-jarosite-SWAla onset temperature was 180.31 °C, the degradation proceeded through 6 steps, and the final degradation temperature was 767.60 °C (Table 1). The derivative mass curve for K-jarosite-SWAla (Fig. 2 h) is very similar to the K-jarosite with 6 discernable peaks except that all of the peaks are shifted towards lower temperatures. These results are similar to the K-jarosite-SWMA which both show shifts in the degradation curves toward lower temperatures compared to K-jarosite, however there are no sharp distinguishable additional peaks that would indicate the presence of alanine. The K-jarosite-PMAla degrades in 6 steps with an onset temperature of 190.27 °C. The K-jarosite-PMAla thermal degradation curve (Fig. 2 i) mimics the thermal degradation curves of the K-jarosite and K-jarosite-SWAla (Fig. 2 a, c) except for the steep initial mass loss (step 1, Table 1), which resembles the degradation curve of alanine alone (Fig. 1 c) The K-jarosite-PMAla derivative mass curve (Fig. 2 j) is similar to the K-jarosite curve with the addition of a sharp peak at 225 °C. The derivative mass peak for alanine (Fig. 1 d) has the indicator peak at 320 °C, however it appears that in the mixture experiments alanine is shifted to lower temperatures indicated by the peak at 225 °C in the K-jarosite-PMAla sample.

The thermal degradation and derivative mass curves for Na-jarosite, Na-jarosite-SWMA, Na-jarosite-PMMA, Na-jarosite-SWAla, and Na-jarosite-PMAla are shown in Fig. 3. The Na-jarosite-SWMA sample began to degrade at 240.12 °C and

proceeded through 4 steps with the final degradation step ending at 725.33 °C (Fig. 3 c). The derivative mass curve for Na-jarosite-SWMA (Fig. 3 d) shows a shift towards higher temperatures for all three major peaks. There are no peaks in the indicator region where methylamine should occur. Qualitatively, the Na-jarosite and Na-jarosite-SWMA are similar in shape and number of degradation steps. As with the K-jarosite and K-jarosite-SWMA, there is a deviation in behavior where the curves are shifted relative to one another. The Na-jarosite-PMMA degradation curve (Fig. 3 e) shows a near perfect match to the K-jarosite-PMMA degradation curve (Fig. 2 c), as well as indicator peaks in the methylamine region of the derivative mass curve (Fig. 3 f) indicating that, similar to the K-jarosite sample suite, it is possible to distinguish the physical mixture from both the standard and the synthesis experiment samples.

The Na-jarosite-SWAla onset temperature was 244.71 °C, the sample proceeded through 5 degradation steps and degradation leveled out at 734.70 °C (Fig. 3 g, Table 1). Similar to the Na-jarosite-SWMA, the Na-jarosite-SWAla samples showed a shift towards higher temperatures compared to Na-jarosite in both the thermal degradation and derivative mass curves with no indicator peaks that are representative of either methylamine or alanine. The Na-jarosite-PMAla onset temperature was 165.12 °C and proceeded through 5 degradation steps with degradation leveling off at 749.19 °C (Fig. 3 i). The derivative mass curve for Na-jarosite-PMAla (Fig. 3 j) shows the same sharp peak at 225 °C that is observed in the K-jarosite-PMAla derivative mass curve. Similar to the Na-jarosite-PMMA, the Na-jarosite-PMAla shows a shift towards lower temperatures (Fig. 2 i, j and Fig. 3 i, j).

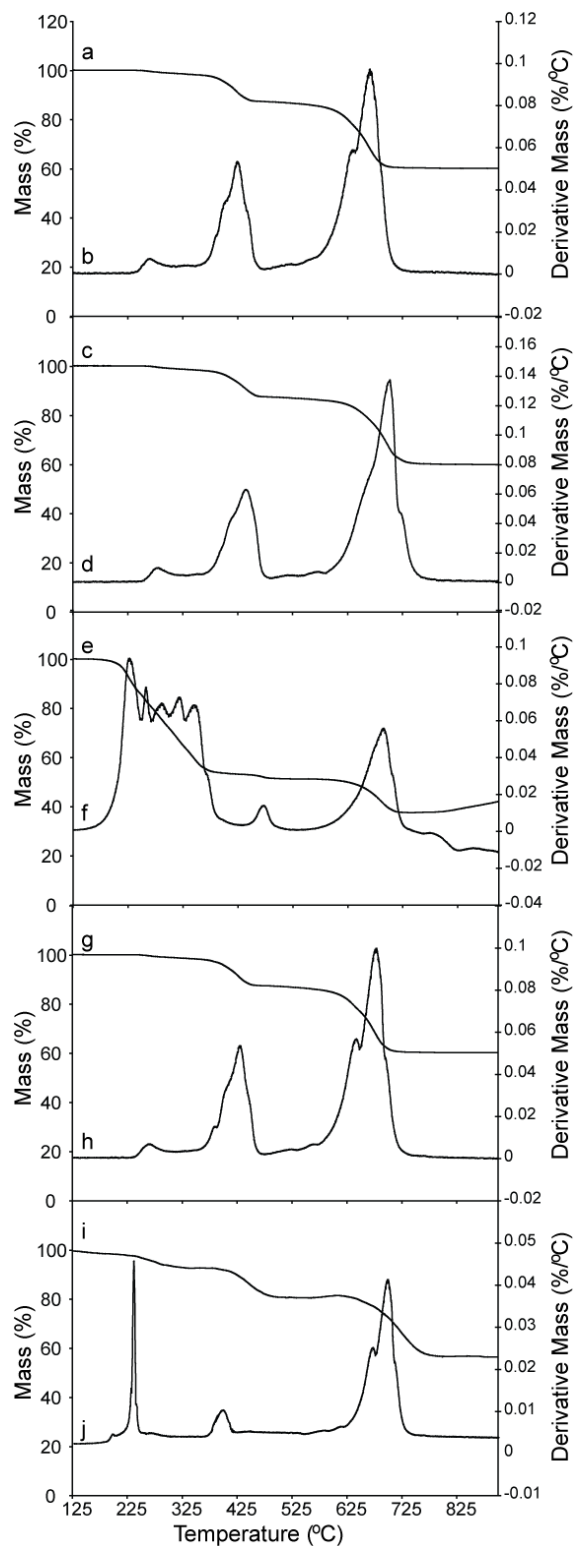


Fig.4. 3 Thermal degradation (TG) and derivative mass (DG) curves for Na-jarosite (a, b) and Na-jarosite-SWMA (c, d), Na-jarosite-PMMA (e, f), Na-jarosite-SWAla (g, h), Na-jarosite-PMAla (i, j).

The results of these experiments show that K-jarosites synthesized in the presence of methylamine can be differentiated from each other by small shifts in thermal degradation and derivative mass curves as well as small peaks in the region where methylamine should be present. The physical mixture of methylamine with K-jarosite (K-jarosite-PMMA) can be distinguished by the presence of additional peaks in the derivative mass curve and shifts in temperature for degradation. It is possible that the concentration of methylamine remaining post synthesis is very low and results in only minor changes in the decomposition behavior, but these results indicate that detection is still possible using thermal analysis. For the K-jarosite-SWAla and K-jarosite-PMAla, both samples can be differentiated by their thermal degradation and derivative mass curves from the K-jarosite standard. In all of the K-jarosite experiments with methylamine and alanine, there is a shift towards lower temperatures in the degradation behavior indicating that if methylamine and alanine are present then the samples are less stable and would degrade at a faster rate.

For the Na-jarosite sample suites, Na-jarosite-SWMA can be differentiated from Na-jarosite and Na-jarosite-PMMA. The Na-jarosite-SWMA shows a shift in decomposition behavior towards higher temperatures. For the Na-jarosite alanine experimental suite, only the Na-jarosite-PMAla can be differentiated from the Na-jarosite standard by the presence of an indicator peak at 225 °C, however shifts in temperature indicate for the Na-jarosite-SWAla sample indicate a difference between the sample and the standard. The shifts in temperature for the alanine peak found in the physical mixture is consistent with other thermal analysis results that state the peaks can be shifted dependent upon how the molecule is associated with the sample

[45]. The shifts towards higher temperatures would indicate that the structure is more stable and less vulnerable to degradation for the Na-jarosite alanine sample suite.

These results indicate that when biomolecules (i.e., methylamine and alanine) are present in the synthetic procedure for jarosite, their detection and behavior is dependent upon both the jarosite end member and the identity of the biomolecule. Jarosite has been identified as a potential storage molecule for biomolecules in the geologic record [14], and other studies have shown that the crystal structure accommodates a series of atomic and molecular substitutions such as ammonium, hydronium and rare earth elements [46, 47], validating the need to probe the limits of jarosite as a target for identifying evidence of pre-biotic and biotic activity in the geologic record on Earth and other planets. Although thermogravimetric techniques are highly sensitive to composition [48] and have been used to differentiate biotic and abiotic mineralization [38, 39], more sensitive techniques may be better able to detect the small amounts and identify the organic material that may be incorporated in the mineral structure.

4.5 CONCLUSIONS

The physical mixtures of the biomolecules methylamine and alanine with both K-jarosite and Na-jarosite can be differentiated from one another by thermal analysis, indicating that specific biomolecules can be identified by thermal analysis in these samples. The ability to detect these biomolecules in physical mixtures is important because they may provide information about biological activity related to jarosite.

Thermal analysis of both the K-jarosite and Na-jarosite synthesized in the presence of methylamine and alanine show slight differences in their degradation curves compared to the standards, however, only the potassium jarosite synthesized in the presence of alanine and the sodium jarosite synthesized in the presence of methylamine show deviations appreciable enough to make conclusions about their effects on the thermal behavior of the samples. Since jarosite is a target for astrobiological investigations, and both alanine and methylamine are key molecules in biologic processes, these results could prove useful for our exploration of the solar system in the search for life.

4.6 ACKNOWLEDGEMENTS

Funding for this research at the University of Montana and the Idaho National Laboratory (INL) comes from the NASA exobiology program (NNX08AP59G). J.M.K. would like to thank the Inland Northwest Research Alliance for graduate support during this project. We would like to thank Christopher Orme of the INL for assistance with thermal analysis. Research performed at the INL under DOE/NE Idaho Operations Office Contract DE-AC07-05ID14517.

4.7 REFERENCES

- 1 G. Klingelhofer, R. V. Morris, B. Bernhardt, C. Schroder, D. S. Rodionov, P. A. de Souza, A. Yen, R. Gellert, E. N. Evlanov, B. Zubkov, J. Foh, U. Bonnes, E. Kankeleit, P. Gutlich, D. W. Ming, F. Renz, T. Wdowiak, S. W. Squyres and R. E. Arvidson, *Science* 306 (2004) 1740.

- 2 R. G. Burns, in *Lun. Plan. Sci.* XVIII (1987).
- 3 R. G. Burns, *Nature* 320 (1989).
- 4 J. Akai, K. Akai, M. Ito, S. Nakano, Y. Maki and I. Sasagawa, *Am. Mineral.* 84 (1999) 171.
- 5 D. G. Karamanev, *J. Biotechnol.* 20 (1991) 51.
- 6 A. K. Baird and B. C. Clark, *Nature* 311 (1984).
- 7 J. Bibring, Y. Langevin, J. Mustard, F. Poulet, R. Arvidson, A. Gendrin, B. Gondet, N. Mangold, P. Pinet and F. Forget, *Science* 312 (2006) 400.
- 8 J. P. Bibring, Y. Langevin, A. Gendrin, B. Gondet, F. Poulet, M. Berthe, A. Soufflot, R. Arvidson, N. Mangold, J. Mustard and P. Drossart, *Science* 307 (2005) 1576.
- 9 R. G. Burns, *Nature* 320 (1986) 55.
- 10 R. G. Burns, *J. Geophys. Res. [Solid Earth]* 92 (1987) E570.
- 11 R. G. Burns, *J. Geophys. Res.* 95 (1990) 14415.
- 12 R. G. Burns, *J. Geophys. Res.* 95 (1990) 14169.
- 13 R. G. Burns, *Geochim. Cosmochim. Acta* 57 (1993).
- 14 J. M. Kotler, N. W. Hinman, B. Yan, D. L. Stoner and J. R. Scott, *Astrobiology* 8 (2008) 253.
- 15 A. Aubrey, H. J. Cleaves, J. H. Chalmers, A. M. Skelley, R. A. Mathies, F. J. Grunthaler, P. Ehrenfreund and J. L. Bada, *Geology* 34 (2006) 357.
- 16 A. M. Skelley, J. R. Scherer, A. D. Aubrey, W. H. Grover, R. H. C. Ivester, P. Ehrenfreund, F. J. Grunthaler, J. L. Bada and R. A. Mathies, *Proceedings of the National Academy of Sciences of the United States of America* 102 (2005) 1041.
- 17 C. Mathews, K. van Holde and K. Ahern, *Biochemistry* (Addison Wesley Longman, San Francisco, 2000).
- 18 H. E. Umbarger, *Annual Review of Biochemistry* 47 (1978) 533.
- 19 R. K. Thauer, *Microbiology* 144 (1998) 2377.
- 20 J. Evans, *Chemistry & Industry* (2009) 10.
- 21 M. J. Mumma, G. L. Villanueva, R. E. Novak, T. Hewagama, B. P. Bonev, M. A. DiSanti, A. M. Mandell and M. D. Smith, *Science* 323 (2009) 1041.
- 22 C. Thomas, O. Mousis, S. Picaud and V. Ballenegger, *Planetary and Space Science* 57 (2009) 42.
- 23 S. Pizzarello and A. L. Weber, *Science* 303 (2004) 1151.
- 24 C. Chyba and C. Sagan, *Origins of Life and Evolution of the Biosphere* 21 (1991) 3.
- 25 W. H. Sorrell, *Astrophysics and Space Science* 253 (1997) 27.
- 26 A. P. Johnson, H. J. Cleaves, J. P. Dworkin, D. P. Glavin, A. Lazcano and J. L. Bada, *Science* 322 (2008) 404.
- 27 M. Schulte and E. Shock, (1995) p. 161-173.
- 28 B. R. T. Simoneit, edited by M. P. Bernstein, M. Kress and R. NavarroGonzalez (2004) p. 88-94.
- 29 R. L. Frost, A. J. Locke and W. Martens, *Journal of Thermal Analysis and Calorimetry* 92 (2008) 887.
- 30 R. L. Frost and D. Wain, (2008) p. 267-274.
- 31 R. L. Frost, M. L. Weier and W. Martens, *Journal of Thermal Analysis and Calorimetry* 82 (2005) 115.

- 32 R. L. Frost, R. A. Wills, J. T. Kloprogge and W. Martens, *Journal of Thermal Analysis and Calorimetry* 84 (2006) 489.
- 33 R. L. Frost, R. A. Wills, J. T. Kloprogge and W. N. Martens, *Journal of Thermal Analysis and Calorimetry* 83 (2006) 213.
- 34 M. C. Hales and R. L. Frost, *Journal of Thermal Analysis and Calorimetry* 91 (2008) 855.
- 35 M. Ozacar, A. Alp and A. O. Aydin, (2000) p. 869-875.
- 36 V. Vagvolgyi, R. L. Frost, M. Hales, A. Locke, J. Kristof and E. Horvath, *Journal of Thermal Analysis and Calorimetry* 92 (2008) 893.
- 37 V. Vagvolgyi, M. Hales, W. Martens, J. Kristof, E. Horvath and R. L. Frosts, *Journal of Thermal Analysis and Calorimetry* 92 (2008) 911.
- 38 F. Stalport, P. Coll, M. Cabane, A. Person, R. N. Gonzalez, F. Raulin, M. J. Vaulay, P. Ausset, C. P. McKay, C. Szopa and J. Zarnecki, *Geophysical Research Letters* 32 (2005).
- 39 F. Stalport, P. Coll, C. Szopa, A. Person, R. Navarro-Gonzalez, M. Cabane, P. Ausset and M. J. Vaulay, *Geophysical Research Letters* 34 (2007).
- 40 D. Baron, Palmer C.D., *Geochimica Et Cosmochimica Acta* 60 (1996) 285.
- 41 A. Navrotsky, F. L. Forray and C. Drouet, *Icarus* 176 (2005) 250.
- 42 J. E. Dutrizac and T. T. Chen, *Canadian Mineralogist* 41 (2003) 479.
- 43 R. L. Frost, M. L. Weier and W. Martens, *Journal of Thermal Analysis and Calorimetry* (2005) 115.
- 44 R. E. Stoffregen, C. N. Alpers and J. L. Jambor, *Sulfate Minerals - Crystallography, Geochemistry and Environmental Significance* 40 (2000) 453.
- 45 L. Patron, G. Marinescu, D. Culita, L. Diamandescu and O. Carp, *Journal of Thermal Analysis and Calorimetry* 91 (2008) 627.
- 46 U. Becker and B. Gasharova, *Physics and Chemistry of Minerals* 28 (2001) 545.
- 47 V. V. Usimov, and Kozlova, P.S., (1972).
- 48 W. W. Wendlandt, *Thermal Analysis* (John Wiley and Sons, New York, 1986).

CHAPTER 5: NEUTRON AND X-RAY DIFFRACTION ANALYSIS OF POTASSIUM JAROSITE, SODIUM JAROSITE, AND AMMONIUM JAROSITE SYNTHESIZED IN THE PRESENCE OF THE AMINO ACID GLYCINE

5.1 ABSTRACT

The amino acid glycine has been found associated with natural samples of the mineral jarosite. A series of synthetic experiments with the jarosite end-members K-jarosite, Na-jarosite and NH₄-jarosite have been conducted adding glycine to the synthesis procedure. The samples were analyzed by X-ray and neutron diffraction to see what effect glycine had on the crystal structure of each of the jarosite end-members. Analysis of the X-ray and neutron diffraction patterns did not show the presence of additional peaks, but did show shifts in peak positions that correspond to changes in unit cell dimensions for the samples synthesized in the presence of glycine. Additional peaks in the sample would have indicated the presence of a secondary phase such as would be expected if jarosite had not been completely synthesized or if glycine was not incorporated into the jarosite sample. Each of the end-members had a different response to the glycine with K-jarosite showing a contraction of the unit-cell along both the a-axis and c-axis, Na-jarosite showed an increase along the a-axis, and NH₄-jarosite showed an expansion along the a-axis and a contraction along the c-axis for the X-ray diffraction studies. In the neutron diffraction study, only the Na-jarosite synthesized with glycine showed a difference in unit cell dimensions compared to the standard, however differences in peak intensities were observed for all the jarosite glycine syntheses compared to the standards.

5.2 INTRODUCTION

Jarosite is a common mineral in terrestrial (ARMSTRONG, 1995; DILL and POLLMAN, 2002; FULIGNATI and SBRANA, 2002; JOHNSTON, 1977) and extraterrestrial environments (BAIRD and CLARK, 1981; BURNS, 1990; CHRISTENSEN et al., 2004b; CLARK et al., 2005; MADDEN et al., 2004), making it a target for studying the depositional environment and the role that microbial life could play its formation. Jarosite was discovered on the surface of Mars by NASA's twin rovers Spirit and Opportunity in 2004 ((CHRISTENSEN et al., 2004a; CHRISTENSEN et al., 2004b; KLINGELHOFER et al., 2004; SQUYRES et al., 2004a; SQUYRES et al., 2004b). Jarosite group minerals belong to the alunite supergroup, which contains over 40 minerals. The supergroup is subdivided based on the trivalent metal cation present in tetrahedral coordination that forms the backbone of the mineral (JAMBOR, 1999). In the jarosite group, the dominant transition metal cation that occupies this site is Fe^{3+} . The jarosite group minerals have the general formula $\text{XFe}_3(\text{SO}_4)_2(\text{OH})_6$, where X is a monovalent cation, the identity of which depends on chemistry of the depositional environment. The most common cations to fill this position are K^+ , Na^+ , Rb^+ , Ag^+ , NH_4^+ , and H_3O^+ . Divalent cations can also be accommodated in the X position resulting in only half of the octahedral sites being filled in the unit cell. The most common divalent cation found in the jarosite group minerals is Pb^{2+} . True end member compositions within the group are rarely found in nature. Most researchers attribute this to the presence of hydronium ions within the primary cation site

(X site) that leads to non-stoichiometry (STOFFREGEN et al., 2000). Deficiencies are also observed for Fe^{3+} leading to incomplete occupation of this site in the crystal lattice.

Extensive work has been done with synthetic varieties of jarosite, and recent reports show that full occupancy of the iron site can be obtained in the laboratory but are rarely found in nature (BASCIANO and PETERSON, 2007a; BASCIANO and PETERSON, 2007b; BASCIANO and PETERSON, 2008a; BASCIANO and PETERSON, 2008b).

An association between amino acids and jarosite minerals have been identified in natural and synthetic jarosite samples related to the search for life on Mars (AUBREY et al., 2006; KOTLER et al., 2008; SKELLEY et al., 2005). A spatial or structural relationship for how the amino acids are associated with the jarosite structure has yet not been identified. A spatial relationship would be defined as molecular proximity based on physical locations of the amino acids and jarosite. A structural relationship would consist of crystallographic substitution of the amino acids. If the relationship is spatial, then the potential biosignatures have a greater chance of being lost during diagenetic processes. If however, the relationship is structural, these potential biosignatures have a greater chance of persisting in the geologic record. Both a spatial and structural relationship would provide vital amino acids to microbial communities, however a structural relationship would be less vulnerable to changes in environmental conditions.

Numerous studies have looked at the jarosite group minerals for crystal structure information and variation within reports are numerous (ALCOBE et al., 2001; BASCIANO and PETERSON, 2007b; BASCIANO and PETERSON, 2008b; BEHERA and RAO, 2007;

BURGER et al., 2009; DUTRIZAC and CHEN, 2006; FORRAY et al., 2005; GREY et al., 2008; GROHOL et al., 2003; MAJZLAN et al., 2006b; PAPIKE et al., 2006; TOUMI and TLILI, 2008). The idealized symmetry for jarosite is trigonal, with space-group R-3m and $Z = 3$. It has been suggested that space-group R-3m and $Z = 3$ should be assumed for jarosite unless structural analysis can confirm otherwise (STOFFREGEN et al., 2000). The R-3m space group has a $Z = 3$, meaning that the formula unit $(XFe_3(SO_4)_2(OH)_6)$ is repeated three times within the unit cell with no stoichiometric deficiencies. Some authors assert that since nonstoichiometry is more the rule than the exception, the lower symmetry space group R3m might be a more appropriate approximation (SZYMANSKI, 1988; TOWNSEND et al., 1986).

This is a study of K-jarosite, Na-jarosite, and NH_4 -jarosite end-member synthetic samples and the end-members synthesized in the presence of the amino acid glycine. The purpose is to determine by X-ray diffraction and neutron diffraction if a structural relationship exists between the amino acid and the crystal structure. Given the variations in unit cell dimensions, space group designations and compositions between synthetic and natural jarosite end-members, this study was conducted using identical synthetic procedures for the end members and glycine syntheses to minimize some of the observed variabilities. Changes in unit cell dimensions, shifts in peak intensities, and the presence of additional peaks in the diffraction patterns were used as indicators of how glycine affected the crystal structure of the different jarosite end-members.

5.3 METHODS

5.3.1 SYNTHESSES

Jarosite ($\text{KFe}_3(\text{SO}_4)_2(\text{OH})_6$), sodium jarosite ($\text{NaFe}_3(\text{SO}_4)_2(\text{OH})_6$), and ammonium jarosite ($\text{NH}_4\text{Fe}_3(\text{SO}_4)_2(\text{OH})_6$) were prepared according to Dutrizac and Chen's (2003) method and also presented in Kotler et al. (2008). Potassium sulfate, sodium sulfate or ammonium sulfate (0.4 M K_2SO_4 , Na_2SO_4 , and $(\text{NH}_4)_2\text{SO}_4$) were added to a 0.4 M FeCl_3 solution in a 100-mL round bottom flask maintaining a stoichiometric ratio of 2:3 sulfate salt to ferric iron during reaction. The solution was stirred under reflux conditions at 100° C for 24 hours. In order to collect the precipitate, the solutions were vacuum filtered while hot using a Buchner funnel and Whatman #4 filter paper (see also Chapters 2, 3, and 4). The precipitates were washed under vacuum three times with 1L of deionized water and air-dried. Substitution experiments were performed by adding 1mM concentrations of glycine to the synthetic procedure using the same temperature, time, and washing procedures as the standard jarosite syntheses. Deuterated samples for neutron diffraction analysis were prepared using 99.9% D_2O and deuterated glycine ($\text{C}_2\text{D}_2\text{NO}_2$) (Cambridge Isotopes, Cambridge, MA). Deuterated jarosite samples are designated with a d before the jarosite sample name.

5.3.2 X-RAY DIFFRACTION

X-ray diffraction was performed at the University of Montana Geology Department and at the Lakehead University Center for Analytical Services (LUCAS) in Thunder Bay, ON. At the University of Montana, powdered samples were mounted on glass slides for random X-ray diffraction (XRD) analysis. X-ray diffraction scans were performed on powdered samples using a Philips APD 3720 X-ray diffractometer using a step size of $0.02^\circ 2\theta$ and a rate of $0.750^\circ 2\theta/\text{min}$. At Lakehead University, samples were prepared using cavity mount slides with a step size of $0.015^\circ 2\theta$ and a rate of $0.250^\circ 2\theta/\text{min}$ (approximately 9 hour scans) and run on the identical Philips APD 3720 X-ray diffractometer used at the University of Montana. Patterns were compared to jarosite synthetic Joint Committee on Powder Diffraction Standards (JCPDS) file 22-0827 and unit cell dimensions were calculated from the hkl {003} and {110} crystallographic reflections.

5.3.3 NEUTRON DIFFRACTION

Neutron diffraction analyses were performed on powdered deuterated jarosite standard syntheses and jarosite glycine syntheses at the High Pressure Preferred Orientation Diffractometer (HIPPO) beam-line of Los Alamos Neutron Science Center (LANSCE), Los Alamos National Laboratory. Samples were deuterated to avoid backscattering of the hydrogen atoms during the experiment and to allow identification of sites within the crystal that would normally be occupied by hydrogen atoms. Diffraction patterns were obtained by integrating the intensities from detectors mounted at diffraction angles of 90° . The collected intensity versus converted to intensity vs. d-spacing for

GSAS refinement. Raw plots of the combined data were used for all of the unit cell and cell volume calculations.

5.4 RESULTS

5.3.1 X-ray diffraction

The diffraction patterns for the K-jarosite, Na-jarosite and NH₄-jarosite standard syntheses (end members) are shown in figure 5.1, and the jarosite glycine syntheses (jarosite-SWG) are shown in figure 5.2. The calculated unit cell dimensions for all of the syntheses are in Table 5.1 and were calculated from the {003} and {110} crystallographic reflections (for detailed discussion of end member jarosite X-ray diffraction see Appendix 2). The K-jarosite standard synthesis (figure 5.1 A) had unit cell dimensions of $a = 7.34 \text{ \AA}$ and $c = 17.28 \text{ \AA}$. The K-jarosite-SWG (figure 5.2 A) had a shorter a -axis at 7.32 \AA and a shorter c -axis of 17.10 \AA . Qualitatively, the patterns are very similar with no visible changes in peak intensities. There are no additional peaks in the K-jarosite-SWG X-ray pattern that would indicate an unbound impurity in the sample.

The Na-jarosite standard synthesis (figure 5.1 B) had unit dimensions of $a = 6.98 \text{ \AA}$ and $c = 16.74 \text{ \AA}$. The Na-jarosite-SWG (figure 5.2 B) showed an increase along the a-axis with dimensions of 7.32 \AA , the c-axis remained the same at 16.74 \AA . The peak patterns are very similar between the two samples with no additional peaks in the Na-jarosite-SWG sample that would indicate the presence of an unbound impurity. Peak intensities between the two samples were also similar. The NH₄-jarosite standard

synthesis (figure 5.1 C) had unit cell dimensions of $a = 7.19 \text{ \AA}$ and $c = 17.50 \text{ \AA}$. The NH_4 -jarosite-SWG sample (figure 5.2 C) showed an increase in the a-axis with dimensions of 7.30 \AA and a decrease along the c-axis with dimensions of 17.41 \AA . The NH_4 -jarosite-SWG X-ray pattern is missing a peak at the $\{021\}$ reflection that is present at $26.53^\circ 2\theta$ in the NH_4 -jarosite X-ray pattern. The peak for the $\{113\}$ reflection is now a doublet peak in the NH_4 -jarosite-SWG pattern possibly representing a shift in the $\{021\}$ position or the addition of a new peak in the spectrum. There is a slight shift in intensity between the $\{110\}$ reflections relative to the $\{104\}$ reflection in the NH_4 -jarosite-SWG X-ray pattern compared to the NH_4 -jarosite pattern.

Table 5.1- X-ray diffraction unit cell dimensions for jarosite end-members and jarosite-SWG.

End member standards	{110}	{003}	Synthesized with glycine	{110}	{003}
K-jarosite $a = 7.34 \text{ \AA}$ $c = 17.28 \text{ \AA}$	$2\theta = 24.223$ $d = 3.67 \text{ \AA}$	$2\theta = 15.343$ $d = 5.76 \text{ \AA}$	K-jarosite-SWG $a = 7.32 \text{ \AA}$ $c = 17.10 \text{ \AA}$	$2\theta = 24.283$ $d = 3.66 \text{ \AA}$	$2\theta = 15.493$ $d = 5.70 \text{ \AA}$
Na-jarosite $a = 6.98 \text{ \AA}$ $c = 16.74 \text{ \AA}$	$2\theta = 25.483$ $d = 3.49 \text{ \AA}$	$2\theta = 15.863$ $d = 5.58 \text{ \AA}$	Na-jarosite-SWG $a = 7.32 \text{ \AA}$ $c = 16.74 \text{ \AA}$	$2\theta = 24.253$ $d = 3.66 \text{ \AA}$	$2\theta = 15.913$ $d = 5.58 \text{ \AA}$
NH_4-jarosite $a = 7.19 \text{ \AA}$ $c = 17.5 \text{ \AA}$	$2\theta = 24.718$ $d = 3.59 \text{ \AA}$	$2\theta = 15.193$ $d = 5.833 \text{ \AA}$	NH_4-jarosite-SWG $a = 7.3 \text{ \AA}$ $c = 17.41 \text{ \AA}$	$2\theta = 24.313$ $d = 3.65 \text{ \AA}$	$2\theta = 15.253$ $d = 5.802 \text{ \AA}$

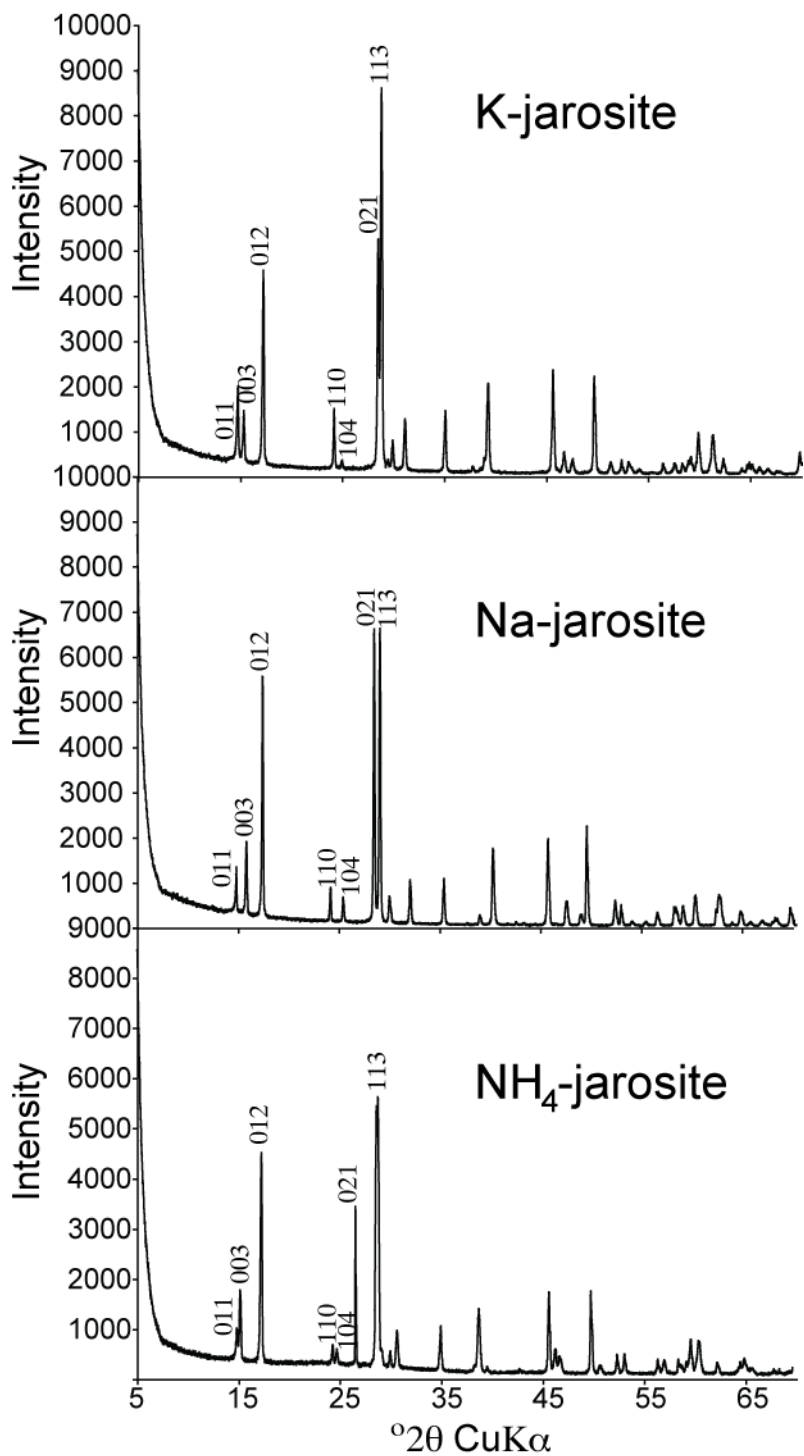


Figure 5.1- X-ray diffraction patterns for K-jarosite (A), Na-jarosite (B), and NH_4 -jarosite (C).

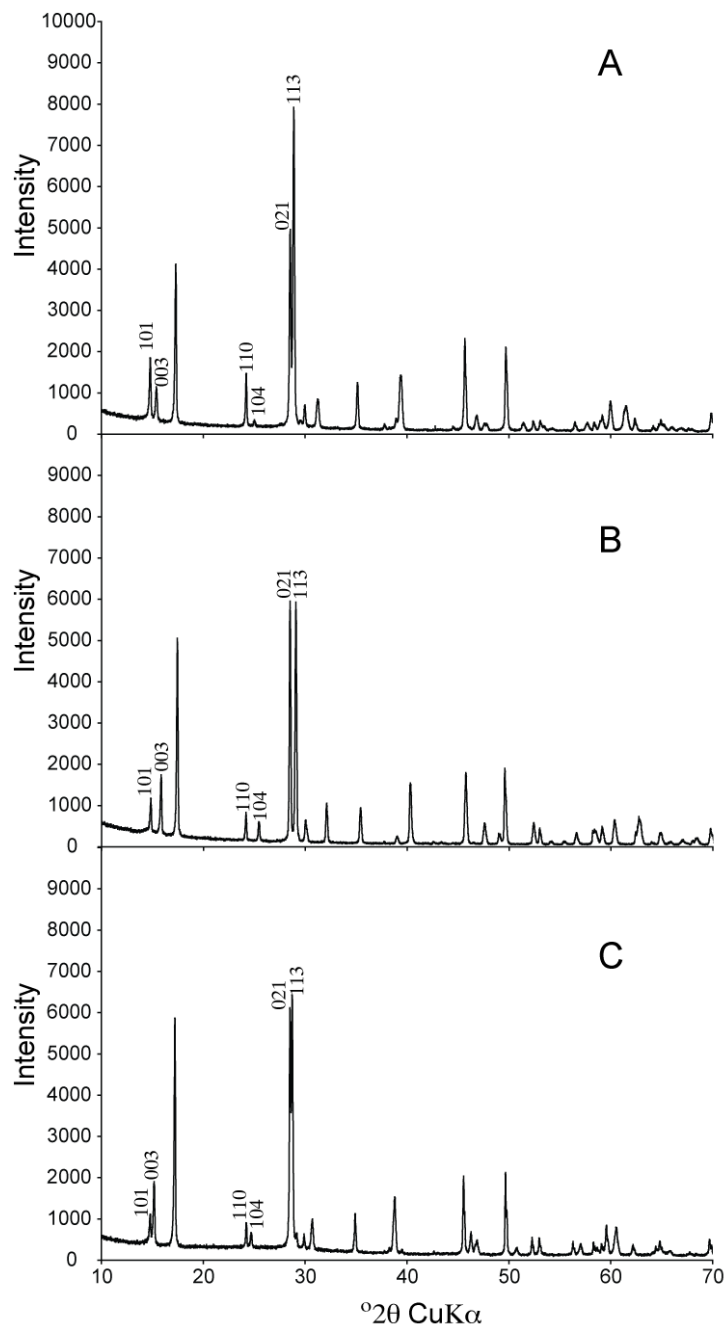


Figure 5.2- X-ray diffraction patterns for K-jarosite-SWG (A), Na-jarosite-SWG (B), and NH₄-jarosite-SWG (C).

5.4.2 NEUTRON DIFFRACTION-

The neutron diffraction patterns for dK-jarosite and dK-jarosite-SWG are shown in figure 5.3 (A, B). Unit cell dimensions were calculated from the {110} and {003} crystallographic reflections and are shown for all the neutron experiments in table 5.2. The unit cell dimensions for both the dK-jarosite and dK-jarosite-SWG are $a = 7.22 \text{ \AA}$ and $c = 17.28 \text{ \AA}$. When the patterns are subtracted (figure 5.4) a difference in intensities for the peaks are shown even though the peak positions are identical. The dK-jarosite-SWG had higher intensities on all peaks.

Figure 5.5 shows the neutron diffraction patterns for dNa-jarosite (A) and dNa-jarosite-SWG (B). The unit cell dimension for dNa-jarosite are $a = 6.97 \text{ \AA}$ and $c = 16.74 \text{ \AA}$ (table 5.2). The dNa-jarosite-SWG showed a shift in unit cell dimensions along both the a and c axes. The unit cell dimensions for dNa-jarosite were $a = 7.02 \text{ \AA}$ and $c = 16.80 \text{ \AA}$. Figure 5.6 shows the pattern subtraction results for dNa-jarosite minus dNa-jarosite-SWG. There are shifts in peak positions and differences in intensities between the samples. Similar to the dK-jarosite dK-jarosite-SWG subtraction results, the dNa-jarosite-SWG overall shows a greater intensity for the diffraction peaks compared to the standard synthesis.

Figure 5.7 shows the neutron diffraction patterns for dNH₄-jarosite (A) and dNH₄-jarosite-SWG (B). The patterns indicate that both samples have the same unit cell dimensions of $a = 7.38 \text{ \AA}$ and $c = 17.58 \text{ \AA}$. The subtracted pattern (figure 5.8) shows that there are differences in the intensities for certain peaks and shifts in positions for certain peaks, although the shifts are not observed for the peaks responsible for the unit cell dimension calculations. Additionally, unlike both the dK-jarosite and dNa-jarosite

subtraction results, the dNH₄-jarosite-SWG did not have more intense peaks than the standard.

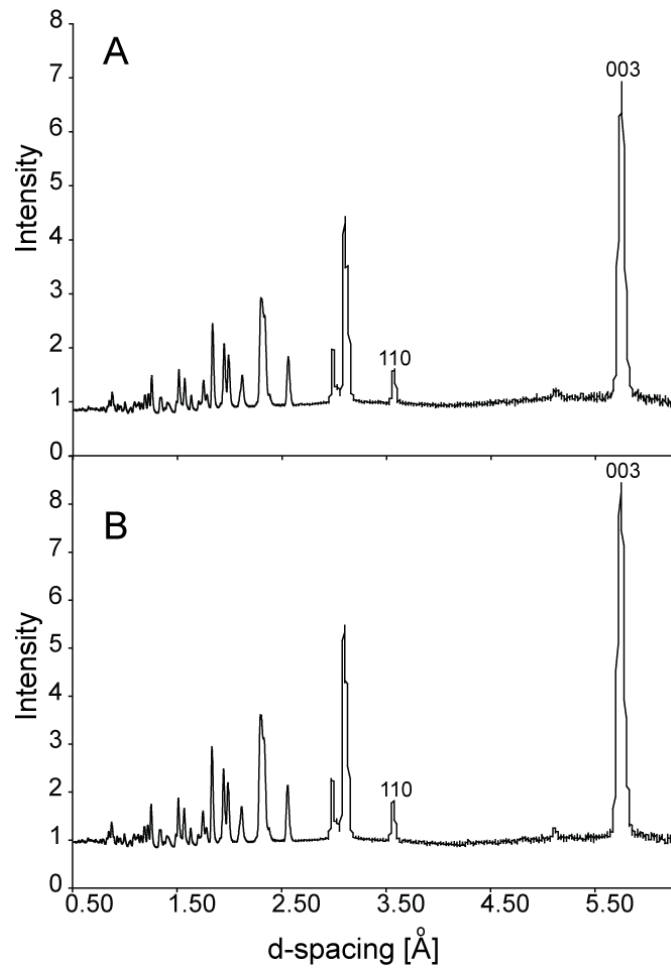


Figure 5.3- Neutron diffraction patterns for dK-jarosite (A) and dK-jarosite-SWG (B).

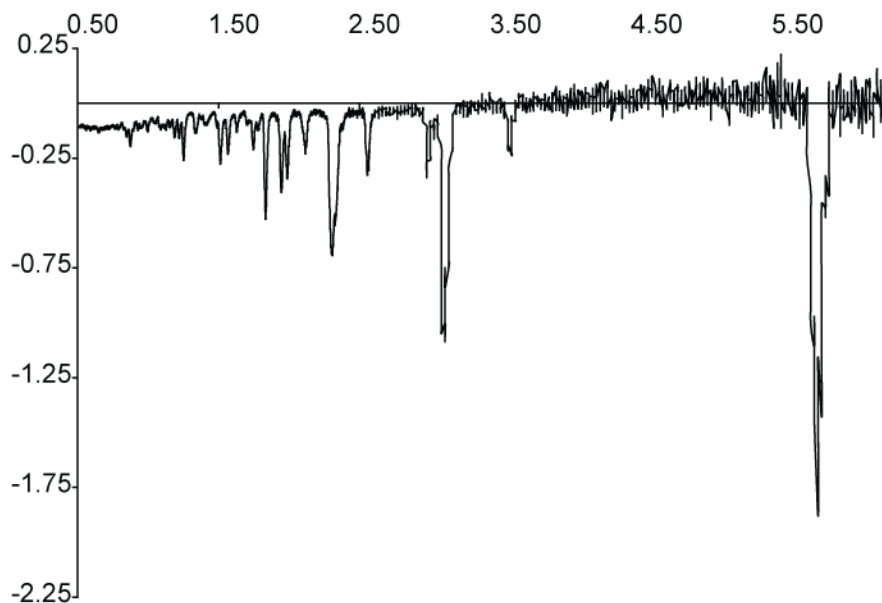


Figure 5.4- Subtracted neutron pattern (dK-jarosite – dK-jarosite-SWG).

Table 5.2- Neutron diffraction unit cell dimensions for the deuterated jarosite end-members and jarosite-SWG.

End member standards	{110}	{003}	Synthesized with glycine	{110}	{003}
dK-jarosite a = 7.22 Å c = 17.28 Å	d = 3.61 Å	d = 5.76 Å	dK-jarosite-SWG a = 7.22 Å c = 17.28 Å	d = 3.61 Å	d = 5.76 Å
dNa-jarosite a = 6.97 Å c = 16.74 Å	d = 3.48 Å	d = 5.58 Å	dNa-jarosite-SWG a = 7.02 Å c = 16.80 Å	d = 3.51 Å	d = 5.60 Å
dNH ₄ -jarosite a = 7.38 Å c = 17.58 Å	d = 3.69 Å	d = 5.86 Å	dNH ₄ -jarosite- SWG a = 7.38 Å c = 17.58 Å	d = 3.69 Å	d = 5.86 Å

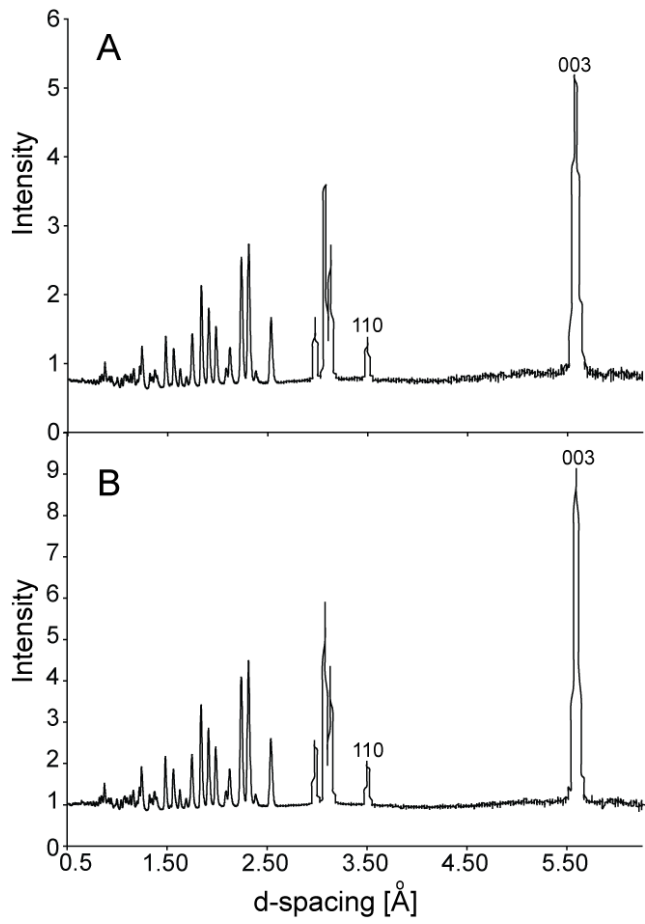


Figure 5.5- Neutron diffraction patterns for dNa-jarosite (A) and dNa-jarosite-SWG (B).

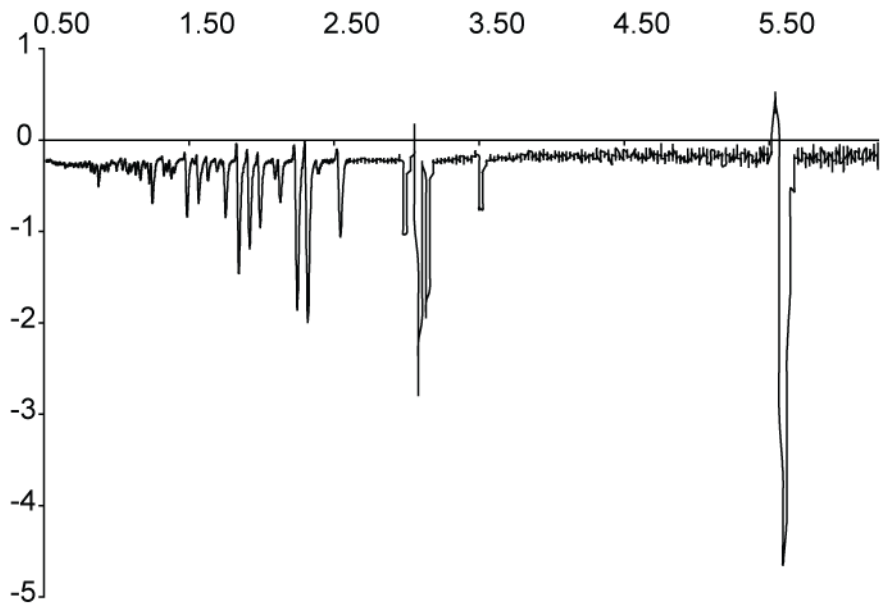


Figure 5.6 - Subtracted neutron pattern (dNa-jarosite – dNa-jarosite-SWG).

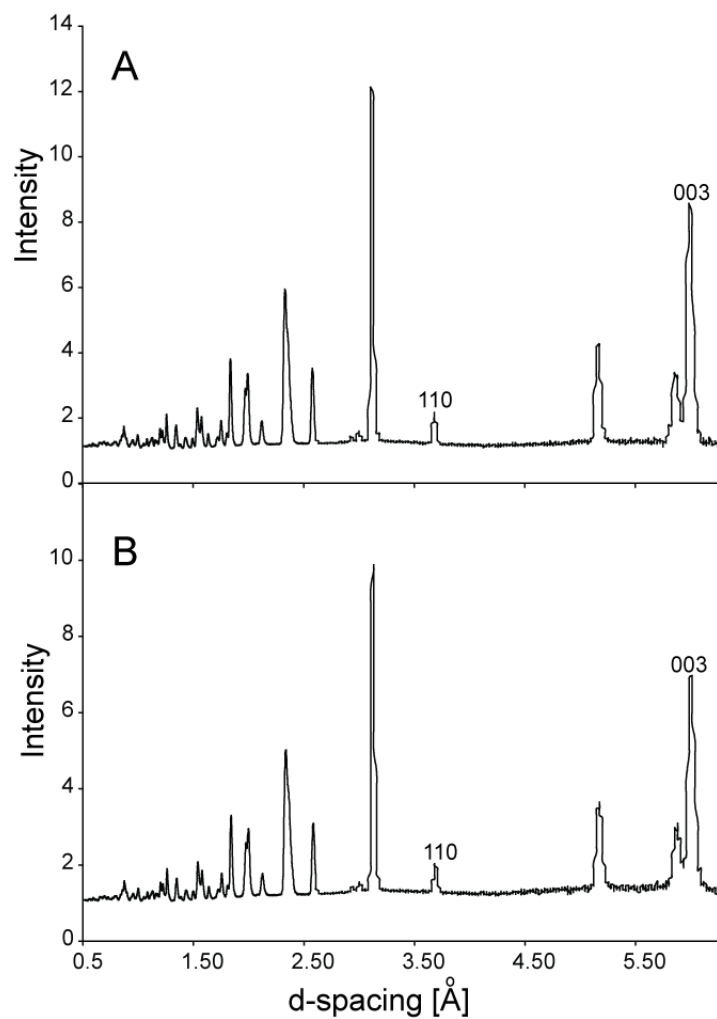


Figure 5.7- Neutron diffraction patterns for dNH₄-jarosite (A) and dNH₄-jarosite-SWG (B).

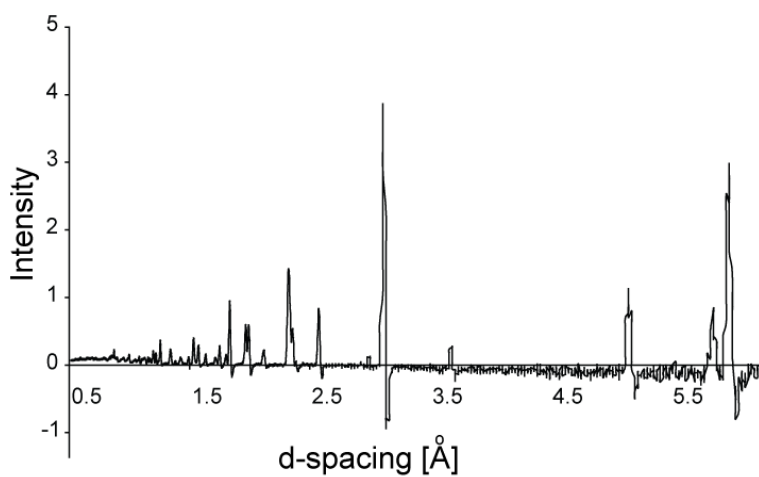


Figure 5.8- Subtracted neutron pattern (dNH₄-jarosite – dNa-jarosite-SWG).

5.5 DISCUSSION

The X-ray diffraction results indicated that K-jarosite-SWG showed a contraction in the a-axis and c-axis compared to the standard. The Na-jarosite-SWG showed an increase along the a-axis with the c-axis remaining the same compared to the standard. The NH₄-jarosite-SWG showed an increase in the a-axis and a decrease in the c-axis compared to the standard and at least one peak showed a shift in position compared to the standard. It is likely that the changes are caused by a contraction of the cell dimensions for the K-jarosite-SWG sample representing a decrease in hydronium ion substitution; although without Rietveld analysis to determine atomic positions this can't be confirmed. It is also unknown if any glycine was substituted in the structure. The expected result would be that the unit cell would increase given the large size of glycine compared to the both K⁺ and H₃O⁺. It is possible that the glycine would also double the unit cell of the crystal because of the charge of glycine at the pH of the experiments (²⁺). This would be a similar effect seen with Pb²⁺ substituting in the crystal structure.

The increase in cell dimensions for the Na-jarosite-SWG along the a-axis would indicate that glycine if present in the structure of the sample it is causing the increased axial dimension. The increase of the NH₄-jarosite-SWG along the same axis would also confirm this assumption. The shift in peak positions of the {021} peak in the NH₄-jarosite-SWG could represent a shift in symmetry for the structure that would accommodate the larger molecule in the structure. There were no peak intensity changes

between the jarosite standards and the jarosite-SWG X-ray diffraction results that would indicate a possible preferred orientation change between the samples.

The X-ray diffraction results are considerably different than the neutron diffraction results. In the X-ray diffraction experiments all three jarosite end members showed changes in the peak positions used for the unit cell dimension calculations after being synthesized in the presence of glycine. For the neutron diffraction experiments, only the dNa-jarosite-SWG showed changes in the peaks used for the unit cell dimension calculations. All of the neutron diffraction patterns for the jarosite standards showed differences in peak intensities for the jarosite glycine syntheses. There were no dominant peak changes that would indicate preferred orientation due to the fact that all of the peaks were shifted relative to one another, not one or two peaks showing a dominant shift.

Further work is in progress to complete Reitveld analysis of all the samples used for both the X-ray and neutron diffraction studies. The results of the Reitveld analysis should provide further clues as to hydronium ion site occupancy to determine if glycine does interfere with hydronium substitution in the samples. Additionally, Reitveld analysis should confirm space group designations for the samples. Reitveld could potentially identify the atomic positions of glycine in the unit cell, although the low concentrations of glycine in the samples could limit the success of this attempt.

The results of this study indicate that glycine can play a structural role when glycine is present in the synthetic procedure. The strength of this effect and the ability to detect changes could be related to the thermodynamic stability of the different jarosite end-members. K-jarosite is the most stable end-member (ALPERS and RYE, 1992; BARON, 1996; FORRAY et al., 2005; MAJZLAN et al., 2006a; MAJZLAN et al., 2004; NAVROTSKY et

al., 2005; STOFFREGEN et al., 2000). It is likely that K-jarosite would be least susceptible to the effects of glycine since it is the most preferred structure. It is likely then that the other jarosite end-members such as Na-jarosite and NH₄-jarosite would make better targets for astrobiological investigations.

5.6 CONCLUSIONS

Additional work needs to be completed on the results of the X-ray and neutron diffraction experiments used in this study. It can be concluded that glycine appears to have a structural effect on jarosite samples when they are co-precipitated from solution. The effect seems to be most strongly noted for the Na-jarosite based on changes to the structure observed in both the X-ray and neutron diffraction analyses.

5.7 REFERENCES

- Alcobe, X., Bassas, J., Tarruella, I., Roca, A., and Vinals, J., 2001. Structural characterization of synthetic Beudantite-type phases by Rietveld refinement. In: Delhez, R. and Mittemeijer, E. J. Eds.).
- Alpers, C. N. and Rye, R. O., 1992. Chemical, Crystallographic and Stable Isotope Properties of Alunite and Jarosite from Acid Hypersaline Australian Lakes. *Chemical Geology* **96**, 203-226.
- Armstrong, D. C., 1995. Acid Sulfate Alteration in a Magmatic Hydrothermal Environment, Barton Peninsula, King George Island, Antarctica. *Mineralogical Magazine* **59**, 429-441.
- Aubrey, A., Cleaves, H. J., Chalmers, J. H., Skelley, A. M., Mathies, R. A., Grunthaner, F. J., Ehrenfreund, P., and Bada, J. L., 2006. Sulfate minerals and organic compounds on Mars. *Geology* **34**, 357-360.
- Baird, A. K. and Clark, B. C., 1981. On the igneous source of Martian fines. *Icarus* **45**.
- Baron, D., Palmer C.D., 1996. Solubility of jarosite at 4-35 degrees C. *Geochimica Et Cosmochimica Acta* **60**, 285-195.

- Basciano, L. C. and Peterson, R. C., 2007a. Jarosite-hydronium jarosite solid-solution series with full iron site occupancy: Mineralogy and crystal chemistry. *American Mineralogist* **92**, 1464-1473.
- Basciano, L. C. and Peterson, R. C., 2007b. The crystal structure of ammoniojarosite, (NH₄)Fe-3(SO₄)(2)(OH)(6) and the crystal chemistry of the ammoniojarosite-hydronium jarosite solid-solution series. *Mineralogical Magazine* **71**, 427-441.
- Basciano, L. C. and Peterson, R. C., 2008a. Crystal chemistry of the natrojarosite-jarosite and natrojarosite-hydronium jarosite solid-solution series: A synthetic study with full Fe site occupancy. *American Mineralogist* **93**, 853-862.
- Basciano, L. C. and Peterson, R. C., 2008b. Crystal chemistry of the natrojarosite-jarosite and natrojarosite-hydronium jarosite solid-solution series: A synthetic study with full Fe site occupancy. *American Mineralogist* **93**, 853-862.
- Behera, J. N. and Rao, C. N. R., 2007. Synthesis, structure and magnetic properties of an amine-templated Mn²⁺ (S=5/2) sulfate with the Kagome structure. *Dalton Transactions*, 669-673.
- Burger, P. V., Papike, J. J., Shearer, C. K., and Karner, J. M., 2009. Jarosite growth zoning as a recorder of fluid evolution. *Geochimica Et Cosmochimica Acta* **73**, 3248-3259.
- Burns, R. G., 1990. Iron-sulfur mineralogy of Mars: magmatic evolution and chemical weathering products. *Journal of Geophysical Research* **95**, 14415-14421.
- Christensen, P. R., Ruff, S. W., Ferguson, R. L., Knudson, A. T., Anwar, S., Arvidson, R. E., Bandfield, J. L., Blaney, D. L., Budney, C., Calvin, W. M., Glotch, T. D., Golombek, M. P., Gorelick, N., Graff, T. G., Hamilton, V. E., Hayes, A., Johnson, J. R., McSween, H. Y., Mehall, G. L., Mehall, L. K., Moersch, J. E., Morris, R. V., Rogers, A. D., Smith, M. D., Squyres, S. W., Wolff, M. J., and Wyatt, M. B., 2004a. Initial results from the Mini-TES experiment in Gusev crater from the Spirit rover. *Science* **305**, 837-842.
- Christensen, P. R., Wyatt, M. B., Glotch, T. D., Rogers, A. D., Anwar, S., Arvidson, R. E., Bandfield, J. L., Blaney, D. L., Budney, C., Calvin, W. M., Faracaro, A., Ferguson, R. L., Gorelick, N., Graff, T. G., Hamilton, V. E., Hayes, A. G., Johnson, J. R., Knudson, A. T., McSween, H. Y., Mehall, G. L., Mehall, L. K., Moersch, J. E., Morris, R. V., Smith, M. D., Squyres, S. W., Ruff, S. W., and Wolff, M. J., 2004b. Mineralogy at Meridiani Planum from the Mini-TES experiment on the Opportunity Rover. *Science* **306**, 1733-1739.
- Clark, B. C., Morris, R. V., McLennan, S. M., Gellert, R., Jolliff, B., Knoll, A. H., Squyres, S. W., Lowenstein, T. K., Ming, D. W., Tosca, N. J., Yen, A., Christensen, P. R., Gorevan, S., Bruckner, J., Calvin, W., Dreibus, G., Farrand, W., Klingelhofer, G., Waenke, H., Zipfel, J., Bell, J. F., Grotzinger, J., McSween, H. Y., and Rieder, R., 2005. Chemistry and mineralogy of outcrops at Meridiani Planum. *Earth and Planetary Science Letters* **240**, 73-94.
- Dill, H. G. and Pollman, H., 2002. Supergene mineralization in mining residues of the Matchless cupreous pyrite deposit (Namibia)- a clue to the origin of modern and fossil duricrusts in semiarid climates. *Journal of Geochemical Exploration* **75**, 43-70.

- Dutrizac, J. E. and Chen, T. T., 2006. Synthesis and characterization of the chromium(III) analogues of jarosite-type compounds. *Canadian Metallurgical Quarterly* **45**, 249-260.
- Forray, F. L., Drouet, C., and Navrotsky, A., 2005. Thermochemistry of yavapaiite $\text{KFe}(\text{SO}_4)_2$: formation and decomposition. *Geochimica Et Cosmochimica Acta* **69**, 2133-2140.
- Fulignati, P. and Sbrana, A., 2002. Formation of rock coating induced by the acid fumarole of plume of the actively degassing volcano of La Fossa (Vulcano Island, Italy). *Journal of Volcanology and Geothermal Research* **115**, 397-410.
- Grey, I. E., Mumme, W. G., Bordet, P., and Mills, S. J., 2008. A NEW CRYSTAL-CHEMICAL VARIATION OF THE ALUNITE-TYPE STRUCTURE IN MONOCLINIC $\text{PbZn}_{0.5}\text{Fe}_3(\text{AsO}_4)_2(\text{OH})_6$. *Canadian Mineralogist* **46**, 1355-1364.
- Grohol, D., Huang, Q. Z., Toby, B. H., Lynn, J. W., Lee, Y. S., and Nocera, D. G., 2003. Powder neutron diffraction analysis and magnetic structure of kagome-type vanadium jarosite $\text{NaV}_3(\text{OD})_6(\text{SO}_4)_2$. *Physical Review B* **68**.
- Jambor, J. L., 1999. Nomenclature of the alunite supergroup. *Canadian Mineralogist* **37**, 1323-1341.
- Johnston, J. H., 1977. Jarosite and Akaganeite from White Island Volcano, New Zealand—an X-ray and Mossbauer study. *Geochimica Et Cosmochimica Acta* **41**, 539-544.
- Klingelhofer, G., Morris, R. V., Bernhardt, B., Schroder, C., Rodionov, D. S., de Souza, P. A., Yen, A., Gellert, R., Evlanov, E. N., Zubkov, B., Foh, J., Bonnes, U., Kankleit, E., Gutlich, P., Ming, D. W., Renz, F., Wdowiak, T., Squyres, S. W., and Arvidson, R. E., 2004. Jarosite and hematite at Meridiani Planum from Opportunity's Mossbauer spectrometer. *Science* **306**, 1740-1745.
- Kotler, J. M., Hinman, N. W., Yan, B., Stoner, D. L., and Scott, J. R., 2008. Glycine identification in natural jarosites using laser desorption Fourier transform mass spectrometry: Implications for the search for life on Mars. *Astrobiology* **8**, 253-266.
- Madden, M. E. E., Bodnar, R. J., and Rimstidt, J. D., 2004. Jarosite as an indicator of water-limited chemical weathering on Mars. *Nature* **431**, 821-823.
- Majzlan, J., Navrotsky, A., McCleskey, R. B., and Alpers, C. N., 2006a. Thermodynamic properties and crystal structure refinement of ferricopiapite, coquimbite, rhomboclase, and $\text{Fe}_2(\text{SO}_4)_3(\text{H}_2\text{O})_5$. *European Journal of Mineralogy* **18**, 175-186.
- Majzlan, J., Speziale, S., Duffy, T. S., and Burns, P. C., 2006b. Single-crystal elastic properties of alunite, $\text{KAl}_3(\text{SO}_4)_2(\text{OH})_6$. *Physics and Chemistry of Minerals* **33**, 567-573.
- Majzlan, J., Stevens, R., Boerio-Goates, J., Woodfield, B. F., Navrotsky, A., Burns, P. C., Crawford, M. K., and Amos, T. G., 2004. Thermodynamic properties, low-temperature heat-capacity anomalies, and single-crystal X-ray refinement of hydronium jarosite, $(\text{H}_3\text{O})\text{Fe}_3(\text{SO}_4)_2(\text{OH})_6$. *Physics and Chemistry of Minerals* **31**, 518-531.
- Navrotsky, A., Forray, F. L., and Drouet, C., 2005. Jarosite stability on Mars. *Icarus* **176**, 250-253.

- Papike, J. J., Karner, J. M., Spilde, M. N., and Shearer, C. K., 2006. Terrestrial analogs of martian sulfates: Major and minor element systematics of alunite-jarosite from Goldfield, Nevada. *American Mineralogist* **91**, 1197-1200.
- Skelley, A. M., Scherer, J. R., Aubrey, A. D., Grover, W. H., Ivester, R. H. C., Ehrenfreund, P., Grunthner, F. J., Bada, J. L., and Mathies, R. A., 2005. Development and evaluation of a microdevice for amino acid biomarker detection and analysis on Mars. *Proceedings of the National Academy of Sciences of the United States of America* **102**, 1041-1046.
- Squyres, S. W., Arvidson, R. E., Bell, J. F., Bruckner, J., Cabrol, N. A., Calvin, W., Carr, M. H., Christensen, P. R., Clark, B. C., Crumpler, L., Des Marais, D. J., d'Uston, C., Economou, T., Farmer, J., Farrand, W., Folkner, W., Golombek, M., Gorevan, S., Grant, J. A., Greeley, R., Grotzinger, J., Haskin, L., Herkenhoff, K. E., Hviid, S., Johnson, J., Klingelhofer, G., Knoll, A., Landis, G., Lemmon, M., Li, R., Madsen, M. B., Malin, M. C., McLennan, S. M., McSween, H. Y., Ming, D. W., Moersch, J., Morris, R. V., Parker, T., Rice, J. W., Richter, L., Rieder, R., Sims, M., Smith, M., Smith, P., Soderblom, L. A., Sullivan, R., Wanke, H., Wdowiak, T., Wolff, M., and Yen, A., 2004a. The Spirit Rover's Athena Science Investigation at Gusev Crater, Mars. *Science* **305**, 794-799.
- Squyres, S. W., Arvidson, R. E., Bell, J. F., Bruckner, J., Cabrol, N. A., Calvin, W., Carr, M. H., Christensen, P. R., Clark, B. C., Crumpler, L., Des Marais, D. J., d'Uston, C., Economou, T., Farmer, J., Farrand, W., Folkner, W., Golombek, M., Gorevan, S., Grant, J. A., Greeley, R., Grotzinger, J., Haskin, L., Herkenhoff, K. E., Hviid, S., Johnson, J., Klingelhofer, G., Knoll, A. H., Landis, G., Lemmon, M., Li, R., Madsen, M. B., Malin, M. C., McLennan, S. M., McSween, H. Y., Ming, D. W., Moersch, J., Morris, R. V., Parker, T., Rice, J. W., Richter, L., Rieder, R., Sims, M., Smith, M., Smith, P., Soderblom, L. A., Sullivan, R., Wanke, H., Wdowiak, T., Wolff, M., and Yen, A., 2004b. The Opportunity Rover's Athena science investigation at Meridiani Planum, Mars. *Science* **306**, 1698-1703.
- Stoffregen, R. E., Alpers, C. N., and Jambor, J. L., 2000. Alunite-jarosite crystallography, thermodynamics, and geochronology. *Sulfate Minerals - Crystallography, Geochemistry and Environmental Significance* **40**, 453-479.
- Szymanski, J. T., 1988. The crystal structure of beudantite, $Pb(Fe, Al)_3[(As, S)_4]_2(OH)_6$. *The Canadian Mineralogist* **26**, 923-932.
- Toumi, M. and Tlili, A., 2008. Rietveld Refinement and Vibrational Spectroscopic Study of Alunite from El Gnater, Central Tunisia. *Russian Journal of Inorganic Chemistry* **53**, 1845-1853.
- Townsend, M. G., Longworth, G., and Roudaut, E., 1986. Triangular-spin, kagome plane in jarosites. *Physical Review B* **33**, 4919-4926.

APPENDIX 1: THE STELLAR STEW: DISTRIBUTION OF EXTRATERRESTRIAL ORGANIC COMPOUNDS IN THE UNIVERSE

J. Michelle Kotler

Department of Geosciences, 32 Campus Drive, University of Montana, Missoula, MT 59812
Phone: (406) 546-9833, Fax: (406) 243-4028, julia.kotler@umontana.edu

C. Doc Richardson

Department of Geosciences, 32 Campus Drive, University of Montana, Missoula, MT 59812
Phone: (406) 396-4626, Fax: (406) 243-4028, charles.richardson@umontana.edu

Nancy W. Hinman

Department of Geosciences, 32 Campus Drive, University of Montana, Missoula, MT 59812
Phone: (406) 243-5277, Fax: (406) 243-4028, nancy.hinman@umontana.edu

Jill R. Scott*

Chemical Sciences, Idaho National Laboratory, 1955 Fremont, MS 2208, Idaho Falls, ID 83415
Phone: (208) 526-0429, Fax: (208) 526-8541, jill.scott@inl.gov

*Corresponding Author

A1 1.1 INTRODUCTION

The universe is composed of heterogeneous environments that range from molecular clouds in the interstellar medium (ISM) to comets and asteroids, as well as to planetary bodies (see Figure A1.1). Currently, the ISM is known to contain organic compounds that are potential precursors to prebiotic molecules. The chemistry in the ISM is driven by variations in temperature, density, and radiation as it relates to the interplay between dust grains and gases. The dust grains and gases are like the broth of a stew as they carry organic compounds from one region to another. The dust grains, along with gas molecules that have condensed on their surfaces, are thought to accrete to form comets, asteroids, meteorites, and planetary bodies. The organic constituents in extraterrestrial objects in our solar system may be altered from their original interstellar organic compositions if the environment induces further chemistry; however, some organic material is thought to remain unaltered from their primordial parent material. Comets, asteroids, meteorites, and interplanetary dust particles (IDPs) bombard planetary bodies delivering various organic molecules that can provide the organic and biochemical building blocks for carbon-based life.

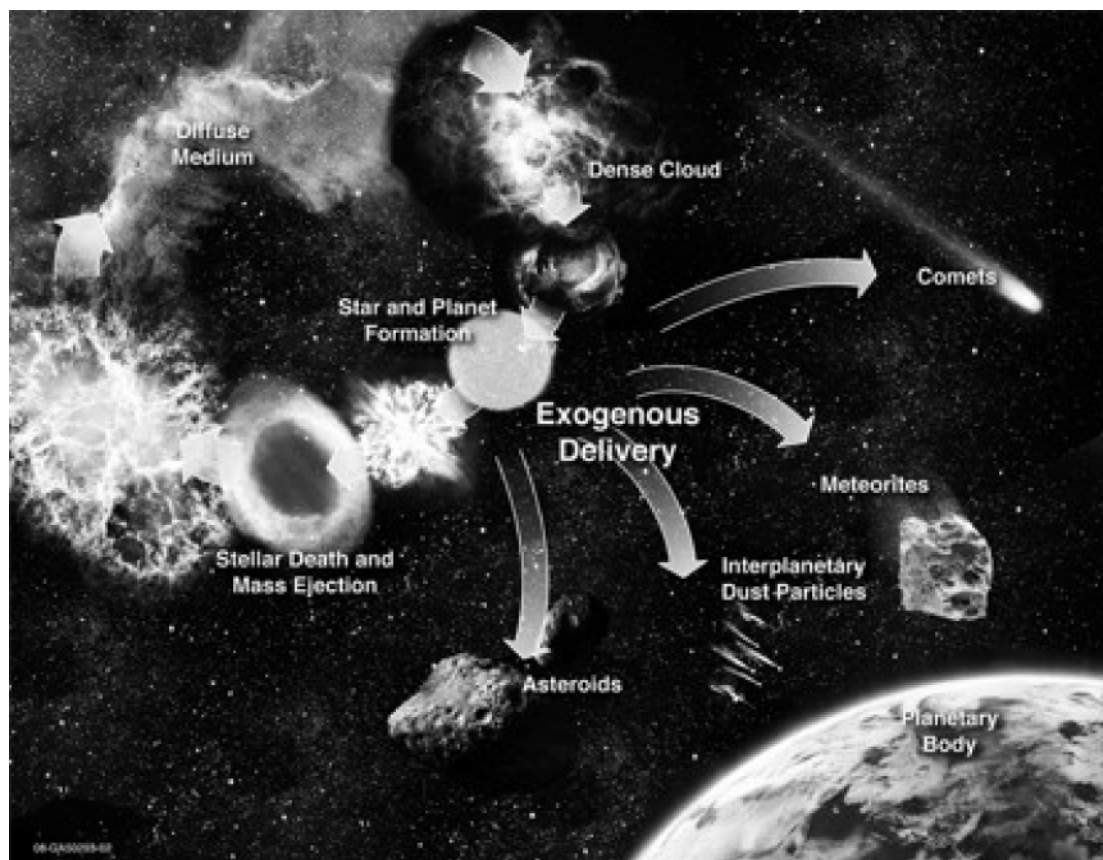


Figure A1.1 Illustration of the various extraterrestrial environments relevant to organic species. Illustration courtesy of Allen J. Haroldsen Idaho National Laboratory.

The most complex extraterrestrial bio/organic molecules, such as prebiotic amino acids, were discovered by directly analyzing extraterrestrial objects that were naturally delivered to Earth, such as chondritic meteorites, with mature analytical techniques. Improvements in telescope technology have enabled remote identification of many organic species. Currently, interrogation of planetary bodies by spacecraft-based probes has not detected complex organic molecules that could represent signs of extant or extinct life, primarily because of the complexities of engineering, sending, and operating complex analytical instrumentation for space-based exploration.

The effort to determine how life originated on Earth, or elsewhere in the universe, involves understanding where and how organic molecules, especially biologically relevant species, are created and then delivered to planetary bodies. After organic compounds have been delivered, it is necessary to understand how terrestrial processes may have contributed to the development of life (see the chapter on “Mineral-induced peptide formation” by Bujdak et al. and the chapter on “The role of clay interactions in chemical evolution” by Negrón-Mendoza et al. for more information). Such an undertaking involves several scientific disciplines, such as astronomy, chemistry, biology, and geology, as well as various branches of engineering. A plethora of scientific literature reports on understanding extraterrestrial organic chemistry, rendering an exhaustive review of all aspects related to extraterrestrial organic compounds prohibitive at best. Therefore, this chapter is an overview of the spatial distribution of organic compounds, the chemistry controlling their fate, and their delivery to various extraterrestrial environments. Thus, this chapter is a generalized ‘Hitchhiker’s Guide’ to extraterrestrial organic compounds.

A1 2.1 INTERSTELLAR MEDIUM ORGANIC COMPOUNDS

The ISM is composed of interstellar dust and gas that interact to produce many molecules, including complex organic species (i.e., neutrals, radicals, and ions). Both dust and gas are modified or processed as they cycle through the various ISM environments, leading to a variety of organic species distributed heterogeneously throughout the ISM. The chemical heterogeneity in the ISM is largely created because of variations in temperature, pressure, and radiation in various environments that affect both the formation and destruction of the organic compounds.

While dust and gas are usually associated with diffuse and dense clouds, the anatomy of the ISM is quite complex and includes translucent clouds whose properties are intermediate between diffuse and dense molecular clouds [1]. In general, diffuse clouds have a low density of

dust and gas resulting in environments exposed to starlight or ultraviolet (UV) radiation and have temperatures from 30–100 K, while dense or dark clouds have high densities of dust and gas resulting in environments that are protected from UV radiation and have temperatures of ~10 K. However, even the environment within a cloud can be heterogeneous, leading to non-uniform distribution of UV radiation and temperatures within a cloud [2]. For example, dense clouds can be “clumpy” and also contain hot molecular cores (HMC) [3,4]. Thus, within a particular region, there are a variety of components that each represents a specific physical and chemical environment (e.g., Orion-KL with a HMC, compact and extended ridges, and a plateau) [5]. As the technology for observing these features has improved, regions such as Orion-KL have proved even more complex than previously thought [6]. The heterogeneous environments present a challenge to astronomers and astrochemists because of potential overlap of different types of cloud environments along a line of sight. Therefore, improvements in technology and methodology are sometimes necessary to “disentangle absorption features” [7].

ISM dust and gas cycle through the various cloud environments multiple times [8,9]. A simple model of the cycling between different cloud types is illustrated in Figure A1.1. Solar winds and explosions expel dust and gas into the diffuse ISM. Diffuse clouds begin to collapse into more dense clouds where stars form. While the core temperature is low, most gas species condense on the surfaces of dust grains forming molecular ices. After the star ignites, the temperature increases allowing organic species to evaporate into the gas phase where chemical reactions can be thermally driven [10]. While some of the dust and gas is consumed in the star or accreted to form larger bodies, other dust and gas remain in the circumstellar disk. Eventually, dust and gas within the circumstellar envelope are returned to the diffuse ISM as mass lost from the dying star’s system [11]. Thus, detecting organic signatures in the various ISM environments is of interest for monitoring the process of star and planetary system formation [12-14] as well as for understanding how extraterrestrial organic compounds may have contributed to the development of carbon-based life.

Identifying the organic species that are created as the dust and gas cycle through the diffuse molecular clouds, dark dense clouds, and hot molecular cores of the ISM requires a variety of approaches from observing and detecting the spectral signatures to laboratory experiments and computational modeling. The organic compounds are observed through various telescopic methods that include UV for electronic transitions, infrared (IR) for vibrational modes, and radio waves for rotational modes. While some organic species are easily observed, others are not. Simple compounds (e.g., H₂O, CO, and CO₂) often have very strong vibrational modes and are present in relatively high abundances, but more complex species tend to have weaker vibrational modes and are less abundant [15]. After spectra are observed, the assignments of the identity of the compounds are usually based on comparison with laboratory experiments designed to mimic the various environments of the ISM (see Figure A1.2) (see the chapter on “High molecular weight complex organics in interstellar space and their relevance to origins of life” by Kobayashi et al.). Theoretical computations are also used to determine if the presence of specific species are possible and if so, what the spectra should look like (see the chapter on “Mechanisms of organic reactions in interstellar medium” by Guillemin). Laboratory experiments and computations are not only used for confirming observed astronomical assignments, but also as guides for searching the ISM by predicting which organic compounds are likely to be produced and survive in different ISM environments. For example, propynal (HC≡CCH=O) was first observed in the laboratory in 1955 [16], over thirty years before it was observed in space within the cold dense cloud Taurus molecular cloud 1 (TMC-1) [17] and Sagittarius B2 (Sgr B2) [18]. Computational studies to determine the mechanism for the formation of propynal were still being performed in 2007 [19]. Another example of the interplay between observations, laboratory experiments, and computations is the case of the “XCN” feature observed at 4.62 μm [20,21]. Schutte and Greenberg [22] originally conjectured that OCN⁻ with NH₄⁺ as the counterion is responsible for the XCN band and many proposed pathways for its formation have been reviewed by Pendleton et al. [23]. Recently, Park and Woon [24] have confirmed the experimental

assignment by Schutte and Greenberg [22] using density functional theoretical calculations. Thus, the assignments of observed astronomical spectral features are often controversial and are only assigned after extensive experimentation and computational modeling.

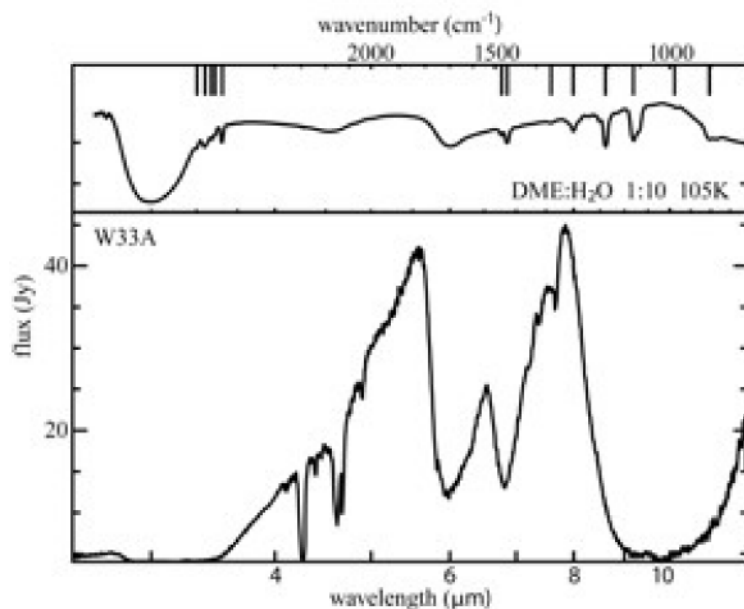


Figure A1.2. Comparison of laboratory acquired spectrum of A) 1:10 mixture of dimethyl ether (CH₃OCH₃) and H₂O at 105 K with B) observed spectrum from the protostar W33A (vertical lines indicate CH₃OCH₃ bands) {Peeters, 2006 #145}. Reprinted with permission from Peeters, et al., *Astronomy & Astrophysics*, 445, 197-204, 2006, Copyright Astronomy and Astrophysics (2008).

The potential presence of amino acids in the ISM is inferred from laboratory synthesis experiments [26-28] and computations [29] that have used precursor species similar to those found in space [30]. Experiments have even shown that homochirality of amino acids could have its origin in space [31]. Therefore, there was great excitement over the announcement that even the simplest amino acid, glycine, had been observed in the ISM (see Figure A1.3) [32]. Because of the enormous implications related to finding a prebiotic molecule in the IMS, the assignment was carefully scrutinized. Snyder et al. [33] noted several “peculiarities” regarding the spectral lines that were used by Kuan et al. [32] to identify glycine and performed a detail analysis of the reported spectra. Snyder et al. [33] suggest that line 21 (see Figure A1.3) is probably from

vibrationally excited ethyl cyanide ($\text{CH}_3\text{CH}_2\text{CN}$). Based on the analysis of this controversy, Snyder et al. [33] suggested criteria for making molecular identifications. Ziurys and co-workers [34] have suggested further guidelines for less ambiguous assignments of large, complex organic species in the ISM. Because large organic species have weak spectral features, better instrumentation with high sensitivity and improved resolution are needed and are currently under construction. The future space-based James Webb Space Telescope (JWST) and Earth-based Atacama Large Millimeter/submillimeter Array (ALMA) are expected to provide the high sensitivity for detection of weak lines from complex species [14,35].

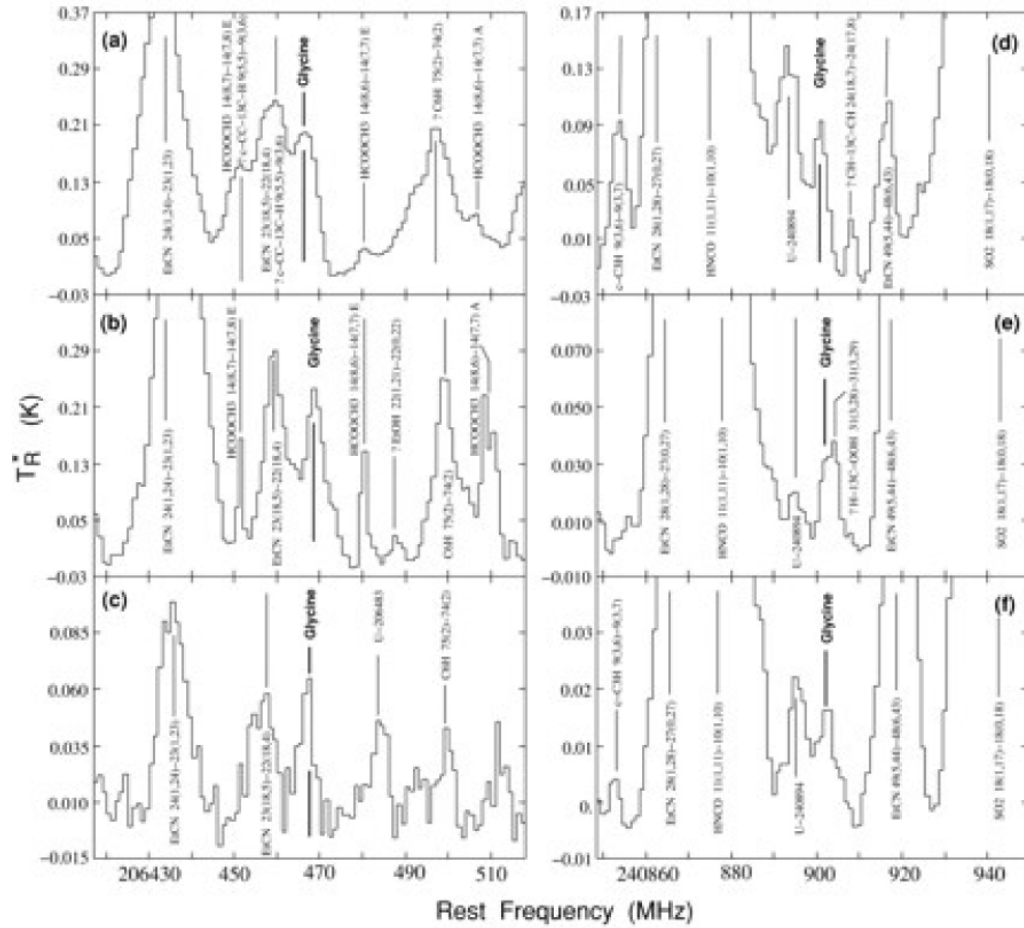


Figure A1.3 Spectral bands indicative of PAHs acquired from several sources: A) 3.3 μm feature and B) 8.6 μm and 11.2 μm features as well as 11.9 μm and 12.8 μm bands for the source WL 16 {Geers, 2007 #71}. Reprinted with permission from Kuan et al., The Astrophysical Journal, 593, 2, 2003, Copyright The American Astronomical Society (2008).

Interstellar dust grains play a critical role in both the physical and chemical processes that control the production of organic species. The surface of dust grains can act as sites for condensation as well as reactive sites that promote chemical reactions [36]. In addition, components of some dust grains can be transformed into large organic species directly. Several reviews have been written about interstellar dust [37-39] as well as its potential role in terrestrial prebiotic chemistry [9]. Dust ejected from stars is often referred to as ‘nuclear ash’ [40] and can be composed of silicates and carbonaceous materials [41]. The carbon-containing material can be graphite, amorphous carbon (AC), hydrogenated amorphous carbon (HAC), microdiamonds, coal, quenched-carbonaceous condensates (QCC), and soot, as well as fullerenes [4,9,42]. The 2880 cm^{-1} band in the aliphatic stretch region is consistent with a tertiary $-\text{CH}$ group. Because of the lower abundance of the $-\text{CH}_2-$ and $-\text{CH}_3$ bands, the $-\text{CH}$ group is likely to be connected to three other carbons; therefore, this band has been assigned to surface carbons of microdiamonds [43,44]. Fullerenes are thought to be produced from shock of carbon soot-like particles [4]. The heating and UV radiation exposure of the carbon material as it cycles through diffuse and dense clouds can lead to processing that results in production of large hydrocarbons [45,46].

Some of these carbonaceous materials can give rise to large organic molecules such as polycyclic aromatic hydrocarbons (PAHs). The carbonaceous grains may be composed of very small carbonaceous grains (VSGs) and PAHs [47,48]. Cesarsky et al. [47] have suggested that the shock waves and/or UV radiation destroys the VSGs, liberating the carriers of the aromatic infrared (IR) bands that are most likely PAHs [48]. Improved observation technologies and techniques have allowed the spectra from these two types of carbonaceous dust grains to be identified [48]. The spectra from interstellar PAHs have emission features at 3.3 μm for C–H stretching as well as 8.6 μm in-plane and 11.3 μm out-of-plane C–H bending (see Figure A1.3) [37]. Although there is little doubt that the spectral features are due to PAHs, specific PAH compounds (e.g., naphthalene, anthracene, etc.) have not been identified [49]. Computational

models suggest that the PAHs in the ISM are probably composed of at least 100 carbon atoms [50]. While PAHs are ubiquitous in space [37,50,51], there are variations in abundance in different locations [1]. Thus, the interest in PAHs is motivated not only because they are large organic molecules, but also because they can be used as diagnostics for stellar radiation [50]. If PAHs are truly formed as stars evolve, then following the distribution and properties should shed light on the evolution of galaxies [52].

Many reviews on extraterrestrial organic compounds are available [54-59]. A list of organic species that have been reported is provided in Table 1. The organic compounds range from small diatomic molecules to larger species, even commonly known compounds such as ethylene glycol [152]. The presence of deuterated species is important because the D/H ratio can be used to discern whether the mechanism producing the molecules occurs in the gas phase or on the grain surface [153,154]. In addition, because isotope ratios in the ISM are different from terrestrial isotope ratios, they can be used to determine the origin of organic species. For example, experiments have shown that photolysis of PAHs in deuterium-enriched interstellar ice analogues can produce isotope ratios that are consistent with the deuterium enrichment of aromatic molecules observed in meteorites and interplanetary dust particles (IDPs), suggesting an interstellar origin [155,156]. The number of detected organic species is growing quickly as better methods and technologies for observing the ISM are brought to bear. However, not all assignments are equally vetted. Websites, such as the Cologne Database for Molecular Spectroscopy, provide updated lists as well as comments regarding the status of the assignments [157,158].

While the ISM is highly complex, three key areas have been thoroughly explored for the presence of organic compounds: (1) diffuse molecular clouds, (2) dark dense clouds, and (3) hot molecular cores within dense clouds. These different environments affect the type of organic species that are observed. Most of the larger, complex organic compounds have been detected in hot molecular cores [129]. However, because most of the hot molecular core observations have been from Sagittarius B2 north (Sgr B2(N)) [159], which has a highly complex structure [160], questions arise about whether the larger molecules are actually in the envelope instead of the hot core [161]. Recently, large organic compounds, such as glycolaldehyde, were detected in the colder interstellar regions, such as the Central Molecular Zone of the Galactic center [161,162]. Possible formation mechanisms in these colder environments may include radicals created by cosmic rays [161,163]. In the case of glycolaldehyde (CH_2OHCHO), the mechanism would involve cleavage of a C–H bond of methanol to create the hydroxymethyl radical (CH_2OH), the H atom would have sufficient energy to overcome the activation barrier to react with CO to form the formyl radical (HCO). Then $\text{HCO}\cdot$ could combine with $\text{CH}_2\text{OH}\cdot$ to form CH_2OHCHO . These recent results illustrate that the understanding of extraterrestrial organic compounds in the ISM continues to evolve as spatial and spectral detection methods improve.

A1 2.2 DIFFUSE MOLECULAR CLOUDS

Typical environments of diffuse molecular clouds cover a temperature of range of 30-100 K, hydrogen density of $100\text{--}500\text{ cm}^{-3}$, and UV radiation of $\sim 10^8\text{ photons cm}^{-2}\text{s}^{-1}$ [54,164]. Snow and McCall [164] have published an excellent, detailed discussion of the physical and chemical properties of diffuse clouds, as well as their interrelationship. Unlike diffuse atomic clouds that are exposed to essentially all UV wavelengths, diffuse molecular clouds are shielded from some UV radiation, specifically the wavelengths that dissociate H_2 , by atomic gases and by self-shielding due to the higher density of H_2 [164]. However, diffuse molecular clouds are still exposed to UV wavelengths that photoionize carbon and photodissociate most organic molecules.

Thus, UV radiation is the controlling factor in diffuse clouds because, once released or produced in the gas phase, many organic molecules are destroyed by photolysis. Therefore, in diffuse clouds, the ability to detect organic species will depend on the relative rates of formation versus destruction by UV radiation.

Given the high level of UV radiation, it is not surprising that most of the observed organic compounds are small. The first diatomic species, CH, CN, and CH⁺, were observed over four decades ago [165-167]. Other common small organic species that have been observed include the following: C₂, CO, CS, HCO⁺, HCN, HNC, and H₂CO [168]. Other triatomic species detected include C₃, CH₂, HCS⁺, and HOC⁺ [58,69,70,78,85,103,109]. More recently, the polyatomic molecules C₂H, *c*-C₃H₂, *l*-C₃H, and C₄H have been reported [169]. While the abundance of some species (e.g., C₂H) in diffuse clouds is similar to the abundance of those observed in dense clouds, the abundance of other species (e.g., *c*-C₃H₂) can vary greatly, in this case being higher than that observed in dense clouds [54]. Nitriles are 5 to 10 times more stable than their corresponding acids when exposed to UV radiation [170]. Thus, regardless of the formation mechanism, organic acids will be less abundant because they are more easily destroyed by photolysis reactions. Nitriles are thought to be intermediates for prebiotic organic acids, including amino acids. Although nitriles are more abundant than acids in space, the opposite is true for carbonaceous meteorites, which is probably due to the easy conversion of nitriles to acids by hydrolysis reactions [170].

Organic compounds enter diffuse clouds from circumstellar envelopes in which their fate is governed by the radiation flux [54,164]. Because the photoionization of H₂ is suppressed, it is available for ion-molecule reactions, such as the formation of HCO⁺ by reaction of H₂ with CO⁺. The facile photoionization of C to C⁺ lead to reactions of the carbon cation with species such as CH and CH₂ that are thought to lead to the formation of PAHs. However, the same UV radiation that promotes formation of these species may also lead to their destruction. Thus, only the most photochemically stable species can survive in the diffuse clouds. Another route to hydrogenation

is on the dust grain surfaces, which have been implicated for production of H₂ and simple hydrides [171]. Modeling studies suggest that large carbon molecules could be formed by ion-molecule reactions or neutral-neutral reactions, probably involving radicals. Such reactions could potentially lead to carbon chains, ring structures, and even fullerenes [172]; however, these have not been definitively observed in diffuse clouds.

Although specific large carbon species have not been observed in diffuse molecular clouds, there is evidence for larger organic compounds [54,164]. The three key spectroscopic features that suggest large carbonaceous compounds: (1) the UV bump at 2200 Å; (2) the diffuse interstellar bands (DIBs) between 4,000 and 10,000 Å; and (3) unidentified infrared bands (UIBs) between 3 and 15 μm. The carrier for the UV bump has not been identified, but candidates for this feature include graphite, HAC, QCC, PAHs, and coal-like material [42,54], possibly generated from the dust grains. The DIBs are assumed to have an organic origin because the rich chemistry of carbon could produce a wide variety of compounds, especially PAHs and carbon chains, that would be needed to explain all of the DIBs [173]. The UIBs are generally thought to be the result of PAHs, but this assignment is not definitive.

Pendleton and Allamandola [174] investigated whether the organic spectral signature from the ISM could have a biological origin. The organic signature was found to be consistent with aromatic and aliphatic carbon with little or no nitrogen or oxygen. The aliphatic components were determined to be composed of small carbon chains of fewer than five carbon atoms. Thus, while the ISM organic compounds contribute to a reservoir of prebiotic precursors, there is no spectral evidence for a biological origin. Other researchers have theorized that aliphatic organic molecules generated in the interstellar medium could have contributed to amphiphilic compounds that may have lead to the development of the first cell membranes on primordial Earth [175].

A1 2.3 DENSE DARK MOLECULAR CLOUDS

Dense interstellar molecular clouds have very low temperatures (10–30 K) and high hydrogen atom densities (10^{4-8} cm^{-3}) compared to the diffuse cloud [54]. At these cold temperatures, most molecules are frozen onto the dust grains as icy coatings or mantles. The UV and visible light is efficiently extinguished by the dust in these dense clouds; hence, the clouds appear dark. However, IR wavelengths can pass through. The dust and molecules in the clouds absorb specific wavelengths depending on their composition and structure. While molecules in the dense dark clouds are shielded from UV light, cosmic rays still penetrate these clouds and affect the chemistry, which governs the types of organic species that are present. TMC-1 and Sgr B2 are prototypical dense dark clouds that have been surveyed for a variety of organic spectral lines [176,177]. However, the types of organic species detected are heterogeneously distributed and not always observed from all dense dark clouds [178].

The chemistry in dark dense clouds is controlled largely by the cold temperatures, which dictate that most reactions have no activation barrier and are most likely to occur on the grain surfaces. At 10 K, only the elements H, D, C, O, and N are mobile enough to move along the grain surface and potentially find a reaction partner [179]. Such cold environments generally produce small, simple species such as CO, N₂, O₂, C₂H₂, C₂H₄, and HCN as well as simple carbon chains [180]. H₂O, CO, and CO₂ are the most abundant species and are easily detected because they have very strong vibrational modes, while less abundant ice species, such as HCOOH and CH₃CHO, have weaker bands (e.g., OH and CH₃ bending modes) [15]. The hydrogenation reactions that give rise to the larger organic molecules are typically thought to involve surface reactions that repetitively hydrogenate CO by atomic hydrogen [181,182]. However, Bishop et al. [15] have shown that some molecules are not as likely to be hydrogenated on ice surfaces as others. Laboratory experiments comparing CO with CO₂ reveal that CO reacts readily with H atoms, while CO₂ is very stable in bulk ice and not likely to react with H atoms unless a catalytic surface is available [15]. The most saturated hydrocarbon

reported from TMC-1 is propylene (CH_2CHCH_3) [183]. Marcelino et al. [183] state that propylene has previously been ignored because there is no known viable pathway for its formation; thus, its detection suggests that the chemistry in dark clouds needs further exploration.

Even though hydrogen is at least 1,000 times more abundant than any other reactive species, most of the observed organic compounds are not fully hydrogenated [184]. Instead, many of the organic species have double and triple bonds, such as cyanoacetylene (HC_3N), vinyl cyanide (CH_2CHCN), and ethyl cyanide ($\text{CH}_3\text{CH}_2\text{CN}$) [185]. The variety of unsaturated carbon chain molecules that have been observed toward TMC-1 include cyanopolyynes (HC_{2n-1}N , $n = 1, 2, 3$) [186], methylcyanopolyynes ($\text{CH}_3\text{C}_{2n-1}\text{N}$, $n = 1, 2, 3$) [83,187,188], and methylpolyynes ($\text{CH}_3\text{C}_{2n}\text{H}$, $n = 1, 2, 3$) [189-193]. The largest methylpolyyne, $\text{CH}_3\text{C}_6\text{H}$, is an 11-atom molecule that was recently reported in 2006 [193]. The formation chemistry for all of the polyynes is thought to be similar because there is a strong correlation between the three different carbon-chain slopes when the total column density of the sequence members are plotted against the number of carbons in the molecules [193]. These molecules may also be formed on the surfaces of interstellar dust grains [83].

Propynal ($\text{HC}\equiv\text{CCH}=\text{O}$) is the simplest conjugated carbonyl compound that has been detected in TMC-1 [194]. However, the mechanism for its formation has been under investigation using laboratory and computational methods for many years [19]. Some of the proposed mechanisms have ranged from ion-molecule ($\text{C}_2\text{H}_3^+ + \text{CO}$) [195,196] to radical-molecule ($\text{C}_2\text{H} + \text{H}_2\text{CO}$) [197] and even neutral-neutral ($\text{C}_3 + \text{H}_2\text{O}$) [198,199] reactions; however, none of these mechanisms are tenable in the environment in a dense dark cloud. A more reasonable reaction has recently been proposed that involves the radical-molecule reaction of C_3H and H_2O on amorphous water ice. This reaction is plausible because the reaction catalyzed on the surface of an icy mantle can be barrierless [19], while the gas-phase reaction would have a considerable energy barrier [200].

Neutral species (e.g., C_nH), and their negative ions (e.g., C_nH^-) have been detected in clouds such as TMC-1. The hydrocarbon anion C_6H^- has been detected in the interstellar medium with an abundance of 1–5% [145]. Assuming that PAHs comprise the grain, then the abundance ratio $n(C_6H^-)/n(C_6H)$ is predicted to follow the ratio of the free electron density to the density of atomic hydrogen [201]. Once the neutral species has at least 5 carbons, then the anion/neutral abundance ratio is estimated to be on the order of a few percent [202]. Laboratory determination of the rotational spectra for the anions butadiyne (C_4H^-) and octatetrayne (C_8H^-) were determined because they are expected to be good candidates for detection in TMC-1 and IRC + 10216 [203]. Indeed, C_8H^- has been detected in TMC-1 and is approximately 5% as abundant as the neutral species, C_8H [204].

Methanol is considered a very important molecule because it could be a precursor to larger organic compounds [54,205]. Typical abundance of approximately $1.5 \times 10^{-9} n_H$ [206,207]. A proposed gas-phase mechanism to produce CH_3OH would involve radiative association of CH_3^+ with H_2O to form protonated methanol followed by recombination with electrons to produce methanol and atomic hydrogen. However, this gas-phase reaction cannot take place in the environment of a dark ISM cloud; therefore, there must be a grain-surface formation process that leads to observed methanol gas-phase abundances [207]. Surface formation of methanol has been investigated [208-210] and is thought to involve sequential hydrogenation of CO by atomic hydrogen, which is still mobile at 10 K [182]. Laboratory experiments have demonstrated that surface reaction such as $H + CO \rightarrow HCO$ and $H + H_2CO \rightarrow CH_3O/CH_2OH$ are efficient at low temperatures even though the activation barriers are on the order of 1000 K [207,210,211]. The abundance of methanol on icy mantles on dust grains is estimated to be approximately $<4 \times 10^{-6} n$ [212]. Therefore, about 0.1% of this methanol would need to get into the gas phase to match observed abundances. However, thermal desorption at 10 K is negligible. Therefore, some other desorption mechanism, such as cosmic ray induced heating [213], must be involved. Recent work

suggests that chemical energy released during grain-surface addition reactions may be sufficient to allow various species, including methanol, to non-thermally desorb from icy mantles into the gas phase [207].

The understanding of low-temperature chemistry in the ISM has been changing because of experimental and computational results related to understanding neutral-neutral reactions. These reactions may have no activation barriers and have fast kinetic rates. Possibly some of these reactions may actually be faster at low temperatures [206]. Experimental results suggest that larger molecules, such as amino acids, can be formed by a variety of reaction pathways [214,215]. Some of the formation pathways on interstellar ice analogues were under conditions that are reasonable for dense clouds. Many pathways for producing amino acids have been predicted or demonstrated. Thus, it will be difficult to sort out what type of ice composition and environment might have led to the production of amino acids and to their isotopic compositions, such as those observed in the Murchison meteorite [216]. While complex organic compounds, such as amino acids, are predicted to form in the dense molecular clouds, they have not yet been observed from these locations or any other ISM location at this time.

A1 2.4 HOT MOLECULAR CORES

Hot molecular cores are one of the regions that can occur in dense clouds associated with massive star formation and anomalously large abundances of complex organic molecules. Hot cores generally have high H₂ densities ranging from 10⁶ to 10⁸ cm⁻³ and high temperatures of 100–300 K. At these temperatures, the icy mantles on dust grains evaporate into the gas phase. The molecules observed in the gas phase of hot cores may be from the evaporation of molecules already present in the icy mantle, molecules formed on the grain during the warming stages, or molecules that are created in the gas phase from reactions of the evaporated species [217]. Thus, evaporation of simple molecular ice mantles drives the gas-phase chemistry in a hot core.

The traditional view of hot molecular cores holds that most reactions require formation of icy mantles at temperatures of ~ 10 K, followed by warming that evaporates the icy mantle into the gas phase to stimulate the array of chemical reactions [218]. Laboratory experiments have confirmed that ice mixtures exposed to UV radiation at 12 K that are allowed to warm up to 300 K can produce a host of complex species, such as esters, carboxylic acids, and amino acids [28,219]. Methanol is thought to play a key role in the formation of these larger molecules [54]. Surface reactions may play important roles in the chemistry of hot cores as demonstrated by the tracking relationship between the abundance of some species (e.g., dimethyl ether $(\text{CH}_3)_2\text{O}$ and vinyl cyanide $(\text{C}_2\text{H}_3\text{CN})$ [129]) and the temperature of the dust. As the dust gets warmer, the abundance of these compounds increases. These compounds were likely formed on the dust grains and then released into the gas phase through evaporation.

Large saturated molecules (e.g., CH_3OH , $\text{CH}_3\text{CH}_2\text{OH}$ and $(\text{CH}_3)_2\text{O}$ [220]) are formed in hot molecular cores as hydrogenation appears to be more efficient than in dense clouds. In the Orion “hot core”, the observed relative abundances of $\text{HC}_3\text{N}:\text{CH}_2\text{CHCN}:\text{CH}_3\text{CH}_2\text{CN}$ are 1:1:7, the reverse of their abundances in dense dark clouds (i.e., HC_3N has the highest abundance) [5,184,221]. These trends are the result of the higher temperatures in the hot cores that enable more gas-phase reactions by providing the thermal energy necessary to surmount the activation barriers.

Methyl formate [222] and dimethyl ether (see Figure A1.2) [25] have been observed in hot molecular cores and are thought to occur in the gas phase. For methyl formate, a gas-phase formation mechanism has been proposed where methanol is first protonated by H_3^+ . The protonated methanol then reacts with formaldehyde to produce protonated methyl formate, which is finally neutralized by dissociative recombination with electrons [223]. Recent calculations have determined that the reaction between CH_3OH_2^+ and H_2CO is very inefficient [224]. Therefore, Garrod and Herbst [225] have proposed that both surface and gas-phase reactions are responsible

for production of methyl formate as well as other species. In their model, the surface processes become more important the longer it takes for a protostar to ‘switch on.’

Glycolaldehyde (CH_2OHCHO) has also been observed [34] and is an isomer of methyl formate (HCOOCH_3) and acetic acid (CH_3COOH) [226]. Similar to methyl formate, the formation of glycolaldehyde is also expected to involve formaldehyde. Halfen et al. [34] determined that the relative ratio of glycolaldehyde to formaldehyde in Sgr B2(N) is 1:27. Based on this ratio, approximately 4% of the H_2CO is converted to CH_2OHCHO . How formaldehyde can be converted to glycolaldehyde has been the subject of debate; however, Halfen et al. [34] have suggested a plausible mechanism (see Figure A1.5). In this reaction scheme, protonated formaldehyde is formed (H_2COH^+), which then reacts with a neutral formaldehyde molecule (H_2CO). After rearrangement, the protonated glycolaldehyde is neutralized by dissociative electron recombination, similar to the mechanism proposed for methyl formate. The reduced alcohol of glycolaldehyde is ethylene glycol ($\text{HOCH}_2\text{CH}_2\text{OH}$), which has also been observed [152]. Hollis et al. [152] note that aldehydes and reduced alcohols appear to dominate the large, complex molecules in the ISM.

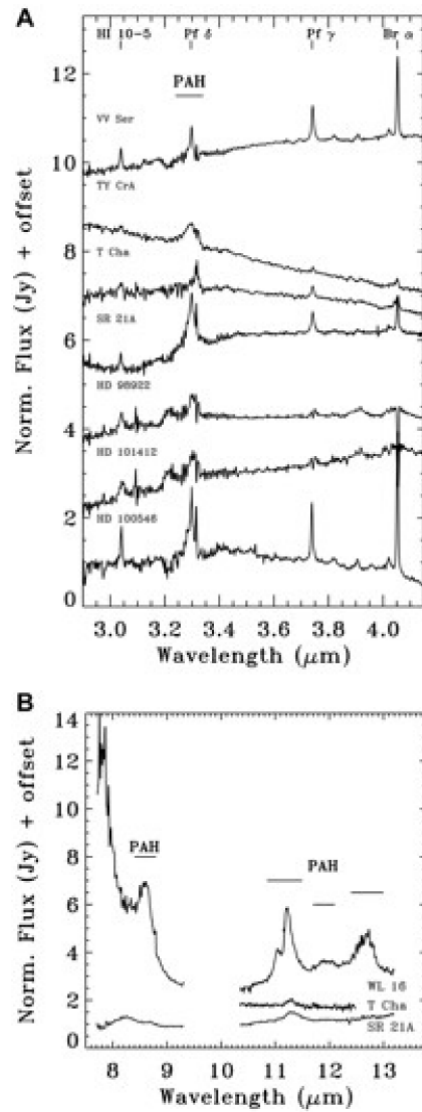


Figure A1.4. Purported glycine spectra for A–C) line 21 at 206,468 MHz and D–F) line 26 240,899 MHz from the three sources Sgr B2(N-LMH), Orion KL, and W51 el /e2, respectively {Kuan, 2003 #108}. Reprinted with permission from Geers et al., *Astronomy and Astrophysics*, 476, 279-289, 2007

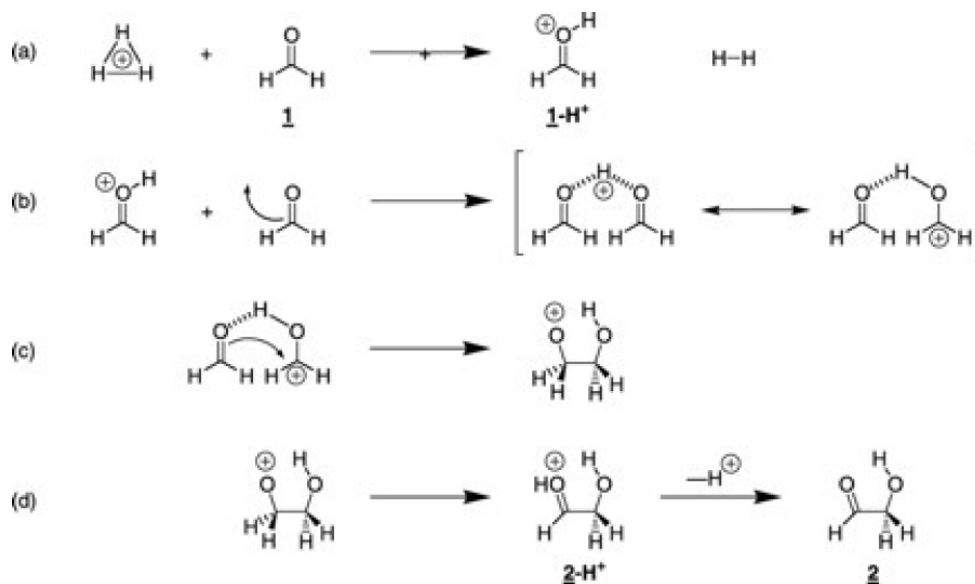


Figure A1.5. Potential gas-phase reaction for synthesis of glycolaldehyde involving four steps: (a) formation of H_2COH^+ , (b) production of a Nazarov-type cations, (c) rearrangement to form protonated glycolaldehyde, and (d) dissociative electron recombination to form the neutral species. Reprinted with permission from Halfen et al., *The Astrophysical Journal*, 639, 237-245, 2006, Copyright The American Astronomical Society (2008).

Although observational evidence for the simple ketose 1,3-dihydroxyacetone ($\text{CO}(\text{CH}_2\text{OH})_2$) has been reported [227,228], Weaver and Blake did stipulate that the assignment would need to be confirmed. Searches by other researchers have not yet been able to verify the existence of 1,3-dihydroxyacetone in the ISM [229,230].

In 2006, Hollis et al. [138] reported the observation of acetamide (CH_3CONH_2) from Sgr B2(N). Transitions for formamide (HCONH_2), which could be the parent molecule for acetamide, were also observed. These compounds would represent the only molecules with NH_2 groups observed in the ISM to date. Thus, acetamide would be the largest molecule currently reported with a peptide bond.

A1 3.1 INTERPLANETARY DUST PARTICLES, ASTEROIDS/CHONDRITIC METEORITES, AND COMETS

Proposed mechanisms and timing of delivery of organic compounds to the Earth, both early in Earth history and throughout Earth evolution, from extraterrestrial objects are speculative. The Earth likely acquires 100,000 to 1,000,000 kg of extraterrestrial material per day [231]. Most extraterrestrial material is thought to be fragments of asteroids that cross Earth's orbit because of the gravitational effects of Jupiter and because of collisions in the asteroid belt located between Mars and Jupiter [232]. A wealth of information has been compiled regarding the composition of these asteroidal fragments and their organic chemical content because of the various samples that have come from the many encounters between Earth and this material [233]. Most of the knowledge about the early solar system comes from samples that can be analyzed directly, such as the carbonaceous chondritic meteorites that have fallen to Earth. A wide variety of organic matter has been detected in these meteorites, and various theories have been proposed to explain the formation and evolution of the organic compounds in these extraterrestrial materials [216].

Knowledge of the composition of extraterrestrial materials is increasing through exploration of the solar system. Comets are generally accepted to be cumulative masses of interstellar dust composed to a large extent of complex organic matter of interstellar origin [234]. The Stardust Discovery Mission launched in 1999 encountered the comet P81/Wild 2 in 2004 and returned an estimated 1000 particles of cometary dust to the Earth in 2006 [235]. This remarkable technological achievement was made possible by the trajectory design of the Stardust spacecraft by Chen-Wan Yen and the development of the aerogel capture medium by Peter Tsou at NASA's Jet Propulsion Laboratory [236]. Brownlee et al. [235,237] have provided an overview of the Stardust Mission including the details of sample collection, sample recovery, mission objectives, and design rationales. The organic matter composition of the returned cometary material is similar (although not identical) to that of interplanetary dust particles and carbonaceous meteorites [238]. For an extensive review of the Stardust Mission organic compound results and

the comparisons to interplanetary dust particles and meteoroids please see Rotundi and Rietmeijer [239].

A1 3.2 INTERPLANETARY DUST PARTICLES

Interplanetary Dust Particles rain down on Earth at a rate of ~30,000 tons/yr [240]. The larger particles heat up during entry into the atmosphere and vaporize as meteors; however, those that survive are estimated to deliver 15 tons/year of unpyrolyzed organic matter composed of aliphatic and carbonyl compounds. IDPs that are carbonaceous can be classified as two types; hydrous and anhydrous chondritic [241]. Both types are classified as being composed of silicate minerals that are in disequilibrium with one another [242,243]. This chemical disequilibrium indicates that the IDPs experienced a complex history as they migrated through the universe, but never experienced significant heating [244-246]. Large D/H ratios suggest that they have not been substantially altered since their initial formation [247].

Interplanetary Dust Particles can contain from 2–10 % carbon by weight [244]. The carbon is present in a several forms including amorphous materials with minor amounts of oxygen and nitrogen [242,248]. A variety of PAH compounds, such as benzene, naphthalene, anthracene, pyrene, chrysene, perylene, benzoperylene, coronene, ovalene, and hexabenzocoronene are also present [244]. Similar PAH compounds found in both the carbonaceous chondrite meteorites and the IDPs indicate that they may both originate from particles of asteroids and comets [244,249,250], which are known by Infrared Astronomy Satellite (IRAS) measurements to expel large quantities of dust [251-253]. The PAH compounds identified in IDPs tend to have higher molecular weights than those found in the carbonaceous chondrites and cometary particles [249]. Raman spectra from some IDPs are similar to interstellar IR emission spectra (see Figure A1.6), which have been attributed to PAHs and HAC [244]. X-ray Absorption Near Edge Structure (XANES) spectroscopy has revealed that the C=O functional group is also present in some IDPs [249]. Because aliphatic and carbonyl species were found to

occur frequently between mineral grains of IDPs, organic compounds apparently act as the “glue” that holds the mineral grains together. This is similar to the concept of “sticky” interstellar grains covered with organic matter [254].

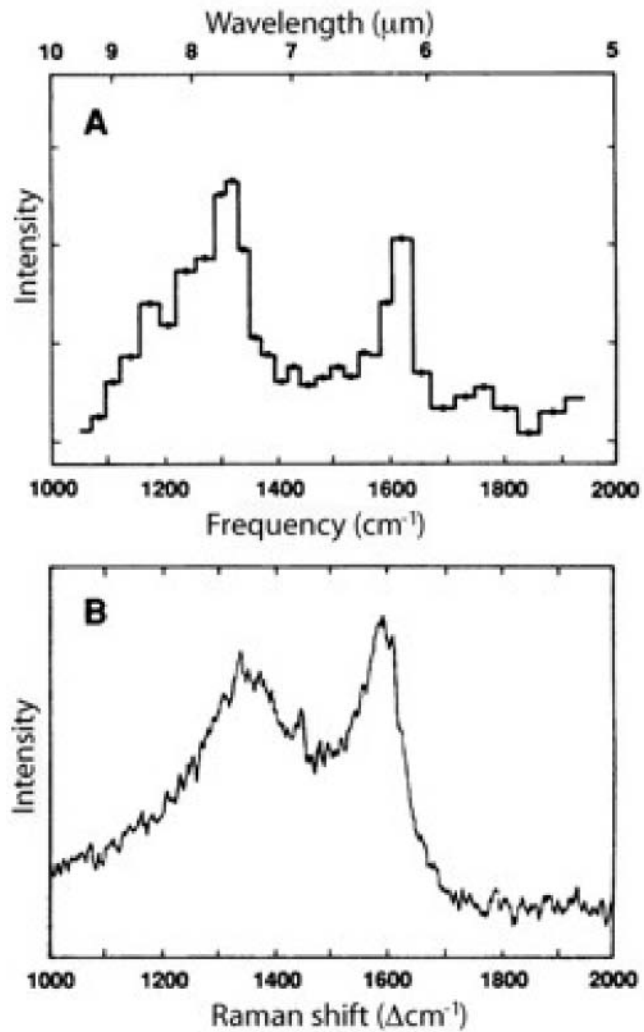


Figure A1.6 Comparison of RAMAN spectra from a laboratory sample with that of an IDP. From Allamandola et al., *Science*, 237, 56-59, 2001. Reprinted with permission from AAAS.

Elemental isotopic anomalies have been observed in IDPs and are thought to indicate the presence of extrasolar phases [241,255,256]. The H and N isotopic anomalies may have originated from chemical reactions in the cold molecular-cloud precursor of our solar system

[255]. Nitrogen isotopic enrichments (^{15}N) are postulated to result from low-temperature interstellar chemistry [257]. Chemical reactions in dense molecular clouds could produce elevated ^{15}N [258,259]; however, these enrichments would fall short of those observed in IDPs [260]. More likely, organic compounds are the source of these enriched nitrogen anomalies, which come from reactions of ^{15}N -rich ammonia with organic hosts in IDPs [261]. The anomalies suggest that heteroatomic organic compounds of interstellar origin are present in the IDPs and that Earth may acquire as much as a centimeter of these exogenous, abiotic nitrogenous organic compounds every million years [261].

A1 3.3 ASTEROIDS/CHONDRITIC METEORITES

Carbonaceous chondrites carry a record of the chemical evolution of the solar system and are thought to have remained ‘unprocessed’ for approximately 4.6 billion years [262].

‘Unprocessed’ means that the meteorite never accreted or differentiated into a planetary body [263]. Carbonaceous chondrites are generally accepted as low-temperature condensates of solar gas, although some questions remain about where condensation of this matter took place. Some scientists prefer the idea of formation from solar nebulae [264,265], while others favor formation in the atmospheres of red giants in interstellar space [266] or in the gaseous envelopes of asteroidal meteorite parent bodies [267,268].

Carbonaceous chondrites are classified using the letter C (indicating elemental carbon percentages upwards of 2%) followed by a letter representing the type specimen (primary chemistry and mineralogy classification) and finally with a number that indicates the petrographic type of the meteorite [216]. The petrographic type is based on the inferred temperatures and alteration processes (aqueous and thermal) the sample has experienced on its asteroidal meteorite parent body before it fell to Earth. The numerical values range from 1–6 (i.e., C1, C2, C3, etc.) with lower numbers (1–3) indicating aqueous alteration and temperatures averaging 150°C to just above 400°C. Higher numbers (4–6), indicate the specimen has seen some degree of thermal

metamorphism with temperatures ranging from 600°C–950°C (detailed petrologic descriptions can be found in Lin et al., [269]). For example, the Murchison meteorite, which fell in Australia in 1969, contains variable amounts of the hydrous silicate mineral serpentine, the anhydrous silicate mineral forsterite, and a diverse suite of carbon compounds and is classified as a CM2 carbonaceous chondrite [270].

Similar to the interstellar dust grains, there are multiple forms of carbon in the carbonaceous chondrites ranging from elemental (diamond and graphite) to inorganic (carbonate, silicon carbide, and trapped gases such as carbon dioxide and carbon monoxide) and a vast array of organic compounds [216]. The composition of the organic matter varies both between the carbonaceous chondrite specimens (see Figure A1.7) and within fragments of individual specimens [270,271]. The compositional variety of the organic matter extends from simple molecules, such as methane and small alkanes, to complex PAHs, kerogen, and fullerenes [272,273]. This section will focus primarily on the more abundant organic compounds that are related to biotic and prebiotic chemical processes that may be of interest to the astrobiology community including some of the accepted abiotic mechanisms for their formation. For a more comprehensive review, please see Sephton [216] and Pizzarello et al. [233].

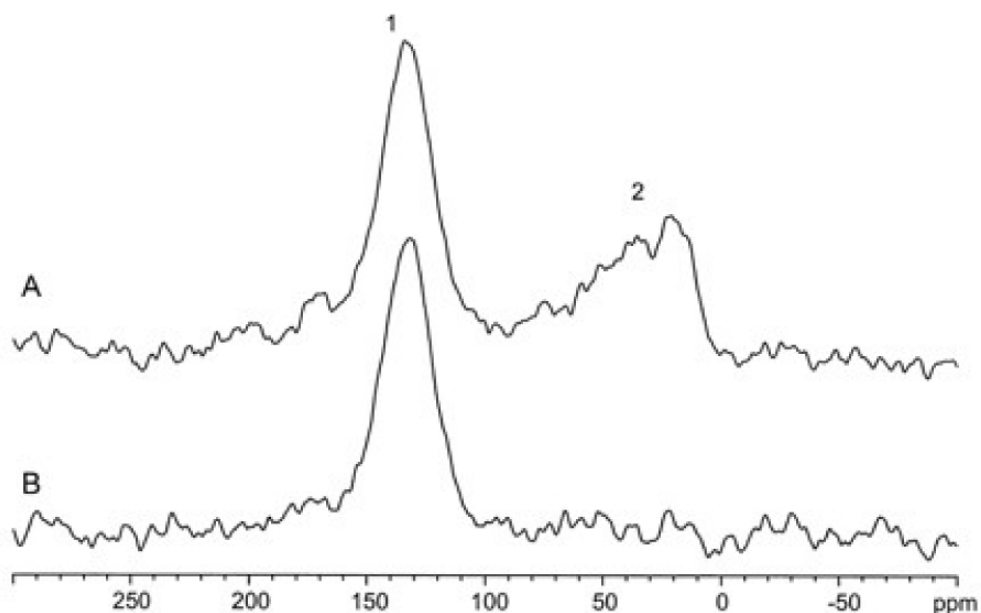


Figure A1.7 Solid-state ^{13}C Nuclear Magnetic Resonance (NMR) spectra of macromolecular material from the (A) Orgueil and (B) Tagish Lake meteorites[33]. The chemical shift differences indicate that the Tagish Lake meteorite insoluble carbon is primarily composed of aromatic compounds, while the Orgueil meteorite's insoluble organic matter contains both aromatic and aliphatic carbon compounds. From Pizzarello et al., *Science*, 293, 2236- 2239, 2001. Reprinted with permission from AAAS.

Since there are such a variety of organic compounds present in the carbonaceous chondrites, many extraction procedures are used to isolate the organic matter from the meteorite. Most of the extraction techniques are based on the functional properties of the organic matter (e.g., solubility in aqueous solutions). Typically, the samples are moderately heated (temperatures above 100°C) in solutions of varying polarity, such as common organic solvents. The less soluble fractions are treated by dissolving the surrounding inorganic material with hydrofluoric acid (HF) to remove the silicates and hydrochloride acid (HCl) to remove the carbonates [216]. More complicated and highly specific extraction procedures have been developed for the analysis of specific organic compounds such as kerogen [275]. The extracts are typically subjected to chromatographic techniques that separate the organic compounds based on elution times. Most chromatographic techniques use a variety of separation methodologies including optimized solutions, stationary phases, and mobile phases for high performance liquid chromatography (HPLC). Gas-phase chromatographic (GC) techniques also use specific column properties that separate the analytes based on the thermal volatility of the different compounds, which controls retention times on the column material [276]. Most chromatographic instruments are coupled to mass spectrometers for chemical identification of compounds with different retention times. Laser desorption mass spectrometry does not require separation based on retention time on a traditional chromatographic column. Figure 8 shows an example of a laser desorption spectra of fullerenes from the Tagish Lake and Murchison meteorites [274]. There are several types of laser desorption mass spectrometric techniques currently employed, and several more are under development to analyze extraterrestrial [277,278] and terrestrial organic compounds [279-282].

Detection and extraction methods introduce some ambiguity into the interpretation of the data. For example, even moderate temperature extractions near or slightly above 100°C provide enough energy to break the hydrogen bonds that hold together ribonucleic acid (RNA) and deoxyribonucleic acids (DNA) [283]. Proteins (amino acid polypeptides) can also be destroyed in these analyses, so that the original macromolecule can be difficult to reconstruct. Even desorption or ablation mass spectrometric techniques can cause molecular clusters ions to form in the desorption plumes, making the identification of the parent molecule difficult to interpret [277,279]. Hence, scientists from several disciplines, including chemistry, biochemistry, analytical chemistry, geology and astronomy, must engage in productive dialogue when analyzing the data and unraveling questions about the origins of life in the universe.

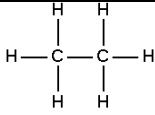
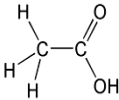
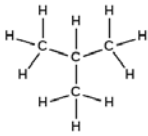
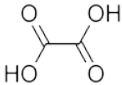
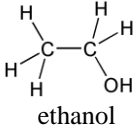
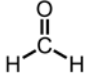
Terrestrial contamination of meteorite samples is another concern that must be considered when interpreting the data. Most of the controversy regarding terrestrial contamination had been cleared up by the early 1970's [284]; however, every subsequent report on the organic chemistry of meteorites contains details of how the issue of contamination was addressed. Pizzarello and co-workers made major progress on issues of contamination while studying organic compounds in the Murchison, Murray, and Tagish Lake meteorites, in which they identified extraterrestrial amino acids (see Pizzarello et al. [285] and references within).

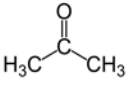
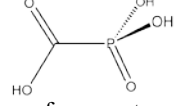
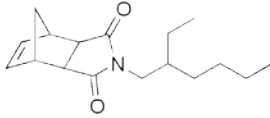
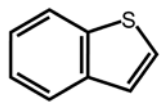
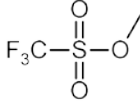
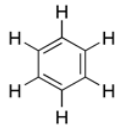
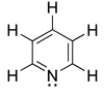
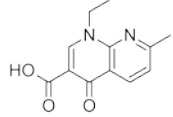
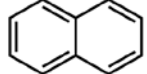
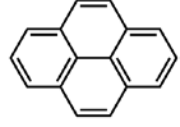
Meteorites can be classified as either 'falls' or 'finds.' A 'fall' is when a meteorite is witnessed to descend to Earth such as the Murchison (1969) and the Tagish Lake (2000) meteorites. These meteorites are considered more 'pristine' and less likely to be contaminated by terrestrial organic compounds or Earth organisms. Examples of the types of organic compounds and their concentrations found in the Murchison and Tagish Lake are provided in Table 1. 'Finds' are meteorites that are found and hence have no record of when they landed on Earth. For example, many of the Antarctic meteorites are finds. Great efforts are needed to ensure that the data from both 'falls' and 'finds' represent original compositions and to rule out terrestrial contamination. One common method used to address contamination is to analyze surface or near

surface fragments and then compare the properties of the surface to the properties of interior pieces. Isotopic data has also helped to constrain extraterrestrial data from terrestrial contamination because the D/H ratios differentiate formation regions [286,287].

Many organic compounds are found in the carbonaceous chondrites. Table A1.2 lists generic examples of some types of compounds. Aromatic compounds, from simple aromatic compounds such as benzene (C₆H₆) and naphthalene to more complex structures such as substituted versions of pyrene [288], have been identified in a variety of samples. Distribution of PAHs is heterogenous; for example, Commins and Harington [289] discovered that some samples of the Cold Bokkeveld meteorite (CM2) had abundant concentrations of fluorene (C₁₃H₁₀) and fluoranthrene (C₁₆H₁₀), while in others phenanthrene (C₁₄H₁₀) and pyrene (C₁₆H₁₀) were the most abundant PAHs. Minimally altered meteorites (C 1-3) contain more volatile aromatic molecules than meteorites of higher petrographic type (C 4-6) [290]. PAHs represent between 15–28% of the organic matter present in carbonaceous chondrites [216]. Research in this area continues to reveal more details on the type and abundance of organic compounds in carbonaceous chondrites.

Table A1.2 Compilation of selected organic compounds found in carbonaceous chondrites including generic structural examples and references. Other compounds, such as amino acids and purine/pyrimidines, are discussed separately in the text.

Carbon compound	Generic examples	Carbon compound	Generic examples
Aliphatic hydrocarbons [32]	 <p>ethane</p>	Monocarboxylic and dicarboxylic acids [32]	 <p>Acetic Acid (mono)</p>
	 <p>isobutane</p>		 <p>Oxalic Acid (di)</p>
Alcohols [50]	 <p>ethanol</p>	Aldehydes [50]	 <p>Formaldehyde</p>

Ketones [50]	 <p>acetone</p>	Phosphonic acids [54]	 <p>fascarnet</p>
Dicarboximides [33]	 <p>N-Octyl bicycloheptene dicarboximide</p>	Benzothiophenes [52]	 <p>benzothiophene</p>
Sulfonic acids [53]	 <p>methyl triflate</p>	Aromatic Hydrocarbons [47]	 <p>benzene</p>
Basic N-heterocycles (pyridines, quinolones) [51]	 <p>pyridine</p>  <p>nalidixic acid</p>	Polyaromatic Hydrocarbons [47]	 <p>naphthalene</p>  <p>pyrene</p>

The nitrogen heterocyclic compounds (nucleic acid bases and precursors) were first reported in the carbonaceous chondrites in the 1960's [296]. These results, immediately called into question, turned out to result from laboratory contaminants [297-299]. Later studies definitively identified several N-heterocyclic compounds including purines (i.e., nucleic acids, adenine, and guanine), as well as several extraterrestrial nitrogen heterocyclic compounds of unknown biological importance, such as guanylyurea, triazines, melamine, and ammeline, from the Orgueil (CI1) carbonaceous chondrite [300-302,303]. Subsequently, Folsom et al. [304,305] failed to detect purines from the carbonaceous chondrites Murchison (CM2), Murray (CM2), and Orgueil (CI1) in the early 1970's suggesting that as analytical technologies and instrumental sensitivity improves, so to does the ability to distinguish indigenous organic compounds from contamination. Currently, the Murchison meteorite is thought to contain several purines (xanthine, hypoxanthine, guanine, and adenine), the pyrimidine uracil, several quinolines/isoquinolines, and pyridines [216]. The pyrimidine, uracil, was positively identified in the Murchison, Murray, and Orgueil meteorites [306,307]. Curiously, the pyrimidine, thymine, which replaces uracil in DNA, was not detected perhaps supporting the theory that the 'RNA' world preceeded the 'DNA' world [308].

The presence of amino acids in the carbonaceous chondrites has generated a great deal of excitement, both as a possible indicator of prebiotic chemistry in the proto-solar nebula and as a way to rule out terrestrial contamination. Amino acids in meteorites have produced a wealth of information and speculation regarding early synthetic pathways for prebiotic chemistry on Earth. Approximately 20 common amino acids comprise proteins in living systems on Earth (see Table A1.3). Amino acids are organic compounds that contain both an α -NH₂ (α - amino group) and an α - COOH (α - carboxylic acid) attached to a common carbon atom. The common carbon can then accommodate several molecular constituents on the side chain of the amino acid. In terrestrial

protein amino acids, a hydrogen (called the α -H) occupies the fourth bonding site on the common carbon. When four different atoms or molecules are bound to the common carbon, that carbon is chiral. Chirality is used to represent molecules of identical composition that differ structurally by how they rotate light. This property can be explained easily by using the term ‘handedness.’ This term becomes useful when describing chirality because human hands are mirror images of one another, but they are not super-imposable. Handedness is pervasive in biomolecules; terrestrial organisms usually prefer one orientation to another, resulting in the concept of homochirality (see the chapter on “The origin of homochirality” by Thiemann, W.H.-P and Bredehöft, J.H.). Chirality is indicated by terms such as R,S enantiomers (organic chemistry nomenclature) and L,D enantiomers (biochemistry nomenclature). Enantiomers are molecules with opposite chirality. Abiotic syntheses of amino acids tend to produce equal quantities of enantiomers (i.e., a 50/50 racemic mixture). Enantiomeric excesses imply preferential synthesis, which could be biologically directed, or preferentially use of one form over another in biological processes; either process would result in an excess of one enantiomer over the other.

Table A1.3. The terrestrial protein amino acids listed with formulas and side chain polarity.

Terrestrial protein amino Acid	Side Chain formula	Side chain polarity
Alanine	$\text{CH}_3\text{-CH(NH}_2\text{)-COOH}$	nonpolar
Arginine	$\text{HN=C(NH}_2\text{)-NH-(CH}_2\text{)}_3\text{-CH(NH}_2\text{)-COOH}$	polar
Asparagine	$\text{H}_2\text{N-CO-CH}_2\text{-CH(NH}_2\text{)-COOH}$	polar
Aspartic Acid	$\text{HOOC-CH}_2\text{-CH(NH}_2\text{)-COOH}$	polar
Cysteine	$\text{HS-CH}_2\text{-CH(NH}_2\text{)-COOH}$	polar
Glutamic Acid	$\text{HOOC-(CH}_2\text{)}_2\text{-CH(NH}_2\text{)-COOH}$	polar
Glutamine	$\text{H}_2\text{N-CO-(CH}_2\text{)}_2\text{-CH(NH}_2\text{)-COOH}$	polar
Glycine	$\text{NH}_2\text{-CH}_2\text{-COOH}$	nonpolar

Histidine	NH-CH=N-CH=C-CH₂-CH(NH₂)-COOH	polar
Isoleucine	CH₃-CH₂-CH(CH₃)-CH(NH₂)-COOH	nonpolar
Leucine	(CH₃)₂-CH-CH₂-CH(NH₂)-COOH	nonpolar
Lysine	H₂N-(CH₂)₄-CH(NH₂)-COOH	polar
Methionine	CH₃-S-(CH₂)₂-CH(NH₂)-COOH	nonpolar
Phenylalanine	Ph-CH₂-CH(NH₂)-COOH	nonpolar
Proline	NH-(CH₂)₃-CH-COOH	nonpolar
Serine	HO-CH₂-CH(NH₂)-COOH	polar
Threonine	CH₃-CH(OH)-CH(NH₂)-COOH	polar
Tryptophan	Ph-NH-CH=C-CH₂-CH(NH₂)-COOH	nonpolar
Tyrosine	HO-Ph-CH₂-CH(NH₂)-COOH	polar
Valine	(CH₃)₂-CH-CH(NH₂)-COOH CH(NH₂)-COOH	nonpolar

Over 100 amino acids were found in the Murchison meteorite, while only approximately 20 amino acids are common in terrestrial systems. Hence, terrestrial biological systems have already trimmed the number of amino acids from the original extraterrestrial inputs; determining the role that exogenous organic compounds might have played in the origins of life on this planet will be challenging [233]. Organics were likely introduced to Earth by carbonaceous chondrites, which may have seeded the planet with prebiotic molecules [309,310]. Life might have been based on achiral molecules, but through evolutionary processes enzymatic processes selected generally only one enantiomer. Biochemical processes use one enantiomer (i.e., L-amino acids and D-sugars) to build proteins (polypeptides), RNA, and DNA; the enantiomers dictate the tertiary structures of biopolymers and ultimately control biopolymer function. Therefore, homochirality is considered essential to terrestrial life [311]. Meteoritic enantiomeric excesses

might have provided a chiral basis capable of directing biosynthesis towards this homochirality [270].

Enantiomeric excesses found during analyses of amino acids in carbonaceous chondrites should be initially regarded as products of terrestrial contamination, and their extraterrestrial origin suspect until proven otherwise because non-racemic mixtures of non-terrestrial amino acids play an important role in demonstrating the extraterrestrial origin of amino acids in carbonaceous chondrites [270]. Several amino acids indigenous to the Murchison meteorite have been carefully selected to investigate this phenomenon. The amino acid, 2-amino-2,3-dimethylpentanoic acid (2-a-2,3-dmpa), has two chiral centers and, consequently, four stereoisomers and has not been found in terrestrial samples. Thus, aqueous processing on the original meteoritic body probably did not alter the configuration of the enantiomeric ratios (i.e., the meteorite has not been affected by terrestrial contamination) [271]. Sarcosine (N-methyl glycine), N-methyl alanine, α -methylnorvaline, isovaline, α -amino-n-butyric acid, and norvaline have also been found in Murchison extracts and are negligible in the terrestrial biosphere [312]. Enantiomeric excesses favoring the L-enantiomer observed in these amino acids; most excesses are considered to be statistically significant [271]. Extraterrestrial amino acids differ from the terrestrial amino acids shown in Table A1.3. Terrestrial biological amino acids are all α -H amino acids, while extraterrestrial amino acids include α -methyl ($-\text{CH}_3$) amino acids. The α -H amino acids and sugars easily racemize in water, making the task of determining and interpreting enantiomeric enrichments in meteorites difficult [313]. However, the amino acid, isovaline, which is not found in terrestrial organisms, is stereochemically stable because it lacks the α -H, thus preventing interconversion between chiral configurations. Meteoritic bombardment early in Earth's history could have provided an extended supply of isovaline, which has an enantiomeric enrichment in meteorites of up to 15% that could have influenced chirality in prebiotic sugar synthesis [314].

The amino acid enantiomeric enrichment data from the Murchison, Murray, and Tagish Lake meteorites suggest that the α -methyl ($-\text{CH}_3$) amino acids may be associated with a distinct meteoritic phase because their concentrations vary systematically relative to the α -H amino acids [315]. Deuterium (D) enrichments in the amino acids suggest that they might be related to interstellar molecules [316]. These α -methyl amino acids coexist with and structurally correspond to a suite of α -hydroxy acids, which could be explained if both were formed by a Strecker-type synthesis (see Figure A1.9) [317]. Since the carbonaceous chondrites have experienced some degree of aqueous processing, Cronin et al. [271] suggested a two-step formation process. The first step is incorporation of precursors to the amino acids, such as the aldehydes, ketones, HCN, and ammonia formed in the molecular cloud, into the meteoritic body; these compounds are often enriched in deuterium, which then provides an isotopic signature for the α -methyl amino acid. Subsequently, a Strecker-type synthesis involving the incorporated components might occur in the meteoritic body, forming amino acids. In 1974, asymmetric organic compounds appeared to have been produced in recurrent photolytic processes by ultraviolet circularly polarized light (UV CPL) [318]; these experiments mimicked recurrent exposure during interstellar cloud collapse [311], which might lead to give large enantiomeric excesses. In UV CPL theory, losses of low-anisotropy organic compounds, such as the amino acids, and higher-anisotropy organic compounds are predicted, which could then act as catalysts for the secondary propagation of optical activity [285]. However, the range of variability for isovaline (upper limit of L-ee = 15.2%) extends well beyond the theoretical boundaries set for amino acid decomposition by UV CPL and would seem to refute the suggestion that UV CPL was the sole causation of the asymmetry observed in certain meteoritic amino acids [285].

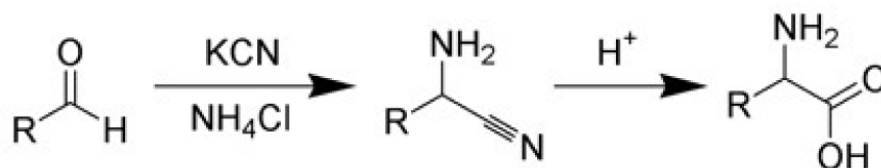


Figure A1.9. Chemical reaction for the formation of amino acids in the Strecker synthesis.

Many authors invoke the Strecker-type synthesis (see Figure A1.9) as the primary formation mechanism for amino acids in carbonaceous chondrites [233]. The Strecker-type synthesis of amino acids from aldehydes and ketones was proposed in the 1850's by Adolph Strecker [319]; an aldehyde condenses with ammonium in the presence of cyanide to form the intermediate compound, α -aminonitrile. The nitrile group is hydrolyzed and replaced by the carboxylic acid to form an amino acid. Figures A1.10 and A1.11 illustrate the roles that the cyano compounds and water play in the formation of amino acids. However, the Strecker-type synthesis does not explain enantiomeric excesses observed in carbonaceous chondrites. Bonner and Rubenstein [320] propose that amino acids formed entirely in the interstellar medium. If true, then the two-stage interstellar-parent body hypothesis (aldehyde and ketone formation followed by the amino acids by Strecker-type synthesis) is not applicable to the non-racemic amino acids. If all of the meteorite amino acids were formed in the interstellar medium, then enantiomeric excesses might be expected in a broader range of organic compounds in comets than in carbonaceous chondrites; comets, discussed below, probably have not experienced aqueous processing, with the attendant possibility of racemization, to the same extent as may have occurred in carbonaceous chondrites [271].

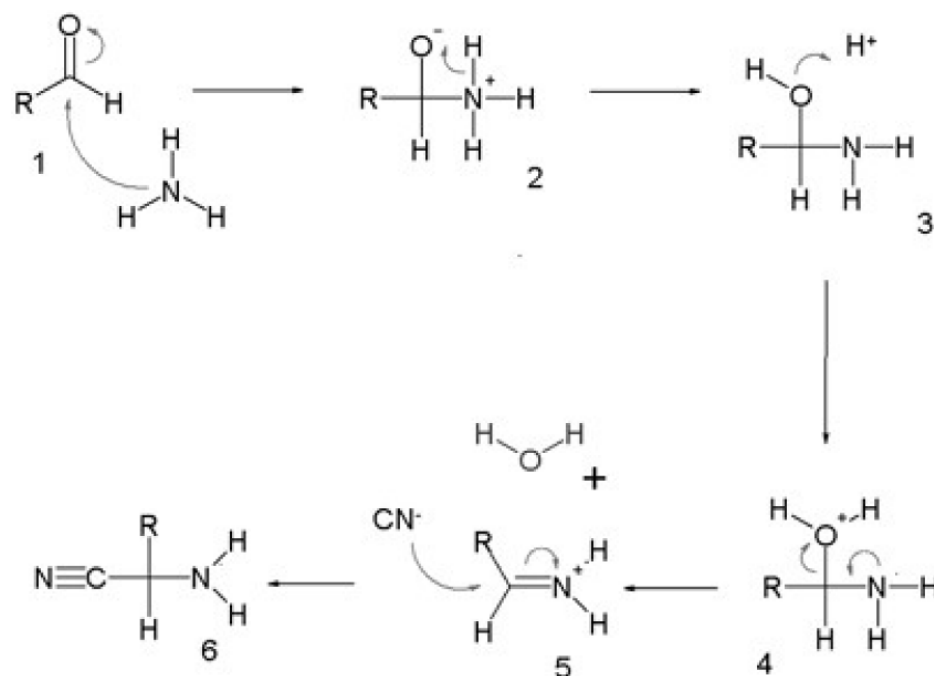


Figure A1.10 Step 1 in the mechanism of the Strecker synthesis illustrating the formation of the α -aminonitrile intermediate.

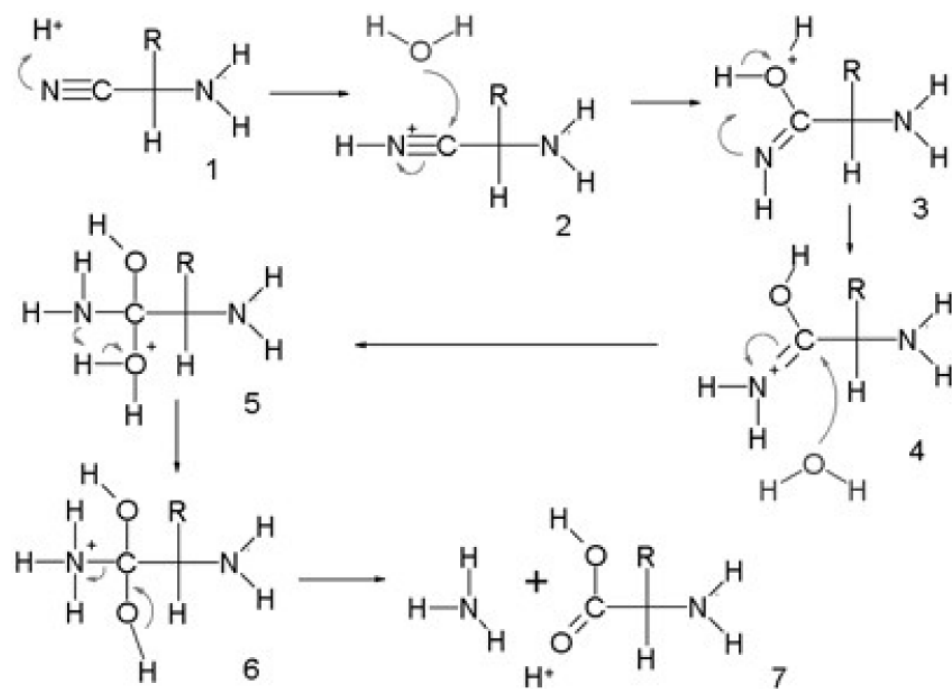


Figure A1.11. Step 2 of the Strecker synthesis showing the mechanism of formation from the α -aminonitrile to the formation of the amino acid and the ammonia by product.

A1 3.4 COMETS

Many observational techniques have been used over the last 30 years to study the particles of interstellar space, including comets (e.g., Hale-Bopp and Hailey), which are considered to be aggregates of interstellar dust [321-325]. These astronomical observations have identified inorganic and organic carbon compounds similar to those discussed in the section on carbonaceous chondrites [238,326]. Comet and dust analogues have been extensively studied in the laboratory [239,327]; however, samples returned from the Stardust Discovery Mission have provided scientists with the opportunity to directly study particles from a comet, specifically, Comet 81P/Wild 2 [235,238,328]. The samples of Comet 81P/Wild 2 are generally nanometer sized grains of Fe-Mg minerals, Fe-Ni minerals, Fe-Ni metal, and other accessory phases [329].

The Stardust Organics Preliminary Examination Team (PET), a group of scientists from 31 government and academic organizations, including international participation from scientists in France, Italy, the United Kingdom, and Germany [238], is currently studying samples returned from Comet 81P/Wild using a full suite of analytical techniques selected to provide information about the chemical nature and abundance of the organic compounds. Techniques included two-step laser-desorption laser-ionization mass spectrometry (L^2MS), secondary ion mass spectrometry (SIMS), time-of-flight SIMS (TOF-SIMS), IR and Raman analysis, X-ray absorption near-edge spectroscopy (XANES), ion chromatography with conductivity detection (IC), liquid chromatography with UV fluorescence detection and time-of-flight mass spectrometry (LC-FD/TOF-MS), and scanning transmission X-ray microscopy (STXM).

Contamination of Stardust samples has been and continues to be a significant concern; understanding how, when, and what type of contamination occurs is critical in distinguishing the

contaminants from the cometary compounds. Organic contamination in the Stardust samples is primarily due to the interaction of the cometary material with the aerogel capture medium. The aerogel capture medium is made of amorphous silica (SiO_2), but a quarter to a few weight percent of the material contains silico-methyl (Si-CH_3) complexes [238]. Consequently, identification of certain carbon compounds may be problematic because an artificial carbon signature could be produced [277]. Further, the cometary material may be altered by high velocity (~ 6.1 km/sec) impact with the aerogel material, which presents a potentially less tractable problem [330]. Impact at these speeds can cause thermal processing of the samples ranging from ‘complete destruction to nearly pristine capture’ [238,330]. The impact velocities and resultant temperature increases could create aromatic organic compounds from the carbon present in the aerogel medium [330] introducing an artificial signature [277].

Organic compounds identified in the aerogel capture media of the Stardust Discovery Mission are varied and heterogeneous even within individual comet particles [239]. There is evidence of aromatic hydrocarbons (although some molecule identifications are not definitive) and chain hydrocarbons of various lengths [239]. The distribution of these aromatic and chain hydrocarbons strongly resembles the matrix material from some IDPs and the Murchison carbonaceous chondrite [331]. Figure 12(A,B) illustrate comparisons between two carbonaceous chondrites of different processing histories [269] and six Stardust samples [238]. Figure A1.12(A) illustrates the range of $1s-\pi^*$ transitions observed from the C,N,O-XANES spectra that is consistent with variable amounts of aromatic, keto/aldehyde, carboxyl moieties, as well as amides and nitriles, that indicate the samples experienced different processing histories. Particles 2 and 3 are comparatively rich in N, with spectra consistent with amide carbon. Glycine, methylamine, and ethylamine were detected in several grains, generating excitement about the possibility of prebiotic molecules in the cometary organic matter [238,328]. Figure A1.12(B) shows that the ratios of O/C and N/C in the Stardust particles are richer in O and N compared to both chondritic organic matter and the composition of comet P/Halley particles [332-335], but are qualitatively

similar to stratospheric IDP's [336,337]. Overall, the Stardust samples are similar to other materials of interstellar/protostellar heritage, even though the heterogeneity of these materials is pervasive.

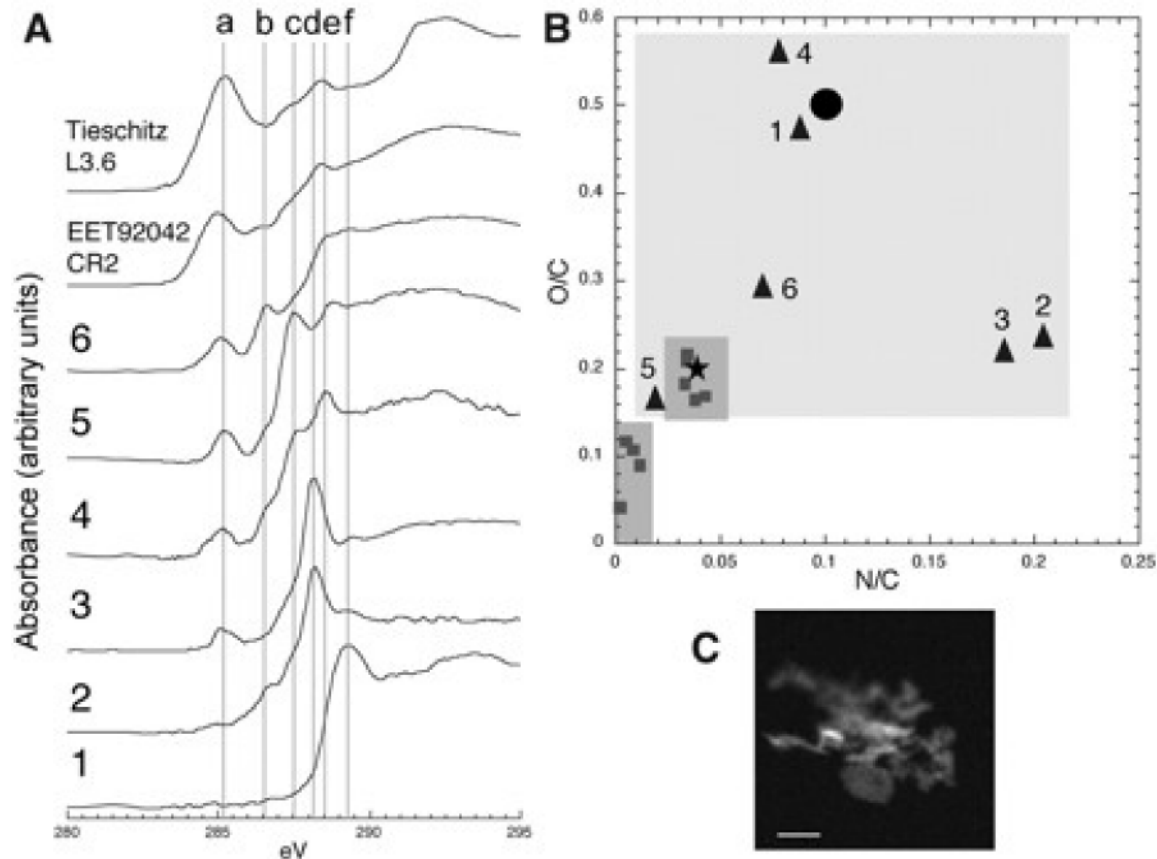


Figure A1.12 Chemical analyses of organic matter from the carbonaceous chondrites EET92042, CR2, and Tieschitz, L3.6 compared to Stardust Comet 81P/Wild 2 samples. (A) C-XANES , (B) O/N and C/N ratios compiled from the C,N,O-XANES spectra and (C) a thin section micrograph of one of the Comet 81P/Wild 2 grains captured in the aerogel medium{Sandford, 2006 #74}. From Sandford et al., Science, 314, 1720, 2006. Reprinted with permission from AAAS.

A1 4.1 PLANETARY BODIES

The emergence of complex organic molecules in our solar system depends, in part, on the occurrence of organic compounds, whose type and distribution are controlled by the processes that form them from existing organic molecules. Thus, Earth-based telescopic and space-based

instrumental detection and characterization of reservoirs of organic compounds is crucial to understanding the formation of organic molecules. The composition of organic molecules and the relationships between organic-molecule reservoirs remain active topics of extraterrestrial research.

With the exception of Mars, Europa, and Titan, planetary bodies are considered unsuitable for extant or extinct life, although these bodies offer valuable insight into surficial and atmospheric organic-chemical processes that lead to formation and accumulation of organic molecules. Therefore, this section will summarize evidence on the distribution and formation of organic molecules on planetary bodies in our solar system; although, it is very exciting that methane has been recently discovered on an extrasolar planetary body by space-based spectroscopy [338]. Reviews of planetary bodies have been published previously [339,340,341].

A1 4.2 THE KUIPER BELT AND CENTAURS

The Kuiper belt is a disk-shaped region between 30 to 200 AU beyond Neptune. The icy objects of the Kuiper belt follow heliocentric orbits. They are variably sized, with tens of thousands of them measuring greater than 100 km in diameter [342]. They have undergone minimal chemical and physical modifications from solar UV radiation [343]. Their current chemical composition likely reflects their original composition and, hence, that of the solar protonebula. Dark refractory material and volatiles dominate the composition, making detection of organic constituents difficult. Unfortunately, chemical characterization of these bodies is also hindered by their small size and great distance from Earth.

Neptune's gravitational field occasionally ejects Kuiper belt objects from their orbits, relegating them to an unstable elliptical orbit among the Jovian planets (Jupiter, Saturn, Uranus, and Neptune) [344]. These objects, called Centaurs, are closer to Earth and, therefore, more easily observed than their parent Kuiper belt objects. Some Centaurs show variations in dust and evaporated gas content and composition, suggesting that Centaurs formed at different

temperatures. Consequently, the compositions of these Centaurs and Kuiper-belt objects may be compositionally similar to short-lived comets [345,346].

Earth-based infrared spectroscopy shows that the surface composition and characteristics of Centaurs vary significantly. Several objects absorb strongly at the same infrared wavelengths as does the organic material, tholin, suggesting it may be present [347,348]. Tholins are high molecular weight, synthetic, macromolecular compounds produced from irradiated gaseous or solid mixtures of simple hydrocarbons, water, or nitrogen. They contain combinations of nitrogen heterocycles, amino acids, pyrimidines, and/or purines [349,350]. Additional surface components of Centaurs are water ice, minor amounts of methanol, $(\text{CH}_2)_6\text{N}_4$ (a photolytic product of methanol), amorphous carbon, and kerogen-like organic molecules [351,352]. The surface compositions of Centaurs are likely representative of all Kuiper belt objects [343].

Organic ices (hydrates) of carbon dioxide and carbon monoxide along with refractory minerals likely comprise the interiors and surfaces of Kuiper belt objects [353]. The largest and most easily studied of the Kuiper-belt objects is Pluto. Spectroscopic data show that Pluto's surface, which is compositionally similar to the Neptunian satellite, Triton, contains varying amounts of CH_4 , CO , and tholin ices (see Figure A1.14) [354]. These CH_4 , CO , and tholin ices, which are produced by photochemical reactions of N_2 and CH_4 in Pluto's atmosphere [355], subsequently condense and precipitate onto Pluto's surface. Like Triton, Pluto also has other complex organic compounds (HCN , C_2H_4 , C_2H_6 , C_2H_2 , and nitriles) that likely formed by photochemical reactions in the atmosphere [356].

A1 4.3 GIANT PLANETS

Atmospheric compositions of the Jovian planets, determined by infrared and ultraviolet spectroscopy from orbiting spacecraft (Voyager 1, Voyager 2, Galileo, and Cassini) and terrestrial-based instruments, are dominated by hydrogen and helium with minor concentrations of CH₄ and other carbon-bearing compounds (see Table 5) [358]. The carbon-bearing compounds are the result of three different mechanisms of CH₄ dissociation. The first is photolysis of singly bonded carbon resulting in CH₃ radicals. The CH₃ radicals subsequently react with atomic H to form simple hydrocarbons, such as ethane (C₂H₆), ethene (C₂H₄), and acetylene (C₂H₂) [359,360]. Other complex organic molecules, such as C₄H₂ and C₆H₆ are produced by further photochemical reactions of the simpler hydrocarbons (ethane, ethane, and acetylene) [361,362]. The second formation mechanism of organic compounds in the Jovian planetary atmospheres is the reaction of magnetically trapped ions (H⁺, CH₃⁻) with atmospheric CH₄, which produces a cloud of simple and more complex hydrocarbons (see Table A1.4) [363]. The last mechanism is the synthesis of organic molecules from CH₄ during lightning storms. This interaction can drive non-equilibrium organic reactions leading to formation of C₂H₆, C₄H₂, and C₆H₆. The exact formation processes of this last mechanism and its relative importance are poorly understood [364,365].

Table A1.4. Chemical composition of atmospheres of the Jovian planets [120-124].

	Jupiter	Saturn	Uranus	Neptune
major compounds	<i>mixing ratio relative to H₂</i>			
H ₂	1	1	1	1
He	0.15	0.06	0.18	0.18
CH ₄	0.001-0.003	0.002	0.03	0.03
minor compounds	<i>ppm</i>			
C ₂ H ₆	1-2	1-3	trace	1-3
C ₂ H ₂	0.03	0.07	0.1	0.1
C ₂ H ₄	0.007	trace		
C ₃ H ₈		trace		
C ₃ H ₄	0.003	trace		
C ₆ H ₆	0.002			

HCN	trace	trace		0.001
CO	0.002	0.002	0.01	1
CO ₂	trace	trace	trace	trace

Hydrogen cyanide (HCN) and its polymers are likely formed in the atmospheres of the Jovian planets by photolysis of CH₄ and NH₃ [366]. The polymers are precursors to polypeptides and amino acids [367,368]. The occurrence of HCN and its polymers may potentially account for Jupiter's banded coloration and for the changes observed after impact of comet P/Shoemaker-Levy 9 with Jupiter in 1994 [367,369]. The occurrence of HCN polymers on Saturn may cause the brown-orange color of the planet [367].

A1 4.4 SATURN'S ICY MOONS

NASA's Cassini spacecraft entered Saturn's orbit in summer 2004. One primary objective of the mission was detection and characterization of surficial and atmospheric composition of Saturn's icy moons (all of Saturn's moons except Titan). Cassini data reveal that the icy moons are physically and chemically diverse.

A1 4.4.1 PHOEBE

Phoebe is Saturn's outermost moon. The elliptical retrograde orbit, unusual for moons, supports one interpretation that it may be a gravitationally captured Kuiper-belt object [375,376]. Further, the surface composition of Phoebe is unlike any surface composition observed in the outer solar system. The unusual, heterogeneous surface composition may reflect a thin veneer of cometary or intersolar material [377].

Spectroscopic data of Phoebe's surface shows the presence of PAHs, CO₂, amorphous carbon, nitriles, tholin, and cyanide compounds bound in a matrix of water ice [377-380]. CO₂ is ubiquitous on Phoebe and, along with these other compounds, accounts for the low albedo of the

surface [377]. The origin of PAHs on Phoebe is still uncertain, although similar molecules are found on another of Saturn's satellites, Iapetus [378].

A1 4.4.2 IAPETUS

Iapetus is Saturn's third largest moon. The surface is divided into a low-albedo hemisphere and a water-rich high-albedo hemisphere [381,382]. This difference in albedos is atypical in the solar system and represents different surface compositions in the two hemispheres. The composition of the high-albedo hemisphere is dominated by water ice with minor, but ubiquitous amounts of tholin [383]. Conversely, the low-albedo hemisphere is composed of several organic compounds; PAHs with aromatic and aliphatic bonds have been detected spectroscopically [378], while modeling experiments suggest the presence of spatially variable tholin, poly-HCN, and low concentrations of water ice [383,384]. Additionally CO₂, a photodissociation product trapped in water ice and organic solids, is ubiquitous in the low-albedo hemisphere [379,385,386]. The occurrence of CO₂ and the existence of PAHs suggest a possible evolutionary link with Phoebe and possibly with carbonaceous meteorites and interstellar dust [377,378].

A1 4.4.3 ENCELADUS

Embedded in Saturn's largest planetary ring is the volcanically active moon, Enceladus. Its atmosphere is composed with minor amounts of CH₄, CO, and CO₂ [387-389]. Additionally, the organic compounds, acetylene and propane, were detected from an outgassing volcanic plume. The presence of these organic compounds suggests that Enceladus potentially has a thermally active carbon-bearing interior [388,390,391], which results in the accumulation of surficial CH₄, CO₂, and water ice [392].

Of the remaining icy moons, few are found to contain carbon-bearing molecules. These moons include Rhea, Hyperion, Mimas, Tethys, and Dione, all of which have trace amounts of

atmospheric CO₂ [393,394]. Atmospheric CO₂ in the moons, detected by Cassini's VIMS (Visible and Infrared Mapping Spectrometer), is likely a dissociation product of interaction of Saturn's magnetosphere with existing tholin and cyanogens [393]. Minor amounts of surficial organic compounds (CH₄, nitriles, and tholin), detected by radiometric and infrared instrumentation are likely interstitially bound in a rock and water ice matrix [395].

A1 4.5 TITAN

The atmosphere of Saturn's moon, Titan, is approximately 90% molecular N₂ with up to 8% CH₄ (see Table 6). CH₄ is essential in the production of atmospheric hydrocarbons, CO₂, CO, nitriles, and amorphous organic solids [339,396,397]. The interaction of cosmic rays, UV radiation, and magnetospheric radiation with CH₄ forms a methyl radical (CH₃) [398], which subsequently reacts to form tholin (see Figure A1.14).

Table A1.5. Organic Inventory on Titan [147,158].

Major constituent	Percentage		
N ₂	82–90		
CH ₄	1–8		
Minor carbon compound	ppm	Minor carbon compounds	ppm
C ₂ H ₆	20	C ₄ H ₂	0.01
C ₂ H ₄	1–4	CO ₂	0.01
C ₂ H ₂	1	CO	10–50
C ₃ H ₈	1–10	HCN	1
C ₃ H ₄	0.01	C ₂ N ₂	0.02
C ₆ H ₆	—	HC ₃ N	0.1–0.03
C ₈ H ₂	—	CH ₃ CN	0.003
C ₄ N ₂	—		

—detected but abundance not determined

Photoionization of N₂ to N ions leads to the formation of nitriles, which subsequently react with methyl radicals to form hydrocarbons [399,400]. These atmospheric reactions are common resulting in formation of increasingly more complex organic compounds (propane,

butane, polyacetylene, and cyanoacetylene) [401-403]. Benzene, a precursor of PAHs, is found in an opaque haze cloud in the upper layers of the atmosphere [397,401,404,405].

Temperature fluctuations in Titan's atmosphere result in continual exchange between surficial and atmospheric CH₄ [396], resulting in a global CH₄ cycle with atmospheric (CH₄ cloud) and liquid reservoirs and evaporation/precipitation transfer mechanisms, analogous to the terrestrial water cycle [406]. Evidence of liquid CH₄ reservoirs derives from morphological, radar backscattering, and climatic models [407]. The CH₄ inventory in these lakes is roughly 30–30,000 km³, a hundred times more than known hydrocarbons reserves on Earth [407]. Further, although temperatures are too cold for liquid water, the high concentrations of CH₄, and abundance of complex organic compounds suggests that life potentially could have evolved during warmer periods during Titan's past.

A1 4.6 TRITON

Neptune's largest moon, Triton, was investigated directly by Voyager 2 spacecraft. Voyager mission data and ground-based telescopic observations suggest solid CO₂, CH₄, CO, and H₂O on Triton's surface [409-411] likely in an N₂-ice matrix [412].

Models of vapor pressure, temperature, atmospheric pressure, and surface organic composition suggest a variety of organic gases should be stable in the atmosphere [343]. Organic gases form by sublimation of N₂, CH₄, and CO ices. These gases are subsequently destroyed by solar winds and photolyzed by UV radiation [413-416], producing small organic compounds, such as HCN, C₂H₂, C₂H₄, and C₂H₆ [343]. These products subsequently condense as a result of Triton's cold temperature and precipitate on the surface [413-415]. However, either because of rapid sublimation or dilution by more abundant N₂, CH₄, and CO, these organic compounds have not been detected on Triton's surface [411]. Of these more abundant gases, CH₄ appears to be

photochemically degraded in the atmosphere and is replenished by either sublimation of solid organic compounds or volcanic outgassing. This CH₄ cycle is apparently similar to that of Saturn's moon, Titan, but differs because of Triton's lower temperature and thinner atmosphere [417].

A1 4.7 GALILEAN SATELLITES

Jupiter's largest moons (Io, Europa, Ganymede, and Callisto) are called the Galilean moons. With the exception of Io, each contains a significant concentration of surficial water ice [418], along with hydrated silicates and trapped volatiles [419]. Furthermore, infrared spectroscopy data from the Voyager and Galileo spacecraft suggest carbon-bearing compounds are incorporated in these surficial components [420-422].

A1 4.7.1 EUROPA

Spectroscopic and gravimetric data confirm that Europa's surface is a 100–150 km thick ice layer overlying a potentially liquid water ocean [422,423]. The existence of the liquid water interior is still uncertain, although magnetic, spectroscopic, and morphologic observations from the Voyager and Galileo spacecrafts support its presence [422,424,425]. A subsurface ocean could contain organic compounds, possibly emanating from hydrothermal vents on the ocean floor [426,427]. Unfortunately, any inferences of the composition of the subsurface ocean are only speculative.

Comets delivered an estimated minimum of 1 to 10 Gt of carbon and other biogenic elements (H, O, P, N, and S) to Europa based on modeling experiments using cometary densities, cometary impact velocities, and escape thresholds of Europa's atmosphere [428]. Hence, Europa has the necessary components for formation of organic compounds.

The presence of liquid water, organic matter, and volcanic activity suggests the possibility of extant or extinct life. These characteristics, in conjunction with past conditions,

could generate biochemical compounds and induce polymerization to provide the necessary ingredients for emergent life.

A1 4.7.2 GANYMEDE AND CALLISTO

Ice on Ganymede, the largest moon in the solar system, covers approximately 50%–90% of the surface and is estimated to be 1,000 km thick [429]. Additionally, the surface has minor concentrations of CO₂, tholin, and cyanogens (compounds with a [CN]₂ component) interstitially bound in the water ice [420]. The presence of these carbon-bearing compounds mirrors organic compounds on Callisto, suggesting similar origin for organic compounds on the two moons [420].

Callisto has a heavy cratered surface devoid of tectonic activity [421] and a CO₂-dominated atmosphere [430]. The CO₂ likely originated from degradation of existing organic compounds supplied by cometary impacts [431] or degassed from the interior [430]. Atmospheric CO₂ is degraded by irradiation from Jupiter's magnetosphere, producing CO and amorphous carbon on both Callisto and Ganymede [420].

A1 4.8 THE TERRESTRIAL PLANETS

The four innermost solar bodies are called the terrestrial planets. Their atmospheres result from internal thermal activity and cometary impacts. Compositionally, these atmospheres differ from the atmospheres of the Jovian planets. Spectroscopic investigations using orbiting spacecraft and Earth-based telescopes show that the terrestrial planets are depleted in organic compounds relative to the large Jovian planets.

A1 4.8.1 MERCURY

The lack of a substantial atmosphere on Mercury and its proximity to the Sun causes temperature to reach 440°C. At this temperature, organic compounds are unstable. Thus, long-term preservation of organic compounds on Mercury is unlikely. Only two spacecraft have investigated Mercury, the Mariner 10 orbiter, which was launched in the mid 1970's, and the

MESSENGER spacecraft, which did a flyby in early 2008 and is scheduled to enter Mercury's orbit in 2011. A future joint mission between Japan's Aerospace Exploration Agency and the European Space Agency is tentatively scheduled for launch in 2013.

A1 4.8.2 VENUS

Venus is the closest planet to Earth and comparable in mass, diameter, density, and chemical composition but lacks liquid water. Further, Venus has a dense corrosive atmosphere (with pressures up to 90 bar) and a runaway greenhouse effect causing surface temperatures to reach 450°C [432,433]. In addition to CO₂, the atmosphere contains trace amounts of CO and possibly carbonyl sulfide (OCS) [434]. The extreme surficial and atmospheric conditions on Venus make it unlikely for synthesis and preservation of organic compounds.

A1 4.8.3 MARS

Viking 1 and 2 were launched in the mid 1970's. A primary objective was the detection of biological processes in the martian soil. Instrumentation aboard the landers was designed to detect photosynthetic, metabolic, and respiration by-products of microbial communities that might be present in the martian regolith. The main instrument for detecting biological processes was a gas chromatography-mass spectrometer with high sensitivity and broad applicability. Unfortunately, no organic carbon was detected using this technique. These results, or lack of results, could be explained by the presence of an oxidant, possibly H₂O₂ [435,436]. Without a protective atmosphere, the martian regolith is continually exposed to solar UV radiation, which could result in photochemical production of oxidants and subsequent oxidation of any organic molecules that might be present [437,438].

The Planetary Fourier Spectrometer aboard the Mars Express Orbiter detected CH₄ in the martian atmosphere [439]. Its presence was confirmed using the Earth-based Fourier Transform Spectrometer [440]. Atmospheric CH₄ concentrations are between 0 and 30 ppbv (parts per

billion by volume), with a global mixing ratio of 10 ppbv [439]. Theories of the origin of atmospheric CH₄ include release as a by-product of methanogenic metabolism in the martian soil [440], emission through degassing by thermal activity [439], and introduction by cometary delivery [441].

In May 2008, Phoenix mission landed in the northern polar region of Mars to look for evidence of liquid water, biologically necessary elements (C, P, N, H), and evidence of organic compounds potentially indicative of life [442]. With only a week on the surface at this time, the Phoenix mission has taken two samples, but no chemical analyses have been completed [443]. NASA's Mars Science Laboratory Rover, scheduled to land in summer 2010 has a primary objective of identifying potential signatures of extinct or extant life [444]. The Sample Analysis at Mars Instrument Suite (SAM), will search for organic compounds using gas chromatography, mass spectrometry, and tunable laser spectrometry. Further, SAM can detect some light biogenic elements, such as H, O, and N.

A1 4.10 SNC METEORITES

The SNC (shergotite-nakhlite-chassignite) meteorite classification system is based primarily on oxygen isotope fractionation in meteoritic materials that indicate an extraterrestrial origin [445] and also correlate with compositional and isotopic measurements of the martian atmosphere taken by Viking spacecraft [446]. The chemistry of gas inclusions in the SNC meteorites (e.g., N₂, CO₂, and various noble gases) serve as geochemical fingerprints linking these meteorites to Mars, which has a unique atmospheric composition [447,448].

Martian meteorites are classified according to their primary mineralogy and petrologic relationships. All martian meteorites are considered to be achondritic stony meteorites. Stony meteorites are similar in composition to terrestrial rocks that have been differentiated or processed by igneous processes resulting in distinct textures and mineralogies; achondritic meteorites are stony meteorites that lack chondrules. Achondritic meteorites account for only 8%

of classified meteorites compared to the iron-nickel and chondritic meteorites that constitute the remaining 92% percent of classified meteorites [449]; some meteorites are still unclassified. The shergotites are named after Shergotty, a 5 kg meteorite that fell in the Bihar State of India in 1865 [449]. There are 6 identified shergotites, all recovered from India, Nigeria, and various localities in Antarctica [445]. The term “shergotites” includes meteorites with basaltic and lherzolithic composition, although the lherzolithic shergotities have only been found in Antarctica [450]. The nakhlites are also igneous rocks and are named after the archetype meteorite, Nakhla, which fell in 1911 at El-Nakhla el-Bahariya in northern Egypt [449]. Two other nakhlites, Lafayette and Governador Valadares, have uncertain histories; they may be from the Nakhla fall [451]. Since 2000, four additional nakhlites have been discovered; two in northwest Africa and two from separate localities in Antarctica [452]. There are only two chassignite (Chassigny) meteorites, which are the only known martian dunite samples. The first was observed to fall in Haute-Marne, France in 1815 [453-455]. The second Chassigny meteorite, NWA 2727, was found in North West Africa [456].

Our understanding of martian organic matter is limited to what is known from the SNC meteorites because of the lack of detection of organic matter by Viking landers. SNC meteorites contain many complex organic molecules. Aromatic, alkyl-substituted aromatic, oxygen-containing, and nitrogen-bearing aromatic hydrocarbons (see Table A1.6) were detected in the Nakhla meteorite, EETA 79001, by pyrolysis GC-MS [459]. Additionally, stepped-heating combustion experiments released CO₂ between 200–400°C, suggesting the presence of carbon-bearing compounds. The amount of CO₂ release is equivalent to approximately 1,000 ppm of carbon [460,461].

Table A1.6 Distribution of organic compounds detected in Martian meteorites [198,201,203].

High mass organic compounds detected in EETA79001^{*,#}	
<i>aromatic and alkyl-substituted</i>	
benzene	C ₆ H ₆

toluene	C_7H_8
naphthalene	$C_{10}H_8$
ethenylbenzene	C_8H_8
<i>oxygen-containing</i>	
phenol	C_6H_5OH
<i>nitrogen-containing</i>	
benzotrile	C_6H_5CN
<hr/>	
High mass organic compounds detected in ALH84001⁺	
phenanthrene	$C_{14}H_{10}$
pyrene	$C_{16}H_{10}$
chrysene	$C_{18}H_{12}$
benzopyrene	$C_{20}H_{12}$
anthanthrene	$C_{22}H_{12}$
benzopenylene	$C_{22}H_{12}$
coronene	$C_{24}H_{12}$
kerogen-like compound	
amino acids (considered to be terrestrial contamination)	
<hr/>	

* a Nakhla meteorite has same organic compounds with addition of biphenyl ($C_{12}H_{10}$),
using pyrolysis-GC-MS,
⁺ using LD-MS

Meteorite ALH84001 does not fall specifically into the SNC classification system, but it is still considered to have a martian origin [457] based on oxygen isotopic composition and gas chemistry [445]. Geochronological investigations estimated the age of the meteorite to be 4.5 ± 0.13 Ga, which is 3 to 4 billion years older than the other SNC class meteorites. Although the age of ALH84001 has raised questions about its designation as the oldest known martian meteorite [458], it is now generally accepted to have originated from Mars [452].

In 1996, McKay et al. [462] issued an astonishing report that ALH84001 contained signs of extraterrestrial life, supported by the appearance of nanofossils, biogenic magnetite, and PAHs. One of the stronger arguments in support of extraterrestrial biogenic influences in ALH84001 is chemical zonation in the carbonate globules. The sequence of Mn-carbonate deposition, followed by Fe-carbonate deposition, followed by Fe-sulfide formation is commonly observed in terrestrial environments where microbial processes control solution chemistry and hence, mineral solubility [463]. The sequence of chemical environments necessary to produce these structures abiotically is complicated. Hence, McKay et al. [462] dismiss an abiotic origin for this sequence as unlikely in

ALH84001's history. Another piece of evidence is the presence of small, elongated, single-crystal magnetite grains. Although McKay et al. [462] acknowledge that some of these structures can form abiotically, their statement that the elongated magnetite crystals in ALH84001 are biogenic is supported by other work that suggests that these structures can be biologically mediated in the form of magnetofossils produced by bacterial magnetosomes [463].

McKay et al. [462] consider possible sources of contamination from Antarctic groundwaters that contain terrestrial organic compounds and microorganisms. Further, they discuss the possibility of sample preparation contaminants and artifacts introduced during some of the analytical procedures. The controversial observation of the nanofossils generated contentious debate and is now considered the weakest evidence for extraterrestrial life. The nanofossils observed by McKay et al. [462] are found in carbonate globules. The nanofossils are purportedly similar in size, shape, and texture to bacterially induced carbonate precipitates in terrestrial samples. Sample-preparation issues, specifically, Au/Pd coatings used in electron-microscopy studies can affect sub-micron morphology. Bradley et al. [464] suggests that Au/Pd imparts fine-scale segmentation and that the segmentation increases as the thickness of the coatings increases. This argument has effectively placed nearly insurmountable doubt on the veracity of purported nanofossils in ALH84001 [462] by calling them 'microscopy artifacts' [465].

McKay et al. [462] boldly conclude that "Although there are alternate explanations for each of these phenomena taken individually, when they are considered collectively, particularly in view of their spatial association, that they are evidence for primitive life on early Mars." While carbon isotopic values and others lines of evidence have discredited the finding of signs of life in ALH84001, examination of the bulk matrix material and carbonate globules indicate that these materials are indeed of extraterrestrial origin based on isotopic studies of the PAHs present in the meteorite [466]. Multiple species of polycyclic aromatic hydrocarbons (see Table 7) [462,467] and amino acids (glycine, serine, alanine) were also detecting using LD-MS and HPLC, but some

were considered to be products of terrestrial contamination [467,468], especially the amino acids that are thought to be contaminants from Antarctic meltwater [466]. Discussions related to martian meteorite ALH84001 are likely to continue. A benefit to the scientific community is that intense scrutiny of the data has altered the rationale and methods in the search for martian life. Multiple methods (e.g., morphological, chemical, mineralogical, and isotopic) are needed to unequivocally identify signs of extraterrestrial life [469,470].

A1 5.1 CONCLUSION

Heterogeneity is a consistent theme in discussions of extraterrestrial organic compounds, in reference to both the types of species observed and the variety of environments. Within the interstellar medium and interplanetary bodies (asteroids, comets, IDPs, and chondritic meteorites), the extraterrestrial organic species range from simple diatomic molecules (e.g., CH) to complex PAH, tholin, and kerogen compounds. This heterogeneity is also pervasive in the organic matter that scientists have detected throughout the solar system, which is driven in part by the types of post-formational processing these materials have experienced. Polycyclic aromatic hydrocarbons appear to be the most ubiquitous class of organic compounds in the universe. Further, even within this class, there are numerous species that have been analyzed both remotely and directly by suites of analytical techniques.

A persistent challenge in data acquisition from all regions of the universe is potential interference and contamination; which can come from spectral interference from different interstellar clouds along overlapping lines of sight, from incorporation of terrestrial organic compounds and organisms into meteorites, from anthropogenic contaminants introduced through sampling design (e.g., carbon impurities in the aerogel capture medium from the Stardust Mission), from contaminants that may be present on spacecraft, or from contaminants introduced during processing of extraterrestrial samples in laboratories here on Earth. Therefore, understanding and characterizing potential sources of contamination will continue to be a critical

issue requiring extraterrestrial organic-compound data to be highly scrutinized to eliminate potential contamination and interference issues.

From an astrobiological perspective, some of the most exciting data come from the identification of extraterrestrial prebiotic building blocks in the ISM and prebiotic molecules in the solar system. These molecules rained down on Earth and other planetary bodies throughout their evolution and continue to provide sources of organic materials. However, the mechanism of the transition from these simple molecules to complex life remains unclear. As data and data-collection techniques continue to improve, the origins of life on this planet and insights into the possibility of extraterrestrial life will continue to intrigue scientists, philosophers, and the general public.

A1 6.1 ACKNOWLEDGEMENTS

The authors would like to thank Gordon E. Holt and Leslie P. Ovard for their assistance in the preparation and review of this manuscript and Allen J. Haroldsen for assistance with the illustration in Figure 1. Work performed at the INL under DOE/NE Idaho Operations Office Contract DE-AC07-05ID14517. Funding for this work was provided by the NASA exobiology program (EXB03-0000-0054). CDR would also like to thank Inland Northwest Research Alliance and Montana Space Grant Consortium for their support.

A1 7.1 REFERENCES

1. F. Verter, L. Magnani, E. Dwek and L. J. Rickard, *Astrophys. J.* **536**, 831 (2000).
2. P. Stauber, S. D. Doty, E. F. van Dishoeck, J. K. Jorgensen and A. O. Benz, *Astron. Astrophys.* **425**, 577 (2004).
3. J. V. Buckle, S. D. Rodgers, E. S. Wirstrom, S. B. Charnley, A. J. Markwick-Kemper, H. M. Butner and S. Takakuwa, *Faraday Discuss.* **133**, 63 (2006).
4. H. J. Fraser, M. R. S. McCoustra and D. A. Williams, *Astron. Geophys.* **43**, 10 (2002).

5. G. A. Blake, E. C. Sutton, C. R. Masson and T. G. Phillips, *Astrophys. J.* **315**, 621 (1987).
6. D. N. Friedel and L. E. Snyder, *Astrophys. J.* **672**, 962 (2008).
7. J. E. Chiar, A. J. Adamson, Y. J. Pendleton, D. C. B. Whittet, D. A. Caldwell and E. L. Gibb, *Astrophys. J.* **570**, 198 (2002).
8. J. M. Greenberg, *Adv. Space Res.* **9**, 13 (1989).
9. V. A. Basiuk and R. Navarrogonzalez, *Origins Life Evol. Biosphere* **25**, 457 (1995).
10. S. Viti, W. Brown, M. McCoustra, H. Fraser, N. Mason and R. Massey, *Astron. Geophys.* **45**, 22 (2004).
11. V. Mennella, *J. Phys.* **6**, 197 (2005).
12. Y. J. Pendleton, *Origins Life Evol. Biosphere* **27**, 53 (1997).
13. E. F. van Dishoeck, *Annu. Rev. Astron. and Astrophys.* **42**, 119 (2004).
14. Y. Aikawa, *Astrophys. Space Sci.* **313**, 35 (2008).
15. S. E. Bisschop, G. W. Fuchs, E. F. van Dishoeck and H. Linnartz, *Astron. Astrophys.* **474**, 1061 (2007).
16. J. A. Howe and J. H. Goldstein, *J. Chem. Phys.* **23**, 1223 (1955).
17. W. Irvine, R. Brown, D. Cragg, P. Friberg, P. Godfrey, N. Kaifu, H. Matthews, M. Ohishi, H. Suzuki and H. Takeo, *Astrophys. J.* **335**, L89 (1988).
18. B. E. Turner, *Astrophys. J. Suppl. S.* **76**, 617 (1991).
19. H. B. Xie, C. B. Shao and Y. H. Ding, *Astrophys. J.* **670**, 449 (2007).
20. S. C. Tegler, D. A. Weintraub, L. J. Allamandola, S. A. Sandford, T. W. Rettig and H. Campins, *Astrophys. J.* **411**, 260 (1993).
21. J. H. Lacy, F. Baas, L. J. Allamandola, S. E. Persson, P. J. McGregor, C. J. Lonsdale, T. R. Geballe and C. E. P. Vandebult, *Astrophys. J.* **276**, 533 (1984).
22. W. A. Schutte and J. M. Greenberg, *Astron. Astrophys.* **317**, L43 (1997).

23. Y. J. Pendleton, A. Tielens, A. T. Tokunaga and M. P. Bernstein, *Astrophys. J.* **513**, 294 (1999).
24. J. Y. Park and D. E. Woon, *Astrophys. J.* **601**, L63 (2004).
25. Z. Peeters, S. D. Rodgers, S. B. Charnley, L. Schriver-Mazzuoli, A. Schriver, J. V. Keane and P. Ehrenfreund, *Astron. Astrophys.* **445**, 197 (2006).
26. V. Blagojevic, S. Petrie and D. K. Bohme, *Mon. Not. R. Astron. Soc.* **339**, L7 (2003).
27. J. M. Hollis, J. A. Pedelty, L. E. Snyder, P. R. Jewell, F. J. Lovas, P. Palmer and S. Y. Liu, *Astrophys. J.* **588**, 353 (2003).
28. M. P. Bernstein, J. P. Dworkin, S. A. Sandford, G. W. Cooper and L. J. Allamandola, *Nature* **416**, 401 (2002).
29. S. Maeda and K. Ohno, *Astrophys. J.* **640**, 823 (2006).
30. P. D. Holtom, C. J. Bennett, Y. Osamura, N. J. Mason and R. I. Kaiser, *Astrophys. J.* **626**, 940 (2005).
31. S. P. Fletcher, R. B. C. Jagt and B. L. Feringa, *Chem. Comm.* **25**, 2578 (2007).
32. Y. J. Kuan, S. B. Charnley, H. C. Huang, W. L. Tseng and Z. Kisiel, *Astrophys. J.* **593**, 848 (2003).
33. L. E. Snyder, F. J. Lovas, J. M. Hollis, D. N. Friedel, P. R. Jewell, A. Remijan, V. V. Ilyushin, E. A. Alekseev and S. F. Dyubko, *Astrophys. J.* **619**, 914 (2005).
34. D. T. Halfen, A. J. Apponi, N. Woolf, R. Polt and L. M. Ziurys, *Astrophys. J.* **639**, 237 (2006).
35. J. P. Gardner, J. C. Mather, M. Clampin, R. Doyon, M. A. Greenhouse, H. B. Hammel, J. B. Hutchings, P. Jakobsen, S. J. Lilly, K. S. Long, J. I. Lunine, M. J. McCaughrean, M. Mountain, J. Nella, G. H. Rieke, M. J. Rieke, H. W. Rix, E. P. Smith, G. Sonneborn, M. Stiavelli, H. S. Stockman, R. A. Windhorst and G. S. Wright, *Space Sci. Rev.* **123**, 485 (2006).
36. Q. Chang, H. M. Cuppen and E. Herbst, *Astron. Astrophys.* **469**, 973 (2007).

37. B. T. Draine and A. Li, *Astrophys. J.* **657**, 810 (2007).
38. E. L. Gibb, D. C. B. Whittet, A. C. A. Boogert and A. Tielens, *Astrophys J. Suppl. S.* **151**, 35 (2004).
39. A. G. Li and J. M. Greenberg, *Astron. Astrophys.* **323**, 566 (1997).
40. B. E. K. Sugerman, B. Ercolano, M. J. Barlow, A. Tielens, G. C. Clayton, A. A. Zijlstra, M. Meixner, A. Speck, T. M. Gledhill, N. Panagia, M. Cohen, K. D. Gordon, M. Meyer, J. Fabbri, J. E. Bowey, D. L. Welch, M. W. Regan and R. C. Kennicutt, *Science* **313**, 196 (2006).
41. L. Piovan, R. Tantalò and C. Chiosi, *Mon. Not. R. Astron. Soc.* **366**, 923 (2006).
42. A. T. Tokunaga and S. Wada, *Adv. Space Res.* **19**, 1009 (1997).
43. L. J. Allamandola, S. A. Sandford, A. Tielens and T. M. Herbst, *Science* **260**, 64 (1993).
44. L. J. Allamandola, S. A. Sandford, A. Tielens and T. M. Herbst, *Astrophys. J.* **399**, 134 (1992).
45. W. W. Duley and D. A. Williams, *Mon. Not. R. Astron. Soc.* **272**, 442 (1995).
46. J. E. Chiar, A. J. Adamson and D. C. B. Whittet, *Astrophys. J.* **472**, 665 (1996).
47. D. Cesarsky, J. Lequeux, C. Ryter and M. Gerin, *Astron. Astrophys.* **354**, L87 (2000).
48. O. Berné, C. Joblin, Y. Deville, J. D. Smith, M. Rapacioli, J. P. Bernard, J. Thomas, W. Reach and A. Abergel, *Astron. Astrophys.* **469**, 575 (2007).
49. P. Thaddeus, *Philos. T. Roy. Soc. B* 361, 1681 (2006).
50. R. Visser, V. C. Geers, C. P. Dullemond, J. C. Augereau, K. M. Pontoppidan and E. F. van Dishoeck, *Astron. Astrophys.* **466**, 229 (2007).
51. E. Peeters, A. L. Mattioda, D. M. Hudgins and L. J. Allamandola, *Astrophys. J.* **617**, L65 (2004).
52. D. W. Hogg, C. A. Tremonti, M. R. Blanton, D. P. Finkbeiner, N. Padmanabhan, A. D. Quintero, D. J. Schlegel and N. Wherry, *Astrophys. J.* **624**, 162 (2005).

53. V. C. Geers, E. F. van Dishoeck, R. Visser, K. M. Pontoppidan, J. C. Augereau, E. Habart and A. M. Lagrange, *Astron. Astrophys.* **476**, 279 (2007).
54. P. Ehrenfreund and S. B. Charnley, *Annu. Rev. Astron. Astrophys.* **38**, 427 (2000).
55. P. Ehrenfreund, S. B. Charnley and O. Botta, in *Astrophysics of Life*, M. Livio, I. N. Reid, and W. B. Sparks, Eds., Space Telescope Science Institute Symposium Series, Baltimore, MD (2005), Vol. 16, p. 1.
56. P. Ehrenfreund and M. A. Sephton, *Faraday Discuss.* **133**, 277 (2006).
57. E. F. van Dishoeck and G. A. Blake, *Annu. Rev. Astron. Astrophys.* **36**, 317 (1998).
58. L. M. Ziurys, *Proc. Natl. Acad. Sci. U. S. A.* **103**, 12274 (2006).
59. L. M. Ziurys, *Astrobiology* **7**, 498 (2007).
60. R. Gredel, J. H. Black and M. Yan, *Astron. Astrophys.* **375**, 553 (2001).
61. R. Gredel, *Astron. Astrophys.* **351**, 657 (1999).
62. D. L. Lambert, Y. Sheffer and S. R. Federman, *Astrophys. J.* **438**, 740 (1995).
63. W. Irvine, P. Friberg, A. Hjalmarson, L. Johansson, P. Thaddeus, R. Brown and P. Godfrey, *B. Am. Astron. Soc.* **16**, 877 (1984).
64. G. Galazutdinov, F. Musaev and J. Krelowski, *Mon. Not. R. Astron. Soc.* **325**, 1332 (2001).
65. J. Hollis, A. Remijan, P. Jewell and F. Lovas, *Astrophys. J.* **642**, 933 (2006).
66. F. Lovas, A. Remijan, J. Hollis, P. Jewell and L. Snyder, *Astrophys. J.* **637**, L37 (2006).
67. G. Fuchs, U. Fuchs, T. Giesen and F. Wyrowski, *Astron. Astrophys.* **444**, 521 (2005).
68. D. A. Neufeld, P. Schilke, K. M. Menten, M. G. Wolfire, J. H. Black, F. Schuller, H. S. P. Muller, S. Thorwirth, R. Gusten and S. Philipp, *Astron. Astrophys.* **454**, L37 (2006).
69. T. Oka, J. A. Thorburn, B. J. McCall, S. D. Friedman, L. M. Hobbs, P. Sonnentrucker, D. E. Welty and D. G. York, *Astrophys. J.* **582**, 823 (2003).
70. G. Galazutdinov, A. Petlewski, F. Musaev, C. Moutou, G. Lo Curto and J. Krelowski, *Astron. Astrophys.* **395**, 969 (2002).

71. J. Mangum and A. Wootten, *Astron. Astrophys.* **239**, 319 (1990).
72. A. Betz, *Astrophys. J.* **244** (1981).
73. J. Lacy, J. Carr, N. Evans, F. Baas, J. Achtermann and J. Arens, *Astrophys. J.* **376**, 556 (1991).
74. J. M. Hollis, in *Astrochemistry: Recent Successes and Current Challenges*, edited D. C. Lis, G. A. Blake and E. Herbst, Cambridge University, Cambridge (2006), Vol. 231, p. 227.
75. National Radio Astronomy Observatory, <http://www.nrao.edu/pr/2006/gbtmolecules/>, accessed on 05/06/2008.
76. J. Cernicharo, A. Heras, A. Tielens, J. Pardo, F. Herpin, M. Guelin and L. Waters, *Astrophys. J.* **546**, L123 (1997).
77. W. S. Adams, *Astrophys. J.* **93**, 11 (1941).
78. A. Fuente, S. Garcia-Burillo, M. Gerin, D. Teyssier, A. Usero, J. R. Rizzo and P. de Vicente, *Astrophys. J.* **619**, L155 (2005).
79. M. Bell and H. Matthews, *Astrophys. J.* **438**, 223 (1995).
80. D. Fosse, J. Cernicharo, M. Gerin and P. Cox, *Astrophys. J.* **552**, 168 (2001).
81. L. Johansson, C. Andersson, J. Elder, P. Friberg, A. Hjalmarsen, B. Hoglund, W. Irvine, H. Olofsson and G. Rydbeck, *Astron. Astrophys.* **130**, 227 (1984).
82. A. Remijan, J. Hollis, F. Lovas, D. Plusquellic and P. Jewell, *Astrophys. J.* **632**, 333 (2005).
83. L. E. Snyder, J. M. Hollis, P. R. Jewell, F. J. Lovas and A. Remijan, *Astrophys. J.* **647**, 412 (2006).
84. S. Weaver and G. Blake, *Astrophys. J.* **624**, L33 (2005).
85. D. Smith, *Philos. T. Roy. Soc.* **324**, 257 (1988).
86. M. Ohishi, S. Ishikawa, C. Yamada, H. Kanamore, W. Irvine, R. Brown, P. Godfrey, N. Kaifu and H. Suzuki, *Astrophys. J.* **380**, L39 (1991).

87. P. Thaddeus, A. Gottlieb, H. Gupta, S. Brunken, M. McCarthy, M. Agundez, M. Guelin and J. Cernicharo, *Astrophys. J.* **677**, 1132 (2008).
88. Y. Kuan, S. Charnley, H. Huang, W. Tseng and Z. Kisiel, *Astrophys. J.* **593**, 848 (2003).
89. L. Snyder, F. Lovas, J. Hollis, D. Friedel, P. Jewell, A. Remijan, V. Ilyushin, E. Alekseev and S. Dyubko, *Astrophys. J.* **619**, 914 (2005).
90. M. Guelin, J. Cernicharo, G. Paubert and B. Turner, *Astron. Astrophys.* **230** (1990).
91. W. Irvine, L. Ziurys, L. Avery, H. Matthews and P. Friberg, *Astrophys. Lett. Comm.* **26**, 167 (1988).
92. W. Irvine, P. Friberg, A. Hjalmarson, S. Ishikawa, N. Kaifu, K. Kawaguchi, S. Madden, H. Matthews, M. Ohishi, S. Saito, H. Suzuki, P. Thaddeus, B. Turner, S. Yamamoto and L. Ziurys, *Astrophys. J.* **334**, L107 (1988).
93. H. S. Liszt, *Astron. Astrophys.* **476**, 291 (2007).
94. D. Halfen, D. Clouthier and L. Ziurys, *Astrophys. J.* **677** (2008).
95. D. Lambert, Y. Sheffer and S. Federman, *Astrophys. J.* **234**, L139 (1979).
96. W. Latter, C. Walker and P. Maloney, *Astrophys. J. Lett.* **419**, L97 (1993).
97. D. Whittet and H. Walker, *Mon. Not. R. Astron. Soc.* **252**, 63 (1991).
98. J. Dickens, W. Irvine, C. De Vries and M. Ohishi, *Astrophys. J.* **479**, 307 (1997).
99. F. J. Lovas, A. J. Remijan, J. M. Hollis, P. R. Jewell and L. E. Snyder, *Astrophys. J.* **637**, L37 (2006).
100. J. Hollis, P. Jewell and F. Lovas, *Astrophys. J.* **438**, 259 (1995).
101. M. Ohishi, D. McGonagle, W. Irvine, S. Yamamoto and S. Saito, *Astrophys. J.* **427**, L51 (1994).
102. M. Ohishi, S. Ishikawa, T. Amano, H. Oka, W. Irvine, J. Dickens, L. Ziurys and A. Apponi, *Astrophys. J.* **471**, L61 (1996).
103. K. Kawaguchi, Y. Kasai, S. Ishikawa, M. Ohishi, N. Kaifu and T. Amano, *Astrophys. J.* **420**, L95 (1994).

104. M. Guelin, J. Cernicharo, M. Travers, M. McCarthy, A. Gottlieb, P. Thaddeus, M. Ohishi, S. Saito and S. Yamamoto, *Astron. Astrophys.* **317**, L37 (1997).
105. L. Snyder and D. Buhl, *Astrophys. J.* **163**, L47 (1971).
106. J. Hollis, F. Lovas, A. Remijan, P. Jewell, V. Ilyushin and I. Kleiner, *Astrophys. J.* **643**, L25 (2006).
107. W. D. Langer, T. Velusamy, T. B. H. Kuiper, R. Peng, M. C. McCarthy, M. J. Travers, A. Kovacs, C. A. Gottlieb and P. Thaddeus, *Astrophys. J.* **480**, L63 (1997).
108. G. Pascoli and M. Comeau, *Astrophys. Space Sci.* **226**, 149 (1995).
109. M. Schenewerk, L. Snyder and A. Hjalmarsen, *Astrophys. J.* **303**, L71 (1986).
110. T. Geballe and T. Oka, *Nature* **384**, 334 (1996).
111. J. Cernicharo, M. Guelin, M. Agundez, K. Kawaguchi, M. McCarthy and P. Thaddeus, *Astron. Astrophys.* **61**, L37 (2007).
112. A. Belloche, K. Menten, C. Comito, H. Muller, P. Schilke, J. Ott, S. Thorwirth and C. Hieret, *Astron. Astrophys.* **482**, 179 (2008).
113. Y. Minh, W. Irvine and M. Brewer, *Astron. Astrophys.* **244**, 181 (1991).
114. C. Walmsley, G. Winnewisser and F. Toelle, *Astron. Astrophys.* **81**, 245 (1990).
115. M. Guelin and J. Cernicharo, *Astron. Astrophys.* **244**, 181 (1991).
116. K. Kawaguchi, M. Ohishi, S. Ishikawa and N. Kaifu, *Astrophys. J.* **201**, L149 (1992).
117. M. Agundez, J. Cernicharo and M. Guelin, *Astrophys. J.* **662**, L91 (2007).
118. Y. Minh, W. Irvine and L. Ziurys, *Astrophys. J.* **334** (1988).
119. B. Turner, H. Liszt, N. Kaifu and A. Kisliakov, *Astrophys. J.* **201**, L149 (1975).
120. J. Cernicharo, M. Guelin and J. R. Pardo, *Astrophys. J.* **615**, L145 (2004).
121. P. Schilke, C. Comito and S. Thorwirth, *Astrophys. J.* **582**, L101 (2003).
122. A. Remijan, J. Hollis, F. Lovas, W. Stork, P. Jewell and D. Meier, *Astrophys. J.* **675**, L85 (2008).
123. M. Guelin, N. Neininger and J. Cernicharo, *Astron. Astrophys.* **335**, L1 (1998).

124. M. Frerking, R. Linke and P. Thaddeus, *Astrophys. J.* **234**, L143 (1979).
125. N. Sakai, T. Sakai, T. Hirota and S. Yamamoto, *Astrophys. J.* **672**, 371 (2008).
126. Nguyen-Q-Rieu, D. Graham and V. Bujarrabal, *Astron. Astrophys.* **138**, L5 (1984).
127. F. J. Lovas, J. M. Hollis, A. J. Remijan and P. R. Jewell, *Astrophys. J.* **645**, L137 (2006).
128. H. Feuchtgruber, F. P. Helmich, E. F. van Dishoeck and C. M. Wright, *Astrophys. J.* **535**, L111 (2000).
129. M. Ikeda, M. Ohishi, A. Nummelin, J. E. Dickens, P. Bergman, A. Hjalmarson and W. M. Irvine, *Astrophys. J.* **560**, 792 (2001).
130. A. Remijan, J. Hollis, L. Snyder, P. Jewell and F. Lovas, *Astrophys. J.* **643**, L37 (2006).
131. M. Bell, P. Feldman, M. Travers, M. McCarthy, A. Gottlieb and P. Thaddeus, *Astrophys. J.* **483**, L61 (1997).
132. P. Goldsmith and R. Linke, *Astrophys. J.* **245**, 482 (1981).
133. C. Ceccarelli, *Planet. Space Sci.* **50**, 1267 (2002).
134. B. Turner, *Astrophys. J.* **362**, L29 (1990).
135. O. Miettinen, J. Harju, L. K. Haikala and C. Pomren, *Astron. Astrophys.* **460**, 721 (2006).
136. Z. Peeters, S. Rodgers, S. Charnley, L. Schriver-Mazzouli, A. Schriver, J. Keane and P. Ehrenfreund, *Astron. Astrophys.* **445**, 197 (2006).
137. N. Kaifu, K. Takagi and T. Kojima, *Astrophys. J.* **198**, L85 (1975).
138. J. M. Hollis, F. J. Lovas, A. J. Remijan, P. R. Jewell, V. V. Ilyushin and I. Kleiner, *Astrophys. J.* **643**, L25 (2006).
139. M. Guelin, S. Muller, J. Cernicharo, A. Apponi, M. McCarthy, A. Gottlieb and P. Thaddeus, *Astron. Astrophys.* **363**, L9 (2004).
140. B. E. Turner and A. J. Apponi, *Astrophys. J.* **561**, L207 (2001).
141. B. Zuckerman, B. Turner, D. Johnson, F. Lovas, N. Fourikis, P. Palmer, M. Morris, A. Lilley, J. Ball and F. Clark, *Astrophys. J.* **196**, L99 (1975).

142. M. Guelin, S. Muller, J. Cernicharo, M. McCarthy and P. Thaddeus, *Astron. Astrophys.* **426**, L49 (2004).
143. J. Cernicharo and M. Guelin, *Astron. Astrophys.* **309**, L26 (1996).
144. B. Turner and B. Zuckerman, *Astrophys. J.* **225**, L75 (1978).
145. M. C. McCarthy, C. A. Gottlieb, H. Gupta and P. Thaddeus, *Astrophys. J.* **652**, L141 (2006).
146. H. Brunken, H. Gupta, A. Gottlieb, M. McCarthy and P. Thaddeus, *Astrophys. J.* **664**, L43 (2007).
147. A. Remijan, J. Hollis, F. Lovas, M. Cordiner, T. Millar, A. Markwick-Kemper and P. Jewell, *Astrophys. J.* **664**, L47 (2007).
148. H. Kroto, C. Kirby, D. Walton, L. Avery, N. Broten, J. MacLeod and H. Oka, *Astrophys. J.* **219**, L133 (2002).
149. A. J. Markwick, S. B. Charnley, H. M. Butner and T. J. Millar, *Astrophys. J.* **627**, L117 (2005).
150. M. Gerin, F. Combes, G. Wlodarczak, P. Encrenaz and C. Laurent, *Astron. Astrophys.* **253**, L29 (1992).
151. N. Marcelino, J. Cernicharo, M. Agundez, E. Roueff, M. Gerin, J. Martin-Pintado, R. Mauersberger and C. Thum, *Astrophys. J.* **665**, L127 (2007).
152. J. M. Hollis, F. J. Lovas, P. R. Jewell and L. H. Coudert, *Astrophys. J.* **571**, L59 (2002).
153. T. J. Millar, E. Roueff, S. B. Charnley and S. D. Rodgers, *Int. J. Mass Spectrom.* **149**, 389 (1995).
154. D. Talbi and E. Herbst, *Astron. Astrophys.* **376**, 663 (2001).
155. S. A. Sandford, M. P. Bernstein, L. J. Allamandola, J. S. Gillette and R. N. Zare, *Astrophys. J.* **538**, 691 (2000).

156. J. P. Dworkin, J. S. Gillette, M. P. Bernstein, S. A. Sandford, L. J. Allamandola, J. E. Elsila, D. R. McGlothlin and R. N. Zare, in *Space Life Sciences: Steps toward Origin(S) of Life*, Kidlington, Oxford, Orlando, FL (2004), Vol. 33, p. 67.
157. H. S. P. Muller, F. Schloder, J. Stutzki and G. Winnewisser, *J. Mol. Struct.* **742**, 215 (2005).
158. Cologne Database for Molecular Spectroscopy, <http://www.astro.uni-koeln.de/vorhersagen/>, accessed on 05/22/2008.
159. J. N. Chengalur and N. Kanekar, *Astron. Astrophys.* **403**, L43 (2003).
160. J. M. Hollis, P. R. Jewell, F. J. Lovas, A. Remijan and H. Mollendal, *Astrophys. J.* **610**, L21 (2004).
161. M. A. Requena-Torres, J. Martin-Pintado, S. Martin and M. R. Morris, *Astrophys. J.* **672**, 352 (2008).
162. M. A. Requena-Torres, J. Martin-Pintado, A. Rodriguez-Franco, S. Martin, N. J. Rodriguez-Fernandez and P. de Vicente, *Astron. Astrophys.* **455**, 971 (2006).
163. C. J. Bennett, S. H. Chen, B. J. Sun, A. H. H. Chang and R. I. Kaiser, *Astrophys. J.* **660**, 1588 (2007).
164. T. P. Snow and B. J. McCall, *Annu. Rev. Astron. Astrophys.* **44**, 367 (2006).
165. A. E. Douglas and G. Herzberg, *Astrophys. J.* **94**, 381 (1941).
166. A. McKellar, *Publ. Astro. Soc. Pacific* **52**, 187 (1940).
167. P. Swings and L. Rosenfeld, *Astrophys. J.* **86**, 483 (1937).
168. R. Lucas and H. S. Liszt, in *Molecules in Astrophysics: Probes and Processes*, edited E. F. van Dishoeck, Kluwer, Dordrecht (1997), p. 421.
169. R. Lucas and H. S. Liszt, *Astron. Astrophys.* **358**, 1069 (2000).
170. M. P. Bernstein, S. F. M. Ashbourn, S. A. Sandford and L. J. Allamandola, *Astrophys. J.* **601**, 365 (2004).

171. R. Wagenblast, D. A. Williams, T. J. Millar and L. A. M. Nejad, *Mon. Not. R. Astron. Soc.* **260**, 420 (1993).
172. D. P. Ruffle, R. P. A. Bettens, R. Terzieva and E. Herbst, *Astrophys. J.* **523**, 678 (1999).
173. T. P. Snow, *Spectrochim. Acta. A* **57**, 615 (2001).
174. Y. J. Pendleton and L. J. Allamandola, *Astrophys. J. Suppl. S.* **138**, 75 (2002).
175. D. Deamer, J. P. Dworkin, S. A. Sandford, M. P. Bernstein and L. J. Allamandola, *Astrobiology* **2**, 371 (2002).
176. S. V. Kalenskii, V. I. Slysh, P. F. Goldsmith and L. E. B. Johansson, *Astrophys. J.* **610**, 329 (2004).
177. A. Remijan, Y. S. Shiao, D. N. Friedel, D. S. Meier and L. E. Snyder, *Astrophys. J.* **617**, 384 (2004).
178. H. Beuther and T. K. Sridharan, *Astrophys. J.* **668**, 348 (2007).
179. A. Tielens and W. Hagen, *Astron. Astrophys.* **114**, 245 (1982).
180. E. Herbst, *Annu. Rev. Phys. Chem.* **46**, 27 (1995).
181. A. Tielens and S. B. Charnley, *Origins Life Evol. Biosphere* **27**, 23 (1997).
182. N. Katz, I. Furman, O. Biham, V. Pirronello and G. Vidali, *Astrophys. J.* **522**, 305 (1999).
183. N. Marcelino, J. Cernicharo, M. Agundez, E. Roueff, M. Gerin, J. Martin-Pintado, R. Mauersberger and C. Thum, *Astrophys. J.* **665**, L127 (2007).
184. J. E. Dickens, W. M. Irvine, C. H. DeVries and M. Ohishi, *Astrophys. J.* **479**, 307 (1997).
185. Y. C. Minh and W. M. Irvine, *Astrophys. Space Sci.* **175**, 165 (1991).
186. M. B. Bell, P. A. Feldman, J. K. G. Watson, M. C. McCarthy, M. J. Travers, C. A. Gottlieb and P. Thaddeus, *Astrophys. J.* **518**, 740 (1999).
187. H. E. Matthews and T. J. Sears, *Astrophys. J.* **267**, L53 (1983).
188. N. W. Broten, J. M. Macleod, L. W. Avery, W. M. Irvine, B. Hoglund, P. Friberg and A. Hjalmarsen, *Astrophys. J.* **276**, L25 (1984).
189. R. B. Loren, A. Wootten and L. G. Mundy, *Astrophys. J.* **286**, L23 (1984).

190. J. M. Macleod, L. W. Avery and N. W. Broten, *Astrophys. J.* **282**, L89 (1984).
191. C. M. Walmsley, P. R. Jewell, L. E. Snyder and G. Winnewisser, *Astron. Astrophys.* **134**, L11 (1984).
192. W. M. Irvine, B. Hoglund, P. Friberg, J. Askne and J. Ellder, *Astrophys. J.* **248**, L113 (1981).
193. A. J. Remijan, J. M. Hollis, L. E. Snyder, P. R. Jewell and F. J. Lovas, *Astrophys. J.* **643**, L37 (2006).
194. W. M. Irvine, R. D. Brown, D. M. Cragg, P. Friberg, P. D. Godfrey, N. Kaifu, H. E. Matthews, M. Ohishi, H. Suzuki and H. Takeo, *Astrophys. J.* **335**, L89 (1988).
195. R. Maclagan, M. J. McEwan and G. B. I. Scott, *Chem. Phys. Lett.* **240**, 185 (1995).
196. G. B. I. Scott, D. A. Fairley, C. G. Freeman, R. Maclagan and M. J. McEwan, *Int. J. Mass Spectrom.* **149**, 251 (1995).
197. S. Petrie, R. P. A. Bettens, C. G. Freeman and M. J. McEwan, *Mon. Not. R. Astron. Soc.* **264**, 862 (1993).
198. S. Ekern, J. Szczepanski and M. Vala, *J. Phys. Chem.* **100**, 16109 (1996).
199. S. Ekern and M. Vala, *J. Phys. Chem. A* **101**, 3601 (1997).
200. H. Dong, Y. H. Ding and C. C. Sun, *J. Chem. Phys.* **122** (2005).
201. D. R. Flower, G. P. D. Forets and C. M. Walmsley, *Astron. Astrophys.* **474**, 923 (2007).
202. T. J. Millar, C. Walsh, M. A. Cordiner, R. Ni Chuimin and E. Herbst, *Astrophys. J.* **662**, L87 (2007).
203. H. Gupta, S. Brunken, F. Tamassia, C. A. Gottlieb, M. C. McCarthy and P. Thaddeus, *Astrophys. J.* **655**, L57 (2007).
204. S. Brunken, H. Gupta, C. A. Gottlieb, M. C. McCarthy and P. Thaddeus, *Astrophys. J.* **664**, L43 (2007).
205. R. Garrod, I. H. Park, P. Caselli and E. Herbst, *Faraday Discuss.* **133**, 51 (2006).
206. I. W. M. Smith, E. Herbst and Q. Chang, *Mon. Not. Roy. Astron. Soc.* **350**, 323 (2004).

207. R. T. Garrod, V. Wakelam and E. Herbst, *Astron. Astrophys.* **467**, 1103 (2007).
208. N. Watanabe, T. Shiraki and A. Kouchi, *Astrophys. J.* **588**, L121 (2003).
209. P. Ehrenfreund and W. A. Schutte, *IAU Symp.* **197**, 135 (2000).
210. N. Watanabe and A. Kouchi, *Astrophys. J.* **571**, L173 (2002).
211. H. Hidaka, N. Watanabe, T. Shiraki, A. Nagaoka and A. Kouchi, *Astrophys. J.* **614**, 1124 (2004).
212. A. Nummelin, D. C. B. Whittet, E. L. Gibb, P. A. Gerakines and J. E. Chiar, *Astrophys. J.* **558**, 185 (2001).
213. T. I. Hasegawa and E. Herbst, *Mon. Not. R. Astron. Soc.* **261**, 83 (1993).
214. G. M. M. Caro, U. J. Meierhenrich, W. A. Schutte, B. Barbier, A. A. Segovia, H. Rosenbauer, W. H. P. Thiemann, A. Brack and J. M. Greenberg, *Nature* **416**, 403 (2002).
215. J. E. Elsila, J. P. Dworkin, M. P. Bernstein, M. P. Martin and S. A. Sandford, *Astrophys. J.* **660**, 911 (2007).
216. M. A. Sephton, *Nat. Prod. Rep.* **19**, 292 (2002).
217. F. Fontani, I. Pascucci, P. Caselli, F. Wyrowski, R. Cesaroni and C. M. Walmsley, *Astron. Astrophys.* **470**, 639 (2007).
218. P. D. Brown, S. B. Charnley and T. J. Millar, *Mon. Not. Roy. Astron. Soc.* **231**, 409 (1988).
219. K. M. Pontoppidan, E. Dartois, E. F. van Dishoeck, W. F. Thi and L. d'Hendecourt, *Astron. Astrophys.* **404**, L17 (2003).
220. A. J. Remijan, F. Wyrowski, D. N. Friedel, D. S. Meier and L. E. Snyder, *Astrophys. J.* **626**, 233 (2005).
221. W. M. Irvine and A. Hjalmarsen, *Origins Life Evol. Biosphere* **14**, 15 (1984).
222. N. Sakai, T. Sakai and S. Yamamoto, *Astrophys. J.* **660**, 363 (2007).
223. T. J. Millar, E. Herbst and S. B. Charnley, *Astrophys. J.* **369**, 147 (1991).

224. A. Horn, H. Mollendal, O. Sekiguchi, E. Uggerud, H. Roberts, E. Herbst, A. A. Viggiano and T. D. Fridgen, *Astrophys. J.* **611**, 605 (2004).
225. R. T. Garrod and E. Herbst, *Astron. Astrophys.* **457**, 927 (2006).
226. A. Remijan, L. E. Snyder, S. Y. Liu, D. Mehringer and Y. J. Kuan, *Astrophys. J.* **576**, 264 (2002).
227. S. L. W. Weaver and G. A. Blake, *Astrophys. J.* **624**, L33 (2005).
228. S. L. W. Weaver and G. A. Blake, *Astrophys. J.* **632**, L163 (2005).
229. A. J. Apponi, J. J. Hoy, D. T. Halfen, L. M. Ziurys and M. A. Brewster, *Astrophys. J.* **652**, 1787 (2006).
230. A. J. Apponi, D. T. Halfen, L. M. Ziurys, J. M. Hollis, A. J. Remijan and F. J. Lovas, *Astrophys. J.* **643**, L29 (2006).
231. R. T. Dodd, *Nature* **290**, 189 (1981).
232. H. F. Levison, L. Dones, C. R. Chapman, S. A. Stern, M. J. Duncan and K. Zahnle, *Icarus* **151**, 286 (2001).
233. S. Pizzarello, *Acc. Chem. Res.* **39**, 231 (2006).
234. J. M. Greenberg, A. Kouchi, W. Niessen, H. Irth, J. Vanparadijs, M. Degroot and W. Hermsen, *J. Biol. Phys.* **20**, 61 (1994).
235. D. Brownlee, P. Tsou, J. Aleon, C. M. O. Alexander, T. Araki, S. Bajt, G. A. Baratta, R. Bastien, P. Bland, P. Bleuet, J. Borg, J. P. Bradley, A. Brearley, F. Brenker, S. Brennan, J. C. Bridges, N. D. Browning, J. R. Brucato, E. Bullock, M. J. Burchell, H. Busemann, A. Butterworth, M. Chaussidon, A. Chevront, M. F. Chi, M. J. Cintala, B. C. Clark, S. J. Clemett, G. Cody, L. Colangeli, G. Cooper, P. Cordier, C. Daghljan, Z. R. Dai, L. D'Hendecourt, Z. Djouadi, G. Dominguez, T. Duxbury, J. P. Dworkin, D. S. Ebel, T. E. Economou, S. Fakra, S. A. J. Fairey, S. Fallon, G. Ferrini, T. Ferroir, H. Fleckenstein, C. Floss, G. Flynn, I. A. Franchi, M. Fries, Z. Gainsforth, J. P. Gallien, M. Genge, M. K. Gilles, P. Gillet, J. Gilmour, D. P. Glavin, M. Gounelle, M. M. Grady, G. A. Graham, P.

G. Grant, S. F. Green, F. Grossemy, L. Grossman, J. N. Grossman, Y. Guan, K. Hagiya, R. Harvey, P. Heck, G. F. Herzog, P. Hoppe, F. Horz, J. Huth, I. D. Hutcheon, K. Ignatyev, H. Ishii, M. Ito, D. Jacob, C. Jacobsen, S. Jacobsen, S. Jones, D. Joswiak, A. Jurewicz, A. T. Kearsley, L. P. Keller, H. Khodja, A. L. D. Kilcoyne, J. Kissel, A. Krot, F. Langenhorst, A. Lanzirotti, L. Le, L. A. Leshin, J. Leitner, L. Lemelle, H. Leroux, M. C. Liu, K. Luening, I. Lyon, G. MacPherson, M. A. Marcus, K. Marhas, B. Marty, G. Matrajt, K. McKeegan, A. Meibom, V. Mennella, K. Messenger, S. Messenger, T. Mikouchi, S. Mostefaoui, T. Nakamura, T. Nakano, M. Newville, L. R. Nittler, I. Ohnishi, K. Ohsumi, K. Okudaira, D. A. Papanastassiou, R. Palma, M. E. Palumbo, R. O. Pepin, D. Perkins, M. Perronnet, P. Pianetta, W. Rao, F. J. M. Rietmeijer, F. Robert, D. Rost, A. Rotundi, R. Ryan, S. A. Sandford, C. S. Schwandt, T. H. See, D. Schlutter, J. Sheffield-Parker, A. Simionovici, S. Simon, I. Sitnitsky, C. J. Snead, M. K. Spencer, F. J. Stadermann, A. Steele, T. Stephan, R. Stroud, J. Susini, S. R. Sutton, Y. Suzuki, M. Taheri, S. Taylor, N. Teslich, K. Tomeoka, N. Tomioka, A. Toppani, J. M. Trigo-Rodriguez, D. Troadec, A. Tsuchiyama, A. J. Tuzzolino, T. Tyliczszak, K. Uesugi, M. Velbel, J. Vellenga, E. Vicenzi, L. Vincze, J. Warren, I. Weber, M. Weisberg, A. J. Westphal, S. Wirick, D. Wooden, B. Wopenka, P. Wozniakiewicz, I. Wright, H. Yabuta, H. Yano, E. D. Young, R. N. Zare, T. Zega, K. Ziegler, L. Zimmerman, E. Zinner and M. Zolensky, *Science* **314**, 1711 (2006).

236. D. S. Burnett, *Science* **314**, 1709 (2006).
237. D. E. Brownlee, P. Tsou, J. D. Anderson, M. S. Hanner, R. L. Newburn, Z. Sekanina, B. C. Clark, F. Horz, M. E. Zolensky, J. Kissel, J. A. M. McDonnell, S. A. Sandford and A. J. Tuzzolino, *J. Geophys. Res.-Planets* **108** (2003).
238. S. A. Sandford, J. Aleon, C. M. O. Alexander, T. Araki, S. Bajt, G. A. Baratta, J. Borg, J. P. Bradley, D. E. Brownlee, J. R. Brucato, M. J. Burchell, H. Busemann, A. Butterworth, S. J. Clemett, G. Cody, L. Colangeli, G. Cooper, L. D'Hendecourt, Z. Djouadi, J. P.

- Dworkin, G. Ferrini, H. Fleckenstein, G. J. Flynn, I. A. Franchi, M. Fries, M. K. Gilles, D. P. Glavin, M. Gounelle, F. Grossemy, C. Jacobsen, L. P. Keller, A. L. D. Kilcoyne, J. Leitner, G. Matrajt, A. Meibom, V. Mennella, S. Mostefaoui, L. R. Nittler, M. E. Palumbo, D. A. Papanastassiou, F. Robert, A. Rotundi, C. J. Snead, M. K. Spencer, F. J. Stadermann, A. Steele, T. Stephan, P. Tsou, T. Tyliczszak, A. J. Westphal, S. Wirick, B. Wopenka, H. Yabuta, R. N. Zare and M. E. Zolensky, *Science* **314**, 1720 (2006).
239. A. Rotundi and F. J. M. Rietmeijer, *Earth Moon Planets* **102**, 473 (2008).
240. G. J. Flynn, L. P. Keller, C. Jacobsen and S. Wirick, in *Space Life Sciences: Steps toward Origin(S) of Life*, (2004), Vol. 33, p. 57.
241. C. Floss, F. J. Stadermann, J. P. Bradley, Z. R. Dai, S. Bajt, G. Graham and A. S. Lea, *Geochim. Cosmochim. Acta* **70**, 2371 (2006).
242. J. P. Bradley and D. E. Brownlee, *Meteoritics* **21**, 339 (1986).
243. S. Sandford and R. Walker, *Sky Telescope* **69**, 388 (1985).
244. L. J. Allamandola, S. A. Sandford and B. Wopenka, *Science* **237**, 56 (1987).
245. P. Fraundorf, *Geochim. Cosmochim. Acta* **45**, 915 (1981).
246. P. Fraundorf, R. I. Patel and J. J. Freeman, *Icarus* **47**, 368 (1981).
247. K. D. McKeegan, R. M. Walker and E. Zinner, *Geochim. Cosmochim. Acta* **49**, 1971 (1985).
248. J. P. Bradley and D. E. Brownlee, *Meteoritics* **19**, 197 (1984).
249. G. J. Flynn, L. P. Keller, M. Feser, S. Wirick and C. Jacobsen, *Geochim. Cosmochim. Acta* **67**, 4791 (2003).
250. G. J. Flynn, L. P. Keller, S. Wirick, C. Jacobsen and S. R. Sutton, *J. Phys. IV* **104**, 367 (2003).
251. L. A. Lebofsky, M. V. Sykes, E. F. Tedesco, G. J. Veeder, D. L. Matson, R. H. Brown, J. C. Gradie, M. A. Feierberg and R. J. Rudy, *Icarus* **68**, 239 (1986).

252. F. J. Low, C. A. Beichman, F. C. Gillett, J. R. Houck, G. Neugebauer, D. E. Langford, R. G. Walker and R. H. White, *Opt. Eng.* **23**, 122 (1984).
253. G. Neugebauer, C. A. Beichman, B. T. Soifer, H. H. Aumann, T. J. Chester, T. N. Gautier, F. C. Gillett, M. G. Hauser, J. R. Houck, C. J. Lonsdale, F. J. Low and E. T. Young, *Science* **224**, 14 (1984).
254. A. Kouchi, T. Kudo, H. Nakano, M. Arakawa, N. Watanabe, S. I. Sirono, M. Higa and N. Maeno, *Astrophys. J.* **566**, L121 (2002).
255. L. P. Keller, S. Messenger, G. J. Flynn, S. Clemett, S. Wirick and C. Jacobsen, *Geochim. Cosmochim. Acta* **68**, 2577 (2004).
256. C. Floss, F. J. Stadermann, J. Bradley, Z. R. Dai, S. Bajt and G. Graham, *Science* **303**, 1355 (2004).
257. D. Alexander, L. K. Harra-Murnion, J. I. Khan and S. A. Matthews, *Astrophys. J.* **494**, L235 (1998).
258. S. Charnley, *Geochim. Cosmochim. Acta* **66**, A131 (2002).
259. R. Terzieva and E. Herbst, *Int. J. Mass Spectrom.* **201**, 135 (2000).
260. S. Messenger, F. J. Stadermann, C. Floss, L. R. Nittler and S. Mukhopadhyay, *Space Sci. Rev.* **106**, 155 (2003).
261. T. Lee, W. F. Calaway, C. Y. Chen, J. F. Moore, M. J. Pellin and I. V. Veryovkin, *Meteorit. Planet. Sci.* **39**, A59 (2004).
262. M. H. Studier, R. Hayatsu and E. Anders, *Science* **149**, 1455 (1965).
263. H. Y. McSween, *Rev. Geophys.* **17**, 1059 (1979).
264. J. W. Larimer, *Geochim. Cosmochim. Acta* **31**, 1215 (1967).
265. L. Grossman, *Geochim. Cosmochim. Acta* **36**, 597 (1972).
266. I. R. Cameron and Z. Top, *Geochim. Cosmochim. Acta* **38**, 899 (1974).
267. H. C. Urey, *Icarus* **7**, 350 (1967).
268. G. Mueller, *Geochim. Cosmochim. Ac.* **4**, 1 (1953).

269. Y. Lin, M. Kimura, B. Miao, D. Dai and A. Monoi, *Meteorit. Planet. Sci.* **41**, 67 (2006).
270. S. Pizzarello and J. R. Cronin, *Geochim. Cosmochim. Acta* **64**, 329 (2000).
271. J. R. Cronin and S. Pizzarello, *Science* **275**, 951 (1997).
272. L. Becker, R. J. Poreda and T. E. Bunch, *Proc. Natl. Acad. Sci. U. S. A.* **97**, 2979 (2000).
273. G. Yuen, N. Blair, D. J. Desmarais and S. Chang, *Nature* **307**, 252 (1984).
274. S. Pizzarello, Y. S. Huang, L. Becker, R. J. Poreda, R. A. Nieman, G. Cooper and M. Williams, *Science* **293**, 2236 (2001).
275. M. P. Bernstein, L. J. Allamandola and S. A. Sandford, *Adv. Space Res.* **19**, 991 (1997).
276. M. J. Berna, B. L. Ackermann and A. T. Murphy, *Anal. Chim. Acta* **509**, 1 (2004).
277. M. K. Spencer and R. N. Zare, *Science* **317** (2007).
278. T. N. Tingle, C. H. Becker and R. Malhotra, *Meteoritics* **26**, 117 (1991).
279. J. M. Kotler, N. W. Hinman, B. Yan, D. L. Stoner and J. R. Scott, *Astrobiology* **8**, 253 (2008).
280. J. R. Scott and P. L. Tremblay, *Rev. Sci. Instrum.* **73**, 1108 (2002).
281. B. Z. Yan, D. L. Stoner, J. M. Kotler, N. W. Hinman and J. R. Scott, *Geomicrobiol. J.* **24**, 379 (2007).
282. B. Z. Yan, D. L. Stoner and J. R. Scott, *Talanta* **72**, 634 (2007).
283. J. Isaksson, S. Acharya, J. Barman, P. Cheruku and J. Chattopadhyaya, *Biochemistry* **43**, 15996 (2004).
284. E. Anders, R. Hayatsu and M. H. Studier, *Science* **182**, 781 (1973).
285. S. Pizzarello, M. Zolensky and K. A. Turk, *Geochim. Cosmochim. Ac.* **67**, 1589 (2003).
286. A. A. Penzias, *Science* **208**, 663 (1980).
287. M. A. Sephton and I. Gilmour, *Mass Spectrom. Rev.* **20**, 111 (2001).
288. H. Naraoka, A. Shimoyama and K. Harada, *Earth Planet. Sc. Lett.* **184**, 1 (2000).
289. B. T. Commins and J. S. Harington *Nature* **212**, 273 (1966).
290. R. J. Olson, J. Oro and A. Zlatkis, *Geochim. Cosmochim. Ac.* **31**, 1935 (1967).

291. G. Jungclauss, J. R. Cronin, C. B. Moore and G. U. Yuen, *Nature* **261**, 126 (1976).
292. G. W. Cooper, W. M. Onwo and J. R. Cronin, *Geochim. Cosmochim. Acta* **56**, 4109 (1992).
293. A. Shimoyama and H. Katsumata, *Chem. Lett.*, 30, 202 (2001).
294. G. W. Cooper, M. H. Thiemens, T. L. Jackson and S. Chang, *Science* **277**, 1072 (1997).
295. P. G. Stoks and A. W. Schwartz, *Geochim. Cosmochim. Acta* **46**, 309 (1982).
296. M. H. Briggs, *Nature* **191**, 1137 (1961).
297. J. Oro, *Nature* **197**, 756 (1963).
298. J. Oro, *Nature* **197**, 862 (1963).
299. J. Oro, *Nature* **197**, 971 (1963).
300. R. Hayatsu, *Science* **150**, 374 (1965).
301. R. Hayatsu, *Science* **149**, 443 (1965).
302. E. Anders, A. Dufresne, F. W. Fitch, A. Cavaille, E. R. Dufresne and R. Hayatsu, *Science* **146**, 1157 (1964).
303. R. Hayatsu, *Science* **146**, 1291 (1964).
304. C. E. Folsome, J. G. Lawless, M. Romiez and Ponnampe.C, *Geochim. Cosmochim. Acta* **37**, 455 (1973).
305. C. Folsome, J. Lawless, M. Romiez and Ponnampe.C, *Nature* **232**, 108 (1971).
306. P. G. Stoks and A. W. Schwartz, *Geochim. Cosmochim. Acta* **45**, 563 (1981).
307. P. G. Stoks and A. W. Schwartz, *Nature* **282**, 709 (1979).
308. W. Gilbert, *Nature* **319**, 618 (1986).
309. C. Chyba and C. Sagan, *Nature* **355**, 125 (1992).
310. A. H. Delsemme, *Adv. Space Res.* **12**, 5 (1992).
311. J. Cronin and J. Reisse, *Lect. Astrobiol.* **1**, 473 (2005).
312. J. L. Bada, *Philos. T. Roy. Soc. B* **333**, 349 (1991).
313. J. L. Bada and S. L. Miller, *Biosystems* **20**, 21 (1987).

314. S. Pizzarello and A. L. Weber, *Science* **303**, 1151 (2004).
315. J.L. Bada, J. R. Cronin, M.S. Ho, K.A. Kvenvolden, J.G. Lawless, S.L. Miller, J. Oro, and S. Steinberg, *Nature* **301**, 294 (1983).
316. S. Epstein, R. V. Krishnamurthy, J. R. Cronin, S. Pizzarello and G. U. Yuen, *Nature* **326**, 477 (1987).
317. E. T. Peltzer and J. L. Bada, *Nature* **272**, 443 (1978).
318. Balavoin.G, Moradpou.A and H. B. Kagan, *J. Am. Chem. Soc.* **96**, 5152 (1974).
319. O. Riant and J. Hannedouche, *Org. Biomol. Chem.* **5**, 873 (2007).
320. U. Meierhenrich, W. H. P. Thiemann and H. Rosenbauer, *Chirality* **11**, 575 (1999).
321. J. M. Greenberg and J. I. Hage, *Astrophys. J.* **361**, 260 (1990).
322. C. X. Quang, A. H. Clark, J. K. W. Lee and N. Hawkes, *Econ. Geol.* **100**, 87 (2005).
323. R. L. Hawkes and R. A. Eaton, *Earth Moon Planets* **95**, 187 (2005).
324. P. Jenniskens, *Abstr. Pap. Am. Chem. S.* **219**, U691 (2000).
325. P. Jenniskens and H. Betlem, *Astrophys. J.* **531**, 1161 (2000).
326. P. Ehrenfreund, R. Ruitkamp, Z. Peeters, B. Foing, F. Salama and Z. Martins, *Planet Space Sci.* **55**, 383 (2007).
327. O. Popova, *Earth Moon Planets* **95**, 303 (2005).
328. S. A. Sandford, *Astrobiology* **7**, 493 (2007).
329. M. E. Zolensky, T. J. Zega, H. Yano, S. Wirick, A. J. Westphal, M. K. Weisberg, I. Weber, J. L. Warren, M. A. Velbel, A. Tsuchiyama, P. Tsou, A. Toppani, N. Tomioka, K. Tomeoka, N. Teslich, M. Taheri, J. Susini, R. Stroud, T. Stephan, F. J. Stadermann, C. J. Snead, S. B. Simon, A. Simionovici, T. H. See, F. Robert, F. J. M. Rietmeijer, W. Rao, M. C. Perronnet, D. A. Papanastassiou, K. Okudaira, K. Ohsumi, I. Ohnishi, K. Nakamura-Messenger, T. Nakamura, S. Mostefaoui, T. Mikouchi, A. Meibom, G. Matrajt, M. A. Marcus, H. Leroux, L. Lemelle, L. Le, A. Lanzirrotti, F. Langenhorst, A. N. Krot, L. P. Keller, A. T. Kearsley, D. Joswiak, D. Jacob, H. Ishii, R. Harvey, K.

- Hagiya, L. Grossman, J. N. Grossman, G. A. Graham, M. Gounelle, P. Gillet, M. J. Genge, G. Flynn, T. Ferroir, S. Fallon, D. S. Ebel, Z. R. Dai, P. Cordier, B. Clark, M. F. Chi, A. L. Butterworth, D. E. Brownlee, J. C. Bridges, S. Brennan, A. Brearley, J. P. Bradley, P. Bleuet, P. A. Bland and R. Bastien, *Science* **314**, 1735 (2006).
330. S. A. Sandford and D. E. Brownlee, *Science* **317** (2007).
331. S. J. Clemett, C. R. Maechling, R. N. Zare, P. D. Swan and R. M. Walker, *Science* **262**, 721 (1993).
332. J. Kissel and F. R. Krueger, *Nature* **328**, 117 (1987).
333. J. Kissel and F. R. Krueger, *Nature* **326**, 755 (1987).
334. J. Kissel, R. Z. Sagdeev, J. L. Bertaux, V. N. Angarov, J. Audouze, J. E. Blamont, K. Buchler, E. N. Evlanov, H. Fechtig, M. N. Fomenkova, H. Vonhoerner, N. A. Inogamov, V. N. Khromov, W. Knabe, F. R. Krueger, Y. Langevin, V. B. Leonas, A. C. Levasseuregourd, G. G. Managadze, S. N. Podkolzin, V. D. Shapiro, S. R. Tabaldyev and B. V. Zubkov, *Nature* **321**, 280 (1986).
335. J. Kissel, D. E. Brownlee, K. Buchler, B. C. Clark, H. Fechtig, E. Grun, K. Hornung, E. B. Igenbergs, E. K. Jessberger, F. R. Krueger, H. Kuczera, J. A. M. McDonnell, G. M. Morfill, J. Rahe, G. H. Schwehm, Z. Sekanina, N. G. Utterback, H. J. Volk and H. A. Zook, *Nature* **321**, 336 (1986).
336. F. Horz, R. Bastien, J. Borg, J. P. Bradley, J. C. Bridges, D. E. Brownlee, M. J. Burchell, M. F. Chi, M. J. Cintala, Z. R. Dai, Z. Djouadi, G. Dominguez, T. E. Economou, S. A. J. Fairey, C. Floss, I. A. Franchi, G. A. Graham, S. F. Green, P. Heck, P. Hoppe, J. Huth, H. Ishii, A. T. Kearsley, J. Kissel, J. Leitner, H. Leroux, K. Marhas, K. Messenger, C. S. Schwandt, T. H. See, C. Snead, F. J. Stadermann, T. Stephan, R. Stroud, N. Teslich, J. M. Trigo-Rodriguez, A. J. Tuzzolino, D. Troadec, P. Tsou, J. Warren, A. Westphal, P. Wozniakiewicz, I. Wright and E. Zinner, *Science* **314**, 1716 (2006).

337. J. M. Sunshine, M. F. A'Hearn, O. Groussin, J. Y. Li, M. J. S. Belton, W. A. Delamere, J. Kissel, K. P. Klaasen, L. A. McFadden, K. J. Meech, H. J. Melosh, P. H. Schultz, P. C. Thomas, J. Veverka, D. K. Yeomans, I. C. Busko, M. Desnoyer, T. L. Farnham, L. M. Feaga, D. L. Hampton, D. J. Lindler, C. M. Lisse and D. D. Wellnitz, *Science* **311**, 1453 (2006).
338. M. R. Swain, G. Vasisht and G. Tinetti, *Nature* **452**, 329 (2008).
339. A. Brack, *Adv. Space Res* **24**, 417 (1999).
340. J. Oro, in *A New Era in Bioastronomy* edited G. Lemarchand and K. Meech, Sheridan Books, Chelsea, MI (2000), Vol. 213, p. 285.
341. Space Studies Board and B. O. C. S. A. Technology, *Exploring organic environments in the solar system*, National Academy of Sciences Press, Washington, D.C. (2007).
342. J. Luu and D. Jewitt, *Annu. Rev. Astron. Astrophys.* **40**, 63 (2002).
343. D. P. Cruikshank, *Space Sci. Rev* **116**, 421 (2005).
344. D. Durda and A. Stern, *Icarus* **145**, 220 (2000).
345. H. Levison and M. Duncan, *Icarus* **127**, 13 (1997).
346. K. Meech and J. Belton, *Astron. J* **100**, 1323 (1990).
347. E. Dotto, M. Barucci and C. De Bergh, *Earth Moon Planets* **92**, 157 (2003).
348. D. P. Cruikshank, H. Imanaka and C. M. Dalle Ore, *Adv. Space Res* **36**, 178 (2005).
349. C. Sagan and B. N. Khare, *Nature* **277**, 102 (1979).
350. G. McDonald, L. Whited, C. DeRuiter, B. N. Khare, A. Patnaik and C. Sagan, *Icarus* **122**, 107 (1996).
351. F. Poulet, J. Cuzzi, D. P. Cruikshank, T. L. Roush and C. M. Dalle Ore, *Icarus* **160**, 313 (2002).
352. M. P. Bernstein, S. Sandford, L. Allamandola, S. Chang and M. Scharberg, *Astrophys. J.* **454**, 327 (1995).
353. J. Luu and D. Jewitt, *Astrophys. J. Suppl. S.* **112**, 2310 (1996).

354. S. Doute, B. Schmitt, E. Quirico, T. C. Owen, D. P. Cruikshank, C. De Bergh, T. R. Geballe and T. L. Roush, *Icarus* **142**, 421 (1999).
355. V. Krasnopolsky and D. P. Cruikshank, *J. Geophys. Res* **104**, 21979 (1999).
356. L. Lara, W. Ip and R. Rodrigo, *Icarus* **130**, 16 (1997).
357. D. Jewitt and J. Luu, *Nature* **432**, 731 (2004).
358. J. Fortney, *Science* **305**, 1414 (2004).
359. T. Encrenaz, *Planet Space Sci.* **51**, 89 (2003).
360. B. Bezard, T. Encrenaz, E. Lellouch and H. Feuchtgruber, *Science* **283**, 800 (1999).
361. G. Gladstone, M. Allen and Y. L. Yung, *Icarus* **119**, 1 (1996).
362. D. Strobel, *J. Atmos. Sci* **30**, 489 (1973).
363. J. Friedson, A. Wong and Y. L. Yung, *Icarus* **158** (2002).
364. S. Desch, W. Borucki, C. Russell and A. Bar-Nun, *Rep. Prog. Phys.* **65**, 955 (2002).
365. J. Magalhaes and W. Borucki, *Nature* **349**, 311 (1991).
366. A. T. Tokunaga, S. Beck, T. R. Geballe, J. Lacy and E. Serabyn, *Icarus* **48**, 283 (1981).
367. C. N. Matthews, *Adv. Space Res* **19**, 1087 (1997).
368. R. Glaser, B. Hodgen, D. Farrelly and E. McKee, *Astrobiology* **7**, 455 (2007).
369. C. Griffith, B. Bezard, T. Greathouse, E. Lellouch, J. Lacy, D. Kelly and M. Richter, *Icarus* **170**, 58 (2004).
370. M. Summers and D. Strobel, *Astrophys. J.* **346**, 495 (1989).
371. W. Hubbard, *Science* **275**, 1279 (1997).
372. J. I. Lunine, *Annu. Rev. Astron. Astrophys.* **31**, 217 (1993).
373. J. Moses, B. Bezard, E. Lellouch, G. Gladstone, H. Feuchtgruber and M. Allen, *Icarus* **143**, 244 (2000).
374. C. Nixon, R. Achterberg, B. Conrath, P. Irwin, N. Teanby, T. Fouchet, P. Parrish, P. Romani, M. Abbas, A. LeClair, D. Strobel, A. Simon-Miller, D. Jennings, F. Flasar and V. Kunde, *Icarus* **188**, 47 (2007).

375. T. Johnson and J. I. Lunine, *Nature* **435**, 69 (2005).
376. D. P. Simonelli, J. Kay, D. Adinolfi, J. Veverka, P. C. Thomas and P. Helfenstein, *Icarus* **138**, 249 (1999).
377. R. N. Clark, R. H. Brown, R. Jaumann, D. P. Cruikshank, R. M. Nelson, B. J. Buratti, T. B. McCord, J. I. Lunine, K. H. Baines, G. Belluci, J. Bibring, F. Capaccioni, G. Cerroni, A. Coradini, V. Formisano, Y. Langevin, D. L. Matson, V. Mennella, P. D. Nicholson, B. Sicardy, C. Sotin, T. M. Hoefen, J. M. Curchin, G. Hansen, K. Hibbitts and K. Matz, *Nature* **435**, 66 (2005).
378. D. P. Cruikshank, E. Wegryn, C. M. Dalle Ore, R. H. Brown, J. Bibring, B. J. Buratti, R. N. Clark, T. B. McCord, P. D. Nicholson, Y. J. Pendleton, T. C. Owen, G. Filacchione, A. Coradini, G. Cerroni, F. Capaccioni, R. Jaumann, R. M. Nelson, K. H. Baines, C. Sotin, G. Belluci, M. Combes, Y. Langevin, B. Sicardy, D. L. Matson, V. Formisano, P. Drossart and V. Mennella, *Icarus* **193**, 334 (2008).
379. B. J. Buratti, K. Soderlund, J. Bauer, J. A. Mosher, M. D. Hicks, D. P. Simonelli, R. Jaumann, R. N. Clark, R. H. Brown, D. P. Cruikshank and T. Momary, *Icarus* **193**, 309 (2008).
380. A. Coradini, F. Tosi, A. Gavrishin, F. Capaccioni, P. Cerroni, G. Filacchione, A. Adriani, R. H. Brown, G. Belluci, V. Formisano, E. D'Aversa, J. I. Lunine, K. H. Baines, J. Bibring, B. J. Buratti, R. N. Clark, D. P. Cruikshank, M. Combes, P. Drossart, R. Jaumann, Y. Langevin, D. L. Matson, T. B. McCord, V. Mennella, G. Hansen, C. A. Hibbitts, M. Showalter, C. Griffith and G. Strazzulla, *Icarus* **193**, 233 (2008).
381. A. R. Hendrix and C. Hansen, *Icarus* **193**, 344 (2008).
382. F. Vilas, S. Larson, K. Stockstill and M. Gaffey, *Icarus* **124**, 262 (1996).
383. B. J. Buratti, D. P. Cruikshank, R. H. Brown, B. C. Clark, J. Bauer, R. Jaumann, T. B. McCord, D. P. Simonelli, C. A. Hibbitts, G. Hansen, T. C. Owen, K. H. Baines, G. Belluci, J. Bibring, F. Capaccioni, G. Cerroni, A. Coradini, P. Drossart, V. Formisano, Y.

- Langevin, D. L. Matson, V. Mennella, R. M. Nelson, P. D. Nicholson, B. Sicardy, C. Sotin, T. L. Roush, K. Soderlund and A. Muradyan, *Astrophys. J.* **622**, L149 (2005).
384. P. Wilson and C. Sagan, *J. Geophys. Res.* **100**, 7531 (1995).
385. E. Palmer and R. H. Brown, *Icarus* **195**, 434 (2008).
386. T. C. Owen, D. P. Cruikshank, C. M. Dalle Ore, T. R. Geballe, T. L. Roush, C. de Bergh, Y. J. Pendleton and B. N. Khare, *Icarus* **149**, 160 (2001).
387. M. Y. Zolotov, *Geophys. Res. Lett.* **34** (2007).
388. M. Y. Zolotov, in *EOS Trans. AGU; Vol. 88* (Fall Meet. Suppl. Abstract P32B-0540, 2007).
389. J. H. Waite, M. Combi, W. Ip, T. E. Cravens, R. L. McNutt, W. Kasprzak, R. Yelle, J. Luhmann, H. Niemann, D. Gell, B. Magee, G. Fletcher, J. I. Lunine and W. Tseng, *Science* **311**, 1419 (2006).
390. D. L. Matson, J. C. Castillo, J. I. Lunine and T. V. Johnson, *Icarus* **187**, 569 (2007).
391. R. P. Hodyss, P. V. Johnson, J. D. Goguen, A. L. Lane, C. S. Boxe, J. L. Kirschvink, Y. L. Yung and I. Kanik, *EOS* **87** (2006).
392. R. H. Brown, R. N. Clark, B. J. Buratti, D. P. Cruikshank, J. W. Barnes, R. M. Mastrapa, J. Bauer, S. Newman, T. Momary, K. H. Baines, G. Belluci, F. Capaccioni, G. Cerroni, M. Combes, A. Coradini, P. Drossart, V. Formisano, R. Jaumann, Y. Langevin, D. L. Matson, T. B. McCord, R. M. Nelson, P. D. Nicholson, B. Sicardy and C. Sotin, *Science* **311**, 1425 (2006).
393. R. N. Clark, R. Brown, K. H. Baines, G. Belluci, J. Bibring, B. J. Buratti, F. Capaccioni, G. Cerroni, M. Combes, A. Coradini, D. P. Cruikshank, P. Drossart, G. Filacchione, V. Formisano, R. Jaumann, Y. Langevin, D. L. Matson, T. B. McCord, V. Mennella, R. M. Nelson, P. D. Nicholson, B. Sicardy, C. Sotin, J. M. Curchin and T. M. Hoefen, *American Astronomical Society* **37**, 705 (2005).

394. G. Filacchione, F. Capaccioni, T. B. C. McCord, A., P. Cerroni, G. Belluci, F. Tosi, E. D'Aversa, V. Formisano, R. H. Brown, K. H. Baines, J. Bibring, B. J. Buratti, R. N. Clark, M. Combes, D. P. Cruikshank, P. Drossart, R. Jaumann, Y. Langevin, D. L. Matson, V. Mennella, R. M. Nelson, P. D. Nicholson, B. Sicardy, C. Sotin, G. Hansen, K. Hibbitts, M. Showalter and S. Newman, *Icarus* **186**, 259 (2007).
395. S. Ostro, R. West, M. Janssen, R. Lorenz, H. Zebker, G. Black, J. I. Lunine, L. Wye, R. M. Lopes, S. Wall, C. Elachi, L. Roth, S. Hensley, K. Kelleher, G. Hamilton, Y. Gim, Y. Anderson, R. Boehmer, W. Johnson and t. C. R. Team, *Icarus* **183**, 479 (2006).
396. C. P. McKay and H. D. Smith, *Icarus* **178**, 274 (2005).
397. S. Atreya, *Science* **316**, 843 (2007).
398. E. Wilson and S. Atreya, *Planet Space Sci.* **51**, 1017 (2003).
399. B. Tran, J. Joseph, J. Ferris, P. Persans and J. Chera, *Icarus* **165**, 379 (2003).
400. S. Atreya, E. Adams, H. Niemann, J. Demick-Montelara, T. C. Owen, M. Fulchignoni, F. Ferri and E. Wilson, *Planet Space Sci.* **54**, 1177 (2006).
401. J. H. Waite, D. T. Young, T. E. Cravens, A. J. Coates, F. J. Crary, B. Magee and J. Westlake, *Science* **316**, 870 (2007).
402. Y. L. Yung, M. Allen and J. P. Pinto, *Astrophys. J. Suppl. S.* **55**, 465 (1984).
403. A. Coustenis, A. Salama, B. Schulz, S. Ott, E. Lellouch, T. Encrenaz, D. Gautier and H. Feuchtgruber, *Icarus* **161**, 383 (2003).
404. K. Rages and J. Pollack, *Icarus* **55**, 50 (1983).
405. D. Clarke and J. Ferris, *Icarus* **127**, 158 (1997).
406. J. I. Lunine and S. Atreya, *Nature Geo.* **1**, 159 (2008).
407. R. M. Lopes, K. Mitchell, S. Wall, G. Mitri, M. Janssen, S. Ostro, R. Kirk, A. Hayes, E. Stofan, J. I. Lunine, R. Lorenz, C. Wood, J. Radebaugh, P. Paillou, H. Zebker and F. Paganelli, *EOS* **88**, 569 (2007).

408. D. Gautier and F. Raulin, in *Huygens: science, payload and mission*, edited A. Wilson, ESA Special Report SP-1177, (1997), p. 359.
409. K. Tryka, R. Brown, V. Anicich, D. P. Cruikshank and T. C. Owen, *Science* **261**, 751 (1993).
410. D. P. R. Cruikshank, T., T. C. Owen, E. Quirico and C. De Bergh, in *Ices in the Solar System*, edited B. Schmitt, C. De Bergh, and M. Festou, Kluwer, Dordrecht (1998), p. 655.
411. E. Quirico, S. Doute, B. Schmitt, C. De Bergh, D. P. Cruikshank, T. C. Owen, T. R. Geballe and T. L. Roush, *Icarus* **139**, 159 (1999).
412. W. Grundy, M. Buie and J. Spencer, *Astron. J.* **123**, 1039 (2002).
413. W. Thompson, S. Singh, B. N. Khare and C. Sagan, *Geophys. Res. Lett.* **16**, 981 (1989).
414. D. Strobel and M. Summers, in *Neptune and Triton*, edited D. P. Cruikshank, University of Arizona Press, Tucson, (1995), p. 1107.
415. J. Elliot, D. Strobel, M. Zhu, J. Stansberry, L. Wasserman and O. Franz, *Icarus* **143**, 425 (2000).
416. R. B. Bohn, S. Sandford, L. Allamandola and D. P. Cruikshank, *Icarus* **111**, 151 (1994).
417. Y. L. Yung and W. DeMore, *Photochemistry of planetary atmospheres*, Oxford, New York (1999).
418. O. Kuskov and V. Kronrod, *Icarus* **151**, 204 (2001).
419. O. Gomis and G. Strazzulla, *Icarus* **194**, 146 (2008).
420. T. B. McCord, W. Carlson, W. Smythe, G. Hansen, R. Clark, C. A. Hibbitts, F. Fanale, J. Granahan, M. Segura, D. L. Matson, T. Johnson and P. Martin, *Science* **278**, 271 (1997).
421. A. Showman and R. Malhotra, *Science* **286**, 77 (1999).
422. M. Kivelson, C. Khurana, C. Russel, R. Volwerk, R. Walker and C. Zimmer, *Science* **289**, 1340 (2000).

423. R. Pappalardo, M. Belton, H. Breneman, M. Carr, C. Chapman, G. Collins, T. Denk, S. Fagents, P. Geissler, B. Giese, R. Greeley, R. Greenberg, J. Head, P. Helfenstein, G. Hoppa, S. Kadel, K. Klaasen, J. Klemaszewski, K. Magee, A. S. McEwen, J. Morre, W. Morre, G. Neukum, C. Phillips, L. Prockter, G. Schubert, D. Senske, R. Sullivan, B. Tufts, E. Turtle, R. Wagner and K. Williams, *J. Geophys. Res.* **104**, 24015 (1999).
424. D. Stevenson, *Science* **289**, 1305 (2000).
425. M. Carr, M. Belton, C. Chapman, M. Davies, P. Geissler, R. Greenberg, A. S. McEwen, B. Tufts, R. Greeley, R. Sullivan, J. Head, R. Pappalardo, K. Klaasen, T. Johnson, J. Kaufman, D. Senske, J. N. Moore, G. Neukum, G. Schubert, J. Burns, P. C. Thomas and J. Veverka, *Nature* **391**, 363 (1998).
426. T. Reynolds, S. W. Squyres, D. Colburn and C. P. McKay, *Icarus* **56**, 246 (1983).
427. C. Chyba, *Nature* **406**, 391 (2000).
428. E. Pierazzo and C. Chyba, *Icarus* **157**, 120 (2002).
429. W. Calvin, R. Clark, R. Brown and J. Spencer, *J. Geophys. Res.* **100**, 19041 (1995).
430. R. Carlson, *Science* **283**, 820 (1999).
431. M. Delitsky and A. L. Lane, *J. Geophys. Res.* **103**, 31391 (1998).
432. W. DeMore and Y. L. Yung, *Science* **217**, 1209 (1982).
433. P. Drossart, G. Piccioni, J. C. Gérard, M. A. Lopez-Valverde, A. Sanchez-Lavega, L. Zasova, R. Hues, F. W. Taylor, B. Bézard, A. Adriani, F. Angrilli, G. Arnold, K. H. Baines, G. Bellucci, J. Benkhoff, J. P. Bibring, A. Blanco, M. I. Blecka, R. W. Carlson, A. Coradin, A. D. Lellis, T. Encrenaz, S. Erard, S. Fonti, V. Formisano, T. Fouchet, R. Garcia, R. Haus, J. Helbert, N. I. Ignatiev, P. Irwin, Y. Langevin, S. Lebonnois, D. Luzi, L. Marinangeli, V. Orofino, A. V. Rodin, M. C. Roos-Serote, B. Saggin, D. M. Stam, D. Titov, G. Visconti, M. Zambelli and C. Tsang, *Nature* **450**, 641 (2007).
434. R. Carlson, K. H. Baines, T. Encrenaz, F. Taylor, P. Drossart, L. Kamp, J. Pollack, E. Lellouch, A. Collard, S. Calcutt, D. Grinspoon, P. Weissman, W. Smythe, A. Ocampo, G.

- Danielson, F. Fanale, T. Johnson, H. Kieffer, D. L. Matson, T. B. McCord and A. Soderblom, *Science* **253**, 1541 (1991).
435. H. Hartman and C. P. McKay, *Planet Space Sci.* **43**, 123 (1995).
436. J. A. Hurowitz, N. J. Tosca, S. M. McLennan and M. A. A. Schoonen, *Earth Planet. Sc. Lett.* **255**, 41 (2007).
437. V. Oyama, B. Berdahl and G. Carle, *Nature* **265**, 100 (1977).
438. T. Encrenaz, B. Bezard, T. Greathouse, L. Richter, J. Lacy, S. Atreya, A. Wong, S. Lebonnis, F. Lefevre and F. Forget, *Icarus* **170**, 424 (2004).
439. V. Formisano, V. Atreya, E. T., N. Ignatiev and M. Giuranna, *Science* **306**, 1758 (2004).
440. V. Krasnopolsky, J. Maillard and T. C. Owen, *Icarus* **172**, 537 (2004).
441. M. Kress and C. P. McKay, *Icarus* **168**, 475 (2004).
442. Phoenix Mars Mission, <http://phoenix.lpl.arizona.edu/science03.php>, accessed on 06/04/08.
443. Phoenix Mars Mission, http://phoenix.lpl.arizona.edu/06_03_pr.php, accessed on 06/04/08.
444. M. Cabane, P. Coll, C. Szopa, G. Israel, F. Raulin, R. Sternberg, P. Mahaffy, A. Person, C. Rodier, R. Navarro-Gonzalez, H. Hiemann, D. Harpold and W. Brinckerhoff, *Adv. Space Res.* **33**, 2240 (2004).
445. R. N. Clayton and T. K. Mayeda, *Geochim. Cosmochim. Acta* **60**, 1999 (1996).
446. M. H. Carr and H. Wanke, *Icarus* **98**, 61 (1992).
447. K. Marti, J. S. Kim, A. N. Thakur, T. J. McCoy and K. Keil, *Science* **267**, 1981 (1995).
448. G. Turner, S. F. Knott, R. D. Ash and J. D. Gilmour, *Geochim. Cosmochim. Acta* **61**, 3835 (1997).
449. H. Y. McSween, *Annu. Rev. Earth Pl. Sc.* **17**, 119 (1989).
450. H. Y. McSween and K. Keil, *Geochim. Cosmochim. Acta* **64**, 2155 (2000).
451. A. H. Treiman, *Meteoritics* **18**, 409 (1983).

452. A. H. Treiman, *Chem. Erde-Geochem.* **65**, 203 (2005).
453. A. Banin, *Adv. Space Res.* **18**, 231 (1996).
454. A. Banin, *Adv. Space Res.* **18**, 233 (1996).
455. R. L. Mancinelli, *Adv. Space Res.* **18**, 241 (1996).
456. P. Beck, J. A. Barrat, P. Gillet, M. Wadhwa, I. A. Franchi, R. C. Greenwood, M. Bohn, J. Cotten, B. V. de Moortele and B. Reynard, *Geochim. Cosmochim. Acta* **70**, 2127 (2006).
457. A. H. Treiman, A. K. Maloy and C. K. Shearer, *Meteorit. Planet. Sci.* **40**, A157 (2005).
458. C. L. Harper, L. E. Nyquist, B. Bansal, H. Wiesmann and C. Y. Shih, *Science* **267**, 213 (1995).
459. M. A. Sephton, I. P. Wright, I. Gilmour, J. W. de Leeuw, M. M. Grady and C. T. Pillinger, *Planet Space Sci.* **50**, 711 (2002).
460. I. Wright, M. Grady and C. Pillinger, *Nature* **340**, 220 (1989).
461. A. Jull, C. Courtney, D. Jeffrey and J. Beck, *Science* **279**, 366 (1998).
462. D. S. McKay, E. K. Gibson, K. L. ThomasKeperta, H. Vali, C. S. Romanek, S. J. Clemett, X. D. F. Chillier, C. R. Maechling and R. N. Zare, *Science* **273**, 924 (1996).
463. R. P. Blakemore, *Annu. Rev. Microbiol.* **36**, 217 (1982).
464. J. P. Bradley, R. P. Harvey and H. Y. McSween, *Nature* **390**, 454 (1997).
465. R. A. Kerr, *Science* **278**, 1706 (1997).
466. L. Becker, B. Popp, T. Rust and J. L. Bada, *Earth Planet. Sc. Lett.* **167**, 71 (1999).
467. L. Becker, B. Popp, T. Rust and J. L. Bada, in *Life Sciences: New Insights Into Complex Organics In Space*, Pergamon, Oxford (1999), Vol. 24, p. 477.
468. J. L. Bada, D. P. Glavin, G. D. McDonald and L. Becker, *Science* **279**, 362 (1998).
469. J. F. Banfield, J. W. Moreau, C. S. Chan, S. A. Welch and B. Little, *Astrobiology* **1**, 447 (2001).
470. J. W. Schopf, A. B. Kudryavtsev, D. G. Agresti, T. J. Wdowiak and A. D. Czaja, *Nature* **416**, 73 (2002).

APPENDIX 2: INVESTIGATION OF SYNTHETIC JAROSITE END MEMBERS (K, NA, NH₄, RB, AND PB) USING LASER DESORPTION FOURIER TRANSFORM MASS SPECTROMETRY AND X-RAY DIFFRACTION

A2.1 ABSTRACT

Jarosite and the jarosite group minerals came to the forefront of planetary geology when jarosite was discovered on the martian surface in 2004. Since then, studies have been in progress to characterize the behavior of the mineral group through a variety of analytical techniques. Determining which techniques provide the most information about the geology and potential biology of both natural and synthetic jarosite samples will assist in selecting instruments for future exploration missions. The primary cation that defines each of the jarosite end members can provide clues to the chemical environment in which it formed. The Mössbauer spectrometers that identified jarosite during the Mars Exploration Rover mission could not determine the identity of the primary cation, therefore, one of the goals of this study was to determine whether laser-desorption Fourier transform mass spectrometry (LD-FTMS) could make this distinction for jarosite samples. Baseline LD-FTMS spectra for the jarosite samples is also needed to determine whether biogenic materials can be identified in natural samples. K-jarosite, Na-jarosite, NH₄-jarosite, and Rb-jarosite were synthesized and analyzed by X-ray diffraction and LD-FTMS. A failed Pb-jarosite synthesis was also analyzed to determine if LD-FTMS could identify the jarosites based only the LD-FTMS results.

A2.2 INTRODUCTION

A new technique has been developed to detect biosignatures in geologic materials, examine the interaction of microorganisms with minerals, and chemically image the minerals within rock samples using laser-desorption Fourier transform mass spectrometry (LD-FTMS) (KOTLER et al., 2008; SCOTT et al., 2006; YAN et al., 2006; YAN et al., 2007). Understanding how synthetic minerals and standards behave during the laser desorption event and what factors determine which molecules or ions can be detected is critical to developing this new technology. Baseline spectra will assist in determining which minerals provide a useful chemical fingerprint that can identify a mineral species. Soft ionization techniques such as LD-FTMS rely on lower energy lasers to release ions and atoms from materials compared to techniques such as Laser Ablation Inductively Coupled Plasma Mass Spectrometry (LA-ICP-MS). This distinction separates an ablation technique from a desorption technique. Soft ionization techniques currently used for solids include particle bombardment, laser desorption/ionization (LDI), and matrix-assisted laser desorption/ionization (MALDI). Among those techniques, LDI has not been widely used because of fragmentation and difficulty in vaporizing polar compounds under UV laser radiation (STUMP et al., 2002). Since its introduction in 1988 (KARAS and HILLENKAMP, 1988; TANAKA et al., 1988), MALDI has become the dominate laser desorption technique because it overcame the limitations of LDI by using photoreactive matrix molecules to transfer large and/or nonvolatile biomolecules (e.g., protein, DNA, and RNA) into the gas-phase as intact ions (STULTS, 1995; STUMP et al., 2002). Because of sample prep constraints, MALDI may not be practical for identifying biomolecules in geologic materials. Consequently, laser desorption and ionization of mineral-associated biomolecules may have to rely on the minerals themselves. Inorganic matrices that are

compositionally similar to natural minerals such as porous silicon powder, silica gel, metal oxide powders or graphite have been used as matrices to detect proteins, peptides, or low molecular weight biomolecules (KINUMI et al., 2000; LAI et al., 1998; YALCIN et al., 2002; ZHANG et al., 2001).

The jarosite minerals belong to the alunite super group, which contains over 40 minerals (STOFFREGEN et al., 2000). The general formula for the jarosite minerals is $XFe_3(SO_4)_2(OH)_6$, where X is typically a monovalent cation. The most common monovalent cations that fill this position are K^+ , Na^+ , NH_4^+ , and H_3O^+ . Divalent cations such as Pb^{2+} can also occupy this position, doubling of the unit cell length along the c-axis (DUTRIZAC, 2004). Other ions including REEs have been shown to substitute in natural samples (USIMOV, 1972). Rb^+ has been synthesized as a jarosite end member, however natural varieties of rubidium jarosite are unknown (STOFFREGEN et al., 2000). The wide variety of ions present in jarosite make it ideal target to study by mass spectrometry.

Jarosite was identified on the surface of Mars in 2004, increasing interest in the mineral group (CHRISTENSEN et al., 2004; CLARK et al., 2005; GROTZINGER et al., 2005; KLINGELHOFER et al., 2004; RIEDER et al., 2004; SODERBLOM et al., 2004; SQUYRES et al., 2004a; SQUYRES et al., 2004b). The end member composition of the jarosite found on Mars could not be determined with the analytical suite on the Mars Exploration Rover (MER) (SQUYRES et al., 2003). However, inferences based on high levels of sodium in the soils at the Meridiani Planum site indicate that it is probably natrojarosite (Na-jarosite) (CLARK et al., 2005). Future planned missions may specifically target the martian jarosite minerals for further investigation (BEEGLE et al., 2007) based on studies

of microbially mediated jarosite formation on Earth (GRISHIN et al., 1988; KAWANO and TOMITA, 2001; SASAKI and KONNO, 2000). For this reason, the jarosite minerals are useful targets for astrobiological investigations (KNOLL et al., 2005).

This is a study to determine baseline LD-FTMS spectra and characterize the synthetic K, Na, NH₄, and Rb-jarosites by X-ray diffraction (XRD) for other planned studies. A failed Pb-jarosite synthesis is also included to test if mineral identification of jarosite can be determined from just the LD-FTMS spectra.

A2.3 METHODS

A2.3.1 SYNTHESSES

K-jarosite (KFe₃(SO₄)₂(OH)₆), Na-jarosite (NaFe₃(SO₄)₂(OH)₆), NH₄-jarosite, Rb-jarosite, and Pb-jarosite were prepared according to the method described in Dutrizac and Chen (DUTRIZAC and CHEN, 2003) as presented in Kotler et al. (KOTLER et al., 2008). Potassium sulfate, sodium sulfate, ammonium sulfate, rubidium sulfate or lead sulfate (0.4 M) were added to a 0.4 M FeCl₃ solution in a 100-mL round bottom flask maintaining a stoichiometric ratio of 2:3 sulfate salt to ferric iron during reaction. The solution was stirred under reflux conditions at 100° C for 24 hours. In order to collect the precipitate, the solutions were vacuum filtered while hot using a Buchner funnel and Whatman #4 filter paper. The precipitates were washed under vacuum three times with 1L of deionized water and air-dried.

A2.3.2 X-RAY DIFFRACTION

Powdered samples were mounted in cavity slides for random X-ray powder

diffraction (XRD) analysis to ensure purity and for phase identification. X-ray diffraction analyses were performed on randomly oriented powders using a Philips APD 3720 X-ray diffractometer using a step size of $0.02^\circ 2\theta$ and a rate of $0.750^\circ 2\theta/\text{min}$ at Lakehead University Centre for Analytical Services. Patterns were compared to jarosite synthetic Joint Committee on Powder Diffraction Standards (JCPDS) file 22-0827.

A2.3.3 LASER DESORPTION-FOURIER TRANSFORM MASS SPECTROMETRY (LD-FTMS)

Powdered samples were formed into pellets using a half-inch Beckman dye with a Carver Laboratory Press at a pressure of 5,000 psi before mounting onto a 316 SS probe tip using epoxy (Devcon 5 minute epoxy, Danvers, MA). Epoxy was allowed to cure to ~70 % dryness before pellet was applied to prevent the sample from absorbing the epoxy. Mass spectra were obtained using a laboratory fabricated Fourier transform mass spectrometer equipped with a 7 Tesla Oxford (Oxford, England) superconducting magnet, a 2-inch cubic cell, and an Odyssey control and data acquisition system (Thermo-Finnigan FT/MS, Bremen, Germany) (SCOTT and TREMBLAY, 2002; YAN et al., 2007). A Nd:YAG laser (Continuum, Santa Clara, CA) operating at 355 nm with a 6 ns pulse width was used for desorption/ionization using a laser fluence of $1 \times 10^8 \text{ W/cm}^2$ focused to a spot having a $\sim 6 \mu\text{m}$ diameter. All spectra were collected from single laser shots. The sample was positioned $\sim 0.5 \text{ cm}$ from the front electrostatic trap plate of the ionization cell. During the ionization event, the potential on the front and rear trap plates was maintained at 0 V. After ionization, a trapping potential of 2 V was applied to both trap plates and maintained until the quench event at the end of the sequence. A delay of

0.5 s was imposed prior to application of a radio frequency chirp excitation applied to opposing plates of the cubic cell over the range of 50 to 4 MHz with a sweep rate of 3600 Hz/ μ s. The ions were detected in direct mode using 64 to 128 K data points. The raw data were baseline corrected, Hamming apodized, zero filled, and Fourier-transformed to produce the mass spectra. Pressure during analysis was $\leq 2 \times 10^{-9}$ Torr.

A2.4 RESULTS/DISCUSSION

A2.4.1 X-RAY DIFFRACTION

The diffraction pattern for the synthetic K-jarosite is shown in Figure A2 1.1 (A). The unit cell dimensions for all of the synthesis experiments are listed in Table A2 1.1. The a-axis was 7.34 Å and the c-axis was 17.28 Å. The Na-jarosite diffraction pattern is shown in Figure A2 1.1 (B). The unit cell dimensions for Na-jarosite are a = 6.98 Å and c = 16.74 Å. Na-jarosite typically has a smaller unit cell given the reduced size of a the sodium ion compared to other ions that can occupy the same site in the jarosite structure (STOFFREGEN et al., 2000). Differences between the K-jarosite and the Na-jarosite diffraction patterns can be seen in the relative intensities and positions of the {101} and {003} reflections (figures A2 1.1 (A) and (B)). The intensity of the {104} reflection is quite low in the K-jarosite pattern, compared to the Na-jarosite where the {104} is almost of equal intensity to the {110}. Additional differences in the patterns exist for the highest intensity peak in the pattern. In K-jarosite the dominant peak is the {113} peak. In the Na-jarosite pattern, the {021} and the {113} peaks are equal in intensity. These

results are consistent with both published data (BASCIANO and PETERSON, 2008) and reference diffraction patterns (JCPDS 22-087).

Table A2 1 1. Unit cell dimensions for the synthetic jarosites calculated from {110} and {003} reflections.

Sample unit cell dimensions	{110}	{003}
K-jarosite $a = 7.34 \text{ \AA}$ $c = 17.28 \text{ \AA}$	$2\theta = 24.223$ $d = 3.67 \text{ \AA}$	$2\theta = 15.343$ $d = 5.76 \text{ \AA}$
Na-jarosite $a = 6.98 \text{ \AA}$ $c = 16.74 \text{ \AA}$	$2\theta = 25.483$ $d = 3.49 \text{ \AA}$	$2\theta = 15.343$ $d = 5.76 \text{ \AA}$
NH ₄ -jarosite $a = 7.19 \text{ \AA}$ $c = 17.5 \text{ \AA}$	$2\theta = 24.718$ $d = 3.59 \text{ \AA}$	$2\theta = 15.193$ $d = 5.833 \text{ \AA}$
Rb-jarosite $a = 7.314 \text{ \AA}$ $c = 17.875 \text{ \AA}$	$2\theta = 24.31$ $d = 3.65 \text{ \AA}$	$2\theta = 14.85$ $d = 5.958 \text{ \AA}$

The diffraction pattern for synthetic NH₄-jarosite is shown in Figure A2 1.3. The unit cell dimensions are $a = 7.19 \text{ \AA}$ and $c = 17.5 \text{ \AA}$. The NH₄-jarosite diffraction pattern differs from both the K-jarosite and Na-jarosite patterns in both the positions and relative intensities of certain peaks (Figures A2 1.1 (A), (B), and (C)). The {011} and {003} peaks are almost overlapping and the peak bases are therefore indistinguishable. In the NH₄-jarosite X-ray pattern the {021} and {113} peaks are separately from each other by a larger margin than in the K-jarosite and Na-jarosite patterns. These results are consistent with the published literature for ammonium jarosite (BASCIANO and PETERSON, 2007).

The Rb-jarosite diffraction pattern is shown in Figure A2 1.1 (D). The unit cell dimensions are $a = 7.314 \text{ \AA}$ and $c = 17.875 \text{ \AA}$. This is the largest unit cell for the synthetic jarosites used in this study. The pattern differs from the other synthetic samples in both position of peaks and number of reflections. The Rb-jarosite pattern is lacking the $\{011\}$ and $\{104\}$ peaks that are in the K-jarosite, Na-jarosite and NH_4 -jarosite diffraction patterns (Figures A2 1.1, 1.2, 1.3, and 1.4). This is likely due to a decrease in the space group symmetry from R-3m to R3m caused by the large size of the Rb^+ ion. Additionally, studies have shown that Rb-jarosite crystallizes at a slower rate than other jarosites (IVARSON et al., 1981) suggesting that a longer synthesis time may have provided a more ordered sample.

Figure A2 1.2 shows the diffraction pattern for the attempted Pb-jarosite synthesis. The $\{003\}$ peak should be at $3.899^\circ 2\theta$ ($d = 11.3 \text{ \AA}$) (DUTRIZAC, 2004), which is below the angle used for the X-ray diffraction measurement, however the absence of other higher angle peaks also confirms that the synthesis was not successful. The most intense peak should be $14.47^\circ 2\theta$ ($d = 3.066 \text{ \AA}$) representing the $\{116\}$ reflection (DUTRIZAC, 2004), this peak is not observed in the diffraction pattern. The failure of the synthesis did provide the opportunity to test whether the LD-FTMS would be able to differentiate this sample from the other jarosites.

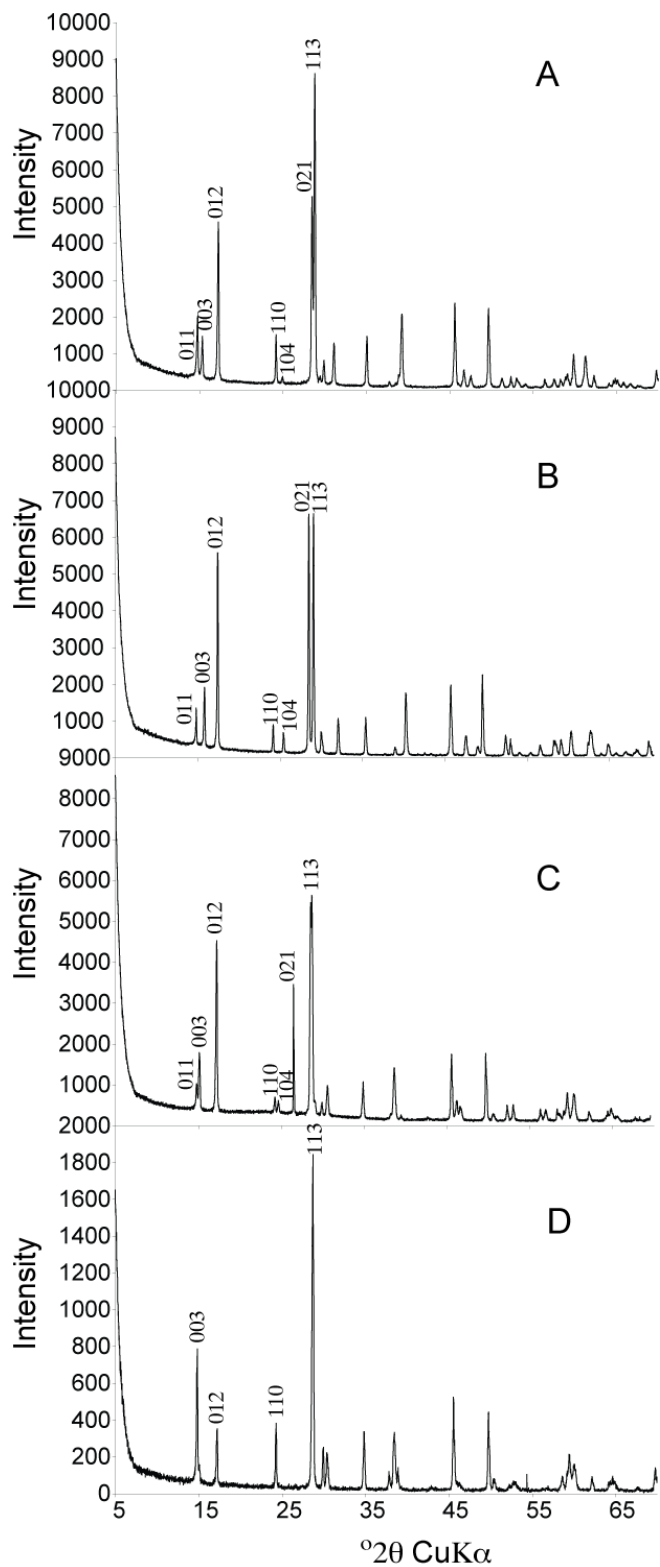


Figure A2 1.1. Powder X-ray diffraction patterns for (A) K-jarosite, (B) Na-jarosite, (C) NH_4 -jarosite, and Rb-jarosite.

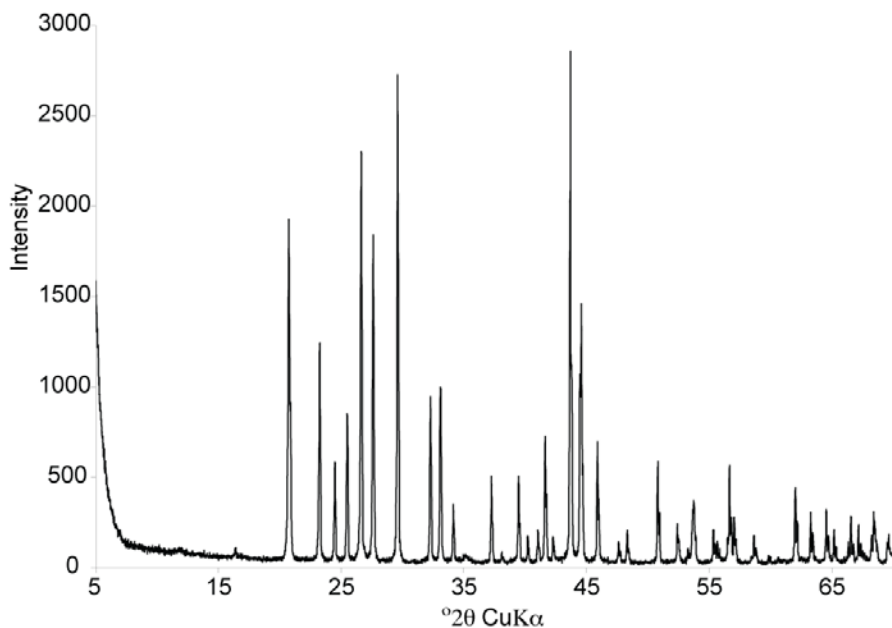


Figure A2 1.2. Pb-jarosite failed synthesis powder X-ray diffraction pattern.

A2.4.2 LD-FTMS

The LD-FTMS spectra for the synthetic jarosites are shown in Figure A2 1.6.

Figure A2 1.3 (A) shows the spectrum for K-jarosite. The two most abundant ions in the spectrum are K^+ at m/z 39.943 and Fe^+ at m/z 55.963. In the formula unit $(KFe_3(SO_4)_2(OH)_6)$, iron is more abundant than potassium by 3:1, however, in the spectrum, potassium is the most abundant ion detected. This is because ions have different ionization energies (HORTAL et al., 2008) and behave differently under UV radiation (FERNANDEZ-LIMA et al., 2008) leading to abundances in the spectra that are not quantitative. Figure A2 1.3 (B) shows the spectrum for the Na-jarosite and Figure A2 1.3 (C) shows the spectrum for NH_4 -jarosite. In both of these spectra, only the Fe^+ ion at m/z 55.963 is observed. No Na^+ and NH_4^+ ions are observed because the mass of sodium (m/z 22) and ammonium (m/z 18) are below the m/z detection of the instrument (SCOTT and

TREMBLAY, 2002). Figure A2 1.3 (D) is the LD-FTMS spectrum for the Rb-jarosite sample. The Rb^+ ion dominates the spectrum, and a peak related to Fe^+ is not observed. Figure A2 1.3 (E) is the LD-FTMS spectrum of the failed Pb-jarosite synthesis. In this spectra a series of Pb^+ ions are detected in the isotope range between m/z 204 – 210. A peak related to Fe^+ is detected at m/z 56.

The positive ions in the jarosite formula produce uncomplicated spectra during LD-FTMS analysis. There are no cluster ions produced during the desorption and ionization events that complicate the spectra. When the positive cations are within range of the instrument, such as with K-jarosite and Rb-jarosite, the spectra is dominated by the alkali cation and detection of Fe^+ ions only occurs in the K-jarosite spectra. Without being able to detect sodium or ammonium ions, identification of these jarosite end members by LD-FTMS is not possible. This would also not allow solid-solutions of these jarosites with K-jarosite to be determined by LD-FTMS. The failed Pb-jarosite spectra did produce the expected positive ions of Pb^+ , and Fe^+ , however, the X-ray diffraction results showed that it would be a misleading to assume that Pb-jarosite was the mineral responsible for this spectra.

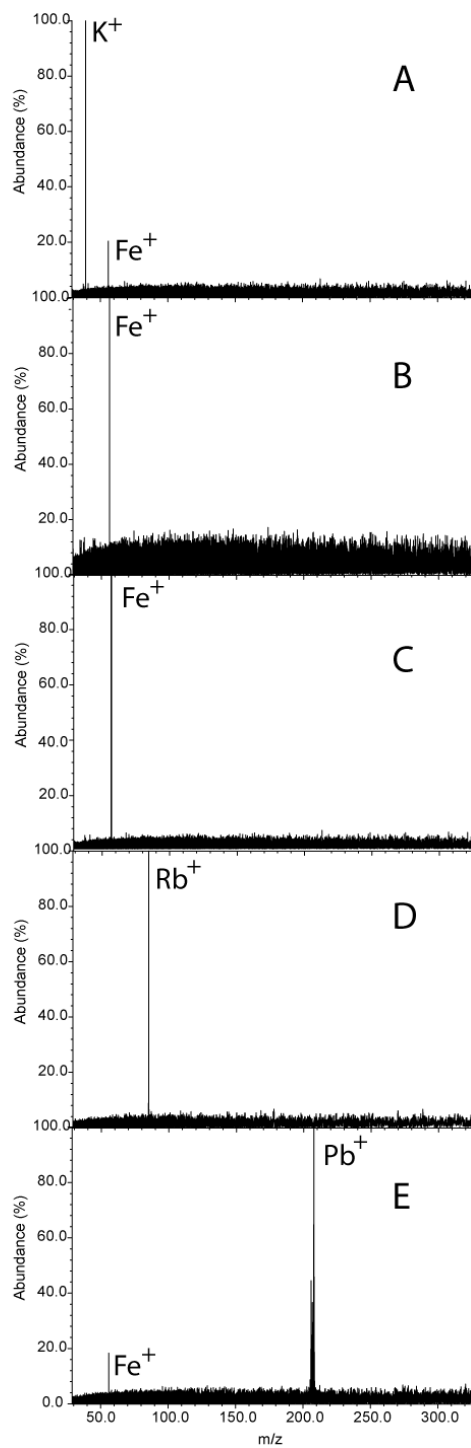


Figure A2 1.3. LD-FTMS spectra of synthetic K-jarosite (A), Na-jarosite (B), NH₄-jarosite (C), Rb-jarosite (D), and Pb-jarosite (E).

A2.5 CONCLUSIONS

The combined X-ray diffraction and LD-FTMS results from this study provide the necessary background data needed to identify some of the potential limitations of LD-FTMS analysis of jarosite samples. The lack of complex cluster ion formation in the spectra allows for the easier identification of impurities when natural jarosites are analyzed.

The findings of this study are as follows:

1. X-ray diffraction patterns for the synthetic jarosite end members are distinct and calculation of unit cell parameters can easily be calculated from the diffraction patterns for phase identification.
2. The synthetic procedure is robust and the same procedure can produce jarosites of various compositions depending on the starting materials used, with the exception of Pb-jarosite.
3. Na, and NH₄-jarosite are not identifiable from the LD-FTMS spectra because of m/z detection levels.
4. The LD-FTMS spectra do not provide quantitative data of one ion to another because of differences in ionization efficiency between the various ions.
5. Jarosite group minerals can not be identified by LD-FTMS spectra alone. Phase identification needs to be done using another method such as X-ray diffraction.
6. The simplistic nature of the LD-FTMS spectra may allow for easier identification of impurities in natural samples.

A2.6 REFERENCES

- Basciano, L. C. and Peterson, R. C., 2007. The crystal structure of ammoniojarosite, $(\text{NH}_4)\text{Fe}_3(\text{SO}_4)_2(\text{OH})_6$ and the crystal chemistry of the ammoniojarosite-hydronium jarosite solid-solution series. *Mineralogical Magazine* **71**, 427-441.
- Basciano, L. C. and Peterson, R. C., 2008. Crystal chemistry of the natrojarosite-jarosite and natrojarosite-hydronium jarosite solid-solution series: A synthetic study with full Fe site occupancy. *American Mineralogist* **93**, 853-862.
- Beegle, L. W., Wilson, M. G., Abilleira, F., Jordan, J. F., and Wilson, G. R., 2007. A concept for NASA's mars 2016 astrobiology field laboratory. *Astrobiology* **7**, 545-577.
- Christensen, P. R., Wyatt, M. B., Glotch, T. D., Rogers, A. D., Anwar, S., Arvidson, R. E., Bandfield, J. L., Blaney, D. L., Budney, C., Calvin, W. M., Faracaro, A., Ferguson, R. L., Gorelick, N., Graff, T. G., Hamilton, V. E., Hayes, A. G., Johnson, J. R., Knudson, A. T., McSween, H. Y., Mehall, G. L., Mehall, L. K., Moersch, J. E., Morris, R. V., Smith, M. D., Squyres, S. W., Ruff, S. W., and Wolff, M. J., 2004. Mineralogy at Meridiani Planum from the Mini-TES experiment on the Opportunity Rover. *Science* **306**, 1733-1739.
- Clark, B. C., Morris, R. V., McLennan, S. M., Gellert, R., Jolliff, B., Knoll, A. H., Squyres, S. W., Lowenstein, T. K., Ming, D. W., Tosca, N. J., Yen, A., Christensen, P. R., Gorevan, S., Bruckner, J., Calvin, W., Dreibus, G., Farrand, W., Klingelhofer, G., Waenke, H., Zipfel, J., Bell, J. F., Grotzinger, J., McSween, H. Y., and Rieder, R., 2005. Chemistry and mineralogy of outcrops at Meridiani Planum. *Earth and Planetary Science Letters* **240**, 73-94.
- DeAngelis, G. and Chicarro, A., 1996. A catalogue of potential landing sites for the INTERMARSNET mission.
- Dutrizac, J. E., 2004. The behaviour of the rare earths during precipitation of sodium, potassium and lead jarosites. *Hydrometallurgy* **73**, 11-30.
- Dutrizac, J. E. and Chen, T. T., 2003. Synthesis and properties of V³⁺ analogues of jarosite-group minerals. *Canadian Mineralogist* **41**, 479-488.
- Farmer, J., Desmarais, D., Greeley, R., Landheim, R., and Klein, H., 1994. SITE SELECTION FOR MARS EXOBIOLGY. In: Greenberg, J. M., Oro, J., Brack, A., Devincenzi, D. L., Banin, A., Friedmann, E. I., Rummel, J. D., Raulin, F., McKay, C. P., Baltscheffsky, H., Schwartz, A. W., Schidlowski, M., and Roessler, K. Eds.).
- Fernandez-Lima, F. A., Ponciano, C. R., and da Silveira, E. F., 2008. UV laser-induced desorption mechanism analyzed through two-layer alkali halide samples. *J. Mass Spectrom.* **43**, 587-593.
- Golombek, M. P., Cook, R. A., Moore, H. J., and Parker, T. J., 1997. Selection of the Mars Pathfinder landing site. *Journal of Geophysical Research-Planets* **102**, 3967-3988.
- Grishin, S. I., Bigham, J. M., and Tuovinen, O. H., 1988. Characterization of Jarosite Formed Upon Bacterial Oxidation of Ferrous Sulfate in a Packed-Bed Reactor. *Applied and Environmental Microbiology* **54**, 3101-3106.
- Grotzinger, J. P., Arvidson, R. E., Bell, J. F., Calvin, W., Clark, B. C., Fike, D. A., Golombek, M., Greeley, R., Haldemann, A., Herkenhoff, K. E., Jolliff, B. L.,

- Knoll, A. H., Malin, M., McLennan, S. M., Parker, T., Soderblom, L., Sohl-Dickstein, J. N., Squyres, S. W., Tosca, N. J., and Watters, W. A., 2005. Stratigraphy and sedimentology of a dry to wet eolian depositional system, Burns formation, Meridiani Planum, Mars. *Earth and Planetary Science Letters* **240**, 11-72.
- Hortal, A. R., Hurtado, P., Martinez-Haya, B., Arregui, A., and Banares, L., 2008. Solvent-free MALDI investigation of the cationization of linear polyethers with alkali metals. *Journal of Physical Chemistry B* **112**, 8530-8535.
- Ivarson, K. C., Ross, G. J., and Miles, N. M., 1981. Formation of rubidium jarosite during the microbological oxidation of ferrous iron at room temperature. *Canadian Mineralogist* **19**, 429-434.
- Jakosky, B. M. and Mellon, M. T., 2001. High-resolution thermal inertia mapping of Mars: Sites of exobiological interest. *Journal of Geophysical Research-Planets* **106**, 23887-23907.
- Karas, M. and Hillenkamp, F., 1988. Laser desorption ionization of proteins with molecular masses exceeding 10000 daltons. *Analytical Chemistry* **60**, 2299-2301.
- Kawano, M. and Tomita, K., 2001. Geochemical modeling of bacterially induced mineralization of schwertmannite and jarosite in sulfuric acid spring water. *American Mineralogist* **86**, 1156-1165.
- Kinumi, T., Saisu, T., Takayama, M., and Niwa, H., 2000. Matrix-assisted laser desorption/ionization time-of-flight mass spectrometry using an inorganic particle matrix for small molecule analysis. *J. Mass Spectrom.* **35**, 417-422.
- Klingelhofer, G., Morris, R. V., Bernhardt, B., Schroder, C., Rodionov, D. S., de Souza, P. A., Yen, A., Gellert, R., Evlanov, E. N., Zubkov, B., Foh, J., Bonnes, U., Kankeleit, E., Gutlich, P., Ming, D. W., Renz, F., Wdowiak, T., Squyres, S. W., and Arvidson, R. E., 2004. Jarosite and hematite at Meridiani Planum from Opportunity's Mossbauer spectrometer. *Science* **306**, 1740-1745.
- Knoll, A. H., Carr, M., Clark, B., Marais, D. J. D., Farmer, J. D., Fischer, W. W., Grotzinger, J. P., McLennan, S. M., Malin, M., Schroder, C., Squyres, S., Tosca, N. J., and Wdowiak, T., 2005. An astrobiological perspective on Meridiani Planum. *Earth and Planetary Science Letters* **240**, 179-189.
- Kotler, J. M., Hinman, N. W., Yan, B., Stoner, D. L., and Scott, J. R., 2008. Glycine identification in natural jarosites using laser desorption Fourier transform mass spectrometry: Implications for the search for life on Mars. *Astrobiology* **8**, 253-266.
- Lai, E. P. C., Owega, S., and Kulczycki, R., 1998. Time-of-flight mass spectrometry of bioorganic molecules by laser ablation of silver thin film substrates and particles. *J. Mass Spectrom.* **33**, 554-564.
- Rieder, R., Gellert, R., Anderson, R. C., Bruckner, J., Clark, B. C., Dreibus, G., Economou, T., Klingelhofer, G., Lugmair, G. W., Ming, D. W., Squyres, S. W., d'Uston, C., Wanke, H., Yen, A., and Zipfel, J., 2004. Chemistry of rocks and soils at Meridiani Planum from the alpha particle X-ray spectrometer. *Science* **306**, 1746-1749.
- Sasaki, K. and Konno, H., 2000. Morphology of jarosite-group compounds precipitated from biologically and chemically oxidized Fe ions. *Canadian Mineralogist* **38**, 45-56.

- Scott, J. R. and Tremblay, P. L., 2002. Highly reproducible laser beam scanning device for an internal source laser desorption microprobe Fourier transform mass spectrometer. *Review of Scientific Instruments* **73**, 1108-1116.
- Scott, J. R., Yan, B. Z., and Stoner, D. L., 2006. Spatially-correlated mass spectrometric analysis of microbe-mineral interactions. *Journal of Microbiological Methods* **67**, 381-384.
- Soderblom, L. A., Anderson, R. C., Arvidson, R. E., Bell, J. F., Cabrol, N. A., Calvin, W., Christensen, P. R., Clark, B. C., Economou, T., Ehlmann, B. L., Farrand, W. H., Fike, D., Gellert, R., Glotch, T. D., Golombek, M. P., Greeley, R., Grotzinger, J. P., Herkenhoff, K. E., Jerolmack, D. J., Johnson, J. R., Jolliff, B., Klingelhofer, G., Knoll, A. H., Learner, Z. A., Li, R., Malin, M. C., McLennan, S. M., McSween, H. Y., Ming, D. W., Morris, R. V., Rice, J. W., Richter, L., Rieder, R., Rodionov, D., Schroder, C., Seelos, F. P., Soderblom, J. M., Squyres, S. W., Sullivan, R., Watters, W. A., Weitz, C. M., Wyatt, M. B., Yen, A., and Zipfel, J., 2004. Soils of eagle crater and Meridiani Planum at the Opportunity Rover landing site. *Science* **306**, 1723-1726.
- Squyres, S. W., Arvidson, R. E., Baumgartner, E. T., Bell, J. F., Christensen, P. R., Gorevan, S., Herkenhoff, K. E., Klingelhofer, G., Madsen, M. B., Morris, R. V., Rieder, R., and Romero, R. A., 2003. Athena Mars rover science investigation. *Journal of Geophysical Research-Planets* **108**.
- Squyres, S. W., Arvidson, R. E., Bell, J. F., Bruckner, J., Cabrol, N. A., Calvin, W., Carr, M. H., Christensen, P. R., Clark, B. C., Crumpler, L., Des Marais, D. J., d'Uston, C., Economou, T., Farmer, J., Farrand, W., Folkner, W., Golombek, M., Gorevan, S., Grant, J. A., Greeley, R., Grotzinger, J., Haskin, L., Herkenhoff, K. E., Hviid, S., Johnson, J., Klingelhofer, G., Knoll, A. H., Landis, G., Lemmon, M., Li, R., Madsen, M. B., Malin, M. C., McLennan, S. M., McSween, H. Y., Ming, D. W., Moersch, J., Morris, R. V., Parker, T., Rice, J. W., Richter, L., Rieder, R., Sims, M., Smith, M., Smith, P., Soderblom, L. A., Sutlivan, R., Wanke, H., Wdowiak, T., Wolff, M., and Yen, A., 2004a. The Opportunity Rover's Athena science investigation at Meridiani Planum, Mars. *Science* **306**, 1698-1703.
- Squyres, S. W., Grotzinger, J. P., Arvidson, R. E., Bell, J. F., Calvin, W., Christensen, P. R., Clark, B. C., Crisp, J. A., Farrand, W. H., Herkenhoff, K. E., Johnson, J. R., Klingelhofer, G., Knoll, A. H., McLennan, S. M., McSween, H. Y., Morris, R. V., Rice, J. W., Rieder, R., and Soderblom, L. A., 2004b. In situ evidence for an ancient aqueous environment at Meridiani Planum, Mars. *Science* **306**, 1709-1714.
- Stoffregen, R. E., Alpers, C. N., and Jambor, J. L., 2000. Alunite-jarosite crystallography, thermodynamics, and geochronology. *Sulfate Minerals - Crystallography, Geochemistry and Environmental Significance* **40**, 453-479.
- Stults, J. T., 1995. Matrix-assisted laser-desorption ionization mass-spectrometry (MALDI-MS). *Curr. Opin. Struct. Biol.* **5**, 691-698.
- Stump, M. J., Fleming, R. C., Gong, W.-H., Jaber, A. J., Jones, J. J., Surber, C. W., and Wilkins, C. L., 2002. MATRIX-ASSISTED LASER DESORPTION MASS SPECTROMETRY. *Applied Spectroscopy Reviews* **37**, 275 - 303.

- Tanaka, K., H. W., Ido, Y., Akita, A., Yoshida, Y., and Yoshida, T., 1988. Protein and polymer analyses up to m/z 100,000 by laser ionization time-of-flight mass spectrometry. *Rapid Communications in Mass Spectrometry* **2**, 151-153.
- Usimov, V. V., and Kozlova, P.S., 1972. Rare Earth natrojarosite.
- Yalcin, T., Wallace, W. E., Guttman, C. M., and Li, L., 2002. Metal powder substrate-assisted laser desorption/ionization mass spectrometry for polyethylene analysis. *Analytical Chemistry* **74**, 4750-4756.
- Yan, B., McJunkin, T. R., Stoner, D. L., and Scott, J. R., 2006. Validation of fuzzy logic method for automated mass spectral classification for mineral imaging. *Applied Surface Science* **253**, 2011-2017.
- Yan, B. Z., Stoner, D. L., Kotler, J. M., Hinman, N. W., and Scott, J. R., 2007. Detection of biosignatures by geomatrix-assisted laser desorption/ionization (GALDI) mass spectrometry. *Geomicrobiology Journal* **24**, 379-385.
- Zhang, Q. C., Zou, H. F., Guo, Z., Zhang, Q., Chen, X. M., and Ni, J. Y., 2001. Matrix-assisted laser desorption/ionization mass spectrometry using porous silicon and silica gel as matrix. *Rapid Communications In Mass Spectrometry* **15**, 217-223.